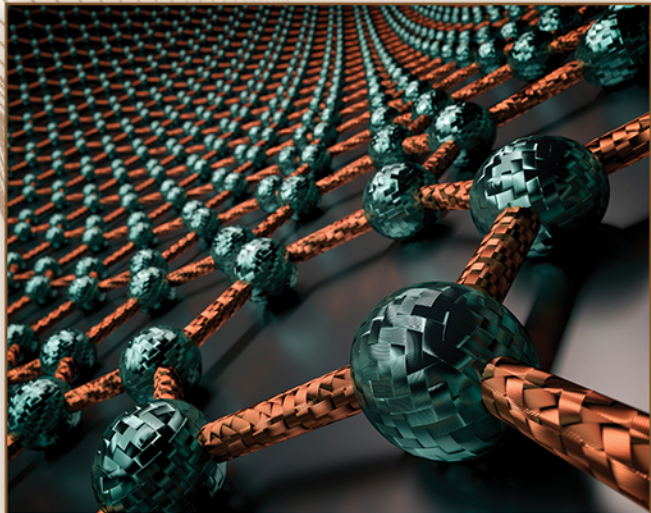


METAL MATRIX COMPOSITES

FABRICATION, PRODUCTION AND 3D PRINTING



EDITED BY

**SUNEEV ANIL BANSAL
VIRAT KHANNA
PALLAV GUPTA**



CRC Press
Taylor & Francis Group
[@seismicisolation](http://seismicisolation.com)

Metal Matrix Composites



Taylor & Francis

Taylor & Francis Group

<http://taylorandfrancis.com>

@seismicisolation
@seismicisolation

Metal Matrix Composites

Fabrication, Production, and
3D Printing (Vol. 1)

Edited by
Suneev Anil Bansal
Virat Khanna
Pallav Gupta



CRC Press

Taylor & Francis Group

Boca Raton London New York

CRC Press is an imprint of the
Taylor & Francis Group, an **informa** business

[@seismicisolation](#)
[@seismicisolation](#)

First edition published 2023
by CRC Press
6000 Broken Sound Parkway NW, Suite 300, Boca Raton, FL 33487-2742

and by CRC Press
4 Park Square, Milton Park, Abingdon, Oxon, OX14 4RN

CRC Press is an imprint of Taylor & Francis Group, LLC

© 2023 selection and editorial matter, Suneev Anil Bansal, Virat Khanna, and Pallav Gupta; individual chapters, the contributors

Reasonable efforts have been made to publish reliable data and information, but the author and publisher cannot assume responsibility for the validity of all materials or the consequences of their use. The authors and publishers have attempted to trace the copyright holders of all material reproduced in this publication and apologize to copyright holders if permission to publish in this form has not been obtained. If any copyright material has not been acknowledged, please write and let us know so we may rectify in any future reprint.

Except as permitted under U.S. Copyright Law, no part of this book may be reprinted, reproduced, transmitted, or utilized in any form by any electronic, mechanical, or other means, now known or hereafter invented, including photocopying, microfilming, and recording, or in any information storage or retrieval system, without written permission from the publishers.

For permission to photocopy or use material electronically from this work, access www.copyright.com or contact the Copyright Clearance Center, Inc. (CCC), 222 Rosewood Drive, Danvers, MA 01923, 978-750-8400. For works that are not available on CCC please contact mpkbookspermissions@tandf.co.uk

Trademark notice: Product or corporate names may be trademarks or registered trademarks and are used only for identification and explanation without intent to infringe.

ISBN: 978-1-032-04853-6 (hbk)

ISBN: 978-1-032-04855-0 (pbk)

ISBN: 978-1-003-19489-7 (ebk)

DOI: 10.1201/9781003194897

Typeset in Times
by SPi Technologies India Pvt Ltd (Straive)

Contents

Preface	vii
Editors	ix
Contributors	xi
Chapter 1 Micro and Nanocomposites Produced by Different Casting Routes and Improved Mechanical and Tribological Properties	1
<i>Sekar Kannan</i>	
Chapter 2 Processing of Metal Matrix Composites (MMCs)	17
<i>Rahul Gupta and Daksh Shelly</i>	
Chapter 3 Copper Matrix Composites: Synthesis and Applications	47
<i>Prateek Mittal, Jimmy Mehta, Seema Mahto and Sahil Mehta</i>	
Chapter 4 A Review on Aluminum Metal Matrix Composites: A Multidimensional Attribute Approach	63
<i>Gurpreet Singh Sokhal, Gurprinder Singh Dhindsa, Gurmali Singh Malhi and Kamaljit Singh Sokhal</i>	
Chapter 5 Multi-scale Computational Analysis of Metal Matrix Nanocomposites	81
<i>Gaurav Arora and Himanshu Pathak</i>	
Chapter 6 Impact of Coating Blends and Coating Techniques on Metal Matrix Composites	117
<i>Jimmy Mehta, Prateek Mittal and Sahil Mehta</i>	
Chapter 7 Effects of Performance Measures of Non-conventional Joining Processes on Mechanical Properties of Metal Matrix Composites	135
<i>Kamaljit Singh, Suneev Anil Bansal, Virat Khanna and Satinder Singh</i>	

Chapter 8	3D Printing of Metal Matrix Composites: A Review and Prospective.....	167
	<i>Gurdyal Singh, Gurpreet Singh, Rajbir Bhatti and Balkar Singh</i>	
Chapter 9	Conventional and 3D Printing Technology for the Manufacturing of Metal Matrix Composite: A Study	197
	<i>Rakesh Kumar, Santosh Kumar, Mohit Kumar and Gaurav Luthra</i>	
Chapter 10	Advancement in Liquid Processing Techniques of Aerospace-Grade 7XXX Series Aluminium Alloy and Composites	225
	<i>Vasanthakumar Pandian and Sekar Kannan</i>	
Index.....		253

Preface

The present book volume, *Metal Matrix Composites: Fabrication, Production, and 3D Printing* will provide great support and basic knowledge of MMCs to readers undergoing different programs related to Mechanical and Materials Technology, irrespective of the stream they opt for. All the engineers and designers are directly or indirectly involved in the manufacturing of metal matrix composites and its related processes. In general, Composites are made of two or more materials with a combination of required properties and are used by both manufacturers and industrialists. Moreover, understanding their manufacturing processes is paramount as these processes vary as do the materials. Hence, engineers and researchers opting for this profession should have deep knowledge about the materials and preparation of MMCs. The users can provide the best feedback and if they happen to be engineers, their feedback may help in better design, cost reduction, alternative material, and the process of making a part or machine or structure. The present book intends to provide in-depth knowledge for easy understanding of concepts. This book brings in the elements of the manufacturing of metal matrix composites with a detailed focus on its fabrication, production, and 3D printing. Real-life examples have also been used in the text rather than just describing the process. Also, the different authors have tried to explain the concepts and reasons in the best possible way.

The entire book has been divided into 10 different chapters thereby covering all the major issues and challenges related to MMCs. Chapter-wise details are as follows:

Chapter 1 discusses in detail the whole process of manufacturing an aluminum composite using various techniques like casting, etc. Also, types of casting have been explained and a case study of A356 alloy has been highlighted.

Chapter 2 is dedicated to the processing of metal matrix composites, where each and every step has been discussed in detail with schematic diagrams.

Chapter 3 discusses copper matrix composites, their properties, synthesis, and their applications in various fields. It also includes the history of copper-based composites, their evolution, and their characteristics.

Chapter 4 covers the review of aluminum-based composites. It also includes the enhancement in a number of applications on a daily basis and continuous improvement in the methodology used in preparing them.

Chapter 5 describes the nanocomposites, properties, and their applications. Micro-scale and macro-scale investigations have been presented with a detailed discussion of elastic and elastoplastic behavior.

Chapter 6 is focused on the available coating layers to effectively enhance the working life of metal matrix composite. Various coating powders, techniques, and blends are discussed and a selection of the best can be made based on their application. The addition of rare earth has also been summarized.

Chapter 7 explains all the joining processes that are presently used by manufacturers. The benefits of non-conventional methods have also been explained with illustrations and examples.

Chapter 8 discusses additive manufacturing and 3D printing, a relatively new process (recognized a decade ago) used in developing complex geometries without any material wastage. Prospective applications and limitations have been discussed in detail.

Chapter 9 discusses both conventional and 3D printing technology, and their advantages and differences. Recent developments and future scope for fabrication techniques are also explained in this chapter.

Chapter 10 focuses on the applications of metal matrix composites and this has been very well explained by the case study using aluminum alloy for the aerospace industry. Mechanical properties and characterization are discussed with most possible outcomes using case studies.

All three editors are thankful to almighty God. Apart from this, Dr. Suneev Anil Bansal and Dr. Virat Khanna are also thankful to their family members for the support extended during the editing of this book. Dr. Pallav Gupta is also thankful to his mother (Beena Gupta), wife (Dr. Ritu Agrahari), and son (Saahas Gupta) for their encouragement as well as their support extended during the entire duration of editing this book.

Dr. Pallav Gupta also would like to extend his heartfelt gratitude to Mr. S. M. Prasad, Joint Director, Council of Science and Technology, Lucknow for the motivation provided during the period while he was editing this book.

We are also thankful to all our contributors who submitted their chapters to the present volume of the book.

We are also thankful to Dr. Gagandeep Singh and Ms. Aditi Mittal along with their entire team of CRC Press (Taylor and Francis Group) for publishing this book in the fastest possible time and in the most efficient manner.

Dr. Suneev Anil Bansal

Dr. Virat Khanna

Dr. Pallav Gupta

Editors



Dr. Suneev Anil Bansal has more than 15 years of diverse experience in industry, research laboratories, and academia. He has served in various key positions in key projects like automobile development at Hero Motor Corp., fighter aircraft development at DRDO, and nanomaterials and manufacturing development at various universities. His research interest is in the fields of micro/nano-manufacturing, materials, 2D materials, graphene, polymer/metal composite materials, sensing, etc. Presently, he is working as professor (associate) Bharat Institute of Engineering and Technology, Hyderabad, India. He has published

more than 50 research papers, holds one patent, and has served as a subject expert for a number of journals.



Dr. Virat Khanna is an Assistant Professor and Head of the Department of Mechanical Engineering at Maharaja Agrasen University, HP, India and has 11 years of teaching experience. He holds a Ph.D. in Mechanical Engineering from Maharaja Agrasen University, HP, India. He completed his M.Tech in Mechanical Engineering in 2013 and B.Tech in Mechanical Engineering in 2008 from I.K. Gujral Punjab Technical University,

Jalandhar, India. His areas of research are aluminum metal matrix nanocomposite (Graphene, CNT, processing techniques, optimization, and mathematical modeling techniques). He has published and presented more than 18 papers in journals and conferences of national and international repute. He has authored one book named *Steady State Creep in Rotating Thick-Walled Composite Cylinders* with Lambert Academic Publishing, Germany (ISBN: 978-3-659-71203-6). He is also the editor of *Emerging and Futuristic Trends in Engineering and Technology* (ISBN: 978-93-82068-14-3).



Dr. Pallav Gupta is presently working as an Assistant Professor (Grade-II) in the Department of Mechanical Engineering, Amity School of Engineering and Technology, Amity University Uttar Pradesh, Noida (INDIA). He completed his B.Tech. (Honors) from Department of Mechanical Engineering, Integral University, Lucknow, INDIA in the year 2009, qualified GATE in 2009 with AIR-3291, and then completed his M.Tech. (Honors) from I.I.T. (B.H.U.), Varanasi, India in 2011 followed by Ph.D. in 2015 from I.I.T.(B.H.U.),

Varanasi, India. His areas of research include material processing, metal matrix composites, coatings/nanocoatings, mechanical behavior, and corrosion. He also has a good command over teaching subjects like Material Science, Engineering Materials, Measurement and Metrology, Advanced Welding Technology, and Composite Materials.

Dr. Gupta has over eight years of teaching and research experience. During this time, he has published over 90+ research papers in peer-reviewed international journals as well as in reputed international and national conferences in India as well as abroad. Apart from this, he has also published seven chapters in books published by Springer. Dr. Gupta has edited one book entitled *Advances in Engineering Materials* (Springer) and has also authored a textbook, *Manufacturing Processes* (IP Innovative Publication Pvt. Ltd.). He has also filed one Indian and one Australian patent as well. Dr. Gupta has completed two sponsored research projects as principal investigator. He also received international travel support from S.E.R.B., Department of Science and Technology, Government of India in the year 2016 for attending and presenting his research work at an International Conference held in Malaysia.

Dr. Gupta also holds memberships of several professional bodies like the Materials Research Society of India, Tribology Society of India, Electron Microscope Society of India, The Indian Society for Technical Education etc. He also has delivered a large number of invited and expert lectures as well as chaired sessions in conferences at various reputed universities and institutes in India and abroad. A large number of students have completed their summer internships, B.Tech. projects, and M.Tech. dissertations under his guidance. Two scholars have completed and six are presently registered for their Ph.D. research work under his supervision in the areas of coatings, metal matrix composites, and polymer matrix composites.

Contributors

Dr. Balkar Singh

IKG Punjab Technical University
Jalandhar, Punjab, India
ptubalkar@gmail.com

Mr. Daksh Shelly

Thapar Institute of Engineering and
Technology
Patiala, India
dakshshelly@gmail.com

Mr. Gaurav Arora

Chandigarh University
Gharuan, Mohali, Punjab, 140413, India
d16053@students.iitmandi.ac.in

Mr. Gaurav Luthra

Department of Clinical Research and
Development Auxein Medical
Private Limited
Sonipat, Haryana, India
gaurav@kaulmed.com

Dr. Gurdyal Singh

Chitkara University Institute of
Engineering and Technology
Chitkara University
Punjab, India
gurdyal.singh@chitkara.edu.in

Dr. Gurmail Singh Malhi

Chandigarh University
Gharuan, Mohali, Punjab
gurmail.malhi@gmail.com

Mr. Gurpreet Singh

Chitkara University Institute of
Engineering and Technology
Chitkara University
Punjab, India
gurpreet.singh@chitkara.edu.in

Dr. Gurpreet Singh Sokhal

Chandigarh University
Gharuan, Mohali, Punjab
singh.gurpreet@thapar.edu

Dr. Gurprinder Singh Dhindsa

Chandigarh University
Gharuan, Mohali, Punjab
guridhindsa@gmail.com

Dr. Himanshu Pathak

Composite Design and Manufacturing
Research Group, School of
Engineering
Indian Institute of Technology Mandi
VPO Kamand, Mandi, Himachal
Pradesh, India 175075
himanshu@iitmandi.ac.in

Dr. Jimmy Mehta

Manav Rachna International Institute
of Research and Studies
Faridabad
jimmy.fet@mriu.edu.in

Mr. Kamaljit Singh

Mechanical Engineering Department
CEC Landran, Mohali, Pb, India
kamaljit36@gmail.com

Dr. Kamaljit Singh Sokhal

University of Winnipeg
Manitoba, Canada
kamaljit.singh@thapar.edu

Mr. Mohit Kumar

Department of Clinical Research and
Development Auxein Medical
Private Limited
Sonipat, Haryana, India
m.kumar@auxein.com

Mr. Prateek Mittal

Manav Rachna International Institute
of Research and Studies
Faridabad
prateekmittal.fet@mriu.edu.in

Mr. Rahul Gupta

Thapar Institute of Engineering and
Technology
Patiala
rahulsliet2008@gmail.com

Dr. Rajbir Bhatti

Mount Royal University
Calgary, Alberta, Canada
rbhatti@mtroyal.ca

Mr. Rakesh Kumar

Department of Regulatory Affairs
(Risk Management)
Auxein Medical Private Limited
Sonipat, Haryana, India
rk05691@gmail.com

Mr. Sahil Mehta

Thapar Institute of Engineering and
Technology
Patiala
sahilmehtha.chd@gmail.com

Dr. Santosh Kumar

Department of Mechanical
Engineering
Chandigarh Group of Colleges
Landran, Mohali, Punjab (India)
santoshdgc@gmail.com

Mr. Satinder Singh

Mechanical Engineering Department
IIT Jammu
NH-44, Village Jagti, PO Nagrota,
J&K, 181221
satinder.singh@iitjammu.ac.in

Ms. Seema Mahto

Manav Rachna International Institute
of Research and Studies
Faridabad
seemamahto.fet@mriu.edu.in

Dr. Sekar Kannan

Department of Mechanical
Engineering
National Institute of Technology
Calicut, NIT Campus
Calicut-673601, Kerala, India
sekar@nitc.ac.in

Dr. Suneev Anil Bansal

Department of Mechanical
Engineering
MAIT, Maharaja Agrasen University
HP, 174103, India
and
Department of Mechanical
Engineering
Bharat Institute of Engineering and
Technology
Mangalpally, Ibrahimpatnam,
Hyderabad, Telangana, 501510,
India
suneev@gmail.com

Mr. Vasanthakumar Pandian

Department of Mechanical
Engineering
National Institute of Technology
Calicut, NIT Campus
Calicut - 673601, Kerala, India
vasanthakumarp76@gmail.com

Dr. Virat Khanna

Department of Mechanical
Engineering
MAIT, Maharaja Agrasen University
HP, 174103, India
khanna.virat@gmail.com

1 Micro and Nanocomposites Produced by Different Casting Routes and Improved Mechanical and Tribological Properties

Sekar Kannan

Department of Mechanical Engineering, National Institute of Technology Calicut, Calicut, India

CONTENTS

1.1	Introduction.....	2
1.2	Review of Different Casting Machine and Properties of A356 Alloy-Al ₂ O ₃ Metal Matrix Composites	2
1.2.1	Introduction.....	2
1.2.2	Different Casting Machine.....	2
1.2.3	Aluminum-Silicon Alloy (A356).....	3
1.2.4	Microstructure and Mechanical Properties of A356 Alloy Made by Different Casting Techniques: Gravity, Vacuum, and Squeeze Casting	5
1.2.5	A356 Alloy-Al ₂ O ₃ Metal Matrix Composites and Mechanical Properties	6
1.3	Review of Heat-Treatment Studies of A356 Alloy-Al ₂ O ₃ Metal Matrix Composites.....	7
1.3.1	T6 Heat-Treatment Studies of Aluminum Material.....	7
1.3.2	Effect of Solutionizing Temperature and Time.....	7
1.3.3	Effect of Quenching Rate	8
1.3.4	Time and Temperature Effect of Aging	8
1.3.5	The T6 Heat-Treated Alloy and Composite Material Properties	8

1.4	Review of Wear Studies of A356 Alloy-Al ₂ O ₃ Metal Matrix Composites.....	9
1.4.1	Wear Studies in Aluminum A356 Alloy	9
1.4.2	Wear in Aluminum and Metal Matrix Composites.....	10
1.4.3	Wear Studies on T6 Heat-Treated Aluminum and MMCs.....	11
1.5	Summary.....	11
	References.....	11

1.1 INTRODUCTION

Most aluminum-silicon (Al-Si) alloy cast parts are utilized in the automobile sector, replacing the use of steel parts and cast irons. Apart from the automobile sector, Al-Si alloys have applications in aerospace and other service industries. Al-Si alloys have good physical properties, high strength, high corrosion resistance, low specific gravity, good castability, and improved mechanical properties.

1.2 REVIEW OF DIFFERENT CASTING MACHINE AND PROPERTIES OF A356 ALLOY-AL₂O₃ METAL MATRIX COMPOSITES

1.2.1 INTRODUCTION

This chapter covers the literature related to the various casting machines, different casting methods, and the performance of casting without and with heat treatment. Existing reviews particularly focus on the mechanical and tribological properties of A356 alloy castings and nano Al₂O₃-particle-based composites. The glaring shortcomings in the literature formed the impetus for this investigation, along with the overall objectives pursued and the scope of the investigations. The survey of such a vast literature has generally been found to be tedious. Thus, the main goal here was to compile the literature in a structured manner.

1.2.2 DIFFERENT CASTING MACHINE

In view of the need for lightweight materials with good strength and stiffness for alloy and metal matrix composites (MMC), Gandhewar et al. (2011) reported that there is no holding time delay the molten metal, reducing the losses, improving the efficiency of a furnace. Ramazan and Bayindir (2007) reported that the design and construction of an electric furnace and efficiency of the furnace have been increased. Oyawale and Olawale (2007) claimed heating and melting rates well over 1000°C within 1 hour, melting the first charge within 95 minutes. Jawad (2010) reported electrical, thermal, and economic problems with the furnace. Xiaohong et al. (2010) claimed that the vacuum achieved during the process was within 1.5 milliseconds. The decreased porosity significantly compared with other conventional die casting methods.

Uchida (2009) reported that the vacuum casting process plays a major role in the die-casting industry for both product quality and mass production efficiency. It also decreases gas porosity and shrinkage porosity. CEng and CEng (2011)

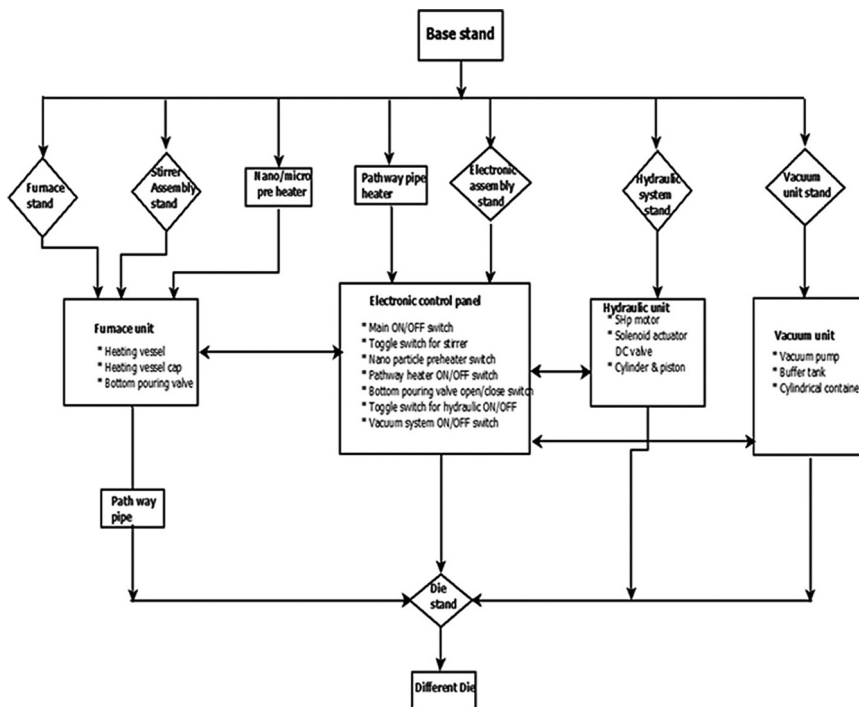


FIGURE 1.1 Flow chart of different units of multiple casting machine.

reported low capital costs, operating costs, and energy consumption, while Sharma and Shukla (2013) found that process and automation help in reducing the production cost and process lead time. This machine has only a gravity casting facility, although smaller machines have been described in the many literatures.

Sekar et al. (2013) developed a multiple casting machine with different casting techniques. This innovative machine could produce castings with minimal casting defects. The flow chart for this machine's workflow is shown in Figure 1.1, while the solid model machine assembly and the fabricated multiple casting machine are shown in Figure 1.2. This multiple casting machine is used to produce defect-free alloy casting and composite materials.

1.2.3 ALUMINUM-SILICON ALLOY (A356)

The wide popularity of cast Al-Si alloys stems from their good casting, better mechanical properties, and corrosion resistance. The following Table 1.1 shows the chemical composition of the A356 alloy.

Gruzleski and Closset (1990), in their book on *The Treatment of Liquid Aluminum-Silicon Alloys*, reported that the energy crisis in the 1970s led to the popularity of the A356 alloy castings in the automotive sector. The demand for the reduction of weight in automobiles stems from the need to improve fuel efficiency.

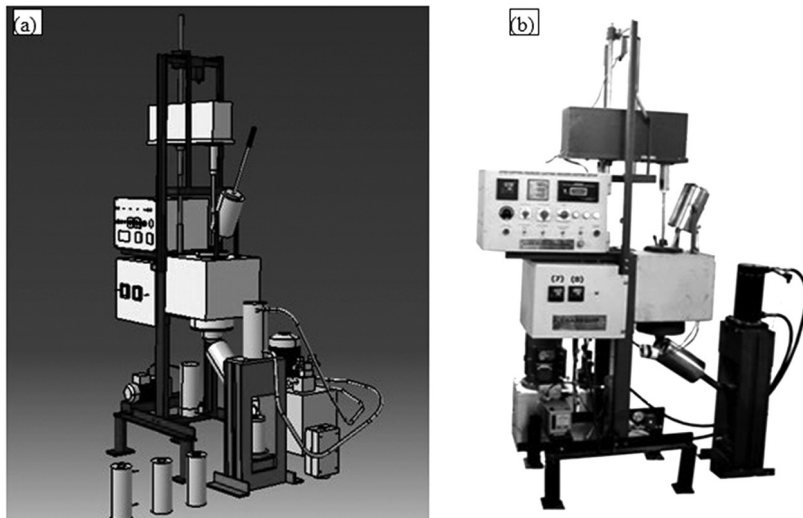


FIGURE 1.2 (a) Solid model machine assembly. (b) Fabricated multiple casting machine.

TABLE 1.1
Chemical Composition of A356 Alloy

Alloy	Composition (wt%)									
	Cu	Si	Mg	Mn	Fe	Ti	Ni	Zn	Tin	Al
A356	0.09	6.65	0.55	0.06	0.32	0.06	0.04	0.004	0.001	Remaining

The A356 alloys find wide applications in the marine, electrical, automobile, and aircraft industries (Gruzleski and Closset 1990).

Environmental concerns have put the onus on automotive manufacturers to develop even lighter and more fuel-efficient vehicles. In this regard, the development of new aluminum (Al) alloys and new techniques has been an ongoing process, where investigations carried out worldwide by Al suppliers, R&D organizations, and by the automotive industry have developed new materials in the production of automobile parts and other applications (Coalition 2002). The following are some of the techniques and treatment methods for further enhancement of the properties that achieve improved performance and reliability of this alloy:

- Grain boundary strengthening
- Chemical modification
- Solid solution strengthening
- Precipitation hardening
- Dispersion strengthening
- Metal matrix composite strengthening.

All the above methods attempt to achieve improved properties and microstructure either via the casting route or heat treatment process. The following sections highlight some of the techniques adopted for A356 alloy strengthening during the casting process.

1.2.4 MICROSTRUCTURE AND MECHANICAL PROPERTIES OF A356 ALLOY MADE BY DIFFERENT CASTING TECHNIQUES: GRAVITY, VACUUM, AND SQUEEZE CASTING

Jiang et al. (2013) reported that the gravity casting process results in a microstructure with defects of dendrites and porosity. Plate-like silicon particles are also observed. Dey et al. (2006) claimed that conventional cast samples were fully dendritic in their microstructure. Jiang et al. (2011) reported well-distributed morphology of dimple fracture when the A356 alloy was made by casting process with a vacuum. Deng-wei et al. (2012) reported that good mechanical properties and void content play a major role, as material yield stress increased with the decrease of void content.

Good mechanical properties can be achieved in the A356 alloy by a vacuum casting. Vacuum pressure casting involves the control of solidification and crystallization, dense microstructure, and excellent mechanical properties. Moreover, Niu et al. (2000) reported that the gas porosity is reduced by vacuum casting. Kim and Kang (2008) also claim that defects can be eliminated by a vacuum casting.

The advanced manufacturing process is the squeeze casting, the high pressure is applied to the molten metal Ghomashchi and Vikhrov (2000), Morton and Barlow (1994). The squeeze-casting components are zero gas porosity, good properties of mechanical. It is reported that, the squeeze cast components are good mechanical properties (Morton and Barlow 1994). The squeeze-casting process is better compared to gravity and vacuum casting routes (Clegg 1991):

- (i) Grain structure is refined
- (ii) Mechanical properties are improved
- (iii) Gas porosity and shrinkage porosity is eliminated
- (iv) Good dimensional accuracy

Sekar (2019a) reported that the squeeze-casting process improved all the mechanical properties. Bai and Zhao (2010) reported that the partial squeeze pressure also produced pore-free microstructure. Lee et al. (2008) claim that the squeeze-casting process to the A356 alloy is improved the material ductility by the squeeze pressure.

Abou El-khair (2005) identified that an increase in squeeze pressure decreased the porosity percentage and increased the metal density and material properties.

Gokhale and Patel (2005) claimed a significant fracture improvement in mechanical properties, while Dey et al. (2006) reported that rheocast alloy showed improved mechanical properties. Guo et al. (2009) claimed that the grain size decrees and the primary α -Al morphology of improved by the squeeze pressure.

Another method of composite making by the stir casting liquid state method involves the ceramic particles being mixed with a molten liquid matrix metal with help of mechanical stirring to achieve a uniform mixing and good wettability of the reinforcement particles with the matrix material.

Ezatpour et al. (2011) reported that the pre-heat-treated nano Al_2O_3 particles were introduced into the molten metal with a stirring system. This system is good for the wettability and distribution of the reinforcement of particles within the aluminum melt. In another study by Chu and Wu (1999), A356 alloy reinforced with alumina particles produced by the squeeze-casting method also showed improved bending strength.

Hajizamani and Baharvandi (2011) claimed that hardness has been found to grow with an increase in the reinforcement content, up to a maximum of 1wt% Al_2O_3 -10 vol. % ZrO_2 , after which it starts a decreasing trend.

Hashim et al. (1999) studied MMC fabricated by the stir casting method and reported good wettability and distribution of reinforcement in substance with less porosity. The results from Balasivanandhaprabu et al. (2006) revealed that more time and stirring speed achieved a good mixing of particles and increased hardness. Kori et al. (2009)'s findings indicate that less Cu (0.1–0.5%) and Mg (0.3–0.7%) improve the mechanical properties.

1.2.5 A356 ALLOY- Al_2O_3 METAL MATRIX COMPOSITES AND MECHANICAL PROPERTIES

A study of published squeeze cast works by Chu and Wu (1999) reported that the Al_2O_3 /A356 composites cleaved Al_2O_3 particles and brittle fracture in that composite.

Meanwhile, Sajjadi et al. (2012) reported that composite material hardness is increased by reinforcement particle weight fraction. Sekar and Vasanthakumar (2020) reported that the composite material mechanical properties increased compared with aluminum alloy. Meanwhile, Sajjadi et al. (2011) found that the hardness and compressive strength increased and decreased porosity. Sekar et al. (2015) identified a significant improvement in strength and hardness with 1 wt% nano Al_2O_3 for stir and squeeze casting.

Ansary Yar et al. (2009) revealed that the 1.5 vol % MgO particles composites improved mechanical properties, while El-Kady et al.'s (2011) results showed that the high content of reinforcement particles on aluminum alloy increased both tensile and yield strength of composite with finer size of nanoparticles. Sekar et al. (2019) reported improved mechanical properties for the microcomposite materials.

Sajjadi et al. (2012) identified improved hardness at 3 wt% nano Al_2O_3 for compo-casting and with 2 %wt nanoparticles in squeeze casting. Sekar and Vasanthakumar (2019) reported improved mechanical properties, and Sekar et al. (2019) showed that the mechanical properties improved in hybrid composite materials.

Mazahery et al. (2009) claimed that the Al_2O_3 reinforcement significantly improved hardness, yield strength, and hardness. Su et al. (2012) presented an

enhancement in yield and ultimate tensile strength; Chou et al. (2006) reported that the mechanical properties of bending strength are increased.

1.3 REVIEW OF HEAT-TREATMENT STUDIES OF A356 ALLOY- Al_2O_3 METAL MATRIX COMPOSITES

1.3.1 T6 HEAT-TREATMENT STUDIES OF ALUMINUM MATERIAL

Heat treatment is used to change the metallurgical structure, mechanical properties, and reduce the residual stress in the metal products. A common heat-treatable alloy group for Al is the A356 alloy. The A356 alloy castings are usually age-hardened to obtain the desired mechanical properties like hardness, bending strength, double shear strength, compressive and impact strength, and good wear resistance and surface roughness.

The heat treatment cycles consider three steps:

- i. Solutionizing
- ii. Quenching for supersaturation
- iii. Aging for precipitation of solute atoms

T6 heat treatment improves the material properties of fracture toughness and ductility by the eutectic Si particles spheroidization with the help of solutionizing treatment (Kumar et al. 2006; Kashyap et al. 1993; Shivkumar et al. 1990; Pedersen and Arnberg 2001). As per the Standard of ASTM B917-01 in the range of 6–12 h at 540°C in water quench, the sand cast A356 alloys are heated for 2–5 h at 155°C and also the permanent mold cast is given 4–12 h of solutionizing at 540°C and then aging at 155°C at 2–5 h. The effect of the A356 alloy T6 heat treatment on the mechanical properties was studied by many researchers (Taylor et al. n.d.; Shivkumar 1989; Emadi et al. 2003; Zhang et al. 2002).

1.3.2 EFFECT OF SOLUTIONIZING TEMPERATURE AND TIME

The solutionizing treatment of cast A356 alloy ranges 400–560°C, the hardening agents dissolve in the α -Al matrix, reducing the Mg, Cu, Mn of micro-segregation in the aluminum alloy and spheroidizing the Si particles in the aluminum alloy (Emadi et al. 2003). The increasing solution treatment temperature at the time rate of dissolution increases, depending on the casting methods of vacuum and gravity casting. The squeeze casting can alter the Si morphology in the matrix material and improve the mechanical properties of the alloy materials Sekar (2019b). The effects of Mg and Si concentration in cast A356 alloy solutionizing temperature were studied by Pedersen and Arnberg (2001). The maximum ultimate tensile strength was obtained in the materials. Emadi et al. (2003) found, in their study on A356 alloy castings, that water quenches at 6–12 h of aging, and at 6 h in the aging of 155°C. The small variation in the temperature can change the solutionizing time (Shivkumar 1989).

1.3.3 EFFECT OF QUENCHING RATE

Quenching is the precipitation and retaining of solute atoms (Zhang and Zheng 1996). Rapid quenching improves strength and ductility (Emadi et al. 2003).

Pedersen and Arnberg (2001). They said that Mg and Si are related to mechanical properties. The quenching rates are reduced after solution heat treatment, leading to a lesser strength due to Mg_2Si precipitates (Zhang and Zheng 1996; Rometsch et al. 2003).

1.3.4 TIME AND TEMPERATURE EFFECT OF AGING

At this stage, the coherent precipitates are formed, increasing with dislocations, strengthening the alloys [64]. Age hardening is possible at natural aging or artificial aging. Generally, for A356 alloys, aging is conducted between 150°C to 200°C ranging from 4 h to 8 h. Like solutionizing, aging is both time and temperature dependent. Aging temperature increases, and the aging time decreases – roughly a 10°C aging temperature increases and decreases by a factor of two while maintaining the tensile properties (ASM Handbook 1995).

Age-hardening behavior of cast A356 alloy was studied by Li (2004), who reported that increased hardness was obtained at a higher aging temperature. The T6 heat-treatment temperature makes morphological changes in the materials (Cavaliere et al. 2004; Murayama et al. 1998; Chaudhury et al. 2003). The heat treatment cycle is preferred, while productivity increases and manufacturing costs are reduced. Most researchers followed the three steps of (1) solutionizing, (2) quenching, and (3) aging, as shown in Figure 1.3.

1.3.5 THE T6 HEAT-TREATED ALLOY AND COMPOSITE MATERIAL PROPERTIES

Merlin et al. (2009) reported that the cast wheel impact energy is less than T6 heat-treated wheels. Jiang et al. (2012) reported that the Si particles are distributed homogeneously at the grain boundary after T6 heat treatment.

Niu et al. (2000) reported that the mechanical properties are improved in the vacuum die-casting process by the T6 heat treatment. Jiang et al. (2012)



FIGURE 1.3 T6 heat-treatment processes of A356 alloy and composites: (a) solutionizing; (b) quenching; (c) aging.

reported that the silicon particles' length, width, and aspect ratio decrease after T6 conditioning.

Chen and Thrope (1996) claimed that the Si particles' size and shape are very small after the T6 conditioning. Bai and Zhao (2010) reported that the tensile properties are improved after T6 heat treatment due to the spheroidization of silicon particles in the alloy and composites. do Lee (2013) claimed it improved the stress amplitudes of A356 alloy.

Sjolander and Seifeddine (2010) reported an increase in the yield strength of materials after aging. Emadi et al. (2003) noted that a 155°C aging treatment when coupled with solutionizing for 4 h at 540°C, followed by cold/warm water quench and 6–12 h preaging offered optimal properties and reproducibility. Penga et al. (2011) reported that the Si and Mg were oversaturated in α -Al. A study by Man et al. (2011) reported a decrease in the mean diameter and roundness of silicon particles in the form of grain refined samples.

Zhu et al. (2012) claimed that the diameter of Si is reduced due to T6 heat treatment. Moller et al. (2008a, 2008b) found that the hardness increased after T6 heat treatment of A356 alloy.

Moller et al. (2008a, 2008b) claimed that the impact properties are improved by T6 heat treatment. Lashgari et al. (2010) showed that the B_4C reinforcement particles strong bonding with aluminum alloy after the T6 treatment conditions and also improve the material properties due to change of eutectic silicon morphology spherical shape. Sekar et al. (2015) reported that the Si particles are homogeneously spread in grain and grain boundary after T6 heat treatment.

Hossein-Zadeth et al. (2014) reported that the compression and hardness strength of the composites is increased by the heat treatment. Mechanical evaluation, such as the hardness test, showed enhancement in the properties. The purpose of this chapter is to investigate changes in the mechanical properties, such as hardness, bending, shear strength, and change of microstructure of gravity, vacuum casting, and squeeze casting, of an A356 alloy, an A356 alloy with the addition of Al_2O_3 nano reinforcement particles by the combined effect of stir and squeeze and heat treatment, and also to discuss the mechanism of improvement.

1.4 REVIEW OF WEAR STUDIES OF A356 ALLOY- Al_2O_3 METAL MATRIX COMPOSITES

1.4.1 WEAR STUDIES IN ALUMINUM A356 ALLOY

The development of A356 alloy casting have created a material with good wear and corrosion resistance, and better castability for automobile and tribological applications and other engineering fields (Lasa and Ibabe 2002; Mabuchi et al. 1997; Apps et al. 2003). Study of wear is an important aspect in tribology, which helps engineers and metallurgists assess the behavior and mechanical properties of materials. Wear is a phenomenon present in any mechanical component, and whenever there is relative motion between the components. Wear is defined as the continued wear loss of material caused by the interaction of two metal surfaces.

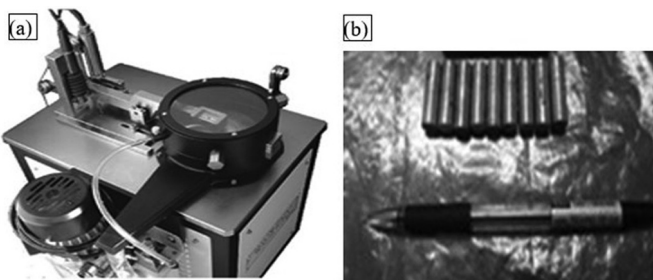


FIGURE 1.4 (a) Pin-on-disk machine. (b) A set of wear specimens.

It is measured as wear rate in the volume loss due to material load (Hutchings and Arnold n.d.). Most researchers study the wear behavior of the cast alloy in different processing conditions of the wear tests. The dry and wet sliding wear tests were carried out in accordance with the ASTM G-99 standard using a pin-on-disk tribometer. The pin-on-disk machine and the wear specimens are shown in Figure 1.4.

1.4.2 WEAR IN ALUMINUM AND METAL MATRIX COMPOSITES

Vencl and Bobic (2010) found that the reinforcement particles were formed as an agglomeration in the composite materials. Sekar (2019) showed the composite material's better wear properties. Vencl et al. (2008) reported that the wear resistance improved at 3 wt% Al_2O_3 reinforcement particles of the composites. Vencl et al. (2008) reported that the better tribological properties of A356 aluminum alloy can be obtained by compo casting process Dearnleya et al. (1999). They reported that all the surface plastic deformation was decreased due to oxidation Al_2O_3 -layer in the composites. Wang and Song (2011) reported that the addition of SiCp particles decreases the tribological properties. Sekar and Singh (2019) reported that the tribological properties are increased in composites compared with aluminum alloy Daoud et al. (2004). They reported that the increase in the content of Al_2O_3 nanoparticles and squeeze pressure on A356 alloy increased hardness, finer structure, decreased porosity and improved wear resistance Sekar et al. (2016). The results showed increased hardness, finer structure, decreased porosity and better tribological properties.

Suresh et al.'s (2003) results revealed significant improvement in wear resistance.

Sekar and Ananda Rao (2020) showed that the mechanical properties and tribological properties of composites were improved compared with aluminum alloy. Vencl et al. (2008) reported that the friction and wear resistance coefficient improved in the composites.

Vencl and Bobic (2010) reported improvement in the wear resistance of the composites. Baradeswaran and ElayaPerumal (2014) showed that with the addition of 5 wt% graphite in the composites, the wear loss and coefficient of friction

decrease due to graphite addition. Sahin et al. (2002) reported that surface roughness values are increased with increasing reinforcement particles. Vinoth et al. (2012) reported that a lubricant film on the wear surface decreases wear rate. This is evident in the SEM micrographs of composites, where the lubricant forms a film in certain regions, partially reducing plowing and delamination.

1.4.3 WEAR STUDIES ON T6 HEAT-TREATED ALUMINUM AND MMCs

The heat treatment processes are carried out to further enhance and refine the wear properties. Investigations on wear behavior of A356 alloy and MMCs Mandal et al. (2009). They reported that the Si and TiB₂ reinforcement-related composites are improved mechanical and tribological properties Gangadhar et al. (2013). They found that the reinforced composites are improved wear resistance, the microstructures are showed the distribution of ceramics particles uniform in the composites. Chen et al. (2000) reported that the T6 heat-treated composites are more wear-resistant and coefficient with friction compared with those without heat-treatment composites. Avinash et al. (2013) reported that the reinforced composites had improved mechanical and wear properties due to the good distribution and bonding of reinforcement particles in the matrix.

1.5 SUMMARY

A comprehensive survey of the literature reveals the importance of die-casting techniques such as gravity casting (GC), vacuum casting (VC), squeeze casting (SqC), and stir casting (SC). These techniques are also needed for the development of good-quality castings. The effect of nanoparticles on the A356 alloy to improve the properties of the castings materials is also reported. Another important aspect of heat treatment (T6) is its ability to enhance the material properties of aluminum alloys. Composites may also replace alloys in achieving improved morphologies with micro and nanoparticle reinforcement additions. The expected improvements in the wear behavior of nanocomposites have a wide scope of usage in diversified industrial areas. Heat treatment is one method of improving material properties. Finally, present and potential engineering applications of various automobile components are additionally presented and reviewed in the present chapter on the basis of various theoretical and practical studies.

REFERENCES

- Abou El-Khair, M.T. (2005). Microstructure characterisation and tensile properties of squeeze-cast Al-Si-Mg alloys, *Material Letters*, vol. 59, pp. 894–900.
- Ansary Yar, A., Montazerian, M., Abdizadeh, H. & Baharvandi, H.R. (2009). Microstructure and mechanical properties of aluminum alloy matrix composite reinforced with nano-particle MgO, *Journal of Alloys and Compounds*, vol. 484(2), pp. 400–404.
- Apps, P.J., Bowen, J.R. & Prangnell, P.B. (2003). The effect of coarse second-phase particles on the rate of grain refinement during severe deformation processing, *Acta Mater.*, vol. 51(10), pp. 2811–2822.

- ASM Handbook, Materials Park, OH, 1995, pp. 785–791 and pp. 823–873.
- Avinash, M.H. Annaiah, Harendra Kumar, H.V., Linge Gowda, S. & Narasimha Murthy, G.S. (2013). The effect of heat treatment on the microstructure, mechanical properties and dry sliding wear behaviour of A356.O reinforced with aluminium, *International Journal of Innovative Research in Science, Engineering and Technology*, vol. 2, pp. 1054–1059.
- Bai, Y. & Zhao, H. (2010). On tensile properties and fracture behaviour of partial squeeze added slow shot die-cast A356 aluminum alloy, *Materials and Design*, vol. 31(9), pp. 4237–4243.
- Balasivanandhaprabu, S., Karunamoorthy, L., Kathiresan, S. & Mohan, B. (2006). Influence of Stirring speed and stirring time on distribution of particles in cast metal matrix composite, *Journal of Material Processing Technology*, vol. 171(2), pp. 268–273.
- Baradeswaran, A. & ElayaPerumal, A. (2014). Study on mechanical and wear properties of Al 7075/Al₂O₃/graphitehybrid composites, *Composites: Part B: Engineering*, vol. 56, pp. 464–471.
- Cavaliere, P., Cerri, E. & Leo, P. (2004). Effect of heat treatments on mechanical properties and fracture behaviour of a thixocast A356 Aluminium alloy, *Journal of Material Science*, vol. 39, pp. 1653–1658.
- CEng, A.P. & CEng, J.H. (2011). Technology for electromagnetic stirring of aluminum reverberatory furnaces. In Lindsay, S.J. (ed) *Light Metals 2011. The Minerals, Metals and Materials Society*, Springer, Cham, pp. 1193–1198.
- Chaudhury, S.K., Shankar, S., Apelian, D. & Van Wert, J. (2003). *Proceedings of the AFS, aluminium structural casting conference*, Orlando, FL, published by AFS, November, pp. 2–4.
- Chen, R., Iwabuchi, A. & Shimizu, T. (2000). The effect of T6 heat treatment on the fretting wear of a SiC particle-reinforced A356 aluminium alloy matrix composite, *International Journal of Wear*, vol. 238(2), pp. 110–119.
- Chen, Z.W. & Thrope, W.R. (1996). The effect of squeeze casting pressure and iron content on the impact energy of Al-7Si-0.7Mg alloy, *Materials Science and Engineering A*, vol. 221(2), pp. 143–153.
- Chou, S.-N., Huang, J.-L., Lii, D.-F. & Lu, H.-H. (2006). The mechanical properties of Al₂O₃/aluminum alloy A356 composite manufactured by squeeze casting, *Journal of Alloys and Compounds*, vol. 419(2), pp. 98–102.
- Chu, S. & Wu, R. (1999). The structure and bending properties of squeeze cast A356 aluminium alloy reinforced with alumina particles, *Composites Science and Technology*, vol. 59(1), pp. 157–162.
- Clegg, A.J. (1991). *Precision casting processes*, Pergamon Press, Oxford.
- Coalition, Cast Metals (2002). *Metal casting industry technology roadmap: Pathway for 2002 and beyond 2003*. Available at: <https://www.yumpu.com/en/document/view/24670819/itp-metal-casting-2002-metal-casting-industry-of-the-future>
- Daoud, A., Abou, M.T., El-Khair, A. & Abdel-Azim, A.N. (2004). Effect of Al₂O₃ particles on the microstructure and sliding wear of 7075 Al alloy manufactured by squeeze casting method, *JMEPEG*, vol. 13(2), pp. 135–143.
- Dearnley, P.A., Gummersbach, J., Weissb, H., Ogwuc, A.A. & Daviesc, T.J. (1999). The sliding wear resistance and frictional characteristics of surface modified aluminum alloys under extreme pressure, *Wear*, vol. 225–229, pp. 127–134.
- Deng-Wei, H., Juan, Y. & Xiang-Yang, Z. (2012). Preparation of open-celled aluminum foams by counter gravity infiltration casting, *Transactions of Nonferrous Metals Society of China*, vol. 22, pp. 85–89.

- Dey, A.K., Poddar, P., Singh, K.K. & Sahoo, K.L. (2006). Mechanical and wear properties of rheocast and conventional die cast A356 alloy, *Materials Science and Engineering A*, vol. 435–436, pp. 521–529.
- do Lee, Choong. (2013). Effect of T6 heat treatment on the defect susceptibility of fatigue properties to micro porosity variations in low-pressure die-cast A356 alloy, *Material Science & Engineering A*, vol. 559, pp. 496–505.
- El-Kady, El-Sayed Y., Mahmoud, T.S. & Sayed, M.A.-A. (2011). Elevated temperatures tensile characteristics of cast A356/Al₂O₃ nano composites fabricated using a combination of rheo-casting and squeeze casting techniques, *Journal of Material Science and Applications*, vol. 2, pp. 390–398.
- Emadi, D. Whiting, L.V. & Sahoo, M. (2003). Optimal heat treatment of A356.2 alloy, *Light Metals*, TMS, pp. 983–989.
- Ezatpour, H.R., Beygi, S.H., Sajjadi, A. & Torabi Parizi, M. (16–17 May 2011). Microstructure and mechanical properties of Al-Al₂O₃ micro and nano composites fabricated by a novel stir casting route, *2nd Conference on Application of Nanotechnology in Science, Engineering and Medicine*, Mashhad-Iran.
- Gandhewar, Vivek R., Bansod, Satish V. & Borade, Atul B. (2011). Induction furnace – a review, *International Journal of Engineering and Technology*, vol. 3(4), pp. 277–284.
- Gangadhar, Amith. D., Annaiah, M.H., Lingegowda, S., Rajiv, T.G. & Harendra Kumar H.V. (2013). The effect of heat treatment on the microstructure, mechanical properties and dry sliding wear behaviour of A356.O reinforced with graphite, *International Journal of Innovative Research in Science, Engineering and Technology*, vol. 2, pp. 1038–1042.
- Ghomashchi, M.R. & Vikhrov A. (2000). Squeeze casting: An overview, *Journal of Material Processing Technology*, vol. 101, pp. 1–9.
- Gokhale, A.M. & Patel, G.R. (2005). Quantitative fractographic analysis of variability in tensile ductility of a squeeze cast Al-Si-Mg base alloy, *Materials Characterization*, vol. 54(1), pp. 13–20.
- Gruzleski, J.E. & Closset, B.M. (1990). *The treatment of liquid aluminium-silicon alloys*, AFS, Illinois, pp. 127–143.
- Guo, H.-M., Yang, X.-J. & Wang, J.-X. (2009). Pressurised solidification of semi-solid aluminium die casting alloy A356, *J. Alloys and Compounds*, vol. 485(2), pp. 812–816.
- Hajizamani, M. & Baharvandi, H. (2011). Fabrication and studying the mechanical properties of A356 alloy reinforced with Al₂O₃-10% vol. ZrO₂ nano particles through stir casting, *Advance in Materials Physics and Chemistry*, vol. 1, pp. 26–30.
- Hashim, J., Looney, J. & Hashmi, M.S.J. (1999). Metal matrix composites production by the stir casting method, *Journal of Material Processing Technology*, vol. 93, pp. 1–7.
- Hossein-Zadeth, M., Mirzaee, O. & Saidi, P. (2014). Structural and mechanical characterization of Al based composite reinforced with heat treated Al₂O₃ particles, *Journal of Materials and Design*, vol. 54, pp. 245–250.
- Hutchings, I.M. & Arnold, Edward (n.d.). *Friction and wear of engineering materials*, 3rd Edition. Edward Arnold, London.
- Jawad, S.K. (2010). Investigation of the dimensions design components for the rectangular indirect resistance electrical furnaces, *American Journal of Engineering and Applied Sciences*, vol. 3(2), pp. 350–354.
- Jiang, W., Fan, Z., Liao, D., Liu, D., Zhao, Z. & Dong, X. (2011). Investigation of microstructures and mechanical properties of A356 aluminum alloy produced by expendable pattern shell casting process with vacuum and low pressure, *Materials and Design*, vol. 32, pp. 926–934.

- Jiang, W., Fan, Z. & Liu, D. (2013). Correlation of microstructure with mechanical properties and fracture behaviour of A356-T6 aluminium alloy fabricated by expendable pattern shell casting with vacuum and low pressure, gravity casting and lost foam casting, *Materials Science and Engineering A*, vol. 560, pp. 396–403.
- Jiang, W., Fan, Z. & Liu, D. (2012). Microstructure, tensile properties and fractography of A356 alloy under as-cast and T6 obtained with expendable pattern shell casting process, *Transactions of Metals Society of China*, vol. 22, pp. 7–13.
- Kashyap, K.T., Murali, S., Raman, K.S. & Murthy, K.S.S. (1993). Casting and heat treatment variables of Al-7Si-Mg Alloy, *Materials Science and Technology*, vol. 9, pp. 189–203.
- Kim, H.H. & Kang, C.G. (2008). Vacuum assisted rheo-forging process of A356 aluminum alloys, *International Journal of Machine Tools and Manufacture*, vol. 48(15), pp. 1626–1636.
- Kori, S.A., Prabhudev, M.S. & Chandrashekharaiyah, T.M. (2009). Studies on the microstructure and mechanical properties of A356 alloy with minor additions of copper and magnesium, *Transactions of The Indian Institute of Metals*, vol. 62(5), pp. 353–356.
- Kumar, N., Hegde, S., Kumar, G. & Prabhu, K.N. (2006). Effect of modification melt treatment and cooling rate on NDT parameters of Al-13wt% Si alloy, *Indian Foundry Journal*, vol. 52(1), pp. 25–32.
- Lasa, L. & Ibabe, J.M.R. (2002). Effect of composition and processing route on the wear behaviour of Al-Si alloys, *Scripta Mater*, vol. 46, pp. 477.
- Lashgari, H.R., Zangeneh, Sh., Shahmir, H., Saghafi, M. & Emamy, M. (2010). Heat treatment effect on the microstructure, tensile properties and dry sliding wear behaviour of A356-10% B4C cast composites, *Journal of Materials and Design*, vol. 31(9), pp. 4414–4422.
- Lee, K., Kwon, Y.N. & Lee, S. (2008). Effect of eutectic silicon particles on the tensile properties and fracture toughness of A356 aluminum alloys fabricated by low-pressure-casting, casting-forging, and squeeze-casting processes, *Journal of Alloys and Compounds*, vol. 461(2), pp. 532–541.
- Li, R.X. (2004). Age-hardening behaviour of cast Al-Si base alloy, *Materials Letters*, vol. 58, pp. 2096–2101.
- Mabuchi, M., Iwasaki, H., Yanase, K. & Higashi, K. (1997). Low temperature super plasticity in an AZ91 magnesium alloy processed by ECAE, *Scripta Materialia*, vol. 36(6), pp. 681–686.
- Man, Z., Gencang, Y., Lijuan, Y. & Yaohe, Z. (2011). Effect of T6 heat treatment on the microstructures and the aging behavior of the grain-refined A356 alloys, *Advanced Materials Research*, vol. 143–144, pp. 1410–1414.
- Mandal, A., Murty, B.S. & Chakraborty, M. (2009). Sliding wear behaviour of T6 treated A356-TiB₂ in-situ composites, *Journal of Wear*, vol. 266(8), pp. 865–872.
- Mazahery, A., Abdizadeh, H. & Baharvandi, H.R. (2009). Development of high performance A356/nano Al₂O₃ composites, *Journal of Materials Science and Engineering A*, vol. 518(2), pp. 61–64.
- Merlin, M., Timelli, G., Bonollo, F. & Garagnani, G.L. (2009). Impact behaviour of A356 alloy fabricated by low- pressure die casting, *Journal of Materials Processing Technology*, vol. 209, pp. 1060–1073.
- Moller, H., Govender, G. & Stumpf, W.E. (2008a). T6 heat treatment of semi-solid metal processed alloy A356. *Open Materials Science Journal*, vol. 2, pp. 6–10.
- Moller, H., Govender, G. & Stumpf, W.E. (2008b). Investigation of the T4 and T6 heat treatment cycles of semi-solid processed aluminium alloy A356. *Open Materials Science Journal*, vol. 2, pp. 11–18.

- Morton, J.R. & Barlow, J. (1994). Squeeze casting from a theory to properties and fracture, *J. Inst. Brit. Foundry Man., Part-1*, vol. 87, pp. 23–28.
- Murayama, M., Hono, K., Saga, M. & Kikuchi, M. (1998). *Material Science and Engineering A*, vol. 250(15), p. 127.
- Niu, A.X.P., Hu, B.H., Pinwill I. & Li, H. (2000). Vacuum assisted high pressure die casting of aluminum alloys, *Journal of Materials Processing Technology*, vol. 105, pp. 119–127.
- Oyawale, F.A. & Olawale, D.O. (2007). Design and prototype development of mini-electric arc furnace, *The Pacific Journal of Science and Technology*, vol. 8(2), pp. 224–230.
- Pedersen, L. & Arnberg, L. (2001). The effect of solution heat treatment and quenchinates on mechanical properties and microstructures in Al-Si-Mg foundry alloys, *Materials Transactions A*, vol. 32A, pp. 525–532.
- Penga, J., Tanga, X., Hea, J. & Xub, D. (2011). Effect of heat treatment on microstructure and tensile properties of A356 alloys, *Trans. Nonferrous Met. Soc. China*, vol. 21(9), pp. 1950–1956.
- Ramazan & Bayindir (2007). Design and construction of an electrical furnace to fire ceramic product, *Journal of Scientific and Industrial Research*, vol. 66, pp. 135–140.
- Rometsch, P.A., Starink, M.J. & Gregson, P.J. (2003). Improvements in quench factor modelling, *Materials Science and Engineering A*, vol. 339, pp. 255–264.
- Sahin, Y., Kok, M. & Celik, B. (2002). Tool wear and surface roughness of Al_2O_3 particle-reinforced aluminium alloy composites, *Journal of Materials Processing Technology*, vol. 128(3), pp. 280–289.
- Sajjadi, S.A., Ezatpour, H.R. & Beygi, H. (2011). Microstructure and mechanical properties of Al– Al_2O_3 micro and nano composites fabricated by stir casting, *Journal of Materials Science and Engineering A*, vol. 528(30), pp. 8765–8771.
- Sajjadi, S.A., Ezatpour, H.R. & Torabi Parizib, M. (2012). Comparison of microstructure and mechanical properties of A356 aluminum alloy/ Al_2O_3 composites fabricated by stir and compo-casting processes, *Journal of Materials and Design*, vol. 34, pp. 106–111.
- Sajjadi, S.A., Torabi Parizi, M., Ezatpour, H.R. & Sedghi, A. (2012). Fabrication of A356 composite reinforced with micro and nano Al_2O_3 particles by a developed compo-casting method and study of its properties, *Journal of Alloys and Compounds*, vol. 511(1), pp. 226–231.
- Sekar, K. (2019a). Fabrication of AA2014 with B4C and graphite hybrid composite by stir-casting method: Study of mechanical and welding properties, *Journal of Physics*, vol. 1240(1), pp. 12–142.
- Sekar, K. (2019b). Mechanical and tribological properties of Al7475-SiCp composites by stir casting method and wear rate modeling using RSM, *Sādhanā*, vol. 44(5), p. 129.
- Sekar, K., Allesu, K., Joseph, M.A. (2013). Design, construction and performance evaluation of multiple casting machine, *Nigerian Journal of Technology*, vol. 32(3), pp. 498–506.
- Sekar, K., Allesu, K. & Joseph, M.A. (2015). Mechanical and wear properties of Al– Al_2O_3 metal matrix composites fabricated by the combined effect of stir and squeeze casting method, *Transactions of the Indian Institute of Metals*, vol. 68(2), pp. 115–121.
- Sekar, K. & Ananda Rao, D.V. (2020). Investigation of hybrid composite A7075/SiC/B4C by stir and squeeze casting method, *Materials Today: Proceedings*, vol. 22, pp. 1398–1408.
- Sekar, K., Manohar, M. & Jayakumar, K. (2016). Investigation of mechanical and tribological properties of A356 alloy Al_2O_3 -SiCp hybrid composites through stir and squeeze casting, *Journal of Advanced Engineering Research*, vol. 3(2), pp. 89–92.

- Sekar, K., Manohar, M. & Jayakumar, K. (2019). Mechanical and tribological properties of A356/Al₂O₃/MoS₂ hybrid composites synthesized through combined stir and squeeze casting, *Advances in Materials and Metallurgy*, pp. 115–125.
- Sekar, K. & Singh, R. (2019). Mechanical and tribological properties of A7050 hybrid composite reinforced with nano Al₂O₃/micro ZrO₂ particles by stir casting method, *Materials Science Forum*, vol. 969, pp. 576–581.
- Sekar, K. & Vasanthakumar, P. (2019). Mechanical properties of Al-Cu alloy metal matrix composite reinforced with B4C, Graphite and Wear Rate Modeling by Taguchi Method, *Materials Today: Proceedings*, vol. 18, pp. 3150–3159.
- Sekar, K. & Vasanthakumar, P. (2020). Mechanical and tribological properties of Al6063 hybrid composites reinforced with SiC/ZrO₂ by stir casting and thixoforming process, *Materials Science Forum*, vol. 979, pp. 47–51.
- Sharma, V. & Shukla, O.P. (2013). Design and development of clamping and ejection system for mould used for gravity die casting machine, *Journal of Engineering Research and Technology*, vol. 2, pp. 890–897.
- Shivkumar, S. (1989). An experimental study to optimize the heat treatment of A356 alloy, *AFS Transactions*, vol. 97, pp. 791–810.
- Shivkumar, S., Ricci, S., Keller, J.C. & Apelian, D. (1990). Effect of solution treatment parameters on tensile properties of cast aluminium alloys, *Journal of Heat Treating*, vol. 8, pp. 63–70.
- Sjolander, E. & Seifeddine, S. (2010). The heat treatment of Al-Si-Cu-Mg casting alloys, *Journal of Materials Processing Technology*, vol. 210(10), pp. 1249–1259.
- Su, H., Gao, W., Feng, Z. & Lu, Z. (2012). Processing, microstructure and tensile properties of nano-sized Al₂O₃ particle reinforced aluminium matrix composites, *Mater Des*, vol. 36, pp. 590–596.
- Suresh, K.R., Nirajan, H.B., MartinJebaraj, P. & Chowdiah, M.P. (2003). Tensile and wear properties of aluminium composites, *Wear*, vol. 255(6), pp. 638–642.
- Taylor, J.A., Zheng, L. & St John, D.J. (n.d.). *Cooperative research centre for cast metals manufacturing*, The University of Queensland.
- Uchida, M. (2009). Development of vacuum die-casting process, *Overseas Foundry*, vol. 6(2), pp. 137–144.
- Vencl, A. & Bobic, I. (2010). Structural, mechanical and tribological properties of A356 aluminum alloy reinforced with Al₂O₃, SiC and SiC⁺ graphite particles, *Journal of Alloys and Compounds*, vol. 506, pp. 631–639.
- Vencl, A., Bobic, I., Jovanovic, M.T., Babic, M. & Mitrovic, S. (2008). Microstructural and tribological properties of A356 Al-Si alloy reinforced with Al₂O₃ particles, *Tribol Lett*, vol. 32, pp. 159–170.
- Vinoth, K.S., Subramanian, R., Dharmalingam, S. & Anandavel, B. (2012). Mechanical and tribological characteristics of stir-cast Al-Si-10Mg and self-lubricating Al-Si-10Mg/MoS₂ composites, *MTAEC*, vol. 46(5), pp. 497–501.
- Wang, Yi qi & Song, Jung-il. (2011). Dry sliding behaviour of Al₂O₃ fiber and SiC particle reinforced aluminium based MMCs fabricated by squeeze casting method, *Trans. Nonferrous Met. Soc. China*, vol. 21(7), pp. 1441–1448.
- Xiaohong, G.E., Hongwu, Huang, Hui, LI & Yadan, L. (2010). Design and verification of an auxiliary system for high vacuum die casting, *Chinese Journal of Mechanical Engineering*, vol. 23, pp. 1–7.
- Zhang, D.L. & Zheng, L. (1996). The quench sensitivity of cast Al-7Si-0.4Mg alloy, *Metallurgical and Materials Transactions A*, vol. 27(12), pp. 3983–3991.
- Zhu, M., Jian, Z., Yang, G. & Zhou, Y. (2012). Effects of T6 heat treatment on the microstructure, tensile properties and fracture behaviour of the modified A356 alloys, *Materials and Design*, vol. 36, pp. 243–249.

2 Processing of Metal Matrix Composites (MMCs)

Rahul Gupta and Daksh Shelly

Thapar Institute of Engineering & Technology,
Patiala, India

CONTENTS

2.1	Introduction.....	17
2.2	Liquid State Processing Techniques	19
2.2.1	Stir Casting Route.....	19
2.2.2	Infiltration Route.....	20
2.2.3	Spontaneous Infiltration Route	21
2.2.4	Forced Infiltration Route.....	22
2.2.4.1	Centrifugal Infiltration Route.....	22
2.2.4.2	Squeeze Infiltration Route.....	24
2.2.4.3	Ultrasonic Infiltration Route	26
2.3	Solid State Processing Techniques	27
2.3.1	Powder Metallurgy Route.....	28
2.3.1.1	High Energy Ball Milling	29
2.3.1.2	Consolidation Techniques	30
2.3.2	Diffusion Bonding Route.....	32
2.4	Phase Deposition Processing Techniques	34
2.4.1	Physical Vapor Deposition Route	34
2.4.1.1	Electron Beam Physical Vapor Deposition (EB-PVD) Process	35
2.4.1.2	Sputtering Deposition Process	36
2.4.2	Spray Deposition Route	37
2.5	Conclusion	40
	References.....	40

2.1 INTRODUCTION

Nowadays, metal matrix composites (MMCs) with good ductility, low density, high modulus and strength, high thermal conductivity and wear resistance, and lower coefficient of thermal expansion have attracted much attention from researchers and industries. The properties offered by MMCs are superior to the

properties offered by conventional materials, i.e., metal and its alloys (Bakshi, Lahiri, & Agarwal, 2010; Shirvanimoghaddam et al., 2017; Gupta, Sharma, Nanda, & Pandey, 2019). The addition of different types of reinforcing material viz. (i) ceramic, (ii) polymer, and (iii) metal were responsible for significant improvement in mechanical, thermal, physical, and electrical properties of metal alloys (Manu, Raag, Rajan, Gupta, & Pai, 2016; Imran & Khan, 2019; Bhoi, Singh, & Pratap, 2020). In addition to this, MMCs have the ability to tailor the properties required for a specific application. The properties of MMCs had varied by changing the weight percentage, particle size, reinforcement material, coating material on reinforcement, etc. Due to their superior and tailorable characteristics, MMCs are used in various applications to make different components of electronic substrates, golf clubs, commercial airliners, and space shuttles, automobile, military, etc. (Shirvanimoghaddam et al., 2017; Gupta et al., 2019; Gupta, Sharma, Nanda, & Pandey, 2020). Various researchers have used Al_2O_3 , TiO_2 , SiC , TiC , Al_2SiO_5 , garnet, zircon, B_4C , TiB_2 , graphite, graphene etc. as a reinforcement material to increase the applicability of metal alloys. These reinforcing materials are available in different forms viz. particles, platelets, whiskers, chopped fibers or continuous fibers (Alaneme & Odoni, 2016; Manu et al., 2016; Akinwamide, Abe, Akinribide, Obadele, & Olubambi, 2020).

There are a number of different methods reported in the literature for the processing of MMCs, such as stir casting, squeeze casting, powder metallurgy, liquid metal infiltration, diffusion bonding, spray deposition, etc. These fabrication methods are classified into three categories, i.e., liquid state processing techniques, solid-state processing techniques and phase deposition processing techniques. This characterization of the fabrication process is done on the basis of the state of a matrix (Torralba, Costa, & Velasco, 2003; Shirvanimoghaddam et al., 2017; Garg et al., 2019). The choice of processing method is the most critical step to getting the desired properties of the final material at the lowest possible cost. The properties of MMCs have been mainly influenced by the dispersion of reinforcement, porosity, chemical reaction, and interfacial bonding between the matrix and reinforcement. The uniform dispersion of reinforcement, minimum porosity, no chemical reaction and good interfacial bonding between reinforcement and matrix is essential to obtain the superior properties for MMCs (Ghomashchi & Vikhrov, 2000; Hewitt & Kibble, 2009; Munir, Kingshott, & Wen, 2015; Zhang, Li, Li, & Zhang, 2018; Arunachalam, Kumar, & Muraliraja, 2019). Out of the above-mentioned processes, powder metallurgy and stir casting are the most commonly used processes. For B_4C and aluminum alloys, the powder metallurgy process is recommended because molten aluminum alloys tend to undergo a chemical reaction with reinforced particles. However, this chemical reaction can be avoided in powder metallurgy due to the solid state of B_4C and Al alloy. On the other hand, the extensive use of the stir casting process attributes to the control of process parameters, simplicity, and lower production cost (Rosso, 2006; Poddar, Srivastava, & Sahoo, 2007; Munir et al., 2015; Kumar, Kumar, & Mukhopadhyay, 2018). The process parameters for the fabrication of MMCs were finalized, depending upon the resultant properties of MMCs. Thus, in this chapter,

a detailed description of the fabrication processes is provided which includes the process parameters, advantages, and disadvantages.

2.2 LIQUID STATE PROCESSING TECHNIQUES

In liquid state processing techniques, the molten matrix material can be reinforced in two different ways. Either reinforcement is directly added into the molten matrix or a preform structure of reinforcement is infiltrated by the molten matrix. Based upon the mechanical force used to infiltrate molten matrix in preform reinforcement, different infiltration processes (IP) are available such as gas pressure IP, vacuum pressure IP, high pressure centrifugal IP, etc. On the other hand, the direct addition of reinforcement is accessed by the formation of a vortex in the molten matrix. Different processes involved in liquid state processing are discussed below.

2.2.1 STIR CASTING ROUTE

The stir casting process is extensively used to fabricate metal matrix composites due to its economical processing, simplicity, suitability for mass production, and flexibility (Deng, Wu, Wu, Nie, & Zheng, 2010; Thandalam, Ramanathan, & Sundarraj, 2015; Nageswaran, Natarajan, & Ramkumar, 2018; Imran & Khan, 2019). The stir casting process involves the melting of selected matrix material in a furnace, which is followed by the addition of reinforcement material and mechanical stirring. Mechanical stirring is done to uniformly dispersed the reinforcement material in molten mass. After stirring, the molten mass is allowed to solidify into a mold (Gupta et al., 2019, 2020; Sharma, Gupta, Nanda, & Pandey, 2021). Figure 2.1 represents the schematic diagram of stir casting process. For uniform dispersion and sound-proof casting, optimum values are required for stir casting parameters, i.e., processing temperature, contact time between matrix and reinforcement, preheating temperature of reinforcement material, design, position, and speed of stirrer in the molten matrix. Due to the high temperature casting, a molten matrix can get oxidized which prevents the uniform dispersion and wetting of reinforcement material in molten mass (Yigezu, Jha, & Mahapatra, 2013;

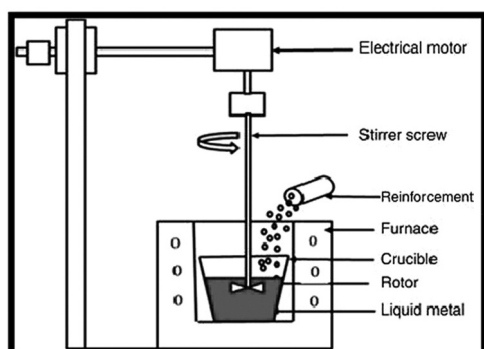


FIGURE 2.1 Schematic diagram of stir casting route (Thandalam et al., 2015).

Arunachalam et al., 2019). To solve this problem, magnesium, borax, K_2TiF_6 flux, etc. are added to the molten mixture during the stirring process (Das, Mishra, Singh, & Pattanaik, 2014; Tirth, 2017; Akinwamide et al., 2020).

2.2.2 INFILTRATION ROUTE

The infiltration process is preferred when the amount of reinforcement added to the matrix material is higher than the amount of reinforcement which can lead to agglomeration in other fabrication processes (Assar, 1999; Michaud & Mortensen, 2001; Manu et al., 2016). In this process, a porous structure of reinforcement was made which is also known as “preform.” This preform has to be made in such a way that it has the capability to sustain the self-weight and also don’t collapse during the filling of liquid matrix material (Manu et al., 2016). When liquid material is poured on the preform then air present in the pores were replaced by the molten mass. After complete filling of pores and solidification of liquid material, the resultant product gives the composite material (Michaud & Mortensen, 2001; Leon-patin & Drew, 2005; Garg et al., 2019). The schematic diagram of the infiltration process is shown in Figure 2.2.

In the infiltration process, filling of liquid material is happened by capillary forces which may lead to incomplete filling of preform structure. Further, it may also lead to non-wetting of liquid material with the reinforcement material (Tuncer, Tasdelen, & Arslan, 2011). The problem of incomplete filling and wetting of preform can be overcome by selecting the proper alloy composition, reinforcement material, surface morphology, time required to fill the preform and liquid temperature. The liquid temperature for the infiltration process needs to be kept at higher values so as to increase the fluidity of the liquid. Due to the increase in fluidity, the chances of completely filling the preform were also increased. However, this may lead to entrapment of gases in the liquid material, which on solidification causes defects in the fabricated composites (Manu et al., 2016). Infiltration time also plays a crucial role as higher infiltration time could lead to a reaction between the preform and matrix material. This interfacial reaction lowers the strength of the resultant composite (Assar, 1999). Due to these two factors, i.e., liquid temperature and infiltration time, the infiltration process is not used for the mass production of composites (Michaud & Mortensen, 2001).

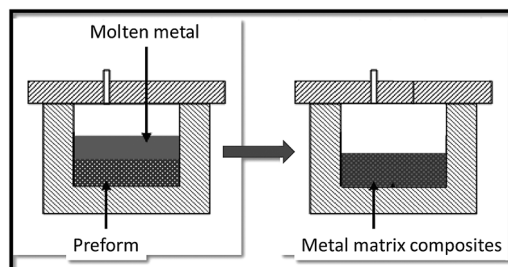


FIGURE 2.2 Schematic diagram of the infiltration process (Garg et al., 2019).

2.2.3 SPONTANEOUS INFILTRATION ROUTE

The spontaneous infiltration process is also known as the pressureless infiltration process. In the spontaneous infiltration process, no external pressure is used to fill the porous preform of ceramics (Leon-patin & Drew, 2005; Garg et al., 2019). However, the filling of the porous preform of ceramics by molten metal alloy is due to the good wetting behavior of metal alloy with ceramic preform. The lower contact angle of metal alloy with ceramic results in lower particle-liquid interfacial energy compared with particle vapor interfacial energy. This difference in interfacial energy generates a negative work of immersion which allows the easy flow of molten metal alloys through the porous preform. Thus, the wetting angle between preform and melt plays a crucial role in the spontaneous infiltration process. The measurement of contact angle can be done by using the sessile drop experiments. The optimum value of contact angle for selection of spontaneous infiltration process was observed to be 50.7° or less. The self-wetting of the preform by the molten metal alloy results in very low residual porosity, high efficiency, and lower production cost (Wang et al., 2018; Zhang et al., 2018). The schematic diagram of the spontaneous infiltration process is shown in Figure 2.3. In this process, a porous preform made up of ceramic was infiltrated by molten metal alloys. The degree of infiltration of molten metal alloy in porous preform depends upon the infiltration time, infiltration temperature, and amount of wettability agent. The increase in infiltration temperature shows a directly proportional relationship with the degree of infiltration (Wang et al., 2018; Zhang et al., 2018). The increase in temperature basically controls the viscosity of the molten metal alloy, which shows it inversely affects the infiltration depth. The relationship between viscosity (η) and infiltration depth (h) is represented by Equation (2.1) (Wang et al., 2018).

$$h^2 = r_{eff} \left(\frac{\sigma \cos \theta}{2\eta} \right) t \quad (2.1)$$

Sometimes the presence of wettability agents like magnesium, titanium, chromium, strontium, titanium, etc. decreases the effect of the increase in infiltration temperature. Wettability agents increase the wettability of ceramics by performing the chemical reaction on the surface of ceramics. The products formed by chemical reaction were acted as a medium to reduce the contact angle between ceramic and molten metal alloy (Manu et al., 2016; Zhang et al., 2019). With the increase in infiltration temperature, the rate of formation of chemical products by wetting agent increases and reduces the alloying element present in the alloy. The decrement in alloying element affects the viscosity and decreases the effect of infiltration temperature. The increase in infiltration time up to an optimal level increases the degree of infiltration. The lower infiltration time doesn't allow the molten metal alloy to completely fill the porous preform of ceramics (Wang et al., 2018; Zhang et al., 2018).

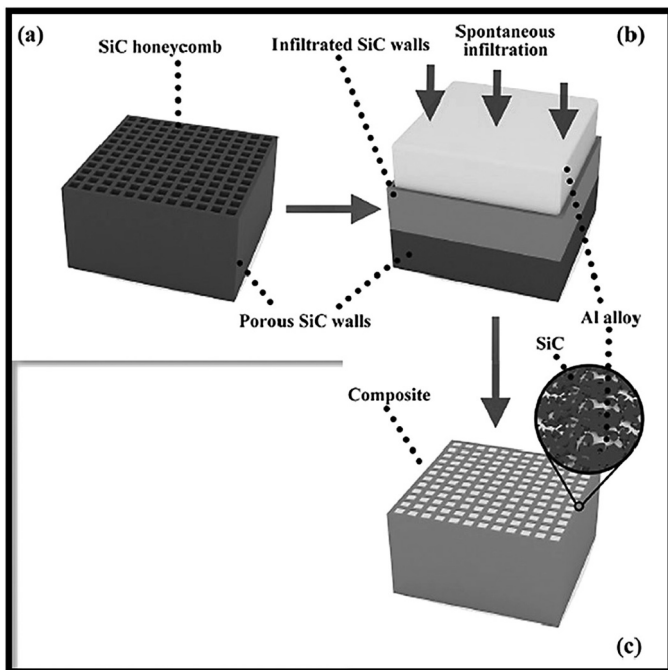


FIGURE 2.3 Illustrative representation of spontaneous infiltration process (Zhang et al., 2019).

2.2.4 FORCED INFILTRATION ROUTE

In the forced infiltration process, an external force is used to infiltrate the porous preform by molten metal and its alloys. The use of external force was done to improve the poor adhesion between matrix and reinforced particles. Further, it is also used in cases where matrix and reinforcement have poor wettability characteristics, i.e., contact angle greater than 90° (Kennedy, Wood, & Weager, 2000; Manu et al., 2016). Various authors have used different types of forces to infiltrate the porous preform, such as:

- Centrifugal infiltration route
- Squeeze infiltration route
- Ultrasonic infiltration route

2.2.4.1 Centrifugal Infiltration Route

In the centrifugal infiltration process, centrifugal force was used to fill the molten metal in the porous preform. The schematic diagram of the centrifugal infiltration process is shown in Figure 2.4. A preform made up of either ceramic or fiber is attached at the end of the cylindrical chamber and the cylindrical chamber was filled with the molten metal alloy. This cylindrical chamber is then fitted onto the

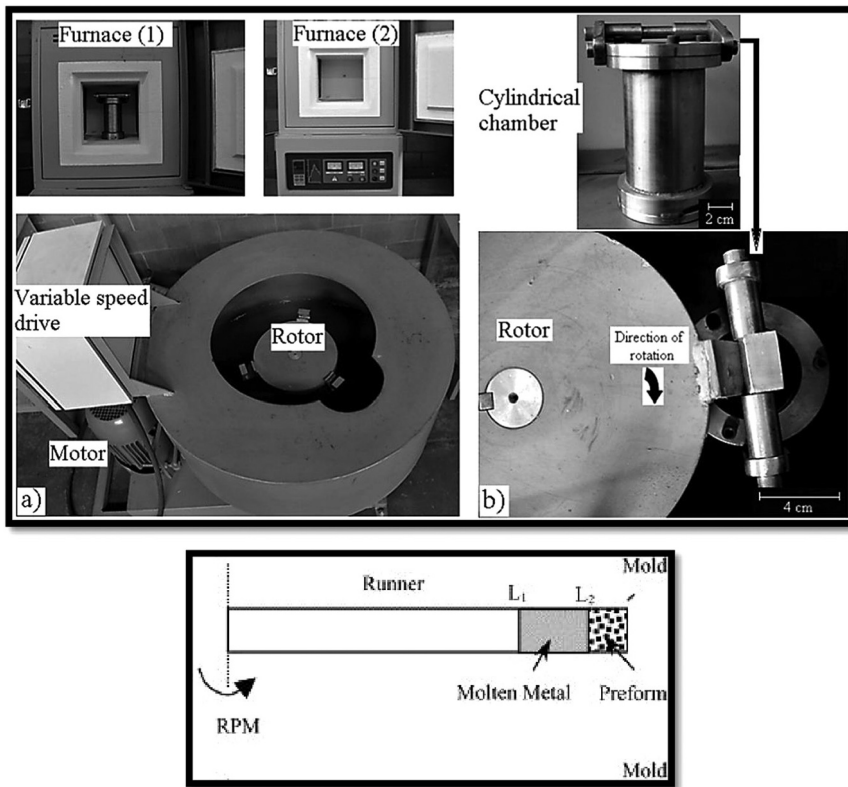


FIGURE 2.4 Schematic representation of centrifugal infiltration process (Wannasin & Flemings, 2005; Sánchez-Martínez, Cruz, González-Nava, & Suárez, 2016).

rotor so that under the action of centrifugal force, preform got filled with molten. This technique is used to make prototypes and series of complex metal pieces (Sánchez, Rams, & Ureña, 2010; Sánchez-Martínez et al., 2016; Akinwamide et al., 2020). The centrifugal force acting on the top surface of the perform is given by the following equation (Sánchez et al., 2010; Manu et al., 2016):

$$F_c = \frac{1}{2} \rho A \omega^2 (L_2^2 - L_1^2) \quad (2.2)$$

where,

F_c = centrifugal force acting on the top surface of the preform

ρ = density of molten metal

ω = rotational speed

L_1 = inner molten metal level from rotational axis (see Figure 2.4)

L_2 = outer molten metal level from rotational axis (see Figure 2.4)

A = area of the top surface of the preform.

2.2.4.2 Squeeze Infiltration Route

In the squeeze infiltration route (Figure 2.5), a preform of reinforced material is made, which is placed in the die attached to the hydraulic press. Besides this hydraulic press, a furnace is set up to melt the metal and its alloys. After pouring molten into the die, the opening of the die is closed and pressurized with the help of a lid attached to the hydraulic press. The pressure on molten metal is maintained until the solidification of melt not completed (Manu et al., 2016; Omrani, Moghadam, Menezes, & Rohatgi, 2016; Zhu et al., 2020). The advantage of applying pressure on molten metal is that it increases the rates of heat flow, eliminates macro/micro shrinkage porosity, and reduces the gas porosity (Ghomashchi & Vikhrov, 2000; Vijayaram, Sulaiman, Hamouda, & Ahmad, 2006). Finally, the component is removed from the die. In some studies, the stir casting process is used to disperse the reinforced particles, which is followed by the process as explained above (Bahrami, Soltani, Pech-Canul, & Gutiérrez, 2016; Arunachalam et al., 2019; Zhu et al., 2020).

The die used for the squeeze infiltration process is subjected to extreme thermal and mechanical stress. These stresses led to thermal fatigue, erosion, cracking, and corrosion of die material. Thus, the design of the die plays an important role in the squeeze infiltration process which involves a selection of material (mostly used H13 tool steel), manufacturing process, and heat treatment (Ghomashchi & Vikhrov, 2000; Vijayaram et al., 2006). The process parameters used in the squeeze infiltration route are pouring temperature, preform preheating temperature, melt volume, melt quantity, die temperature, and squeeze pressure. The cavity or preform present in the die has to be completely filled by the molten melt. Thus, the selection of proper amount of molten melt became essential as no gating and runner system is used in the process. However, this problem can be solved by diverting the excess molten into a region which can be machined after the process. The quality of metal also plays an important role as the presence of inclusion in molten metal led to turbulence, die coat, and increases the dead time (Ghomashchi & Vikhrov, 2000; Vijayaram et al., 2006). The application of applied pressure on

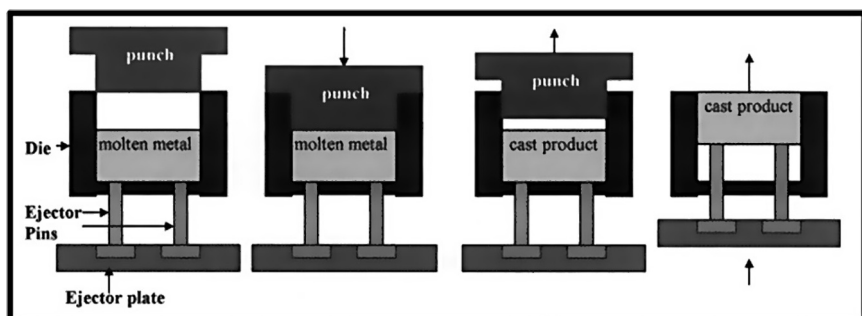


FIGURE 2.5 Schematic diagram of the squeeze infiltration process (Ghomashchi & Vikhrov, 2000).

the preform or mixture of matrix and reinforcement shows a significant effect on the mechanical and microstructural properties of the fabricated component (Dhanashekhar & Kumar, 2014; Arunachalam et al., 2019). A relation between solidification temperature and the applied pressure is given by the Clauclius–Clapeyron equation (see Equation (2.3)) (Akinwamide et al., 2020):

$$\frac{\Delta T}{\Delta P} = \frac{T_f * \Delta V}{H_f} \quad (2.3)$$

where,

P = applied pressure

T_f = freezing temperature

H_f = latent heat of fusion

ΔV = change in volume during solidification.

During solidification, the shrinkage and transfer of heat from the melt led to negative values of change in volume of melt (ΔV) and latent heat of fusion (H_f), respectively. The negative values of ΔV and H_f led to a positive value of $\Delta T/\Delta P$, which signifies the increase in melt temperature with a rise in applied pressure. Besides influencing melting temperature, it also affects the transfer of heat during the solidification process. As the solidification process proceeds, the gap between the wall of the die and solidified material increases due to the shrinkage of molten melt. The increase in gap led to a decrease in heat transfer coefficient but under the action of applied load, the plastic deformation of casting was helpful in maintaining the contact (Vijayaram et al., 2006; Dhanashekhar & Kumar, 2014; Akinwamide et al., 2020). The preform and die temperature should be kept in the range of 200–300°C when the processing of ferrous material has to be done. However, for aluminum alloys, the preferable temperature is kept between 150 and 200°C (Hu, 1998; Ghomashchi & Vikhrov, 2000). The preheating of preform and die temperature is done to maintain a balance between the transfer of heat from molten to the preform and die. This transfer of heat led to premature solidification of the melt and generates cold laps on the surface of the solidified component. Further, this temperature difference generates thermal stresses on the surface of the tool – and if the tool gets overheated, then defects like hot spots and shrinkage pores can affect the fabricated product (Vijayaram et al., 2006; Manu et al., 2016; Arunachalam et al., 2019). The pouring temperature of molten metal in preform affects the life of the die and the quality of the product formed. If the pouring temperature is too low, then molten will have lower fluidity which results in incomplete filling of the preform and die cavity. However, if the pouring temperature is too high, then molten may extrude through the interface of the lid, die, and casting. The extrusion of molten metal will then lead to blocking of the lid. Simultaneously, a high pouring temperature reduces the life of the die and can also increase the shrinkage porosity in thick sections (Hu, 1998; Vijayaram et al., 2006; Manu et al., 2016).

2.2.4.3 Ultrasonic Infiltration Route

The ultrasonic infiltration process is mostly used to make metal matrix composites when fibers are used as a reinforcement (Matsunaga, Ogata, Hatayama, Shinozaki, & Yoshida, 2007). The schematic diagram representing the ultrasonic infiltration process is shown in Figure 2.6. In this process, a spool of fiber is used, which acts as a preform in metal matrix composites. For fiber to act as a preform, a bundle of fiber is twisted to form a multifilament yarn. Before passing this multifilament yarn of fiber into molten metal, it is passed through a furnace for preheating in a nitrogen atmosphere. This preheating of fiber is done to remove the sizing agent present on fibers and the use of nitrogen atmosphere is done to avoid the oxidation of fibers. Further, this preheated multifilament yarn of fibers is passed through the molten metal (Matsunaga, Matsuda, Hatayama, Shinozaki, & Yoshida, 2007; Matsunaga, Ogata, et al., 2007; Manu et al., 2016). The ultrasonic waves produced by a horn can be used in two ways to infiltrate the molten metal in multifilament yarn of fibers, i.e., (i) by placing the fibers beneath the ultrasonic horn, or (ii) by passing the fibers through a hole in ultrasonic horn. The latter method is observed to be more efficient in infiltrating the multifilament yarn fiber with molten metal. When ultrasonic waves are bombarded on the fibers, then the half tensile cycle of ultrasonic wave led to separation of multifilament yarn fibers which allows the penetration of molten metal into empty space between the fibers. During the half compressive cycle of ultrasonic wave, the penetrated molten metal

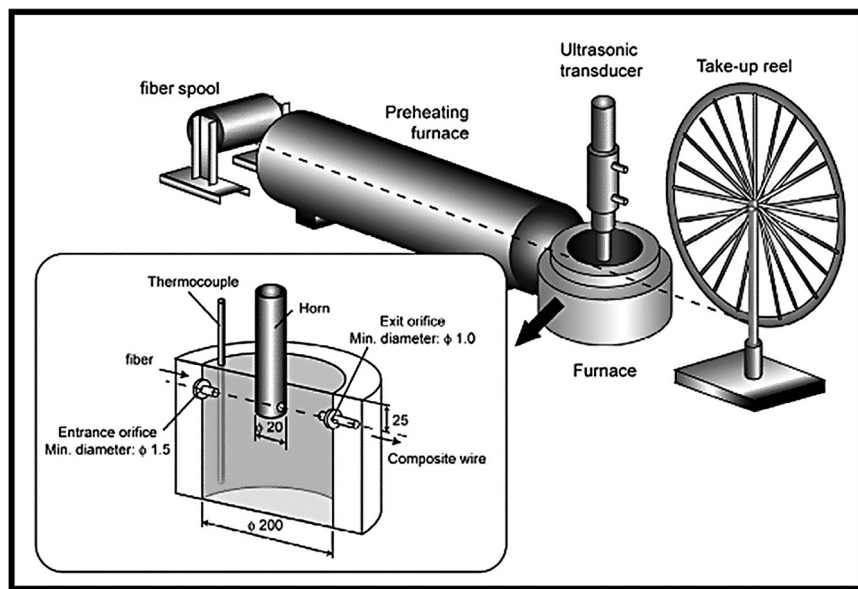


FIGURE 2.6 Schematic diagram of ultrasonic infiltration process (Matsunaga, Ogata, et al., 2007).

is forcibly infiltrated into multifilament yarn of fibers and results in the formation of metal matrix composite (Heng et al., 1993).

The factors affecting the ultrasonic infiltration process are fabrication speed, power of ultrasonication, the temperature of molten metal, and diameter of the hole in the ultrasonic horn (Heng et al., 1993; Matsunaga, Ogata, et al., 2007). The increase in ultrasonic power led to the increase in infiltration of aluminum in the multifilament yarn of fibers. This is attributed to an increase in the cavitation process caused by the ultrasonic waves. However, this cavitation process has a negative effect on the tensile strength of the fabricated metal matrix composites. With the increase in ultrasonic power beyond the optimum value, an increase in damage to the multifilament yarn of fibers is reported which decreases the properties of fabricated composites (Heng et al., 1993). The fabrication speed used in the ultrasonic infiltration process is directly correlated with the contact time of molten metal with the multifilament yarn of fibers. The use of high fabrication speed led to a reduction in the chemical reaction that can occur between matrix and reinforced fiber. If a lower fabrication speed is used, then molten metal and fiber will get enough time to undergo the chemical reaction. The product formed by this chemical reaction is responsible for degradation of the tensile strength of metal matrix composites. Hence, an optimum value of fabrication speed should be selected to avoid the chemical reaction between matrix and reinforced fibers (Matsunaga, Matsuda, et al., 2007). The occurrence of chemical reaction depends on the temperature of molten metal. The use of high temperature for molten metal is also responsible for initiation of chemical reaction at the interfacial region of fibers which degrades the strength of metal matrix composites (Heng et al., 1993). The increase in hole diameter in the ultrasonic horn shows an increment in efficiency of infiltration of molten melt in the fibers. If the size of hole in horn is small, then the acoustic energy generated by ultrasonic wave will not be sufficient to infiltrate the molten metal in multifilament yarn of fibers. Hence, an optimum value of size of hole in ultrasonic horn should be used. If the hole size is greater than the optimum value, then the wave pressure amplitude decreases and the proper separation of fibers for infiltration process will not be attained (Matsunaga, Matsuda, et al., 2007; Manu et al., 2016).

2.3 SOLID STATE PROCESSING TECHNIQUES

Solid state processing techniques are commonly used methods for fabrication of various industrial products such as cemented carbides, diamond tools, etc. In the solid state processing techniques, both matrix and reinforced particles were blended together in solid state by avoiding the phase transformation in both the material. The bonding between matrix and reinforced particles is attained by mutual diffusion of material at high temperature and pressure conditions. In solid state processing, two type of process is mainly used, i.e., powder metallurgy process and diffusion bonding process, which are discussed in the following sections.

2.3.1 POWDER METALLURGY ROUTE

In initial step of powder metallurgy, the matrix powder and reinforcement are mixed to attain uniform distribution of reinforced particles in the matrix. This mixing of powder is done by using a high-energy ball milling process, which is also known as the mechanical alloying process. In the mechanical alloying process, the powder mixture is blended by using balls made up of hard materials such as stainless steel, zirconium oxide, etc. After mechanical alloying, the powder mixture is filled in a die made up of steel or graphite for the compaction process. In the compaction process, pressure is applied to the powder for a certain period of time to form a solid sample. Further, this solid sample is kept in the furnace for the sintering process (Shirvanimoghaddam et al., 2017; Yue et al., 2017; Bhoi et al., 2020). In the sintering process, the temperature of the furnace is kept near the melting point of the matrix material. During the initial stage of heating, the development of thermal gradient in the sample and low penetration of heat lead to the formation of good interfacial bonding and an increase in matrix grain size. However, as the process progresses, this phenomenon changes and results in attainment of dense and homogenous microstructure for fabricated metal matrix composites (Bhoi et al., 2020). The schematic diagram of powder metallurgy process is shown in Figure 2.7. Powder metallurgy process is considered as better processing technique for fabrication of metal matrix composites in comparison with liquid state processing techniques. This was attributed to the ability of the powder metallurgy process to fabricate a wide range of product which has restrictions in size and composition of composite. Further, the scrap produced from this process is much less (Bhoi et al., 2020). In addition to this, the process parameters involved in different steps of powder metallurgy process are discussed as follows.

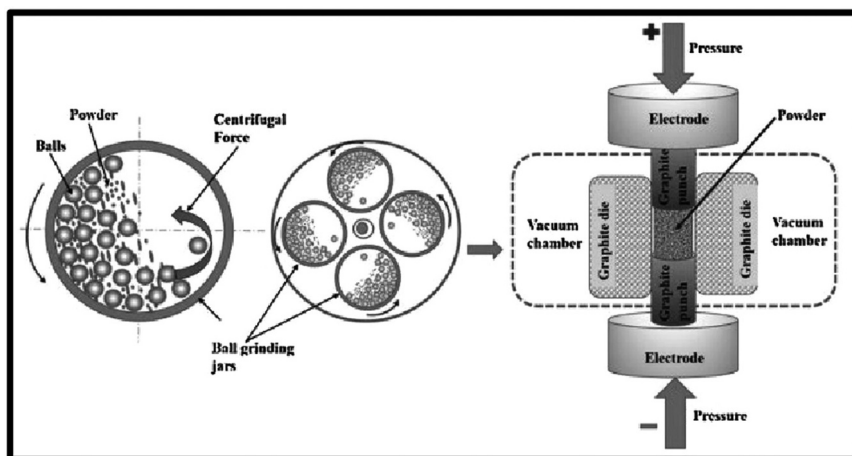


FIGURE 2.7 Schematic diagram of powder metallurgy (Arunachalam et al., 2019).

2.3.1.1 High Energy Ball Milling

The high-energy ball milling process is used in the powder metallurgy process to attain the uniform distribution of reinforced particles in the matrix. This uniform distribution is attained by undergoing the deformation, cold welding, and fracturing of particles, referred to as the DCF process. To accomplish the DCF process, a container containing hardened balls and powder mixture is rotated in planetary motion, as shown in Figure 2.8 (Hewitt & Kibble, 2009; Bakshi et al., 2010; Munir et al., 2015). The high-energy ball milling process is influenced by various parameters, such as the ball-to-powder ratio, processing time, processing speed, ball diameter, and the container's internal diameter (Bhoi et al., 2020). Processing speed (v) in the high-energy ball milling process is considered a crucial factor whose value should be less than the critical speed (v_c). Critical speed is when centrifugal force due to the rotation of the disk and container is equal to the gravitational force acting on the hardened balls. This critical speed shows a direct correlation with the diameter of ball (d) and the diameter of container (D) as shown in Equation (2.4). If the processing speed is higher than the critical speed, then the centrifugal force acting on the ball exceeds the gravitational force. This results in the pinning of hardened balls to the container walls, which decreases the deformation process due to the collision of hardened balls under the action of gravitational force. Hence, the processing speed of the high-energy ball milling process is kept below the critical speed (Munir et al., 2015).

$$v_c = \frac{1}{2 * \pi} \sqrt{\frac{2 * g}{(D - d)}} \quad (2.4)$$

The processing time of the high-energy ball milling process affects uniform distribution, agglomeration, and fracturing of the particle. If processing time is low, then reinforced particles start clustering in the matrix, which degrades the

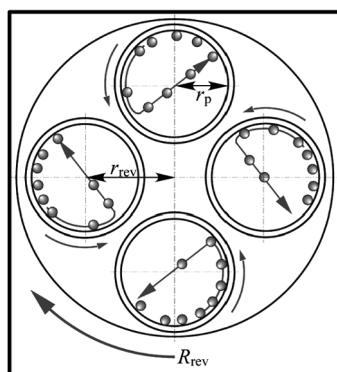


FIGURE 2.8 Schematic diagram of high energy ball milling setup (Asano, Enoki, & Akiba, 2009).

properties of metal matrix composites. On the other hand, if the processing time is too high, then a hardened ball leads to extensive damage to the reinforced particles, affecting the properties of metal matrix composites. Hence, for the mixing of particles, an optimum value of processing time should be selected (Hewitt & Kibble, 2009; Bhoi et al., 2020).

The use of a low ball-to-powder ratio in the ball milling process led to a decrease in impact energy caused by the impact of the hardened balls. This further decreases the degree of homogenous reinforced particles in the matrix. Conversely, a higher ball-to-powder ratio led to an increase in the impact, which can either fracture the mixture of particles or contaminate the mixture by wearing the hardened balls. Thus, an optimal ball-to-powder ratio value should be used for the ball milling process (Hewitt & Kibble, 2009).

2.3.1.2 Consolidation Techniques

After the ball milling process, the obtained mixture of powder was compacted and sintered by using the various techniques reported in the literature, such as (i) conventional sintering, (ii) hot pressing sintering, and (iii) spark plasma sintering. With the help of these techniques, desired mechanical and physical properties are provided to the compacted samples of MMCs. The detailed discussion related to these techniques is as follows:

2.3.1.2.1 Conventional Sintering

In conventional sintering, the blended mixture of matrix and reinforcement is first compacted under the influence of applied pressure to form the pallets of MMCs. To compact the mixture of powders, a punch and die system was used in which desired pressure was applied using the hydraulic press (Samal, Parihar, & Chaira, 2013; Wan, Li, Tieu, Xue, & Zhu, 2019; Bhoi et al., 2020). The applied pressure during compaction results in sliding of the particles, filling the gap between adjacent particles and in densification of the MMCs. This densification of pallets can be attained up to a certain pressure as a further increase in pressure will lead to the deformation of the particles and the generation of cracks in the pallets (Mukhopadhyay & Basu, 2007; Wan et al., 2019). Further, the formed pallets of MMCs are placed in the furnace to attain the desired strength and physical properties (Samal et al., 2013; Wan et al., 2019; Bhoi et al., 2020). This process is known as the sintering process, which depends on the sintering time and temperature. If sintering time and sintering temperature are low, then the fabricated pallets have lower strength and physical properties. On the other hand, the selection of higher sintering temperature and time results in coarsening of the grain, which again decreases the mechanical and physical properties of MMCs. In general, the sintering temperature was kept just below the melting point of the matrix (Mukhopadhyay & Basu, 2007; Hewitt & Kibble, 2009; Yue et al., 2017).

2.3.1.2.2 Hot Pressing Sintering

In conventional sintering, pallets of samples are kept at a high temperature and processed for longer. To reduce the processing time and temperature, an activation

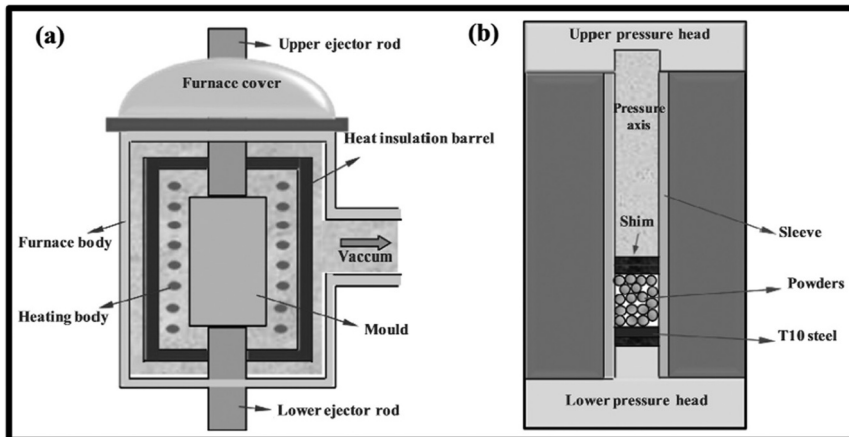


FIGURE 2.9 Schematic diagram of hot-pressing sintering process (Ge et al., 2017).

force is required, increasing the sintering process's kinetics. This activation force can be applied by increasing the temperature of pallets during the compaction process (Mukhopadhyay & Basu, 2007; Chang, Lin, & Huang, 2020). Further, the sintering process also depends upon the particle size of the mixture used. With the increase in a mixture's particle size, the pressure required to compact the mixture shows an increasing trend, which is attributed to increased particle sliding. This sliding of particles creates an opposing force to the applied pressure and increases the applied compacting pressure. This problem can also be solved by increasing the kinetics of the sintering process, as discussed earlier (Mukhopadhyay & Basu, 2007; Hewitt & Kibble, 2009). In hot pressing sintering, the powder mixture was kept in a die made up of either carbon or graphite. Further, a compaction pressure is applied to the mixture by placing the die in an electric furnace and under an inert atmosphere to avoid oxidation of the pallets (Munir et al., 2015; Bhoi et al., 2020). The schematic diagram of the hot-pressing sintering process used to apply CuZrAlTiNi powder coating on T10 steel substrate is shown in Figure 2.9. The increase in sintering temperature showed an increasing trend in densifying the pallets of MMCs, which is also higher than the conventional sintering process. Further, the increase in sintering pressure reduces the time required for the full densification of pallets (Munir et al., 2015; Chang et al., 2020).

2.3.1.2.3 Spark Plasma Sintering

In spark plasma sintering, the consolidation of a mixture of particles is done using a combination of two activation sintering forces. The first activation sintering force is heat, which is supplied by using the electric current, and the second one is the mechanical force, which is applied to the powder through a punch and die system (Bakshi et al., 2010; Samal et al., 2013; Khodaei, Yaghobizadeh, Baharvandi, & Dashti, 2018). This process is similar to the hot-pressing sintering process – the only difference is the source of heat supplied. In the case of hot-pressing

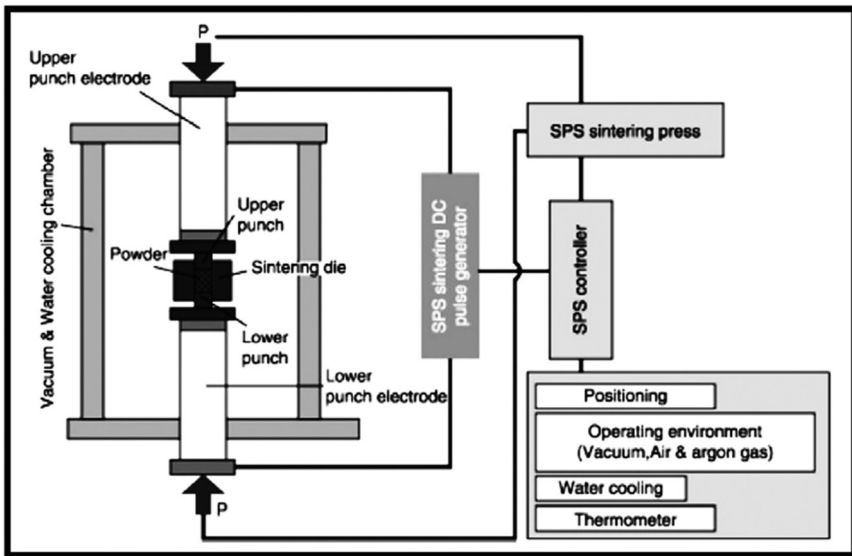


FIGURE 2.10 Schematic diagram of spark plasma sintering process (Khodaei et al., 2018).

sintering, heat is supplied by using the electric furnace; however, in the case of spark plasma sintering, electric current is passed through the punch, die and mixture of powder which generates the electric discharge within the powder and is considered as a source of heat (Mukhopadhyay & Basu, 2007). The advantages of spark plasma sintering over the previously explained sintering process are that it has a low processing time, avoids interfacial reactions, nanoparticles can be easily processed, and inhibits grain growth (Munir et al., 2015). The schematic diagram of the spark plasma sintering process showing different components is presented in Figure 2.10.

During spark plasma sintering, mechanical force is applied throughout the process. However, the electric current to punch, die, and powder can be applied in two ways, i.e., continuous or pulsed supply of DC. In context to the mechanism of heat generation, it is stated in the literature that at the contact of particles, a small insulation film is present, which acts as a small capacitor. This small capacitor led to the generation of electric discharge, which helps consolidate the mixture of particles (Mukhopadhyay & Basu, 2007).

2.3.2 DIFFUSION BONDING ROUTE

The diffusion bonding process is another solid-state welding process used for the fabrication of MMCs, which is mainly used for the material having different chemical and metallurgical properties (Wei, Aiping, Guisheng, & Jiale, 2008; Mahendran, Balasubramanian, & Senthilvelan, 2010; Feng, Chen, Xiong, & Guo,

2013). In the diffusion bonding process, MMCs are fabricated under different temperature and pressure conditions, which allows the development of strong interfacial bonding between the matrix and reinforced particles. Due to experimental conditions of the diffusion process, fabricated materials can avoid the formation of brittle phases and bonding defects (i.e., segregation, distortion, and cracking) (He, Feng, Zhang, & Qian, 2003; Mahendran et al., 2010; Assari & Eghbali, 2019). The schematic diagram of the diffusion bonding process showing the fabrication of carbon-fiber-reinforced MMCs is presented in Figure 2.11.

In the diffusion bonding process, a matrix is used in the form of foils on which a layer of reinforcement is made. The layer of reinforcement can be made by either placing the preform, fiber, or particles on the foil of the metal matrix. In this way, multiple layers of reinforcement and matrix material are stacked to form the MMCs. Further, this stack of MMCs is placed in the furnace at a temperature of 50–80% of the melting point of the matrix or below the temperature of the phase having the lowest melting point (Shirzadi, Assadi, & Wallach, 2001; He et al., 2003; Shirvanimoghaddam et al., 2017). In addition to this, pressure is also applied to the stack of MMCs, which is kept in the vacuum environment to avoid oxidation of the sample. The value of applied pressure should be selected so that the gap present between the asperities of contact surfaces gets filled by undergoing the deformation process. Further, to obtain the high strength of interfacial bonding, the joined surfaces of both materials should be oxide-free, as

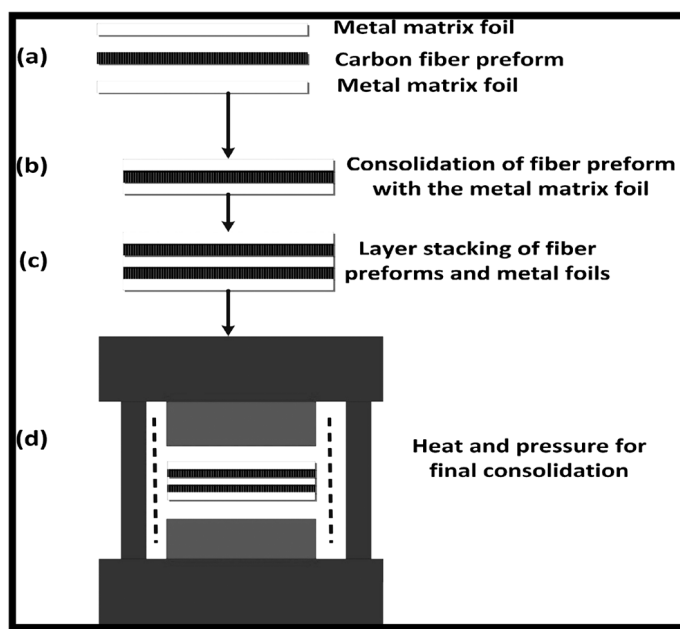


FIGURE 2.11 Schematic diagram of diffusion bonding process (Shirvanimoghaddam et al., 2017).

oxide formation results in less diffusion of material at the interface of matrix and reinforced particle (Mahendran et al., 2010; Maity & Pal, 2012; Prikhodko et al., 2020). Various techniques are used to clean the surfaces of the material, such as dipping of material in alkaline or acid solutions, ion beam cleaning, coating of different materials on matrix and reinforcement, etc. In addition to these techniques, some researchers have also used the transient liquid diffusion bonding process to overcome restrictions in material diffusion caused by the formation of an oxide layer (Shirzadi et al., 2001; Wei et al., 2008; Maity & Pal, 2012). In this method, a metal foil is incorporated between the two mating surfaces. The function of this metal foil is to undergo the eutectic or peritectic reaction with the mating surface as the processing temperature reaches the melting point of the metal foil. This reaction helps remove the oxide layer present on the mating surfaces and results in the formation of strong interfacial bonding upon solidification of the metal foil (Shirzadi et al., 2001; Mahendran et al., 2010; Maity & Pal, 2012). The other advantages of using the transition liquid diffusion bonding process are that the pressure required for the processing is very low, no deformation is observed in the mating parts, and formation of intermetallic can be controlled based on the requirement of the applications (Atabaki & Idris, 2012; Maity & Pal, 2012).

2.4 PHASE DEPOSITION PROCESSING TECHNIQUES

Phase deposition processing techniques are used to form a coating on the reinforced particles. The purpose of using this coating is to increase the wettability of the reinforcement with the matrix material. Thus, the material selected for coating should have good wettability characteristics with the matrix material. If the metal matrix has good wettability characteristics with the reinforcement, then the coating of the metal matrix can also be done on the reinforcement material. After coating the reinforcement material, a consolidation process is used to obtain a consolidated metal matrix composite. The various techniques used for processing of metal matrix composites under phase deposition are discussed below.

2.4.1 PHYSICAL VAPOR DEPOSITION ROUTE

The physical vapor deposition (PVD) technique is basically used to form the coating of different elements, compounds, polymers, and alloys on various substrates. In this process, the material deposition is done by converting it into a vapor state. Then, this vapor state is allowed to pass through a gaseous or low-pressure environment and impinged to the surface of the substrate. After the coating process, a consolidation technique is used to combine the different substrates for making a metal matrix composite. The coating thickness observed for this process ranges from a few angstroms to 1000 angstroms. In addition to this, the deposition temperature used in this process is also low. The physical vapor deposition process is classified based on the energy used to convert the deposition material into vapor. In general, two techniques are used to form the vapors of deposition material, i.e.,

electron beam and sputtering process. Both the processes are discussed in the following sections.

2.4.1.1 Electron Beam Physical Vapor Deposition (EB-PVD) Process

The EB-PVD setup mainly consists of an electron beam gun assembly, substrate, and copper crucible in which material to be evaporated is placed. The copper crucible used in this process is further attached to the water-cooling system (Singh & Wolfe, 2005; Gong & Wu, 2011). The schematic diagram of the EB-PVD process is shown in Figure 2.12.

During the coating process, a focused beam of high-energy electrons is allowed to fall on the material whose coating has to be performed on the substrate. To avoid electron scattering, the bombardment of the electron beam is done in a vacuum chamber. Due to the high kinetic energy of the bombarded electrons, the coating material gets heated up and reaches evaporation temperature. The formed vapors of the material are then allowed to condense on the substrate material, which is directly in the line of sight of the vapors (Fuke, Prabhu, & Baek, 2005; Gong & Wu, 2011; Vasile, Birca, Surdu, Neacsu, & Ionut, 2020). The distance between substrate and source of vapor is mainly kept in the range of 10–100 cm. With an increase in the distance from 10 cm, the deposition area of coated material can be increased. However, the decrease in distance (i.e., below 10 cm) results in the heating of the substrate due to optical radiation (Rossnagel, 2003; Fuke et al., 2005). The coating formed using the EB-PVD process usually has high density, uniform microstructure, low contamination, and a good surface finish. In addition to this, the EB-PVD process has a high deposition rate with high flexibility in the processing parameters (Singh & Wolfe, 2005; Vasile et al., 2020). The deposition of coating material depends upon the mean free path of the vapor generated from coating material. The mean free path should be greater than the distance between the substrate and the vapor source. The use of a higher distance between substrate and source of vapors leads to scattering of the vapors, which reduces the deposition rate. Further, this mean-free path also depends upon the vacuum pressure. With the increase in the mean-free path, the vacuum pressure

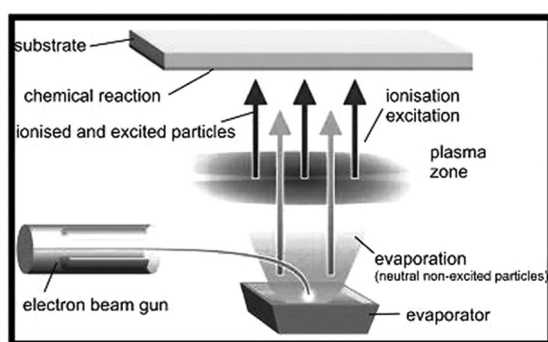


FIGURE 2.12 Schematic diagram of EB-PVD process (Bewilogua et al., 2009).

required for the process has to be decreased to get the desired deposition of the coating material. For a mean-free path of 5 cm, the optimum vacuum pressure required for the system is 1 mTorr (Rossnagel, 2003). Another factor that influences the coating in the EB-PVD process is the temperature of the substrate. This factor mainly comes into existence when film thickness exceeds a few hundred nanometers. For direct condensation of vapor into the solid state, the temperature of substrate (T_s) should be less than two-thirds of the melting temperature of the coating material (T_c). On the other hand, the higher temperature of the substrate leads to a change in the vapor phase to the liquid state, which forms the crystalloids upon reaching a certain size of droplets. Further, the ratio of substrate temperature and melting temperature also showed a direct influence on the microstructure of coating material. If the value of the ratio of $\left(\frac{T_s}{T_c}\right)$ is less than 0.3, then a dome of columnar structure is formed with improper diffusion of the coating material to the substrate material. However, if the value lies between 0.3 and 0.5, then a dense columnar structure is formed in which condensation is governed by surface diffusion and grain size shows an increasing trend with a rise in substrate temperature. At last, if the value of the ratio lies between 0.5 and 1, then a recrystallized structure is formed which is governed by the volume diffusion (Rossnagel, 2003; Singh & Wolfe, 2005; Gong & Wu, 2011).

2.4.1.2 Sputtering Deposition Process

In the physical sputtering process, an energetic particle is allowed to bombard the coating material. There are a number of particles used as energetic particles, e.g., neutral atom, molecule, any ion, or photon but usually, an inert gas ion is used as an energetic particle. As energetic particles bombard the coating material, the energy carried by the particle is used to dislodge the atoms present on the surface of the coating material. In the same way, the dislodged atoms try to penetrate deep into the coating material by dislodging the neighboring atoms. This dislodging process continues until the energy carried by the dislodged atom is lacking to dislodge the neighbor atoms. The insufficient energy carried by the atom gets dissipated by raising the local temperature of the coating material. During dislodging process, the atoms having energy greater than the surface binding energy get emitted from the coating surface. These atoms are then allowed to deposit on the substrate (Rossnagel, 2003; Bewilogua et al., 2009; Mehran, Fazal, Bushroa, & Rubaiee, 2018). The schematic showing the sputtering deposition process is shown in Figure 2.13. On comparison with the EB-PVD process, a dense and smooth thin film is formed in the sputtering deposition process as the energy acquired by the sputtered atom is 10 times higher than the vaporized atom, but the deposition rate of the sputtering deposition process is low, i.e., in the range of nanometer per second (Rossnagel, 2003; Bewilogua et al., 2009).

The characteristics of the sputtering deposition process are defined on the basis of sputter yielding. Sputter yielding is defined as the number of atoms emitted from the coating material upon bombardment of a single energetic particle on the

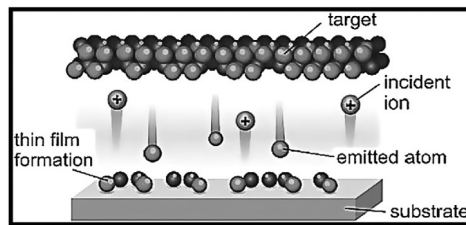


FIGURE 2.13 Schematic diagram of sputtering deposition process (Bewilogua et al., 2009).

coating surface. This factor depends upon the angle of incidence of bombarded particle, the surface binding energy of the substrate, the energy of the bombarded particle, and the relative mass of the energetic particle and coating material (Mattox, 1999; Rossnagel, 2003). The sputtering yield can be increased by two to three times when the angle of incident of an energetic particle is normal to the substrate material. However, the decrease in incident angle results in a decrement in sputtering yield, which is attributed to the low transfer of energy from the particle to the coating material (Rossnagel, 2003). The sputtering deposition process depends upon the surface binding energy of the coating material. If oxides or nitrides are present on the surface of the coating material, then the value of sputtering yield will be low. The decrease in sputtering yield is attributed to high surface binding energy compared to the oxide and nitride-free coating material. Thus, the coating material used in the process should be oxide and nitride free to obtain a high sputtering yield (Mattox, 1999). In addition to this, the sputtering process also depends upon the plasma voltage. If plasma voltage is set between 0.05 and 2.00 KeV, then a condition of knock-on sputtering is developed at the surface of coating material which is essential for thin film coating. With a further increase in voltage from 2 KeV to 50 KeV, a collision cascade condition is developed, making it unsuitable for the thin film application. For voltages higher than 50 KeV, the penetration of incident energetic particles is high, resulting in dissipation of energy within the material, i.e., not on the surface of the coating material. This further results in a decrement of the sputtering yield and, thus, not recommended for the sputtering process (Mattox, 1999; Rossnagel, 2003).

2.4.2 SPRAY DEPOSITION ROUTE

The spray deposition process is classified based on the method used to form the droplets of the matrix material. The droplets of the metal matrix can be formed either by premelting or passing the matrix through a rapid heating source. The process in which droplets are formed by pre-melting of the matrix is designated as a spray forming process, whereas the other method is designated as a thermal spray process (Bakshi et al., 2010; S. Kumar, Singh, & Hashmi, 2019; Si, Tang, Zhang, Wang, & Wu, 2017; Singh & Wolfe, 2005).

In the spray forming process, the molten metal matrix is allowed to atomize under the action of a high-pressure gas jet. This results in the formation of droplets of the micron size and then feed with the reinforced particles. The combination of matrix and reinforced particles, i.e., the atomized beam, is then allowed to deposit on the substrate (Torralba et al., 2003; Shabani & Mazahery, 2013; Si et al., 2017). The schematic diagram of the spray forming process is shown in Figure 2.14. The flow rate of the atomized beam is kept at approximately 5 kg/min, which results in the formation of a deposited layer with a density of around 95%. Further, the high solidification rate of the atomized beams helps reduce any undesirable and interfacial compound between the reinforced and liquid metal. The microstructure obtained after this process has a fine grain structure and can have high solubility of the alloying elements (Torralba et al., 2003; Chaudhury, Sivaramakrishnan, & Panigrahi, 2004; Singh & Wolfe, 2005).

The gas pressure used for atomization of the liquid metal should be optimized because high-pressure gas leads to the development of turbulence in the atomized beam. On the other hand, the low-pressure gas avoids the generation of an atomized beam (Reddy, Maity, & Pandey, 2019). In addition to this, the atomization of liquid metal depends on the viscosity and density. The viscosity of liquid metal is affected by the temperature of the matrix material. Thus, the small deviation in the molten metal temperature greatly affected the atomization process, resulting in the formation of droplets having different sizes. The material having higher liquid density takes longer to atomize the molten metal as the force acting for atomization takes longer to form the droplets of the liquid (Antipas, 2013). The size of

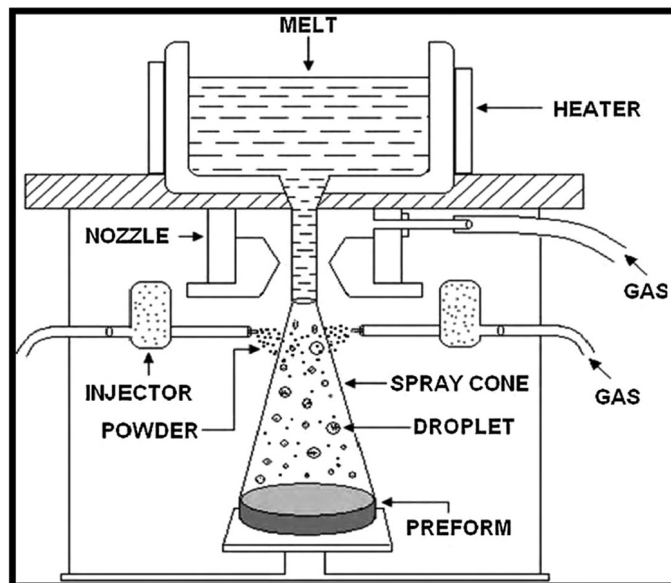


FIGURE 2.14 Schematic diagram of spray forming process (Kaur & Pandey, 2010).

droplets formed from liquid metal also depends upon the distance between the nozzle and substrate. The increase in distance shows a decreasing trend in the size of droplets and deposition rate. However, the decrease in distance beyond the optimum value results in a backflow of molten material, which degrades the properties of the formed coating (Reddy et al., 2019).

In the thermal spray method, the matrix material is either in the form of wire or powder. The selected metal matrix is allowed to feed into a spray gun, in which the melting of matrix material is done by using high-temperature heating sources. The heating is provided by ionizing inert gas with the help of arc generation. This ionization of inert gas results in the formation of a plasma region, which is used to melt the powder or wire of the matrix. The arc generation can be done by applying the voltage between the cathode of tungsten and the anode of concentric copper. This process is defined as a direct current thermal spray process. On the other hand, the use of high-frequency radio waves generated by using the electromagnetic field originating from an induction coil leads to the radiofrequency thermal spray process. After melting the matrix material, high-pressure expanding gas is used to spray the atomized form of metal on the substrate. Before deposition of the liquid metal, reinforced particles are injected into the droplets of the metal matrix (Sampath & Herman, 1993; Smith & Knight, 1996; Singh & Wolfe, 2005; Bakshi et al., 2010). The schematic of the thermal spray method is shown in Figure 2.15.

The temperature and flow field of plasma is influenced by the constituents, pressure and volume of gas used. If the flow of gas volume is low, it will result in lower compression of the plasma jet, which has a direct influence on the velocity

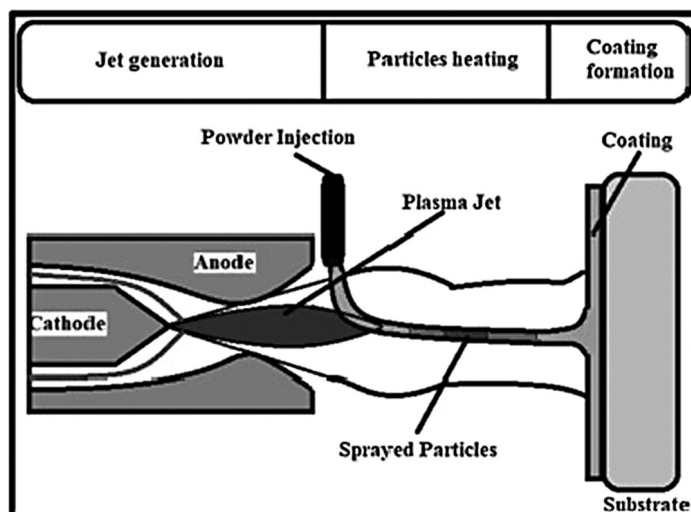


FIGURE 2.15 Schematic diagram of thermal spray process (Henao, Poblano-Salas, Monsalve, Corona-Castuera, & Barceinas-Sanchez, 2019).

of the droplets impacting the substrate. Further, this also increases the loss of heat occurring on the nozzle. On the other hand, the high flow of volume of gas increases the turbulence in the plasma jet, increasing the heat loss and decreasing the quality of the coating process. The heat generated by gas ionization is influenced by the property of the gas. If the heat generated by the ionization of gas is low, then the matrix material will not be able to melt the matrix, whereas the high generation of heat could result in evaporation of the matrix (Fang & Xu, 2002; Wenzelburger, Silber, & Gadow, 2010).

2.5 CONCLUSION

MMCs have exceptional significance in the niche of materials owing to their myriad applications like train disk brakes, critical rotating parts in the aviation industry, etc. MMCs are used for items from tool materials to engine parts due to their exceptional properties such as low density, high thermal conductivity, high stiffness, and strength etc. Numerous processing techniques are available for the fabrication of metal matrix composites. And each process used for the fabrication of metal matrix composites has its characteristics. The processing technique selected is based on the purpose of the fabricated product. The quality of fabricated metal matrix composite depends upon the different parameters used in the processing technique. For the applicability of the metal matrix composites, the fabricated component should be defect-free and also have desirable values of the properties for which the material is designed. This makes the selection of processing technique and its parameter a crucial step for a superior and effective product.

REFERENCES

- Akinwamide, S. O., Abe, B. T., Akinribide, O. J., Obadele, B. A., & Olubambi, P. A. (2020). Characterization of microstructure, mechanical properties and corrosion response of aluminium-based composites fabricated via casting—a review. *The International Journal of Advanced Manufacturing Technology*, 9(6), 1–15.
- Alaneme, K. K., & Odoni, B. U. (2016). Mechanical properties, wear and corrosion behavior of copper matrix composites reinforced with steel machining chips. *Engineering Science and Technology, an International Journal*, 19, 1593–1599. <https://doi.org/10.1016/j.jestch.2016.04.006>
- Antipas, G. S. E. (2013). Review of gas atomisation and spray forming phenomenology. *Powder Metallurgy*, 56(4), 317–330. <https://doi.org/10.1179/1743290113Y.0000000057>
- Arunachalam, R., Kumar, P., & Muraliraja, R. (2019). A review on the production of metal matrix composites through stir casting – furnace design, properties, challenges, and research opportunities. *Journal of Manufacturing Processes*, 42, 213–245. <https://doi.org/10.1016/j.jmapro.2019.04.017>
- Asano, K., Enoki, H., & Akiba, E. (2009). Synthesis of HCP, FCC and BCC structure alloys in the Mg-Ti binary system by means of ball milling. *Journal of Alloys and Compounds*, 480(2), 558–563. <https://doi.org/10.1016/j.jallcom.2009.01.086>
- Assar, A. M. (1999). Fabrication of metal matrix composite by infiltration process—part 2: experimental study. *Journal of Materials Processing Technology*, 86, 152–158.

- Assari, A. H., & Eghbali, B. (2019). Solid state diffusion bonding characteristics at the interfaces of Ti and Al layers. *Journal of Alloys and Compounds*, 773, 50–58. <https://doi.org/10.1016/j.jallcom.2018.09.253>
- Atabaki, M. M., & Idris, J. (2012). Low-temperature partial transient liquid phase diffusion bonding of Al/Mg₂Si metal matrix composite to AZ91D using Al-based interlayer. *Materials and Design*, 34, 832–841. <https://doi.org/10.1016/j.matdes.2011.07.021>
- Bahrami, A., Soltani, N., Pech-Canul, M. I., & Gutiérrez, C. A. (2016). Development of metal-matrix composites from industrial/agricultural waste materials and their derivatives. *Critical Reviews in Environmental Science and Technology*, 42(2), 143–207. <https://doi.org/10.1080/10643389.2015.1077067>
- Bakshi, S. R., Lahiri, D., & Agarwal, A. (2010). Carbon nanotube reinforced metal matrix composites – a review. *International Materials Reviews*, 55(1), 41–64. <https://doi.org/10.1179/095066009X12572530170543>
- Bewilogua, K., Brauer, G., Dietz, A., Gabler, J., Goch, G., Karpuschewski, B., & Szyszka, B. (2009). Surface technology for automotive engineering. *CIRP Annals – Manufacturing Technology*, 58, 608–627. <https://doi.org/10.1016/j.cirp.2009.09.001>
- Bhoi, N. K., Singh, H., & Pratap, S. (2020). Developments in the aluminum metal matrix composites reinforced by micro/nano particles – a review. *Journal of Composite Materials*, 54(6), 813–833. <https://doi.org/10.1177/0021998319865307>
- Chang, S., Lin, L., & Huang, K. (2020). In situ TEM observation of the microstructural characteristics and mechanical properties of vacuum hot-press sintered Co–30Cr–6Mo alloys. *Vacuum*, 176, 109333. <https://doi.org/10.1016/j.vacuum.2020.109333>
- Chaudhury, S. K., Sivaramakrishnan, C. S., & Panigrahi, S. C. (2004). A new spray forming technique for the preparation of aluminium rutile (TiO₂) ex situ particle composite. *Journal of Materials Processing Technology*, 145, 385–390. <https://doi.org/10.1016/j.jmatprotec.2003.09.006>
- Das, D. K., Mishra, P. C., Singh, S., & Pattanaik, S. (2014). Fabrication and heat treatment of ceramic – reinforced aluminium matrix composites – a review. *International Journal of Mechanical and Materials Engineering*, 1(6), 1–15.
- Deng, K. K., Wu, K., Wu, Y. W., Nie, K. B., & Zheng, M. Y. (2010). Effect of submicron size SiC particulates on microstructure and mechanical properties of AZ91 magnesium matrix composites. *Journal of Alloys and Compounds*, 504, 542–547. <https://doi.org/10.1016/j.jallcom.2010.05.159>
- Dhanashekhar, M., & Kumar, V. S. S. (2014). Squeeze casting of aluminium metal matrix composites – an overview. *Procedia Engineering*, 97, 412–420. <https://doi.org/10.1016/j.proeng.2014.12.265>
- Fang, J. C., & Xu, W. J. (2002). Plasma spray forming. *Journal of Materials Processing Technology*, 129, 288–293.
- Feng, K., Chen, H., Xiong, J., & Guo, Z. (2013). Investigation on diffusion bonding of functionally graded WC–Co/Ni composite and stainless steel. *Materials and Design*, 46, 622–626. <https://doi.org/10.1016/j.matdes.2012.11.006>
- Fuke, I., Prabhu, V., & Baek, S. (2005). Computational model for predicting coating thickness in electron beam physical vapor deposition. *Journal of Manufacturing Processes*, 7(2), 140–152.
- Garg, P., Jamwal, A., Kumar, D., Sadashivuni, K. K., Hussain, C. M., & Gupta, P. (2019). Advance research progresses in aluminium matrix composites: manufacturing & applications. *Journal of Materials Research and Technology*, 8(5), 4924–4939.
- Ge, W., Wu, B., Wang, S., Xu, S., Shang, C., Zhang, Z., & Wang, Y. (2017). Characterization and properties of CuZrAlTiNi high entropy alloy coating obtained by mechanical alloying and vacuum hot pressing sintering. *Advanced Powder Technology*, 28(10), 2556–2563. <https://doi.org/10.1016/j.apt.2017.07.006>

- Ghomashchi, M. R., & Vikhrov, A. (2000). Squeeze casting: an overview. *Journal of Materials Processing Technology*, 101, 1–9.
- Gong, S., & Wu, Q. (2011). Processing, microstructures and properties of thermal barrier coatings by electron beam physical vapor deposition (EB-PVD). *Thermal Barrier Coatings*(pp. 115–131). <https://doi.org/10.1533/9780857090829.2.115>
- Gupta, R., Sharma, S., Nanda, T., & Pandey, O. P. (2019). A comparative study of dry sliding wear behaviour of sillimanite and rutile reinforced LM27 aluminium alloy composites. *Materials Research Express*, 7, 016540. <https://doi.org/10.1088/2053-1591/ab61a2>
- Gupta, R., Sharma, S., Nanda, T., & Pandey, O. P. (2020). Wear studies of hybrid AMCs reinforced with naturally occurring sillimanite and rutile ceramic particles for brake-rotor applications. *Ceramics International*, 46(10B), 16849–16859. <https://doi.org/10.1016/j.ceramint.2020.03.262>
- He, P., Feng, J. C., Zhang, B. G., & Qian, Y. Y. (2003). A new technology for diffusion bonding intermetallic TiAl to steel with composite barrier layers. *Materials Characterization*, 50, 87–92. [https://doi.org/10.1016/S1044-5803\(03\)00122-0](https://doi.org/10.1016/S1044-5803(03)00122-0)
- Henao, J., Poblan-Salas, C., Monsalve, M., Corona-Castuera, J., & Barceinas-Sanchez, O. (2019). Bio-active glass coatings manufactured by thermal spray: a status report. *Journal of Materials Research and Technology*, 8(5), 4965–4984. <https://doi.org/10.1016/j.jmrt.2019.07.011>
- Heng, H. M., Lin, Z. H., Zhou, B. L., Zhen, Z. G., Kobayashi, K., & Uchiyama, Y. (1993). Preparation of carbon fibre reinforced aluminium via ultrasonic liquid infiltration technique. *Materials Science and Technology*, 9, 609–614. <https://doi.org/10.1179/mst.1993.9.7.609>
- Hewitt, S. A., & Kibble, K. A. (2009). Effects of ball milling time on the synthesis and consolidation of nanostructured WC-Co composites. *International Journal of Refractory Metals and Hard Materials*, 27, 937–948. <https://doi.org/10.1016/j.ijrmhm.2009.05.006>
- Hu, H. (1998). Squeeze casting of magnesium alloys and their composites. *Journal of Materials Science*, 33, 1579–1589.
- Imran, M., & Khan, A. R. A. (2019). Characterization of Al-7075 metal matrix composites: a review. *Journal of Materials Research and Technology*, 8(3), 3347–3356. <https://doi.org/10.1016/j.jmrt.2017.10.012>
- Kaur, K., & Pandey, O. P. (2010). Microstructural characteristics of spray formed zircon sand reinforced LM13 composite. *Journal of Alloys and Compounds*, 503, 410–415. <https://doi.org/10.1016/j.jallcom.2010.04.249>
- Kennedy, A. R., Wood, J. D., & Weager, B. M. (2000). The wetting and spontaneous infiltration of ceramics by molten copper. *Journal of Materials Science*, 35, 2909–2912.
- Khodaei, M., Yaghobizadeh, O., Baharvandi, H. R., & Dashti, A. (2018). Effects of different sintering methods on the properties of SiC-TiC, SiC-TiB₂ composites. *International Journal of Refractory Metals*, 70, 19–31. <https://doi.org/10.1016/j.ijrmhm.2017.09.005>
- Kumar, A., Kumar, S., & Mukhopadhyay, N. K. (2018). Introduction to magnesium alloy processing technology and development of low-cost stir casting process for magnesium alloy and its composites. *Journal of Magnesium and Alloys*, 6(3), 245–254. <https://doi.org/10.1016/j.jma.2018.05.006>
- Kumar, S., Singh, R., & Hashmi, M. S. J. (2019). Metal matrix composite: a methodological review. *Advances in Materials and Processing Technologies*, 6(1), 13–24. <https://doi.org/10.1080/2374068X.2019.1682296>

- Leon-Patino, C. A., & Drew, R. A. L. (2005). Role of metal interlayers in the infiltration of metal–ceramic composites. *Current Opinion in Solid State and Materials Science*, 9, 211–218. <https://doi.org/10.1016/j.cossms.2006.04.006>
- Mahendran, G., Balasubramanian, V., & Senthilvelan, T. (2010). Influences of diffusion bonding process parameters on bond characteristics of Mg-Cu dissimilar joints. *Transactions of Nonferrous Metals Society of China*, 20, 997–1005. [https://doi.org/10.1016/S1003-6326\(09\)60248-X](https://doi.org/10.1016/S1003-6326(09)60248-X)
- Maity, J., & Pal, T. K. (2012). Transient liquid-phase diffusion bonding of aluminum metal matrix composite using a mixed Cu-Ni powder interlayer. *Journal of Materials Engineering and Performance*, 21(7), 1232–1242. <https://doi.org/10.1007/s11665-011-0037-7>
- Manu, K. M. S., Raag, L. A., Rajan, T. P. D., Gupta, M., & Pai, B. C. (2016). Liquid metal infiltration processing of metallic composites: a critical review. *Metallurgical and Materials Transactions B*, 47B, 2799–2819. <https://doi.org/10.1007/s11663-016-0751-5>
- Matsunaga, T., Matsuda, K., Hatayama, T., Shinozaki, K., & Yoshida, M. (2007). Fabrication of continuous carbon fiber-reinforced aluminum–magnesium alloy composite wires using ultrasonic infiltration method. *Composites Part A: Applied Science and Manufacturing*, 38, 1902–1911. <https://doi.org/10.1016/j.compositesa.2007.03.007>
- Matsunaga, T., Ogata, K., Hatayama, T., Shinozaki, K., & Yoshida, M. (2007). Effect of acoustic cavitation on ease of infiltration of molten aluminum alloys into carbon fiber bundles using ultrasonic infiltration method. *Composites Part A: Applied Science and Manufacturing*, 38, 771–778. <https://doi.org/10.1016/j.compositesa.2006.09.003>
- Mattox, D. M. (1999). Physical vapor deposition (PVD) Processes. *Metal Finishing*, 97(1), 417–430.
- Mehran, Q. M., Fazal, M. A., Bushroa, A. R., & Rubaiee, S. (2018). A critical review on physical vapor deposition coatings applied on different engine components. *Critical Reviews in Solid State and Materials Sciences*, 43(2), 158–175. <https://doi.org/10.1080/10408436.2017.1320648>
- Michaud, V., & Mortensen, A. (2001). Infiltration processing of fibre reinforced composites: governing phenomena. *Composites Part A: Applied Science and Manufacturing*, 32, 981–996.
- Mukhopadhyay, A., & Basu, B. (2007). Consolidation-microstructure-property relationships in bulk nanoceramics and ceramic nanocomposites: a review. *International Materials Reviews*, 52(5), 257–288. <https://doi.org/10.1179/174328007X160281>
- Munir, K. S., Kingshott, P., & Wen, C. (2015). Carbon nanotube reinforced titanium metal matrix composites prepared by powder metallurgy – a review. *Critical Reviews in Solid State and Materials Sciences*, 40(1), 38–55. <https://doi.org/10.1080/10408436.2014.929521>
- Nageswaran, G., Natarajan, S., & Ramkumar, K. R. (2018). Synthesis, structural characterization, mechanical and wear behaviour of Cu-TiO₂-Gr hybrid composite through stir casting technique. *Journal of Alloys and Compounds*, 768, 733–741. <https://doi.org/10.1016/j.jallcom.2018.07.288>
- Omrani, E., Moghadam, A. D., Menezes, P. L., & Rohatgi, P. K. (2016). Influences of graphite reinforcement on the tribological properties of self-lubricating aluminum matrix composites for green tribology, sustainability, and energy efficiency—a review. *The International Journal of Advanced Manufacturing Technology*, 83(1–4), 325–346. <https://doi.org/10.1007/s00170-015-7528-x>

- Poddar, P., Srivastava, V. C., & Sahoo, K. L. (2007). Processing and mechanical properties of SiC reinforced cast magnesium matrix composites by stir casting process. *Materials Science & Engineering A*, 460–461, 357–364. <https://doi.org/10.1016/j.msea.2007.01.052>
- Prikhodko, S. V., Savvakin, D. G., Markovsky, P. E., Olexander, O., Penney, J., Shirzadi, A. A., ... Markovsky, P. E. (2020). Diffusion bonding of TiC or TiB reinforced Ti-6Al-4V matrix composites to conventional Ti-6Al-4V alloy. *Science and Technology of Welding and Joining ISSN:*, 25(6), 518–524. <https://doi.org/10.1080/13621718.2020.1751403>
- Reddy, B. V. R., Maity, S. R., & Pandey, K. M. (2019). Characterization of spray formed Al-alloys—a review. *Reviews on Advanced Materials Science*, 58, 147–158.
- Rossnagel, S. M. (2003). Thin film deposition with physical vapor deposition and related technologies. *Journal of Vacuum Science & Technology A*, 21(5), S74–S87. <https://doi.org/10.1116/1.1600450>
- Rosso, M. (2006). Ceramic and metal matrix composites: routes and properties. *Journal of Materials Processing Technology*, 175(1–3), 364–375. <https://doi.org/10.1016/j.jmatprotec.2005.04.038>
- Samal, C. P., Parihar, J. S., & Chaira, D. (2013). The effect of milling and sintering techniques on mechanical properties of Cu-graphite metal matrix composite prepared by powder metallurgy route. *Journal of Alloys and Compounds*, 569, 95–101. <https://doi.org/10.1016/j.jallcom.2013.03.122>
- Sampath, S., & Herman, H. (1993). Plasma spray forming metals, intermetallics, and composites. *The Journal of The Minerals, Metals & Materials Society*, 45, 42–49.
- Sánchez, M., Rams, J., & Urefía, A. (2010). Fabrication of aluminium composites reinforced with carbon fibres by a centrifugal infiltration process. *Composites Part A: Applied Science and Manufacturing*, 41, 1605–1611. <https://doi.org/10.1016/j.compositesa.2010.07.014>
- Sánchez-Martínez, A., Cruz, A., González-Nava, M., & Suárez, M. A. (2016). Main process parameters for manufacturing open-cell Zn-22Al-2Cu foams by the centrifugal infiltration route and mechanical properties. *Materials and Design*, 108, 494–500. <https://doi.org/10.1016/j.matdes.2016.07.032>
- Shabani, M. O., & Mazahery, A. (2013). Fabrication of AMCs by spray forming: setting of cognition and social parameters to accelerate the convergence in optimization of spray forming process. *Ceramics International*, 39, 5271–5279. <https://doi.org/10.1016/j.ceramint.2012.12.028>
- Sharma, S., Gupta, R., Nanda, T., & Pandey, O. P. (2021). Influence of two different range of sillimanite particle reinforcement on tribological characteristics of LM30 based composites under elevated temperature conditions. *Materials Chemistry and Physics*, 258, 123988. <https://doi.org/10.1016/j.matchemphys.2020.123988>
- Shirvanimoghaddam, K., Hamim, S. U., Akbari, M. K., Fakhrhoseini, S. M., Khayyam, H., Pakseresht, A. H., ... Naebe, M. (2017). Carbon fiber reinforced metal matrix composites: fabrication processes and properties. *Composites Part A: Applied Science and Manufacturing*, 92, 70–96. <https://doi.org/10.1016/j.compositesa.2016.10.032>
- Shirzadi, A. A., Assadi, H., & Wallach, E. R. (2001). Interface evolution and bond strength when diffusion bonding materials with stable oxide films. *Surface And Interface Analysis*, 31, 609–618. <https://doi.org/10.1002/sia.1088>
- Si, C., Tang, X., Zhang, X., Wang, J., & Wu, W. (2017). Microstructure and mechanical properties of particle reinforced metal matrix composites prepared by gas-solid two-phase atomization and deposition technology. *Materials Letters*, 201, 78–81. <https://doi.org/10.1016/j.matlet.2017.04.150>

- Singh, J., & Wolfe, D. E. (2005). Nano and macro-structured component fabrication by electron beam-physical vapor deposition (EB-PVD). *Journal of Materials Science*, 40, 1–26.
- Smith, R. W., & Knight, R. (1996). Thermal spraying II: recent advances in thermal spray forming. *The Journal of The Minerals, Metals & Materials Society*, 48, 16–19.
- Thandalam, K. S., Ramanathan, S., & Sundarajan, S. (2015). Synthesis, microstructural and mechanical properties of ex situ zircon particles ($ZrSiO_4$) reinforced metal matrix composites (MMCs): a review. *Journal of Materials Research and Technology*, 4(3), 333–347. <https://doi.org/10.1016/j.jmrt.2015.03.003>
- Tirth, V. (2017). Dry sliding wear behavior of 2218 Al-alloy- $Al_2O_3(TiO_2)$ hybrid composites. *Journal of Tribology*, 140(2), 21603. <https://doi.org/10.1115/1.4037697>
- Torralba, J. M., Costa, C. E., & Velasco, F. (2003). P/M aluminum matrix composites: an overview. *Journal of Materials Processing Technology*, 133, 203–206.
- Tuncer, N., Tasdelen, B., & Arslan, G. (2011). Effect of passivation and precipitation hardening on processing and mechanical properties of B4C-Al composites. *Ceramics International*, 37, 2861–2867. <https://doi.org/10.1016/j.ceramint.2011.05.007>
- Vasile, B. S., Birca, A. C., Surdu, V. A., Neacsu, I. A., & Ionut, A. (2020). Ceramic composite materials obtained by electron-beam physical vapor deposition used as thermal barriers in the aerospace industry. *Nanomaterials*, 10(370), 1–17. <https://doi.org/10.3390/nano10020370>
- Vijayaram, T. R., Sulaiman, S., Hamouda, A. M. S., & Ahmad, M. H. M. (2006). Fabrication of fiber reinforced metal matrix composites by squeeze casting technology. *Journal of Materials Processing Technology*, 178, 34–38. <https://doi.org/10.1016/j.jmatprotec.2005.09.026>
- Wan, S., Li, H., Tieu, K., Xue, Q., & Zhu, H. (2019). Mechanical and tribological assessments of high-vanadium high-speed steel by the conventional powder metallurgy process. *International Journal of Advanced Manufacturing Technology*, 103, 943–955. <https://doi.org/10.1007/s00170-019-03547-y>
- Wang, H., Tao, Z., Li, X., Yan, X., Liu, Z., & Guo, Q. (2018). Graphite fiber/copper composites prepared by spontaneous infiltration. *Applied Surface Science*, 439, 488–493. <https://doi.org/10.1016/j.apsusc.2018.01.035>
- Wannasin, J., & Flemings, M. C. (2005). Fabrication of metal matrix composites by a high-pressure centrifugal infiltration process. *Journal of Materials Processing Technology*, 169, 143–149. <https://doi.org/10.1016/j.jmatprotec.2005.03.004>
- Wei, Y., Aiping, W., Guisheng, Z., & Jialie, R. (2008). Formation process of the bonding joint in Ti/Al diffusion bonding. *Materials Science & Engineering A*, 480, 456–463. <https://doi.org/10.1016/j.msea.2007.07.027>
- Wenzelburger, M., Silber, M., & Gadow, R. (2010). Manufacturing of light metal matrix composites by combined thermal spray and semisolid forming processes — summary of the current state of technology. *Key Engineering Materials*, 425, 217–244. <https://doi.org/10.4028/www.scientific.net/KEM.425.217>
- Yigezu, B. S., Jha, P. K., & Mahapatra, M. M. (2013). The key attributes of synthesizing ceramic particulate reinforced Al-based matrix composites through stir casting process: a review. *Materials and Manufacturing Processes*, 28, 969–979. <https://doi.org/10.1080/10426914.2012.677909>
- Yue, H., Yao, L., Gao, X., Zhang, S., Guo, E., Zhang, H., ... Wang, B. (2017). Effect of ball-milling and graphene contents on the mechanical properties and fracture mechanisms of graphene nanosheets reinforced copper matrix composites. *Journal of Alloys and Compounds*, 691, 755–762. <https://doi.org/10.1016/j.jallcom.2016.08.303>

- Zhang, B., Li, W., Li, H., & Zhang, H. (2018). Spontaneous infiltration and wetting behaviors of a Zr-based alloy melt on a porous SiC substrate. *International Journal of Minerals, Metallurgy and Materials*, 25(7), 817–823.
- Zhang, Z., Shi, Z., Yang, B., Ge, B., Zhang, X., & Guo, Y. (2019). Preparation and anisotropic thermophysical properties of SiC honeycomb/Al-Mg-Si composite via spontaneous infiltration. *Progress in Natural Science: Materials International*, 29, 177–183. <https://doi.org/10.1016/j.pnsc.2019.02.004>
- Zhu, J., Jiang, W., Li, G., Guan, F., Yu, Y., & Fan, Z. (2020). Microstructure and mechanical properties of SiCnp/Al6082 aluminum matrix composites prepared by squeeze casting combined with stir casting. *Journal of Materials Processing Technology*, 283, 116699. <https://doi.org/10.1016/j.jmatprotec.2020.116699>

3 Copper Matrix Composites

Synthesis and Applications

Prateek Mittal, Jimmy Mehta and Seema Mahto

Manav Rachna International Institute of Research and
Studies, Faridabad, India

Sahil Mehta

Thapar Institute of Engineering and Technology,
Patiala, India

CONTENTS

3.1	Introduction.....	48
3.1.1	Types of Cu MMCs.....	48
3.1.2	Reinforcement Materials	49
3.1.2.1	Fibrous Material.....	50
3.1.2.2	Particles.....	50
3.1.3	Cu Matrix.....	50
3.2	Synthesis.....	50
3.2.1	Liquid State Processing Techniques	50
3.2.1.1	Stir Casting.....	50
3.2.1.2	Liquid Infiltration Process.....	51
3.2.1.3	Squeeze Casting.....	52
3.2.1.4	In Situ Process.....	53
3.2.2	Solid State Processing Techniques	55
3.2.2.1	Powder Metallurgy (P/M)	55
3.2.2.2	Extrusion	56
3.2.2.3	Spark Plasma Sintering	56
3.2.3	Gaseous State Processing	57
3.2.3.1	Physical Vapor Deposition (PVD)	57
3.3	Applications.....	58
	References.....	59

3.1 INTRODUCTION

Metals have been an integral part of human life for thousands of years. In the past few decades, the need for some extraordinary properties in metals has seen an unusual rise due to rapid urbanization and modernization. This need for extraordinary properties in metals has led to the research and development of metal matrix composites (MMCs). MMCs are basically materials wherein metal or metal alloys act as a binding or holding material called matrix for some other foreign material, and generally known as reinforcement, although holding or binding the reinforcement is not the sole purpose of the matrix material. MMCs can be said to be a combination of two or more than two distinct phases (in case of hybrid composites) of which one is the metal phase, which acts as the holding material for the reinforcements. The properties of an MMC are generally quite different from the ones possessed by the individual components (Al-Aqeeli et al. 2015). Fibrous and particulate phases are quite popular in use in Cu MMCs (Choy 2003). As discussed above, the extraordinary properties which are desired from the Cu MMCs arise out of the reinforcements, processing techniques and need of the applications in which they are used (Ahmad et al. 2020). Cu MMCs are most commonly used in thermal management applications, electrical devices, aerospace and defense applications, medical devices, automotive components, and structures (Jamwal, Seth et al. 2020). The aforesaid applications require these composites to give high-quality performance (Jamwal et al. 2019). The properties which are generally desired from an MMC in different applications are enlisted below:

- Low weight-to-strength ratio
- High thermal stability
- High creep resistance
- High wear and corrosion resistance
- High thermal and electrical conductivity
- Low coefficient of thermal expansion, etc.

The properties mentioned above may be application specific in nature, i.e., different properties may be required in different applications.

3.1.1 TYPES OF Cu MMCs

Cu MMCs can primarily be classified on the basis of type of reinforcement used. Such a classification leads to the following different types of Cu MMCs (Figure 3.1):

- Laminated or layered
- Whisker reinforced
- Continuous fiber reinforced
- Particle reinforced
- Nanoparticle reinforced
- Nanotube reinforced

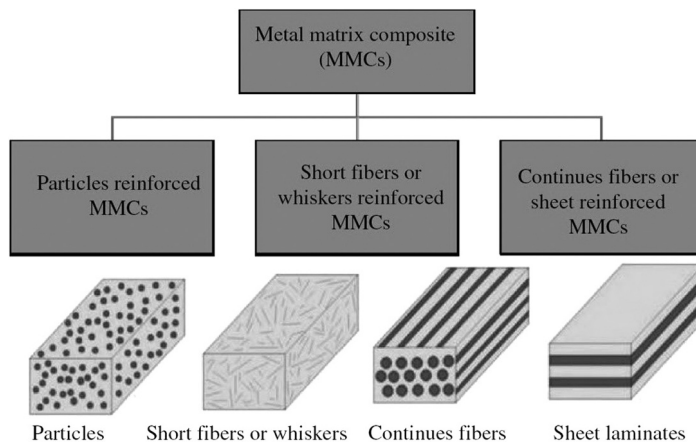


FIGURE 3.1 Classification of Cu MMCs based on the type of reinforcement (Mistry and Gohil 2018).

3.1.2 REINFORCEMENT MATERIALS

Reinforcement materials can be quite diverse depending on the type of application and the properties desired in the MMC. Table 3.1 (Chawla 2016) indicates the reinforcement materials used in the Cu MMCs.

The reinforcements are generally in the form of particles or fiber. Particle-reinforced composites are less expensive compared to continuous fiber-reinforced composites (Karbalaei Akbari et al. 2015). Length (L) to diameter (D) ratio is generally considered to differentiate between the type of reinforcements (Ramanathan et al. 2019). For instance, L/D ratio of infinity leads to long continuous fiber, while the L/D ratio of 1 leads to equiaxed material (Chawla 2016). The processing may be done by various techniques such as casting and powder metallurgy, which are discussed in the subsequent sections of this chapter.

TABLE 3.1
Reinforcement Materials Suitable for Different type of Reinforcements

Type of Reinforcement	Reinforcement Materials
Laminated or layered	Ceramics or polymers
Whisker reinforced	Carbon, silicon carbide, alumina, zirconia, etc.
Continuous fiber reinforced	Silicon carbide, alumina, zirconia, etc.
Particle reinforced	Silicon carbide, alumina, zirconia, etc.
Nanoparticle reinforced	Carbon, silicon carbide, alumina, zirconia, etc.
Nanotube reinforced	Carbon

3.1.2.1 Fibrous Material

Fibrous reinforcements are generally identified by the L/D ratio, which in this case is above 100. The thickness of fiber is generally less than 250 μm . Fibers may be of metals, ceramics, or polymers. These are generally seen to possess a small cross-sectional area and large aspect ratio. Fibrous material tends to give higher strength than the original bulk material and imparts very good flexibility to the composite. The Young's modulus of the fibers is generally low, which gives them the capability to elongate sufficiently upon application of load. Also, the low value of Young's modulus indicates a high degree of flexibility. Carbon fibers are most commonly used in Cu composites. The density of these fibers is around 2.27 g/cc. The carbon fibers also serve as the source of other reinforcements such carbon nano-tubes (CNTs), nano-wires, and graphene after the drawing or extrusion process (Chawla 2016). CNTs are tubes with less than 50nm diameter. The length ranges in a few microns. These single-walled or multi-walled hollow tubes with low relative density.

3.1.2.2 Particles

Particles are generally used in case of ceramics and some allotropes of carbon. Commonly used particles are SiC, Al_2O_3 , WC, etc. (Bhoi et al. 2020). Carbon black may be added to some materials to control the particle size while preparation of the particles (Seetharaman and Gupta 2021). Ball milling and other crushing and milling techniques may be used for the preparation of powders.

3.1.3 Cu MATRIX

Copper matrix acts as the embodiment for the reinforcements. Cu has a density of 8.96 g/cc. Cu has a face-centered cubic structure, which makes it an extraordinary conductor of heat and electricity. Copper matrix composites are mostly used in electrical and thermal applications such as superconductors, electrical contacts, wires, transmission lines, heat sinks, thermal management devices and structures etc. Apart from this, copper matrix composites are used in medical, aerospace, marine and dental implant applications. The Cu MMC made components can be formed in different intricate shapes due to the ductility and soft nature of copper.

3.2 SYNTHESIS

3.2.1 LIQUID STATE PROCESSING TECHNIQUES

3.2.1.1 Stir Casting

Stir casting is the process of producing MMCs wherein metal is melted and reinforcement particles are added to it. Metal is melted in a furnace and reinforcement particles are added to the molten metal, which is kept in a crucible (Das et al. 2006). This melt consisting of the reinforcements and molten metal is stirred for one hour or more to allow the reinforcement material particles to uniformly disperse throughout the metal matrix. The stirring action mainly contributes to the

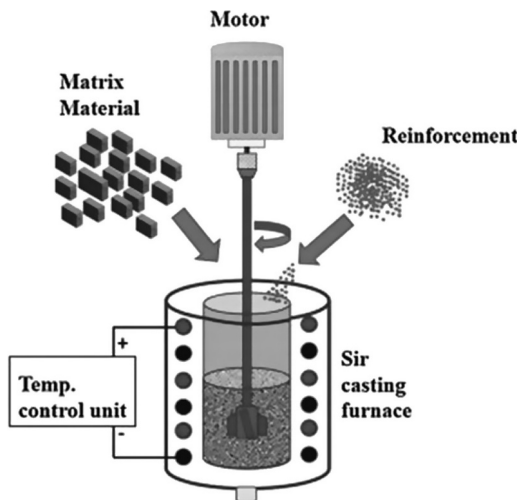


FIGURE 3.2 Schematic diagram of stir casting techniques (Ramanathan et al. 2019).

proper dispersion and wetting of the reinforcement particles within the matrix (Raju et al. 2018). This liquid state processing technique can induce some porosity in the MMC, and thus interaction of the melt with the atmospheric air needs to be inhibited by using a vacuum chamber furnace (Mohanavel et al. 2017). Also, reinforcement particles need to be pre-heated before mixing in the molten metal matrix to remove any moisture (Jamwal, Mittal et al. 2020). It has been seen in past research that the longer the time of stirring higher is the homogeneity in the dispersion of reinforcements in the matrix (Mittal, Raghav et al. 2020). Figure 3.2 indicates the schematic diagram of the stir casting process in detail. Stirring action and stirring time are the important factors on which the quality of the MMC depends (Mittal et al. 2021). In past research, it has been seen that the longer the stirring time, the better is the dispersion of the reinforcement phase in the metal matrix, and the more uniform are the mechanical and thermo-physical properties in the MMC at every cross-section (Kowalski et al. 1992).

3.2.1.2 Liquid Infiltration Process

The liquid infiltration process is another liquid state processing technique wherein an inert gas (usually Argon) is used as the pressurizing agent for the metal to infiltrate the preform (Chawla 2016). The preform may be fiber or particles. The molten metal is pushed to infiltrate the preform which is generally made in the shape of the required component to get the desired composite in the required shape and size (Akbulut et al. 1998). The preform is kept in a die, which allows the molten metal to enter, while inert gas which pressurizes the molten metal keeps the pressure until the melt is solidified in the preform. Both the die containing the preform and the molten metal are kept in a complete vacuum (Deng et al. 2018). Vacuum is of prime importance in any liquid state processing technique as there are very

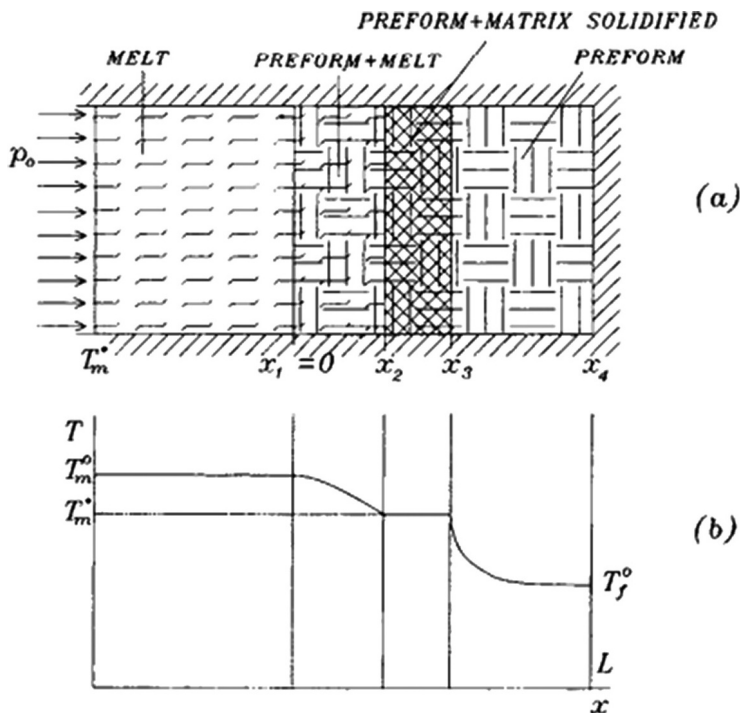


FIGURE 3.3 Schematic diagram of liquid infiltration technique (Mileiko 1997).

high chances of the liquid metal interacting with the environment. This generally creates a layer of oxides and other unwanted compounds. Also, gases may get trapped and can cause other defects to happen in the final composite. Gas entrainment is more prominent in the stir casting process. The temperature of the fibers is also one of the factors affecting the operating temperature. Higher the temperature of the fibers, the more time the molten metal will take to solidify (Ho et al. 2008). The lower the temperature of the fibers, the shorter the time taken in solidification, which may lead to premature solidification, i.e., solidification may occur prior to the complete infiltration of the preform by the molten metal. This induces porosity and brittleness in the composite. This process is quite suitable for intricate shapes which are difficult to achieve by other methods. Figure 3.3 indicates the schematic diagram of the liquid infiltration process.

3.2.1.3 Squeeze Casting

Squeeze casting is another variant of the liquid infiltration process. The difference between the two is that in liquid infiltration an inert gas is used to apply pressure and a vacuum is generated (Akbulut et al. 1998). In squeeze casting firstly a preform is made as shown in Figure 3.4. The preform is prepared by two techniques. The first one involves agitation and squeezing while the second one involves

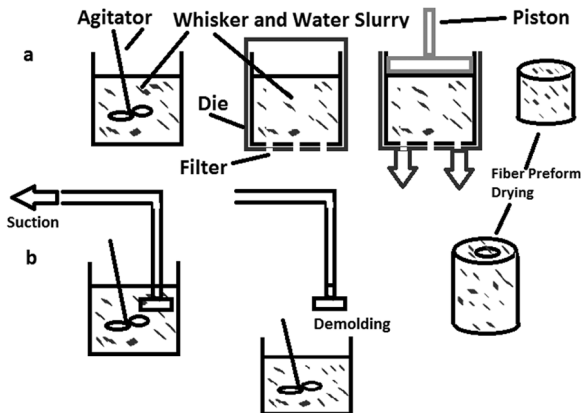


FIGURE 3.4 Generation of performs for the squeeze casting process.

agitation, suction, and demolding (Seetharaman and Gupta 2021), as indicated in Figure 3.4. Firstly, the mix of water and whiskers (short fibers) is agitated by using an agitator, so that the whiskers get completely wet and dispersed (Chawla 2016). Then this mix is put in a die and a squeezing action is applied to get the mix into the desired shape followed by a drying process to provide it with sufficient strength and stability.

After the generation of the preform, it is kept in a preheated die and liquid metal is poured into the die, which is supposed to fill the spaces inside the preform and also completely wet it. The wettability of the metal with the reinforcement preform is of prime importance here. The higher the wettability of the metal with the material of the perform the more homogeneous the composite will be in its composition (Xing et al. 2005). The infiltration of the molten metal is done through a ram, as shown in Figure 3.5. The pressure of the ram is kept up to 100 MPa. The molten metal is kept at a higher temperature than the preform in order to achieve a fine grain structure (Ho et al. 2008).

3.2.1.4 In Situ Process

The in situ process is generally of two types, namely reactive and non-reactive. In the reactive process, the ceramic particles are formed in the matrix alloy with high reinforcement concentration. The parent alloy is then diluted by the addition of this matrix alloy in it. The concentration of the reinforcement particles is controlled by the amount of dilution in the parent alloy. The particle size ranges from 0.25 microns to 1.0 microns. For example, boron and titanium are made to react with each other in the presence of aluminum, giving TiB_2 in the aluminum matrix. Also, the temperature of the reaction can be one of the controlling variables for controlling the particle size. This process has an edge over other processes, i.e., the drawbacks associated with the poor wettability of the matrix material with the reinforcement particles are eliminated due to the reaction between each element.

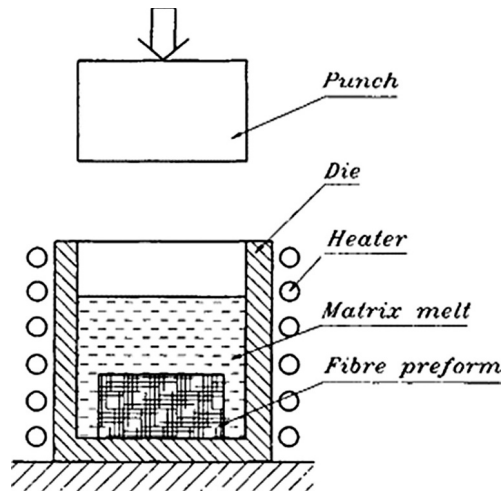


FIGURE 3.5 Schematic diagram of the squeeze casting process (Mileiko 1997).

The non-reactive process is the one wherein a precast reinforcement is kept in a crucible, which has a heating arrangement through induction. The preform is melted in the crucible. This process works on two phase systems. These systems are kept separated from each other by creating a temperature gradient. The molten metal is allowed to enter the precast reinforcement (Mittal, Paswan et al. 2020). The heating is provided by the induction heater and the crucible is chilled from the bottom. The temperature gradient thus generated keeps both the phases apart and the composite is obtained. Non-traditional methods like electron beam heating may also be used when working with elements having very high reactivity like titanium (Chawla 2016). Figure 3.6 shows the schematic diagram of the in situ production process.

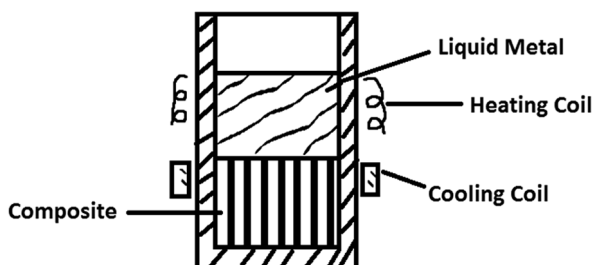


FIGURE 3.6 Schematic diagram of In Situ process.

3.2.2 SOLID STATE PROCESSING TECHNIQUES

3.2.2.1 Powder Metallurgy (P/M)

This process is generally used to produce powder-reinforced MMCs. In powder metallurgy, metal powders are mixed or blended together (Figure 3.7) to form a homogeneous mixture. The metal powders may be obtained through the ball milling process. After achieving a homogeneous mixture, the mixture is cold pressed, which is also known as the green body. This green body has 80% of the final achievable density of the composite (Tu et al. 2002). The green body is then put in a container, sealed, and any gases present are removed. The metal powders, especially aluminum powder, have an oxide layer which does not get removed on degassing (Onat et al. 2007). This oxide layer can break down and enter the composite to be formed, thereby deteriorating its quality and composition (Anderson and Foley 2001). Hot pressing is then done which makes the composite completely dense (Moon and Do Kim 1985). Hot pressing is followed by an extrusion process. In extrusion, there is very little or no deformation in the reinforcement particles while the matrix material gets significantly deformed (Estrada et al. 1991). The ratio of particle size in reinforcement to the particle size in matrix is also an important factor in determining the quality of the composite. This ratio is preferably kept in unity. Powder metallurgy is considered to be costly because a lot of expenditure is involved in the preparation of the powders. Many researchers prefer other less expensive methods of producing MMCs such as stir casting. The following are the main parts of the P/M process:

1. Die and mould
2. Punch for compaction
3. Heater

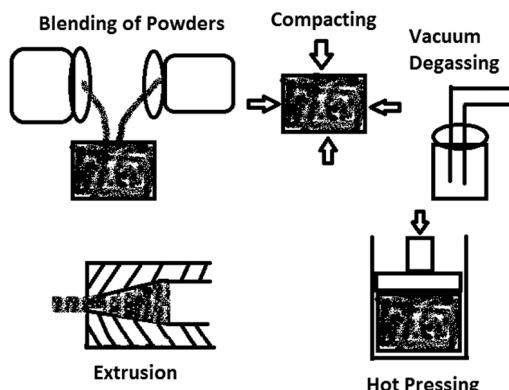


FIGURE 3.7 Schematic diagram of the powder metallurgy process.

3.2.2.2 Extrusion

The extrusion process is a conventional metal forming process wherein metal is pushed into an opening to get deformed into the desired shape and size. The process also provides sufficient strength to the metal due to strain hardening. A lot of MMCs are produced using extrusion as the fabrication technique. Primarily there are three types of extrusion process, as used for the synthesis of MMCs. The first one is the direct extrusion wherein metal is forced to pass from a small opening, thereby creating a dead region where metal cannot flow. In the conventional extrusion process, the die is tapered in shape thereby allowing the metal to flow easily but the problem of crimped or wrinkled edges is seen in conventional extrusion. This happens because of increased shear stresses at the die-metal interface. In this process, die friction plays an important role in the ragged edges of the formed composite. This effect is seen predominantly in the MMCs with a high concentration of the reinforcement particles which contribute to the increased frictional resistance and thus shear stresses. Figure 3.8 indicates the extrusion process. The extrusion process has an inherent advantage of breaking the oxide layers due to the high shear stresses generated during the process.

3.2.2.3 Spark Plasma Sintering

Sintering is conventionally used for producing ceramic products wherein powders are heated and compacted to allow diffusion bonding to form the final product. Spark plasma sintering (SPS) is the process which uses the simultaneous application of high heating rate and high pressure to produce the composite (Faraji et al. 2018). In the SPS process, a high DC pulse is generated between the graphite electrodes using a DC power source. Initially the powders are taken in a graphite crucible and kept in the SPS furnace wherein they are heated by the internal heat produced by the pulse. This heat rate can be as high as 400°C/minute, which makes reaching temperatures of the order of 1200°C/minute a matter of minutes. This heat rate is quite high as compared to the conventional sintering process where the heat rates are around 10°C/minute. This is the prime reason that creates a difference between conventional sintering and SPS as far as time consumption in the process is concerned (Moustafa et al. 2002). During heating, the temperature is kept below the melting point, which makes the diffusion of the atoms possible on the application of high pressures. The furnaces are vacuum sealed or are provided with an inert gas environment. The process has another advantage over conventional sintering in that high relative densities are achievable in a short span of time due to the simultaneous application of high temperature and pressure

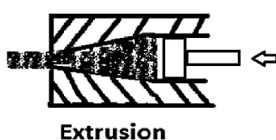


FIGURE 3.8 Schematic of extrusion process.

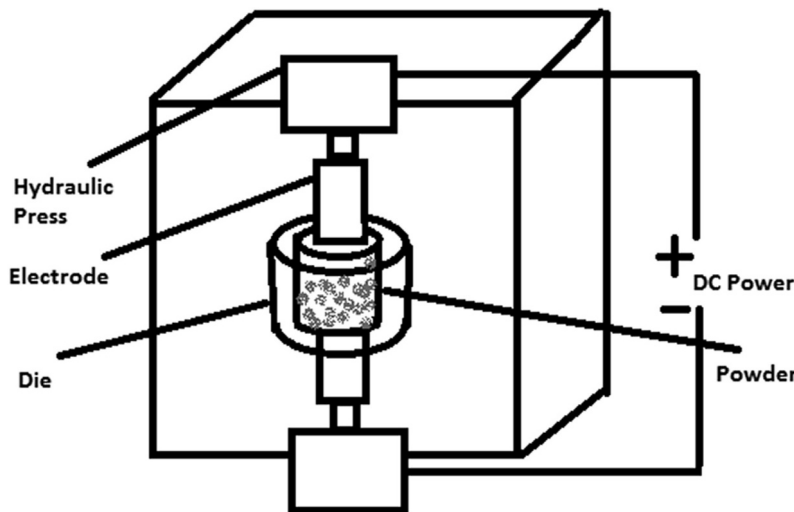


FIGURE 3.9 Schematic diagram of spark plasma sintering technique.

and thus inhibiting the grain growth. This makes this process suitable for nano-powders as well. Figure 3.9 indicates the schematic diagram of the SPS process. SPS process is known to produce high quality composites provided the variables are controlled in the appropriate manner. The SPS process is one of the very few processes to generate the MMCs, wherein heat and mass transfer take place simultaneously. This is only possible due to the diffusion of atoms which takes place at a high temperature due to the DC pulse spark produced at the interface of the electrode and the powder.

3.2.3 GASEOUS STATE PROCESSING

3.2.3.1 Physical Vapor Deposition (PVD)

Physical vapor deposition (PVD) is a process that utilizes metal vapor to be deposited on a substrate which is usually a conducting substance (Mahan 2000; Mehta et al. 2021). Figure 3.10 indicates the schematic diagram of the PVD process. Common physical processes are ion plating and sputtering. The temperature of the surface on which vapor is to be deposited is kept quite lower than the material from which vapors are generated. The transfer of material happens at the atomic level. The following are the steps involved in the PVD process (Shang and Zeng 2013):

1. Vapors of the material to be deposited are formed through plasma or generation of vacuum at high temperature.
2. The vapors are transported to the surface (substrate) on which they need to be deposited.
3. The vapor after undergoing condensation gets deposited forming a thin film.

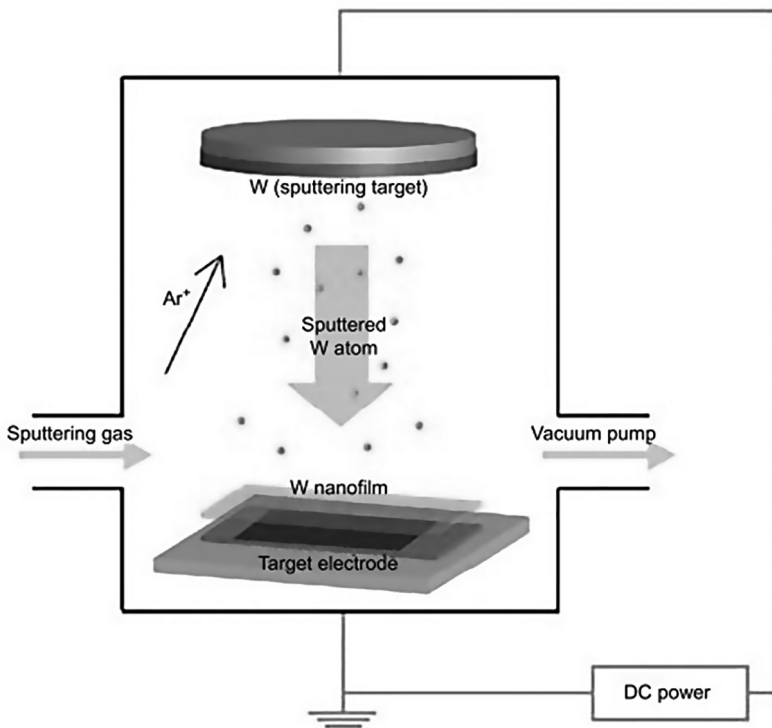


FIGURE 3.10 Schematic diagram of physical vapor deposition (Rafique et al. 2020).

3.3 APPLICATIONS

Characteristics possessed by Cu MMCs make them suitable for a large number of applications. Cu MMCs are the most preferred ones for applications requiring good thermal and electrical properties (Zhou, Yao, Xiao, et al., 2019). Copper has a face-centered cubic (FCC) structure and is flexible and ductile enough to be formed in different shapes and sizes including the most intricate ones. Tribological properties of Cu MMCs are also enhanced when ceramic reinforcements are used and can provide exceptional wear resistance (Ahamad et al. 2021). The following points indicate the application areas of Cu matrix composites:

1. The thrust chambers of rocket engines need to withstand extremely high heat flux. Cu-based composites are the most preferred materials for rocket thrust chambers (SUN et al. 2000).
2. In electronic packaging, highly conductive materials are required to take away the heat released in the electronic devices. Cu composites serve this purpose to a great extent.

3. Devices with extraordinarily high heat generation like heavy-duty motors, fancy lighting setups, etc. need copper as a part of their structure to conduct heat quickly to the environment (Qu et al. 2011).
4. Nb-Ti filaments in Cu matrix are used for producing superconducting magnets, which are used in magnetic resonance imaging machines in hospitals (Patel et al. 2019).
5. Electrical contacts and conductors not only require a material to be a good conductor but also require the material to have a high melting temperature. Copper is a better conductor than aluminum and also has a melting point above 1000°C, which is sufficiently higher than aluminum. Hence, it is the preferred material for electrical contacts and conductors. Its only demerit is the cost, as it is more expensive than aluminum.
6. Heat sinks and heat exchangers require a material with high thermal conductivity, low coefficient of thermal expansion, and sufficient strength (v Müller et al. 2020). Cu composites fulfill these requirements and hence are popularly used in these areas (Qu et al. 2011; Hidalgo-Manrique et al. 2019).
7. Dental implantation is another application where copper composites are used. Copper coated carbon nano tubes are used in some dental implant applications (Sasani et al. 2014; Singh et al. 2017)
8. Brake pads in high-speed trains are also made up of Cu MMCs (Xiao et al. 2018; Zhou, Yao, Gong, et al., 2019)).

REFERENCES

- Ahamad, N., Mohammad, A., Sadasivuni, K. K., & Gupta, P. (2020). Phase, microstructure and tensile strength of Al-Al₂O₃-C hybrid metal matrix composites. *Proceedings of the Institution of Mechanical Engineers, Part C: Journal of Mechanical Engineering Science*, 234(13), 2681–2693.
- Ahamad, N., Mohammad, A., Sadasivuni, K. K., & Gupta, P. (2021). Wear, optimization and surface analysis of Al-Al₂O₃-TiO₂ hybrid metal matrix composites. *Proceedings of the Institution of Mechanical Engineers, Part J: Journal of Engineering Tribology*, 235(1), 93–102.
- Akbulut, H., Durman, M., & Yilmaz, F. (1998). High temperature Young's modulus of alumina short fibre reinforced Al-Si MMCs produced by liquid infiltration. *Materials Science and Technology*, 14(4), 299–305.
- Al-Aqeeli, N., Mohammad, K., Laoui, T., & Saheb, N. (2015). The effect of variable binder content and sintering temperature on the mechanical properties of WC-Co-VC/Cr₃C₂ nanocomposites. *Materials and Manufacturing Processes*, 30(3), 327–334.
- Anderson, I. E., & Foley, J. C. (2001). Determining the role of surfaces and interfaces in the powder metallurgy processing of aluminum alloy powders. *Surface and Interface Analysis: An International Journal Devoted to the Development and Application of Techniques for the Analysis of Surfaces, Interfaces and Thin Films*, 31(7), 599–608.
- Bhoi, N. K., Singh, H., & Pratap, S. (2020). Developments in the aluminum metal matrix composites reinforced by micro/nano particles – a review. *Journal of Composite Materials*, 54(6), 813–833.
- Chawla, N. (2016). *Metal Matrix Composites*. Springer-Verlag, New York.

- Choy, K. L. (2003). Chemical vapour deposition of coatings. *Progress in Materials Science*, 48(2), 57–170.
- Das, S., Udhayabanu, V., Das, S., & Das, K. (2006). Synthesis and characterization of zircon sand/Al-4.5 wt% Cu composite produced by stir casting route. *Journal of Materials Science*, 41(14), 4668–4677.
- Deng, H., Yi, J., Xia, C., & Yi, Y. (2018). Improving the mechanical properties of carbon nanotube-reinforced pure copper matrix composites by spark plasma sintering and hot rolling. *Materials Letters*, 210, 177–181.
- Estrada, J. L., Duszczycy, J., & Korevaar, B. M. (1991). Gas entrapment and evolution in prealloyed aluminium powders. *Journal of Materials Science*, 26(6), 1431–1442.
- Faraji, G., Kim, H. S., & Kashi, H. T. (2018). *Introduction Severe Plastic Deformation*. Elsevier, Amsterdam.
- Hidalgo-Manrique, P., Lei, X., Xu, R., Zhou, M., Kinloch, I. A., & Young, R. J. (2019). Copper/graphene composites: a review. *Journal of Materials Science*, 54(19), 12236–12289.
- Ho, P. W., Li, Q. F., & Fuh, J. Y. H. (2008). Evaluation of W–Cu metal matrix composites produced by powder injection molding and liquid infiltration. *Materials Science and Engineering: A*, 485(1–2), 657–663.
- Jamwal, A., Mittal, P., Agrawal, R., Gupta, S., Kumar, D., Sadasivuni, K. K., & Gupta, P. (2020). Towards sustainable copper matrix composites: manufacturing routes with structural, mechanical, electrical and corrosion behaviour. *Journal of Composite Materials*, 54(19), 2635–2649.
- Jamwal, A., Prakash, P., Kumar, D., Singh, N., Sadasivuni, K. K., Harshit, K., ... & Gupta, P. (2019). Microstructure, wear and corrosion characteristics of Cu matrix reinforced SiC-graphite hybrid composites. *Journal of Composite Materials*, 53(18), 2545–2553.
- Jamwal, A., Seth, P. P., Kumar, D., Agrawal, R., Sadasivuni, K. K., & Gupta, P. (2020). Microstructural, tribological and compression behaviour of copper matrix reinforced with graphite-SiC hybrid composites. *Materials Chemistry and Physics*, 251, 123090.
- Karbalaei Akbari, M., Rajabi, S., Shirvanimoghaddam, K., & Baharvandi, H. R. (2015). Wear and friction behavior of nanosized TiB₂ and TiO₂ particle-reinforced casting A356 aluminum nanocomposites: a comparative study focusing on particle capture in matrix. *Journal of Composite Materials*, 49(29), 3665–3681.
- Kowalski, L., Korevaar, B. M., & Duszczycy, J. (1992). Some new aspects of the theory of oxidation and degassing of aluminium-based alloy powders. *Journal of Materials Science*, 27(10), 2770–2780.
- Mahan, J. E. (2000). *Physical Vapor Deposition of Thin Films* (p. 336). Wiley, New York.
- Mehta, J., Grewal, J. S., Mittal, P., Malhotra, P., & Gupta, P. (2021). Comparison of dry and lubricated wear behaviour of 22MnB5 uncoated ultra high strength steel. *Materials Today: Proceedings*, 47(12) doi:10.1016/j.matpr.2021.03.293.
- Mileiko, S. T. (1997). Liquid Infiltration. In *Composite Materials Series* (Vol. 12, pp. 547–586). Elsevier, Oxford.
- Mistry, J. M., & Gohil, P. P. (2018). Research review of diversified reinforcement on aluminum metal matrix composites: fabrication processes and mechanical characterization. *Science and Engineering of Composite Materials*, 25(4), 633–647.
- Mittal, P., Paswan, M. K., Sadasivuni, K. K., & Gupta, P. (2020). Structural, wear and thermal behaviour of Cu–Al₂O₃–graphite hybrid metal matrix composites. *Proceedings of the Institution of Mechanical Engineers, Part L: Journal of Materials: Design and Applications*, 234(8), 1154–1164.

- Mittal, P., Raghav, V., Chawla, D., Mehta, J., Paswan, M. K., & Gupta, P. (2020). Structural, wear and thermal behavior of copper metal matrix composites: a review. *Advances in Engineering Materials: Select Proceedings of FLAME 2020*, 319.
- Mittal, P., Sengar, S. S., Sorabh, M. K. P., Mehta, J., Chawla, D., & Gupta, P. (2021). Challenges and opportunities in synthesis of hybrid Cu-Al₂O₃-C and Cu-ZrO₂-C composites through stir casting route. *Advances in Engineering Materials*, 1, 1154–1164.
- Mohanavel, V., Rajan, K., Senthil, P. V., & Arul, S. (2017). Mechanical behaviour of hybrid composite (AA6351+ Al₂O₃+ Gr) fabricated by stir casting method. *Materials Today: Proceedings*, 4(2), 3093–3101.
- Moon, I. H., & Do Kim, Y. (1985). Relationship between workability and structural features of tungsten produced by activated sintering. In *Modern Developments in Powder Metallurgy* (pp. 77–87). Metal Powder Industries Federation, Princeton, NJ, USA.
- Moustafa, S. F., Abdel-Hamid, Z., & Abd-Elhay, A. M. (2002). Copper matrix SiC and Al₂O₃ particulate composites by powder metallurgy technique. *Materials Letters*, 53(4–5), 244–249.
- Onat, A., Akbulut, H., & Yilmaz, F. (2007). Production and characterisation of silicon carbide particulate reinforced aluminium–copper alloy matrix composites by direct squeeze casting method. *Journal of Alloys and Compounds*, 436(1–2), 375–382.
- Patel, D., Kim, S. H., Qiu, W., Maeda, M., Matsumoto, A., Nishijima, G., ... & Kim, J. H. (2019). Niobium-titanium (Nb-Ti) superconducting joints for persistent-mode operation. *Scientific Reports*, 9(1), 1–7.
- Qu, X. H., Zhang, L., Mao, W. U., & Ren, S. B. (2011). Review of metal matrix composites with high thermal conductivity for thermal management applications. *Progress in Natural Science: Materials International*, 21(3), 189–197.
- Rafique, M. S., Rafique, M., Tahir, M. B., Hajra, S., Nawaz, T., & Shafiq, F. (2020). Synthesis methods of nanostructures. In *Nanotechnology and Photocatalysis for Environmental Applications* (pp. 45–56). Elsevier, Oxford, UK.
- Raju, P. V. K., Rajesh, S., Rao, J. B., & Bhargava, N. R. M. R. (2018). Tribological behavior of Al-Cu alloys and innovative Al-Cu metal matrix composite fabricated using stir-casting technique. *Materials Today: Proceedings*, 5(1), 885–896.
- Ramanathan, A., Krishnan, P. K., & Muraliraja, R. (2019). A review on the production of metal matrix composites through stir casting–furnace design, properties, challenges, and research opportunities. *Journal of Manufacturing Processes*, 42, 213–245.
- Sasani, N., Khaki, J. V., & Zebarjad, S. M. (2014). Characterization and nanomechanical properties of novel dental implant coatings containing copper decorated-carbon nanotubes. *Journal of the Mechanical Behavior of Biomedical Materials*, 37, 125–132.
- Seetharaman, S., & Gupta, M. (2021). *Fundamentals of metal matrix composites*. <https://doi.org/10.1016/B978-0-12-819724-0.00001-X>
- Shang, S. M., & Zeng, W. (2013). Conductive nanofibres and nanocoatings for smart textiles. In *Multidisciplinary Know-How for Smart-Textiles Developers* (pp. 92–128). Woodhead Publishing, Sawston, Cambridge, United Kingdom.
- Singh, A., Prabhu, T. R., Sanjay, A. R., & Koti, V. (2017). An overview of processing and properties of Cu/CNT nano composites. *Materials Today: Proceedings*, 4(2), 3872–3881.
- Sun, S., Mao, L., Liu, Z., Hu, J., & Liu, J. (2000). High strength and high conductivity copper based composites. *Journal-Hebei University of Science and Technology*, 21(1), 19–22.
- Tu, J. P., Wang, N. Y., Yang, Y. Z., Qi, W. X., Liu, F., Zhang, X. B., ... & Liu, M. S. (2002). Preparation and properties of TiB₂ nanoparticle reinforced copper matrix composites by in situ processing. *Materials Letters*, 52(6), 448–452.

- v Müller, A., Böswirth, B., Cerri, V., Greuner, H., Neu, R., Siefken, U., ... & You, J. H. (2020). Application of tungsten–copper composite heat sink materials to plasma-facing component mock-ups. *Physica Scripta*, 2020(T171), 014015.
- Xiao, Y., Zhang, Z., Yao, P., Fan, K., Zhou, H., Gong, T., ... & Deng, M. (2018). Mechanical and tribological behaviors of copper metal matrix composites for brake pads used in high-speed trains. *Tribology International*, 119, 585–592.
- Xing, H., Cao, X., Hu, W., Zhao, L., & Zhang, J. (2005). Interfacial reactions in 3D-SiC network reinforced Cu-matrix composites prepared by squeeze casting. *Materials Letters*, 59(12), 1563–1566.
- Zhou, H., Yao, P., Gong, T., Xiao, Y., Zhang, Z., Zhao, L., ... & Deng, M. (2019). Effects of ZrO_2 crystal structure on the tribological properties of copper metal matrix composites. *Tribology International*, 138, 380–391.
- Zhou, H., Yao, P., Xiao, Y., Fan, K., Zhang, Z., Gong, T., ... & Ling, P. (2019). Friction and wear maps of copper metal matrix composites with different iron volume content. *Tribology International*, 132, 199–210.

4 A Review on Aluminum Metal Matrix Composites

A Multidimensional Attribute Approach

*Gurpreet Singh Sokhal, Gurprinder Singh
Dhindsa and Gurmail Singh Malhi*
Chandigarh University, Gharuan, India,

Kamaljit Singh Sokhal
Thapar Institute of Engineering & Technology,
Patiala, India

CONTENTS

4.1	Introduction.....	64
4.2	Literature Review.....	64
4.3	Methodology	67
4.3.1	Identification of Research Papers	67
4.3.2	Grouping of Research Papers	67
4.3.3	Cause and Effect Analysis for Attributes	67
4.3.4	Attributes	67
4.3.5	Coding of Research Paper.....	68
4.4	Procedure to Develop a Decision Matrix.....	71
4.5	Advantages of Decision Matrix	72
4.6	Gap Analysis	72
4.7	Examples of Decision Matrix	73
4.7.1	SWOT Analysis	73
4.7.2	SWOT Analysis for Manufacturer	74
4.7.3	SWOT Analysis for Designer	74
4.7.4	SWOT Analysis for Researcher	74
4.7.5	Step by Step Procedure for Attributes-Based Literature Review	75
4.8	Conclusion	77
	References.....	77

4.1 INTRODUCTION

The focus of this paper is on aluminum metal matrix composites. The attributes discussed in this chapter are from the manufacturing viewpoint for the various tests performed on the composites. Aluminum metal matrix composite is composed of two phases: the matrix phase, and the reinforcement phase. In a matrix phase, an excess amount of reinforcement material is embedded in it. The main function of the matrix phase is to hold the reinforcement materials.

The other phase is the reinforcement phase, which is present in less quantity but has a considerable effect on the properties of the composites. The main function of the reinforcement phase is to provide strength to the composites. It also improves other properties like wear resistance, hardness, Young's Modulus, etc. Aluminum metal matrix composites play an important role in the industrial and research fields to invent light metal alloys with improved properties. This is the reason composites are used at a large scale in various fields like aerospace and the automobile industries, etc., when there is a discussion on the charge of heavy alloys with light weighted to allow the aluminum alloys can be improved as per requirements with the addition of suitable reinforcement materials. Aluminum alloys are good from a cost point of view. And this is even better due to the reinforcement materials used to improve the properties of the metal. Sometimes even industrial waste materials are also good as reinforcement materials, like Fly Ash, China Clay, etc.

4.2 LITERATURE REVIEW

Johnson et al. [1] explained the design of composite wings and the effects of impact load on it.

Das et al. [2] meanwhile has explained the effect of heat treatment on Al alloy and Al. Alloy composites also explained the effect of the angle of impingement from 15 to 90 degrees on the solid particle erosion. Hassen et al. [3, 4] have explained the influence on the mechanical properties of Al-6061 matrix reinforced with Al_2O_3 and graphite. Gupta et al. [5] studied the production of a new generation of metal-stable aluminum-titanium materials. Richard et al. [6] studied the mechanical behavior of precipitation-strengthened Al-0.17wt% Sc alloys containing 30 vol % Al_2O_3 dispersions studied during 250,300 and 350°C aging treatments.

Urappa et al. [7] discussed the challenges and opportunities of aluminum matrix composites and variation in their properties with various reinforcements. Flores Zamora et al. [8] discussed the SEM characterization of pure Aluminum alloy reinforcement with Al_2Co_3 partials having size range 100–80 μm . Snaher et al. [9] has studied the stir caster design for the production of metal matrix composites with uniform distribution of partials by varying stirring speed from 200 to 800 rpm and varying other parameters, i.e., volume fraction and shear period for producing aluminum composites. Jalham et al. [10] studied the effect of reinforcement

content on the hot strength of Al-based composite by comparing the various network approaches like radial base function network, multi-layer precipitation network, and neuro. The fuzzy systems approach etc. effect of Al_2O_3 on strain rate, flow stress, and temperature on composite was also studied.

Kannan et al. [11] investigated the effect of cutting parameters and particulate properties like particle size and volume fraction on the microhardness variation of the aluminum matrix on a machined surface. Mandal et al. [12] studied the effect of steel fibers reinforced on microstructure and mechanical properties like tension, strength, and relative strength. The steel fibers are used are of three types: uncoated, copper-coated, and nickel-coated as reinforced material. It has been observed that there is a significant effect on the properties of Al-Mg alloy when steel fibers are added with the vortex method. Prabu et al. [13] studied the effect of stirring time and speed on the distribution of reinforced particles. It was observed that the stirring time was 10 min and the stirring speed 540 rpm. The distribution of particles was uniform and cluster formation reduced.

Mota et al. [14] discussed the diametric tensile strength and microhardness of nano-filled composites by using two techniques ANOVA and turkey statistical tests to compare the results.

Rajan et al. [15] studied the solidification casting interfacial heat transfer characteristics of aluminum matrix composites reinforced with different volume fractions of Sic and graphite. The cooling curves were compared and the effect of the cooling rate was observed during casting.

Kozdin et al. [16] studied the effect of Al_2CO_3 particles in Al-2024 on the wear resistance properties. The tests were carried out on pin on disk apparatus with varying loads and abrasive papers on disk. Rajan et al. [17] looked at the effect of fly ash particles sized 13 μm embedded in Al-75–0.35 mg alloy. The casting routes are used to compare the results, i.e., stir casting, compo casting. Meanwhile, Kannan et al. [18] studied the tribological aspects of machining aluminum meta matrix composites like tool wear, surface integrity, and chip formation under both dry and wet conditions. Taha et al. [19] studied the workability of aluminum reinforced with SIC and Al_2O_3 prepared by different methods like stir casting, powder metallurgy, and squeeze casting with different volume fractions of reinforced particles. Harsha et al. [20] studied the effect of the orientation of fibers on the erosive behavior of epoxy-based composites. Rao et al. [21] studied the effect of sliding distance on the wear and friction behavior of heat-treated Al-SiCp composites with the variation of applied pressure.

Wahab et al. [22] studied the effect of stirring speed, time, and temperature on the characteristics of aluminum metal composites reinforced with aluminum particles. Reddy et al. [23, 24] carried out an experiment on SSM slurry performed under continuous cooling conditions from liquids temperature. The adhesive wear test has been performed under different loads.

Rahiman et al. [25] examined the effect of particle size, sintering temperature, and time on metallurgical properties. Dolata et al. [26] investigated the parameters

used for selection of a ceramic stirrer, while another investigation was pursued for prototype and different software like FEM. Regarding solid works to analyze the strength of ceramic stirrer, Zaho et al. [27] studied the properties of $\text{Al}_2\text{O}_3/\text{ZrO}_3$ -reinforced ceramic composites prepared by combustion synthesis under high gravity. After manufacturing, the effect on properties like toughness, stress, flexure strength etc. was studied. Wanga et al. [28, 29] studied the effect of various volume fractions of SiC content on the water resistance properties of Al359 alloy produced by the semi-solid recast technique.

Kumar et al. [30] studied Al6061 and Al7075 reinforced with SiC and Al_2O_3 , respectively. The effect on various properties like density, hardness, and wear resistance was also studied. Prabhu et al. [31, 32] examined the strength on heat treatment and abrasive wear behavior of Al6061 alloy reinforced with SiC particles. Kumaret al. [33] looked at the effect of particle size and volume fraction on Al7075 reinforced and with SiC particles and studied the wear behavior by using response surface methodology. Seelan et al. [34] researched the comparison of performance characteristics between two different manufacturing processes, powder metallurgy and stir casting. Jokhio et al. [35] studied the effect of the composition of Al_2O_3 on the mechanical properties of 7000 series aluminum alloys by using the stir casting method.

Umarnath et al. [36] studied the friction and wear behavior of hybrid composites produced by Al 601 alloy reinforced with SiC and Al_2O_3 particles in dry conditions. Rehiman et al. [37] studied the effect of production parameters of powder metallurgy on microstructure and wear resistance.

Vineet [38] has discussed the effect of heat treatment on the morphology and micrography of Al2218 alloy reinforced with 5% Al_2O_3 hybrid MMCs. Metin [39] investigated the effect of surface roughness factors in machining Al 2024 reinforced with Al_2O_3 particles by using the Taguchi method, orthogonal arrays, and ANOVA to compare the wear resistance and machining parameters. Goyal et al. [40] studied the effect on the microhardness of ceramic micro and nanocomposites by using the Halpin–Tsai modal. Gupta et al. [41] studied the effect of active cooling through nickel-coated corban fibers in the solidification process of aluminum matrix composites.

Kumar et al. [42] studied the effect of mechanical properties of Al 6061 reinforced with fly ash and glass fiber by varying volume fractions. Rao et al. [43] studied the effects of SiC content and sliding speed on the wear behavior of aluminum composites. Zhra et al. [44] investigated the effect of particle size on the tribological behavior of the Ni_3Al matrix on high-temperature self-lubricating composites.

Ruteeka et al. [45] studied the effect of Al/SiC composite on various parameters like fatigue, creep, and monotonic loading conditions. Sajjadi et al. [46] compared the microstructure and mechanical properties of Al 356/ Al_2O_3 composites fabricated by stir casting and compo-casting processes.

As discussed above, the present way of doing a literature review has many limitations because it does not provide the appropriate knowledge about all the attributes that are described in any paper.

4.3 METHODOLOGY

In this chapter, a new methodology is proposed over the present way of doing a literature review. This methodology is more useful and knowledge based. The methodology used in this paper is called matrix methodology. In this methodology, an ‘M*N’ matrix is obtained. There are many steps followed to develop the final matrix. From the matrix, we easily find out the academic value of any paper based on the attributes discussed in the paper. The various steps to form an ‘M*N’ matrix are followed.

4.3.1 IDENTIFICATION OF RESEARCH PAPERS

The first step is to identify the various papers and research publications related to the field of aluminum metal matrix composites. The research papers characterized from the past few years onwards. The research papers are identified from various journals and publications.

4.3.2 GROUPING OF RESEARCH PAPERS

The next step is the grouping of research papers according to the year of publications. The papers are divided into four groups. In the first group, the paper is grouped from 1995 to 2000 and the second group from 2001 to 2005, the third group is from 2006 to 2010, and the fourth group is from 2011 onwards. In the present paper, 50 papers are grouped into four groups according to their year of publication. The grouping of the papers is done to provide knowledge about the changing trends of the research for past years to the present. The steps provide knowledge about the various developments done in the field of the aluminum metal matrix.

4.3.3 CAUSE AND EFFECT ANALYSIS FOR ATTRIBUTES

Cause and effect attributes analyses are used for identifying attributes and their effects to decide their academic value. In this chapter, we discuss the various causes that are important for producing a good-quality composition and then the various effects which are related to that cause are formed in branches. Cause and effect analysis is one such tool which is most commonly used to produce quality products for many years. Using a cause and effect diagram identifies all the groups and subgroups of attributes to be studied. Figure 4.1 shows the cause-and-effect diagram of aluminum metal matrix composite.

4.3.4 ATTRIBUTES

The next step in the methodology is to identify the attributes from the different research publications. The attributes are identified as those having a significant effect on various characteristics of aluminum composites. The attributes are

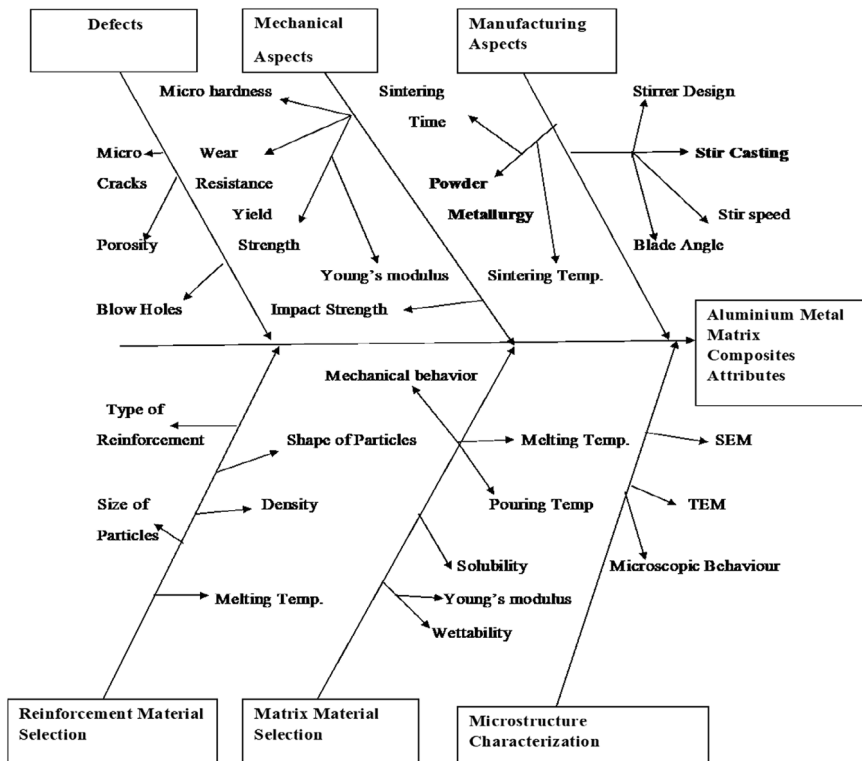


FIGURE 4.1 Cause and effect analysis for attributes.

identified from the manufacturing to the applications of the aluminum composites in various fields; for example, stir blade angle and stir speed – stir time has a significant effect on the distribution of the reinforcement particles in the matrix metal. Besides these, there are many other factors like strength of reinforcement, particle size, type of matrix metal, and reinforcement, etc. Table 4.1 shows the various attributes which are identified from the different research papers and have a significant effect on aluminum matrix composites. In this table, 175 attributes were found from the 50 papers which have related to the aluminum matrix composites and affect the various characteristics in different ways. Besides the direct identification of the attributes, the various aspects or attributes and their effect can be found by using cause-effect analysis.

4.3.5 CODING OF RESEARCH PAPER

The next step in the formation of the matrix is the coding of the papers. The coding of the papers is done from values 0–5. There are various factors to keep in mind to provide the code value: the depth of analysis on a particular attribute, the journal in which a paper is published, etc. (Table 4.2).

TABLE 4.1
List of Various Attributes Identified from Different Research Publications

1. Manufacturing Aspects

- | | |
|--------------------------|----------------------|
| a) Stir casting | b) Powder metallurgy |
| c) Stirrer material | d) Rod material |
| e) Type of furnace | f) Blade angle |
| g) Stirring speed | h) Stirring time |
| i) Degassing | j) Sintering time |
| k) Sintering temperature | l) Compo casting |
| m) Blade height | n) Vortex motion |

2. Defects

- | | |
|--------------------------|------------------------|
| a) Clusters | b) Porosity content |
| c) Micro cracks | d) Cavities |
| e) Blow holes | f) Transverse cracking |
| g) Longitudinal cracking | h) Impurities |
| i) Crack propagation | |

3. Mechanical Aspects

- | | |
|---------------------------------------|------------------------------|
| a) Degree of fracture | b) Yield strength |
| c) Ultimate tensile strength | d) Percent elongation |
| e) Young's modulus | f) Strain rate |
| g) Hardness | h) Modulus of elasticity |
| i) Strength | j) Toughness |
| k) Loading time | l) Strain |
| m) Threshold stress | n) Creep |
| o) Micro hardness | p) Tensile strength |
| q) Ultimate compressive strengthening | r) Monotonic loading |
| s) Stiffness | t) Machining |
| u) Fatigue | v) Chip formation |
| w) Machining forces | x) Workability |
| y) Workability index | z) Thermal residual stresses |
| aa) Impact velocity | bb) Cutting speed |
| cc) Applied pressure | dd) Grooving |
| ee) Seizure pressure | ff) Indentation |
| gg) Normalized pressure | hh) Extrusion |
| ii) Compaction pressure | jj) Thermal stresses |
| kk) Shear modulus | ll) Formability |
| mm) Stress gradient | nn) Fracture toughness |
| oo) Flexural strength | pp) Rupture |

4. Matrix Material Selection

- | | |
|------------------------|------------------------|
| a) Melting temperature | b) Pouring temperature |
| c) Solubility | d) Wettability |
| e) Young's modulus | f) Mechanical behavior |

5. Reinforcement Material Selection

- | | |
|---------------------------|--------------------------|
| a) Type of reinforcement | b) Size of the particles |
| c) Shape of the particles | d) Density |
| e) Melting temperature | f) Young's modulus |

6. Microstructure Aspects

- | | |
|-------------------------|-----------------|
| a) SEM | b) Orientation |
| c) Phase | d) XRD |
| e) Etching | f) Fiber radius |
| g) Inter fiber distance | |

(Continued)

TABLE 4.1 (Continued)**List of Various Attributes Identified from Different Research Publications****7. Wear Aspects**

- a) Wear rate
- b) Angle of impingement
- c) Erosion rate
- d) Shape of erodent
- e) Size of erodent
- f) Abrasion resistance
- g) Wear resistance
- h) Sliding wear resistance
- i) Tool wear
- j) Degree of abrasion
- k) Erosion efficiency
- l) Steady state erosion
- m) Wear tracks
- n) Adhesive wear
- o) Dry wear
- p) Wear volume
- q) Lubricant wear
- r) Craters
- s) Erosion pits
- t) Plow grooves
- u) Speed of erodent

8. General Aspects

- a) Heat treatment
- b) Recrystallization
- c) Thermal aging
- d) Morphology
- e) Nucleation
- f) Type of interface
- g) Chemical composition
- h) Solidification
- i) Lattice spacing
- j) Cooling rate
- k) Volumetric percentage
- l) Metastable phase
- m) Interfacial integrity
- n) Diffusion
- o) Precipitation strengthening
- p) Dispersoid strengthening
- q) Growth kinetics
- r) Aging time
- s) Thermal expansion coefficient
- t) Diffusion bonding
- u) Cutting environment
- v) Particle spacing
- w) Phase
- x) Thermal conductivity
- y) Thermal diffusivity
- z) Grit size of reinforcement
- aa) Micro ploughing
- bb) Coolant
- cc) Coolant concentration
- dd) Curing
- ee) Incubation period
- ff) Dispersion
- gg) Intermetallic phases
- hh) Wetting agent
- ii) Preheating
- jj) Quenching medium
- kk) Hybrid ratio
- ll) Artificial aging
- mm) Availability
- nn) Diffusion coefficient
- oo) Dispersion hardening
- pp) Dislocation
- qq) Interfacial energies
- rr) Berger's vector
- ss) Relative humidity
- tt) Grain growth
- uu) Transient cooling time
- vv) Weld ability
- ww) Solid solubility
- xx) Globular phase
- yy) Surface geometry
- zz) Cooling velocity

TABLE 4.2**Coding of the Research Papers**

Categories	Codes
Attributes which are highly or deeply studied with respect to its corresponding paper	5
Attributes which are average studied with respect to its corresponding paper	3
Attributes which are discussed much less or just introduced	1
Attributes which are not studied or absent in paper	0

4.4 PROCEDURE TO DEVELOP A DECISION MATRIX

- a. In the decision matrix, all the rows represent the number of attributes which are related to the aluminum metal matrix composites and have significant effects on the various physical and mechanical properties. The attributes are represented by “Ai,” where i varies from 1 to m, where m represents the attributes, and all the column represents the no. of papers. The papers are represented by “Pj” where j varies from 1 to n, where n represents the paper. Then there is formulation of $m \times n$ matrix.
- b. First column of the matrix representing the first paper.
- c. First row represents the first attribute find out from the research publications.
- d. In this decision matrix “aij” represents the code value of the paper with respect to the attributes. The code value depends upon the depth of analysis on a particular attribute in the paper. The code value is from 0 to 5.
- e. $\sum P_n$ denotes the submission total of all the values which are given to a particular paper to the corresponding attributes.
- f. $\sum A_i$ denotes the submission total of all the values of attributes to the corresponding papers.
- g. \sum Total represents the total sum corresponding to both attribute and paper.

From the $\sum A_i$ and $\sum P_n$, the academic value of the paper is decided. Table 4.3 shows the decision matrix for the academic value of the corresponding paper with respect to particular attributes. The summation of the attributes and paper was laid out as follows:

The first step is to find the total of the particular attribute or paper:

$$\sum A_m = A_1 + A_2 + A_3 + \dots + A_m$$

$$\sum P_n = P_1 + P_2 + P_3 + \dots + P_n.$$

TABLE 4.3
Decision Matrix “m × n”

Papers	Attributes	P1	P2	P3	.	Pj	Pn	$\sum A_i$
A1		.						$\sum A_1$
A2		.						$\sum A_2$
A3		.						$\sum A_3$
Ai		.				Aij		$\sum A_i$
Am								$\sum A_m$
$\sum P_n$		$\sum P_1$	$\sum P_2$	$\sum P_3$.	$\sum P_j$.	$\sum P_n$

The value of a particular attribute “I” in a paper “j” is $\sum A_{ij}$

$$\sum A_{ij} = \sum A_i + \sum P_j$$

$\sum A_m$ = Sum of the “m” attributes $\sum P_n$ = Sum of “n” papers.

4.5 ADVANTAGES OF DECISION MATRIX

The decision matrix above formed has a large number of advantages. A decision matrix is a useful source of deriving information and knowledge for researchers/designers/manufacturers for basic and commercial research. The methodology is also useful in respect of time, cost, efforts, knowledge, storage, retrieval, and upgrading. etc. Some of the useful attributes of the methodology are:

- (a) A decision matrix is useful for researchers as a source of knowledge and information. This matrix provides the appropriate knowledge about the attributes discussed in a particular paper.
- (b) The matrix is useful for designers and manufacturers to derive knowledge for commercial research.
- (c) The matrix is useful from a time point of view because it saves a lot of time analyzing the research publications.
- (d) The decision matrix reduces the efforts and costs involved to derive out the information from research publications.
- (e) The matrix behaves like a database/software which is used for storage and retrieval of the information which can be updated and enlarged as per requirements and changing needs and trends of research.
- (f) The library should maintain and upgrade this software for the advantage of all the customers, stakeholders, and researchers.

4.6 GAP ANALYSIS

A further step is gap analysis or finding the gap from the past work. With a decision matrix, it is easy to find out the gap in the literature, i.e., in what direction one can make his/her contribution. Gap analysis is different for different areas. The following explains how the gap analysis importance is found, according to various ideas:

1. **Researcher** – From the decision matrix it is easy for a researcher to find the gap between the work that has been done and what has not been done. It is well known that Ph.D. students spend more than a year on a literature review to find out the gap in the research and this literature review is continuously going up to their course work. Using this methodology, the software can be developed in the library of colleges which can be updated as the new research is explored. Even for master's or undergraduate students, it is essential to do a literature review to find the gap in their research work.

2. **Designer** – Every industry has its own research and development department to update its product quality as times change. Designers go through a number of studies to improve or develop a new design that can be a boost for the industry to increase productivity and profit with minimum input cost. By using this type of decision matrix, the designer can go through research and find out the various aspects which can be useful to make the design better.
3. **Manufacturer** – When any manufacturer has to produce a new product, there are various manufacturing aspects that affect the different properties in different ways. But there are some products for which manufacturers have more requirements. With the use of the decision matrix, it is easier to evaluate what are the various manufacturing aspects that can give the desired properties. What are the manufacturing parameters that make a good quality and cost-effective product? Even if someone establishes a new industry, it becomes easy for them to forget the manufacturing aspects to give a boost to the newly established industry.
4. **Short-term and long-term strategic points** – Decisions can be important for various firms to make their strategy. They can easily know the changing trend of the research, i.e., one can know how the research is changed in the past two or five years. According to that, a strategy can be made.

4.7 EXAMPLES OF DECISION MATRIX

The following Table 4.4 shows an example of a decision matrix. In this matrix, 20 attributes are selected from the corresponding 20 papers. Then according to the coding given in the table, three codes are given to the corresponding papers. After coding has been done, the sum of the row and column is found (Table 4.5).

4.7.1 SWOT ANALYSIS

SWOT analysis is a strategic planning method used to evaluate the strengths, weaknesses, limitations, opportunities, and threats in a project, research, or business venture.

- Strength: it is a characteristic of a project team that gives an advantage over others.
- Weakness: it is a characteristic that places the team at a disadvantage relative to others.
- Opportunity: these are the external chances to improve the performance.
- Threats: external elements in the environment that cause trouble for the project.

In this paper, SWOT analysis is done according to the manufacturer, designer, and researchers' points of view.

4.7.2 SWOT ANALYSIS FOR MANUFACTURER

Strength

- Cost effective producer
- Serve maximum customer satisfaction
- Integrated production facility
- A number of projects

Weaknesses

- Present production capacity is no adequate to meet the rising high demand
- Technology is not upgraded to mark as compare to global giants in aluminum industry

Opportunities

- R & D collaboration with universities and another research organization
- More emphasis on downstream production of value-added products
- Recycling should be adopted as routine production
- Raising more finance from marketing for more acquisition and merger for consolidating position in the global market

Threats

- Innovative revolution in plastic and steel industry
- Fall in price of Al, in neighboring country

4.7.3 SWOT ANALYSIS FOR DESIGNER

Strength

- Large no. of software applications are available to reduce efforts and time
- More innovative research is available in various journals

Weaknesses

- Less investment in R&D sector
- Technology is not updated with time in industries
- Limited constraints

Opportunities

- R & D collaboration with universities
- Various model analyses like FMEA, etc.
- Dedicated team effort

Threats

- Technology is updated day by day
- Competitive environment
- Lack of skill

4.7.4 SWOT ANALYSIS FOR RESEARCHER

Strength

- Large no. of journals is available to update the knowledge
- A vide knowledge is easily available on internet
- Experience
- Expert advice

Weaknesses

- Gap in generation
- Poor motivation
- Less experience
- Non availability of resources
- Cost involved in some researches

Opportunities	Threats
<ul style="list-style-type: none"> • Opportunities to work on various gaps in any research you can find in any area • Opportunities to involve in the live projects in universities sponsored by governments • Opportunities to work on the problems faced by industries 	<ul style="list-style-type: none"> • Competitive environment • Lack of skill • Variability in resources available at different universities • Non experienced guidance

4.7.5 STEP BY STEP PROCEDURE FOR ATTRIBUTES-BASED LITERATURE REVIEW

- (1) Researchers/designers/manufactures/user should decide the area aim and objectives of literature review and gap analysis.
- (2) Using cause and effect diagram identify all the groups, subgroups of attributes required to be studied.
- (3) Prepare a list of all the attributes from published literature and cause and effect diagram information.
- (4) Characterize a paper with the help if these “m” attributes as

$$P_j = \{A_{1j}, A_{2j}, A_{3j}, \dots, A_{ij}, \dots, A_{mj}\} \text{ i.e. } i = 1, 2, 3, \dots, m \text{ define } 'm \times n'$$

- (5) Define “m × n” knowledge base matrix where rows represent attributes and columns represents research papers.
- (6) Every attribute is coded in the interval scale of 0–5 based on the depth. It has studied in a particular paper. Zero represents absent while five represents the attribute is highly studied in depth.
- (7) Prepare a comprehensive knowledge base matrix for all the “n” papers collected from all the sources related to the area under consideration. Preferably, develop a user-friendly software for permanent storage retrieval and upgrading.
- (8) Summation of weights of all the attributes in the “I” row represents the academic importance of the paper.
- (9) Through interactive with the software of knowledge base matrix, one can select top few papers of his choice in a particular attribute or set of attributes to be studied.
- (10) This knowledge base clearly highlights what has not been studied at all, has been studied partially, or in detail.
- (11) It is recommended that researchers/designers/manufacturers/should carry out their own SWOT analysis before deciding on short-term and long-term strategy.
- (12) It is necessary to upgrade knowledge base matrix with new publications and can observe changing trends/interest of researcher with based on new challenges. The knowledge bases on the proposed methodology are to be developed and maintained and upgraded by the libraries.

TABLE 4.4
Attributes Research Publication/Papers

S. No	Attributes	Research Publications																			
		P1	P2	P3	P4	P5	P6	P7	P8	P9	P10	P11	P12	P13	P14	P15	P16	P17	P18	P19	P20
1	Stir casting	0	3	1	0	0	3	1	0	1	1	0	0	0	0	3	3	3	3	1	0
2	Stir speed	0	1	1	0	0	3	1	0	0	1	0	0	0	0	1	1	1	5	1	0
3	Stir time	0	1	0	0	0	3	1	0	0	1	0	0	0	0	1	1	1	5	1	0
4	Particle size	3	3	3	0	1	1	2	1	1	1	5	1	1	5	1	1	3	3	1	3
5	Particle distribution	5	3	3	0	1	1	1	0	0	0	1	0	3	1	3	1	3	3	0	1
6	Preheating	0	1	1	0	0	1	1	0	0	1	0	0	0	0	1	1	1	0	1	1
7	Powder metallurgy	0	0	0	0	0	0	0	0	0	5	0	3	3	0	0	0	0	0	0	5
8	Sintering temperature	0	0	0	0	0	0	0	0	0	0	5	0	1	3	0	0	0	0	0	3
9	Sintering time	0	0	0	0	0	0	0	0	0	0	5	0	1	3	0	0	0	0	0	3
10	Machining	1	0	1	5	0	0	0	5	0	0	0	0	0	1	0	0	0	1	0	0
11	Solubility	3	0	0	0	1	1	0	0	0	0	3	0	0	0	1	0	1	1	0	0
12	Wear rate	0	0	0	3	5	3	3	0	5	5	0	5	5	3	0	5	0	5	5	5
13	Sliding distance	0	0	0	0	0	3	0	0	5	5	0	3	0	0	0	5	0	0	3	5
14	Dry wear	0	0	0	0	1	2	2	0	5	5	0	3	0	0	0	5	0	0	3	3
15	Wettability	3	1	1	0	0	1	0	0	0	0	0	1	0	0	0	1	0	1	3	0
16	Porosity content	1	0	1	1	3	1	1	1	0	0	0	0	0	1	0	1	1	3	1	0
17	Microhardness	3	0	3	1	3	0	0	0	3	3	0	0	0	0	3	3	0	3	0	3
18	Heat treatment	5	0	0	0	3	0	5	0	0	3	0	1	0	0	5	0	0	0	0	0
19	Cooling rate	0	0	0	0	1	0	3	0	0	0	0	1	0	0	0	0	0	0	0	0
20	Micro structure	5	5	5	3	3	3	3	3	3	3	3	3	3	3	5	3	5	3	1	5
	ΣP_n	29	18	20	13	22	327	29	10	23	29	28	19	22	26	25	30	22	31	17	38

TABLE 4.5
The References for the Papers used in the Example for Review

S.no.	Papers	References	S.no.	Papers	References
1	Paper 1	[3]	11	Paper 11	[24]
2	Paper 2	[8]	12	Paper 12	[29]
3	Paper 3	[12]	13	Paper 13	[33]
4	Paper 4	[18]	14	Paper 14	[44]
5	Paper 5	[28]	15	Paper 15	[38]
6	Paper 6	[30]	16	Paper 16	[36]
7	Paper 7	[31]	17	Paper 17	[46]
8	Paper 8	[39]	18	Paper 18	[13]
9	Paper 9	[16]	19	Paper 19	[43]
10	Paper 10	[21]	20	Paper 20	[36]

4.8 CONCLUSION

Existing research papers contain research contributions in the form of data. The decision matrix converts this data into information related to attribute research. The present method of literature review is not an effective way to provide appropriate knowledge about the research publication. This paper presents the attributes-based decision matrix methodology. This methodology is very helpful and efficient if the decision matrix is prepared in a very careful and proper way. The decision matrix is a database that can be enlarged as the new researches are upgraded. The library of an institution can be integrated into the computer software, which is helpful for different researchers, designers etc. and can be updated or extended from time to time. The decision matrix methodology provides the knowledge to the designers and manufacturers from one respective field to another respective field. In-depth analysis of the decision matrixes $\sum P_i$'s and $\sum A_j$'s leads to the creation of knowledge and wisdom.

REFERENCES

1. Johnson, A. F., Kempe, G., & Simon, J. (2000). "Design of composite wing access cover under impact loads," *Applied Composite Materials* 7, 219–229.
2. Das, S., Mondal, D.P., & Sawla, S. (2004). "Solid particle erosion of Al ALLOY And Al-alloy composites: effect of heat treatment and angle of impingement," *Metallurgical and Materials Transactions A* 35(4), 1369–1379.
3. Gomez De Salazar, J. M., & Barrena, M. I. (2002). "The influence of Si and Mg rich phases on the mechanical properties of 6061 Al-matrix composites reinforced with Al_2O_3 ," *Journal of Materials Science* 37, 1497–1502.
4. Hassan, A. M., Hayajneh, M. T., & Al-Omari, M. A. (2002). "The effect of the increase in graphite volumetric percentage on the strength and hardness of Al-4 weight percent Mg-graphite composites," *Journal of Materials Engineering and Performance* 11(3), 250.

5. Gupta, M., Yee Chung-E, F., & Srivatsan, T. S. (2003). "Synthesis of new metastable aluminum-titanium alloy by defying equilibrium in an equilibrium process," *Materials and Manufacturing Processes* 18, 891–902.
6. Karnesky, R. A., Meng, L., Seidman, D. N., & Dunand, D. C. (2003). "Mechanical properties of a heat-treatable Al-Sc alloy reinforced with Al_2O_3 dispersoids," *MS & T* 215–224.
7. Surappa, M. K. (2003). "Aluminium matrix composites: Challenges and opportunities," *sadhana*, 28, 319–334.
8. Flores-Zamora, M. I., Segura-Cedillo, I., Santos-Beltrán, A., Estrada-Guel, I., Barajas-Villaruel, J. I., & Martínez-Sánchez, R. (2004). "SEM characterization in Al-C- Al_2O_3 composites produced by stir casting," *Microsc Microanal* 10, 45–49.
9. Naher, S., Brabazon, D., & Looney, L. (2004). "Development and assessment of a new quick quench stir caster design for the production of metal matrix composites," *Journal of Materials Processing Technology* 166, 430–439.
10. Jalham, I. S. (2005). "A comparative study of some network approaches to predict the effect of the reinforcement content on the hot strength of Al-base composites," *Journal of Materials Processing Technology* 166, 392–397.
11. Kannan, S., & Kishawy, H. A. (2006). "Surface characteristics of machined aluminium metal matrix composites," *International Journal of Machine Tools & Manufacture* 46, 2017–2025.
12. Mandal, D., Dutta, B. K., & Panigrahi, S. C. (2006). "Microstructure and mechanical properties of Al-2Mg alloy base short steel fiber-reinforced composites prepared by vortex method," *J Mater Sci* 41, 4764–4770.
13. Balasivanandha Prabu, S., Karunamoorthy, L., Kathiresan, S., & Mohan, B. (2006). "Influence of stir speed and stirring time on distribution of particles in cast metal matrix composite," *Journal of Material Processing Technology* 171, 268–273.
14. Eduardo, G. (2006). "Evaluation of diametral tensile strength and knoop micro hardness of five nanofilled composites in dentin and enamel shades," *Baltic Dental and Maxillofacial Journal* 8, 67–90.
15. Rajan, T. P. D., Narayan Prabu, K., Pillai, R. M. & Pai, B. C. (2007). "Solidification and casting/mould interfacial heat transfer characteristics of aluminium matrix composites," *Composites Science and Technology* 67, 70–78.
16. Kok, M. & Ozdin, K. (2007). "Wear resistance of aluminium alloy and its composites reinforced by Al_2O_3 particles," *Journal of Materials Processing Technology* 183, 301–309.
17. Rajan, T. P. D., Pillai, K. R. M., Pai, B. C., Satyanarayana, K. G. & Rohatogi, P. K. (2007). "Fabrication and characterization of Al-7Si-0.35Mg/fly ash metal matrix composites processed by different stir casting routes," *Composites Science and Technology* 67, 3369–3377.
18. Kannan, S. & Kishawy, H. A. (2008). "Tribological aspects of machining aluminium metal matrix composites," *Journal of Materials Processing Technology* 198, 399–406.
19. Mohamed A. T., Nahed A. E. & Ahmed M. E. (2008). "Some experimental data on workability of aluminium-particulate-reinforced metal matrix composites," *Journal of Materials Processing Technology* 202, 380–385.
20. Harsha, A. P., & Jha, S. K. (2008). "Erosive wear studies of epoxy-based composites at normal incidence," *Wear* 265, 1129–1135.

21. Rao, R. N. & Das, S. (2011). "Effect of sliding distance on the wear and friction behavior of as cast and heat-treated Al-SiCp composites," *Materials and Design* 32, 3051–3058.
22. Wahab, M. N., Daud, A. R., & Ghazali, M. J. (2009). "Preparation and characterization of stir cast-aluminum nitride reinforced aluminum metal matrix composites," *International Journal of Mechanical and Materials Engineering (IJMME)* 4, 115–117.
23. Reddy, T. V. S., Dwivedi, D. K., & Jain, N. K. (2009). "Adhesive wear of stir cast hypereutectic Al-Si-Mg alloy under reciprocating sliding conditions," *Wear* 266, 1–5.
24. Mehdi, R., Naser, E., Nader, P., & Hamid, B. (2009). "The effect of particle size, sintering temperature and sintering time on the properties of Al-Al₂O₃ composites, made by powder metallurgy," *Journal of Materials Processing Technology* 209, 5387–5393.
25. Xianhui, W., Shuhua, L., Ping, Y., & Zhikang, F. (2009). "Effect of Al₂O₃ particle size on vacuum breakdown behavior of Al₂O₃/Cu composite," *Vacuum* 83, 1475–1480.
26. Dolata-Grosz, A., Hufenbach, W., Sleziona, J., Gude, M., & Czulak, A. (2009). "Design, manufacture and technological verification of SiC/C composite stirrer," *Archives of Materials Science and Engineering* 39, 29–37.
27. Zhao, Z. M., Zhang, L., Song, Y. G., Wang, W. G. & Liu, H. B. (2009). "Composition, microstructures and properties of Al₂O₃/ZrO₂ (Y₂O₃) self-growing ceramic composites prepared by combustion synthesis under high gravity," *Journal of Physics: Conference Series* 152, 012085.
28. Curle, U. A. & Ivanchev, L. (2010). "Wear of semi-solid rheocast SiCp/Al metal matrix composites," *Trans. Nonferrous Met. Soc. China* 20, 852–856.
29. Wanga, Y. Q., Afsara, A. M., Jangb, J. H., Hanb, K. S. & Songa, J. I. (2010). "Room temperature dry and lubricant wear behaviors of Al₂O₃f/SiCp/Al hybrid metal matrix composites," *Wear* 268, 863–870.
30. Veeresh Kumar, G. B., Rao, C. S. P., Selvaraj, N., & Bhagyashekar, M. S. (2010). "Studies on Al₆O₆₁-SiC and Al_{70.75}-Al₂O₃ metal matrix composites," *Journal of Minerals & Materials Characterization & Engineering* 9, 43–55.
31. Prabhu Swamy, V., Ramesh, C. S. & Chandrasekhar, T. (2010). "Effect of heat treatment on strength and abrasive wear behaviour of Al6061-SiCp composites," *Bulletin of Materials Science* 33, 49–54.
32. Rao, R. N. & Das, S. (2011). "Effect of sliding distance on the wear and friction behavior of as cast and heat-treated Al-SiCp composites," *Materials and Design* 32, 3051–3058.
33. Kumar, S., & Balasubramanian, S. (2010). "Effect of reinforcement size and volume fraction on the abrasive wear behavior of AA7075 Al/SiCp P/M composites—A statistical analysis," *Tribology International* 43, 414–422.
34. Jayaseelan, V., Kalaichelvan, K., Kannan, M., & Vijay Ananth, S. (2010). "Extrusion characterizes of Al/Sic by different manufacturing process," *International Journal of Applied Engineering Research* 1, 194–197.
35. Muhammad, H. J., Muhammad, I. P., & Mukhtiar, A. U. (2011). "Manufacturing of aluminum composite material using stir casting process," *Mehran University Research Journal of Engineering & Technology* 30, 53–64.

36. Umanath, K., Selvamani, S. T., & Palani, K. (2011). "Friction and wear behaviour of Al₆O₆₁alloy (SiCp +Al₂O₃p) hybrid composites," *International Journal of Engineering Science and Technology (IJEST)*, 3, 5441–5451.
37. Mehdi, R., Nader, P., & Naser, E. (2011). "The effect of production parameters on microstructure and wear resistance of powder metallurgy Al-Al₂O₃ composite," *Materials and Design* 32, 1031–1038.
38. Vineet, T. (2011). "Development and micrography of AA2218 based heat treated 5 Wt% Al₂O₃ (TiO₂) hybrid MMCs," *MIT International Journal of Mechanical Engineering* 1, 41–48.
39. Metin, K. (2011). "Modelling the effect of surface roughness factors in the machining of 2024Al/Al₂O₃ particle composites based on orthogonal arrays," *International Journal of Advanced Manufacturing Technology* 55, 911–920.
40. Goyal, R. K., Tiwari, A. N., & Negi, Y. S. (2008). "Microhardness of PEEK/ceramic micro- and nanocomposites: correlation with Halpin–Tsai model," 491, 230–236.
41. Gupta, N., Nguyen, Q., & Rohatgi, P. K. (2011). "Analysis of active cooling through nickel coated carbon fibers in the solidification processing of aluminum matrix composites," *Composites: Part B* 42, 916–925.
42. Kumar, A., & Swamy, R. P. (2011). "Evaluation of mechanical properties of Al₆O₆₁, flyash and e-glass fiber reinforced hybrid metal matrix composites," *ARPN Journal of Engineering and Applied Sciences* 6(5), 40–44.
43. Rao, R. N., & Das, S. (2011). "Effect of SiC content and sliding speed on the wear behavior of aluminium matrix composites," *Materials and Design* 32, 1066–1071.
44. Shengyu, Z., Qinling, B., Jun, Y., Weimin, L., & Qunji, X. (2011). "Effect of particle size on tribological behavior of Ni3Al matrix high temperature self-lubricating composites," *Tribol Int* 2011, 1–10.
45. Rutecka, A. (2011). "Damage development of Al/SiC metal matrix composite under fatigue, creep and monotonic loading conditions," *Procedia Engineering* 10, 1420–1425.
46. Sajjadi, S. A., Ezatpour, H. R., & Torabi Parizi, M. (2012). "Comparison of microstructure and mechanical properties of A356 aluminium alloy/Al₂O₃ composites fabricated by stir and compo-casting processes," *Materials and Design* 34, 106–111.

5 Multi-scale Computational Analysis of Metal Matrix Nanocomposites

Gaurav Arora

Chandigarh University, Mohali, India

Himanshu Pathak

Indian Institute of Technology Mandi, VPO Kamand,
Mandi, Himachal Pradesh, India

CONTENTS

5.1	Introduction.....	82
5.2	Few Critical Applications of MMNCs.....	85
5.2.1	Automotive Sector	85
5.2.2	Aerospace Sector	85
5.2.3	Medical Sector.....	86
5.2.4	Electronic Packaging and Other Sectors.....	86
5.3	Modeling Methods.....	86
5.3.1	Micromechanics.....	86
5.3.1.1	Voigt and Reuss Models.....	87
5.3.1.2	Hashin–Shtrikman Bounds	89
5.3.1.3	Self-Consistent Method	89
5.3.1.4	Strength of Materials.....	90
5.3.1.5	Mori–Tanaka Homogenization Method	91
5.3.1.6	Finite Element Method	93
5.3.2	Multi-scale Approach.....	94
5.4	Effective Material Properties of MMNCs.....	97
5.4.1	Influence of Volume Fraction of the Nanofillers.....	98
5.4.2	Influence of Orientation of the Nanofillers	100
5.4.3	Influence of Interphase Between the Constituents.....	101
5.4.4	Influence of Aspect Ratio of the Nanofillers.....	104
5.5	Hybrid Metal Matrix Nanocomposites (HMMNCs)	106
	References.....	111

5.1 INTRODUCTION

Metal matrix composites (MMCs) are defined as the composites containing the primary phase metal as matrix and the secondary phase in particle or fiber form as reinforcement. MMCs have been developed and put to use for the past 50 years. The three chief types of MMCs are dispersion strengthened, fiber-reinforced, and particle-reinforced. These three categories of MMCs are extensively used in space, automobile, and military fields. Out of these three, fiber-reinforced is the most unusual. An increase in the development of low-cost fibers has attracted these MMCs to medical fields, as these fiber-reinforced MMCs are anisotropic. The anisotropic nature depends on the orientation and volume fraction of the fibers reinforced in the metal. The foremost part of the fibers is to carry the load, although the matrix, i.e., metals, transfer the load to the fibers and further distributes among them. But this transfer and distribution are mainly dependent on the interfacial bonding between the constituents. Also, the mechanical properties of these MMCs depend primarily on the adhesion between the constituents and fiber properties. A few potential advantages of MMCs for their usage in structural materials are shown in Figure 5.1.

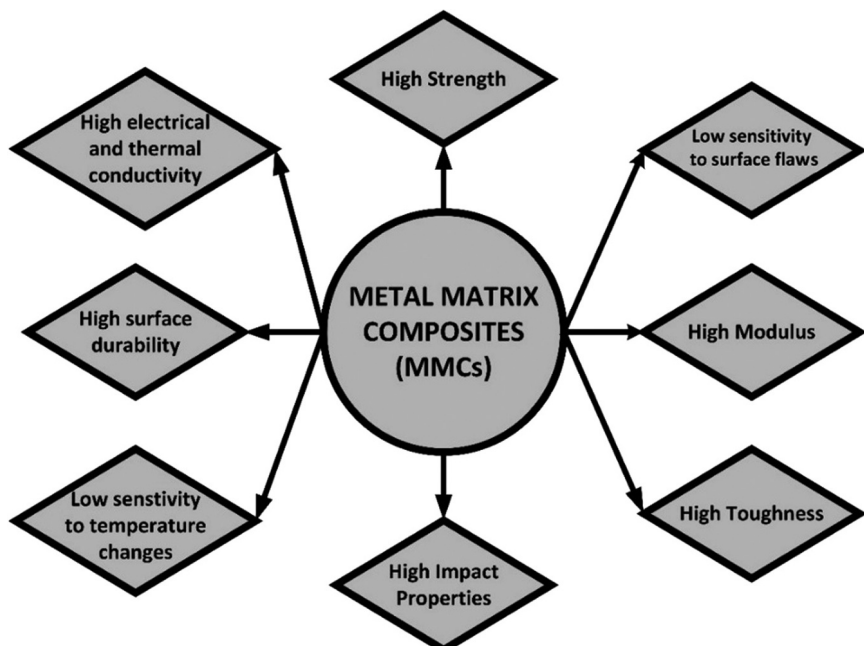


FIGURE 5.1 Advantages of MMCs.

For their use in structural materials, properties like strength retention at elevated temperature, higher toughness, and resistance to the severe environment are the essential requirements of these composites. These properties can also be achieved by discontinuous fiber-reinforced MMCs. Popularly, many discontinuous fiber MMCs are available in the market and can be found in automobile parts and sports equipment nowadays.

Commonly used metals as a matrix in MMCs are as follows:

- Aluminum-based composites (AlCs)
- Copper-based composites (CuCs)
- Magnesium-based composites (MgCs)
- Titanium-based composites (TiCs)
- Super-alloy-based composites (SACs)

AlCs are widely used compared with MgCs in the aerospace and automotive industries. The low thermal conductivity of MgCs restricts their use, but the low density of MgCs encourages their use for the space industry. TiCs have excellent strength and corrosion resistance compared with AlCs, and MgCs thus inspires their use in high-speed applications like missiles, aircraft etc. CuCs have high-temperature strength and high thermal conductivity compared to other MMCs. Gas turbine blades use SACs for manufacturing due to their sustainability at high speed and temperature. All these metals are reinforced with carbides and oxides for the successful production of MMCs.

For better performance of the MMCs, traditional fillers have been replaced with newly developed nanofillers to serve the planned function under the severe mechanical and thermal conditions (El-Kady and Fathy 2014; Gupta and Wong 2015; Mohammad Kazem Hassanzadeh-Aghdam et al., 2018a; Moradgholi et al. 2017; Salehi et al. 2014; Yang and Lu 2013). Nanofillers popularly used during the experimental and computational analysis to predict the enhanced overall properties of MMCs are Silicon carbide (SiC) and graphene nanoplatelets (GNP). SiC are nanoparticles, and graphene nanoplatelets are 2D nanofiller. Artificial or synthetic fibers were developed in the year 1664. But as technology advances, new 3D nanosynthetic fibers were developed. Carbon nanotubes (CNTs) were produced in the year 1993 (Iijima and Ichihashi 1993). CNTs have a single or multi-walled 3D structure. The purpose of the development of CNTs was to increase the interfacial area such that there was significant improvement in the electrical, mechanical, and thermal properties of MMCs. MMCs reinforced with these nanofillers are commonly known as metal matrix nanocomposites (MMNCs).

SiC, GNP, and CNTs have astonishing mechanical, electrical, and thermal properties (for example, CNTs have Young's modulus 1–5.5 TPa (Muhammad et al. 2015), tensile strength 13–53 GPa (Muhammad et al. 2015), axial thermal conductivity $3500 \text{ W}\cdot\text{m}^{-1}\cdot\text{K}^{-1}$ (Pop et al. 2005), and electric current density with

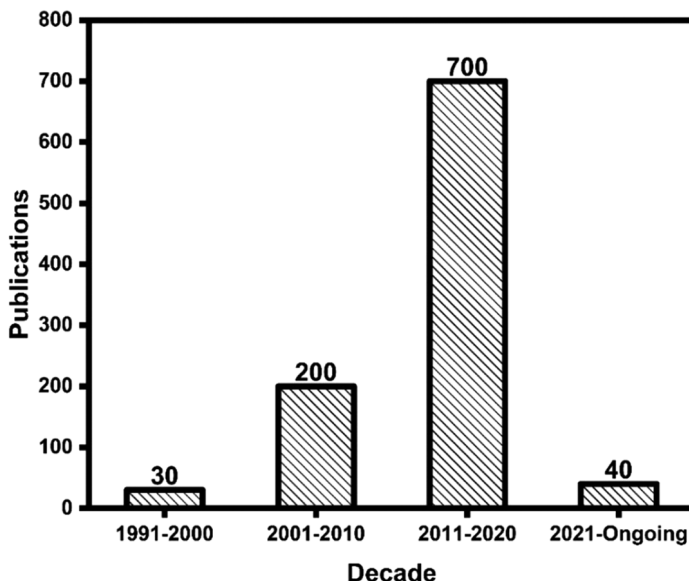


FIGURE 5.2 Publications on multi-scale modeling in a decade.

metals 4×10^9 A/cm²(Hong and Myung 2007). Compared to metals, these properties are far higher. Therefore, reinforcing nanofillers in the metal enhances the overall properties of the nanocomposites. These nanocomposites consist of two phases, i.e., metal as macro-scale material and nanofillers as nano-scale material. As these two phases are of different length scales, therefore the properties of the nanocomposites may vary at each scale. Hence, it is essential to study the properties at two different length scales. The studying of properties at different length scales through proper theoretical modeling is called a multi-scale modeling technique.

Multi-scale modeling is popular to study the responses like elastic, elasto-plastic, visco-elastic, visco-elastoplastic, thermoelastic, and thermo-elastoplastic etc., of the nanocomposites from the structural point of view (Xia et al. 2001; Chawla et al. 2004; Liu and Sun 2005; Sawant and Muliana 2009; Thilly et al. 2009; Gao et al. 2017; Pundhir et al. 2020; Wang et al. 2020; Arora et al. 2021; Arora and Pathak 2021; Hu and Yang 2021; Iacobellis and Behdinan 2021; Pakseresht et al. 2021; Qiu et al. 2021) Multi-scale modeling problems can also be used to study the electrical and thermal behavior of nanocomposites. The number of publications on multi-scale modeling techniques in a decade is illustrated in Figure 5.2. Therefore, it is evident that multi-scale modeling has become an essential method to study the response of the MMNCs as time passes.

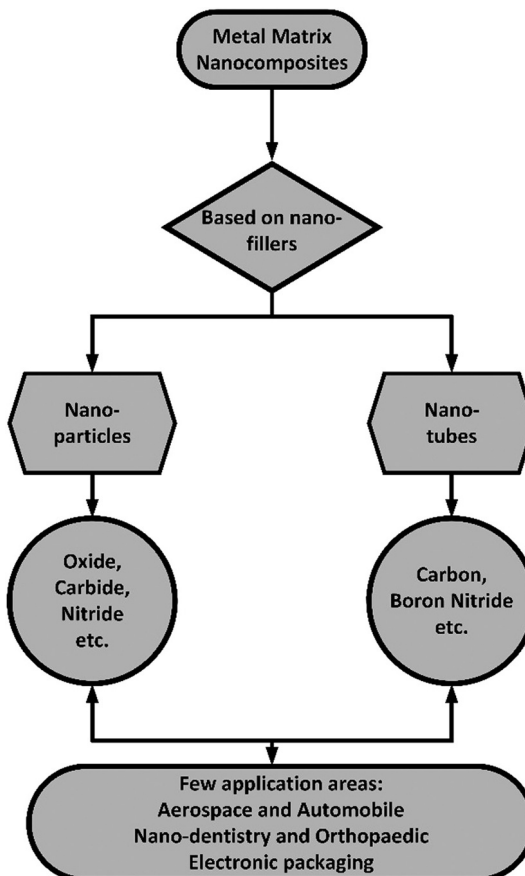


FIGURE 5.3 Metal matrix nanocomposites based on nanofillers.

5.2 FEW CRITICAL APPLICATIONS OF MMNCs

5.2.1 AUTOMOTIVE SECTOR

Diesel engine with reinforced pistons, cylinder bores of engine blocks of AlCs, calipers, disks, intake and exhaust valves, rotors, crankshafts main bearing caps and hybrid and electric car using power module components of MMNCs, gears, and brake shoes.

5.2.2 AEROSPACE SECTOR

Door covers of fuel access, fan exit guide vanes and ventral fins of aircraft, nozzle actuator links in engines, swash plates and sleeves of rotor blades of helicopters, structural radiators, high-gain antenna boom.

5.2.3 MEDICAL SECTOR

Glucose sensing applications, titanium oxide nanotubes for implants, nanodentistry using CNT-reinforced nanocomposites for implants, and Mg-based nanocomposites for orthopedic applications.

5.2.4 ELECTRONIC PACKAGING AND OTHER SECTORS

Heat sinks, hydrogen storage, microbeams and gears, solders, and anode manufacturing and coatings.

5.3 MODELING METHODS

5.3.1 MICROMECHANICS

MMNCs are heterogeneous and anisotropic materials. Thus, micromechanics allows studying these anisotropic materials and predicting their responses (shown in Figure 5.4) under the diverse loading environment analytically and numerically. The various micro-mechanics methods are illustrated in Figure 5.5. The precious advantage of micro-mechanics approaches is that it saves experimental time and cost by performing the virtual test on MMNCs. These heterogeneous nanocomposites are studied based on the geometry and properties of the constituents by the technique called a homogenization method or technique.

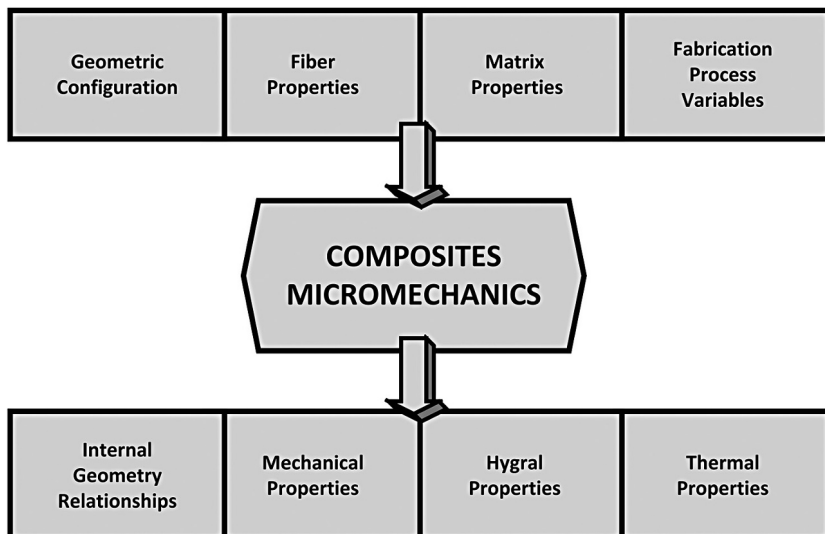


FIGURE 5.4 Definition of composites micromechanics.

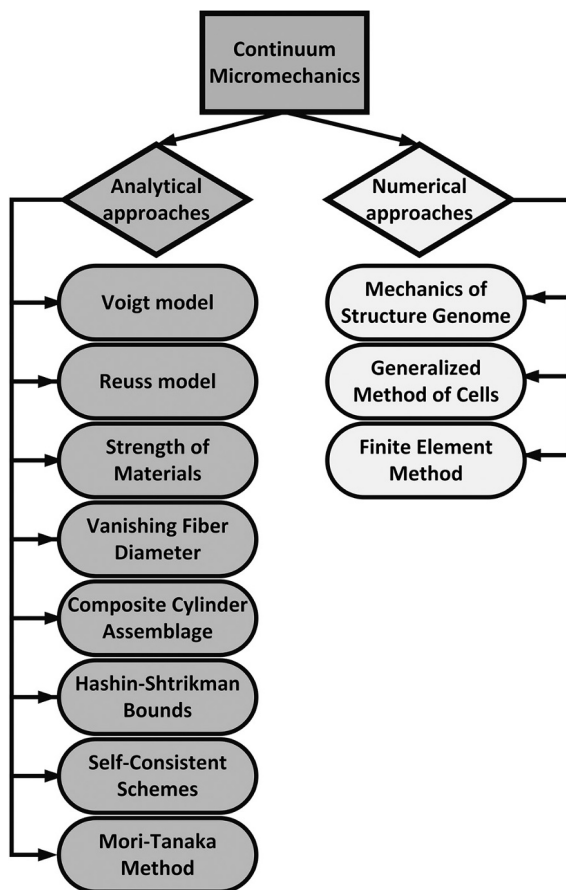


FIGURE 5.5 A tree of analytical and numerical continuum micromechanics approaches.

5.3.1.1 Voigt and Reuss Models

Some analytical methods were studied in the early 90s. Voigt and Reuss have given simple approximations to obtain the overall properties of the heterogeneous materials (linear elastic) (Watt 1976). Voigt model predicted the overall properties by considering the materials in parallel connection, whereas Reuss model predicted the overall properties by considering the materials in series. These approaches considered the average stresses and strains as defined by Hill in 1963 (Watt 1976).

The rule of the mixture is used to define the relationship between the total averaged tensors and material averages, as follows:

$$\langle \chi \rangle = \sum_{p=0}^1 V_p \langle \chi \rangle^p; \quad (5.1)$$

where χ represents the stress and strain, 0 and 1 represents the matrix and inclusion, and V represents the volume fraction. Equation (2) illustrates the relationship between the concentration tensor (\aleph), average material properties $\langle \chi \rangle^p$, and total composite properties $\langle \chi \rangle$.

$$\langle \chi \rangle^p = \aleph \langle \chi \rangle \quad (5.2)$$

where \aleph represents the corresponding stress concentration tensor (A) and strain concentration tensor (B). Hill defines the average strain and stress in inclusions with the alternate strain and stress tensors, respectively, as follows:

$$\langle \chi \rangle^l = \tilde{\aleph} \langle \chi \rangle^0 \quad (5.3)$$

Therefore, the relation between \aleph and $\tilde{\aleph}$ can be defined from Equations (5.1), (5.2) and (5.3) as follows:

$$\aleph = \tilde{\aleph} \left[(1 - V_1) I + V_1 \tilde{\aleph} \right]^{-1} \quad (5.4)$$

The relation between the average stiffness and compliance of the composite can be related to corresponding concentration tensors as follows:

$$\mathbb{C}^{\text{eff}} = \mathbb{C}^0 + V_1 (\mathbb{C}^1 - \mathbb{C}^0) \aleph \quad (5.5)$$

where \mathbb{C} represents the stiffness or compliance matrix corresponding to stress or stain concentration tensors, i.e., \aleph .

According to Voigt model, the average strain tensors in inclusions are equal to the average strain tensor in the composite; therefore, Equation (5.5) can be written as:

$$\mathbb{C}^{\text{VM}} = \mathbb{C}^0 + V_1 (\mathbb{C}^1 - \mathbb{C}^0) \quad (5.6)$$

where \mathbb{C}^{VM} is the effective stiffness of the composite, and Equation (5.6) represents the simple rule of mixture.

Reuss model assumes that the constituents experience constant stress; therefore, Equation (5.5) can be modified as follows:

$$\mathbb{C}^{\text{RM}} = \mathbb{C}^0 + V_1 (\mathbb{C}^1 - \mathbb{C}^0) \quad (5.7)$$

where C^{RM} represents the effective compliance of the composites and is also called an inverse rule of mixture. The relations represented in Equations (5.6) and (5.7) are called upper-bound and lower-bound relations.

5.3.1.2 Hashin–Shtrikman Bounds

The variational principle applied to the n-phase composite for the bounding of the moduli as follows:

$$\left. \begin{aligned} K_-^\dagger &= K_1 + \left[A_1 (1 + \varsigma_1 A_1) \right] \\ K_+^\dagger &= K_n + \left[A_n (1 + \varsigma_n A_n) \right] \end{aligned} \right\} \quad (5.8)$$

The terms ς and A are represented as follows:

$$\varsigma_i = -\frac{3}{3(K_i + 4\mu_i)} \text{ and } A_i = \sum_{j=1}^n \frac{V_j}{(K_j - K_i)^{-1} - \varsigma_i} \text{ where } i = 1, n \quad (5.9)$$

$$\left. \begin{aligned} \mu_-^\dagger &= \mu_1 + \left[B_1 (1 + \psi_1 B_1) \right] \\ \mu_+^\dagger &= \mu_n + \left[B_n (1 + \psi_n B_n) \right] \end{aligned} \right\} \quad (5.10)$$

The terms ψ and B are represented as follows:

$$\psi_i = \frac{-3(K_i + 2\mu_i)}{5\mu_i(3K_i + 4\mu_i)} \text{ and } B_i = \sum_{j=1}^n \frac{V_j}{\left[2(\mu_j - \mu_i)^{-1} - \psi_i \right]} \quad (5.11)$$

Here,

$$\text{Here, } K_-^\dagger \leq K^\dagger \leq K_+^\dagger \quad \text{and} \quad \mu_-^\dagger \leq \mu^\dagger \leq \mu_+^\dagger \quad (5.12)$$

K_i and μ_i are the smallest and largest moduli as i is equal to 1 and n , respectively.

5.3.1.3 Self-Consistent Method

For the higher volume fraction of the inclusions, self-consistent methods are the best. It has an assumption that the matrix surrounding the inclusion is the effective matrix for the effective evaluation of the properties. According to Eshelby's model, the strain concentration tensor is as follows:

$$A^{\text{Eshelby}} = \left[I + \xi S^0 (C^1 - C^0) \right]^{-1} \quad (5.13)$$

where ξ is the fourth-order Eshelby's tensor and A^{Eshelby} is the stain concentration tensor defined by Eshelby's model. The equation (Gao et al. 2017) can be replaced for determining the strain concentration tensor of a self-consistent method by substituting the matrix stiffness with the composite's stiffness.

$$A^{\text{SCM}} = \left[I + \xi S(C^l - C) \right]^{-1} \quad (5.14)$$

where A^{SCM} is the strain concentration tensor of the self-consistent method.

5.3.1.4 Strength of Materials

The evaluation of moduli using the strength of materials approach utilizes the equilibrium equations, continuity equations, and stress-strain relationships (Noor and Shah 1993). The mechanical, thermal, and hygral properties of uni-directional composites can be derived using these equations.

Mechanical properties include the prediction of using simplified micromechanics equations for a uni-directional composite, shown in Figure 5.6, are longitudinal Young's modulus (E_{11}), transverse Young's modulus (E_{22}), shear moduli (G_{12}, G_{23}) and Poisson's ratio (ν_{12}, ν_{23}). The equations of the moduli solved using the strength of the material approach are as follows (Reifsnider et al. 1986; Noor and Shah 1993):

$$\text{Longitudinal Young's modulus : } E_{11} = V_f \ E_{f11} + V_m \ E_{m11} \quad (5.15)$$

$$\text{Transverse Young's modulus : } E_{22} \text{ or } E_{33} = \frac{E_m}{\left(1 - \sqrt{V_f} \left(1 - \frac{E_m}{E_{f22}} \right) \right)} \quad (5.16)$$

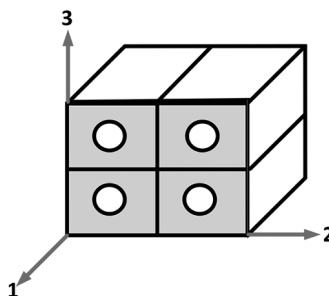


FIGURE 5.6 Uni-directional composite.

$$G_{12} \text{ or } G_{13} = \frac{G_m}{\left(1 - \sqrt{V_f} \left(1 - \frac{G_m}{G_{f12}}\right)\right)} \quad \text{Shear moduli : and} \quad (5.17)$$

$$G_{23} = \frac{G_m}{\left(1 - V_f \left(1 - \frac{G_m}{G_{f23}}\right)\right)}$$

$$\nu_{12} \text{ or } \nu_{13} = V_f \nu_{f12} + V_m \nu_m \quad \text{Poisson's ratios : and} \quad (5.18)$$

$$\nu_{23} = \frac{E_{22}}{(2G_{23} - 1)}$$

E_m , E_f , G_m , G_f , ν_m , and ν_f represent the matrix Young' modulus, fiber Young's modulus, matrix shear modulus, fiber shear modulus, matrix Poisson's ratio, and fiber Poisson's ratio, respectively.

5.3.1.5 Mori–Tanaka Homogenization Method

The analytical technique, i.e., Mori–Tanaka method, is the homogenization method based on Eshelby's equivalent inclusion method. Eshelby's method is considered a lone spherical inclusion in the matrix and proposed the homogenization scheme. The single inclusion in the matrix is considered as the representative volume element (RVE). Therefore, the Mori–Tanaka method is regarded as an RVE-based homogenization technique. On another side, the numerical method, i.e., finite element method (FEM), is based on the deformation study of RVE of adequate geometrical information to predict the behavior or response of MMNCs. The strain or force loading can be applied to the RVE to find out the equivalent homogenized properties.

For a heterogeneous and anisotropic material, the generalized Hooke's law is defined as:

$$\sigma_{ij} = C_{ijkl} \varepsilon_{ij} \quad (5.19)$$

C_{ijkl} is the stiffness matrix of the composite, which contains 36 constants. Depending on the fiber spreading and orientation in the matrix, these constants can be determined by the following continuum micro-mechanics approaches.

An RVE is selected considering microscopic heterogeneous and macroscopic homogenous materials, as illustrated in Figure 5.7. The boundary conditions are

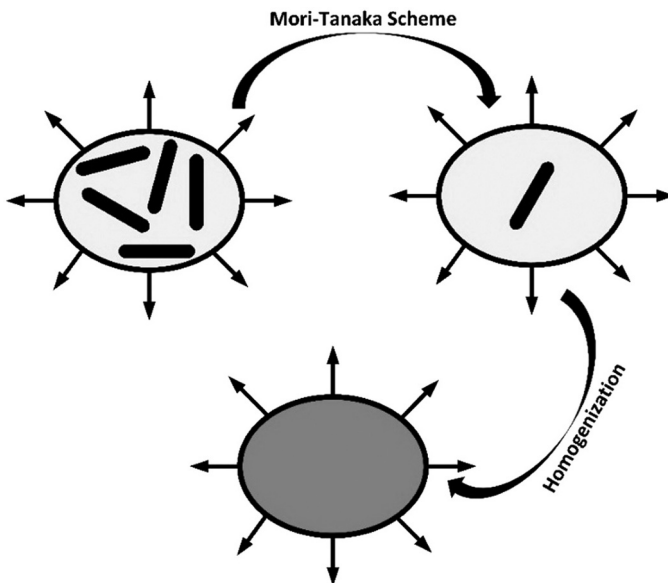


FIGURE 5.7 Illustration of Mori–Tanaka model.

framed in terms of linear displacement vectors or macro-field traction vectors. The RVE is assumed to be deformable and in an equilibrium state. Inertial and body forces are neglected. Thus, the comparable properties of the system are represented as (Arora and Pathak 2020b):

$$C_{abcd}^{\text{eff}} = \frac{1}{V} \int_V c_{abij}(r) A_{ijcd}(r) dV \quad (5.20)$$

All the information related to microstructure is carried by the unknown parameters, which are defined by the strain concentration tensor \mathbf{A} . In other terms, the C^{eff} and \mathbf{A} are described as (Arora and Pathak 2020b):

$$C^{\text{eff}} = c^0 + \sum_{X=1}^N v_X (c^X - c^0) : \mathbf{A}^X \quad (5.21)$$

where c^0 and c^X represents the uniform stiffness tensor of matrix and phase, \mathbf{A}^X represents the global strain concentration tensor and v_X is the volume fraction of phase X.

$$\left\{ \begin{array}{l} \mathbf{A}^X = \mathbf{a}^X : \langle \mathbf{a}^X \rangle^{-1} \\ (\mathbf{a}^X)_0 = \mathbf{X} \\ (\mathbf{a}^X)_{i+1} = (\mathbf{X} + \mathbf{T}^I : \Delta c^X)^{-1} : \left(\mathbf{X} - \sum_{J=0}^N \mathbf{T}^J : \Delta c^J : (\mathbf{a}^J)_i \right) \\ \mathbf{X} = 0, 1, 2, \dots, N \end{array} \right\} \quad (5.22)$$

With \mathbf{a}^X representing the local strain concentration tensor, $\Delta c^X = c^J - C^{rh}$ and C^{rh} is termed the uniform stiffness tensor of homogenous reference medium. \mathbf{T}^I is the tensor representing the interaction between the inclusions in the RVE. It is expressed as (Arora and Pathak 2020b):

$$\mathbf{T}^I = \frac{1}{V^I} \int \int \Gamma(r - r') dV dV' \quad (5.23)$$

where $\Gamma(r - r')$ is the modified Green tensor. The medium used as reference is replaced by matrix when the Mori–Tanaka scheme is selected for homogenization. Inside the matrix, the average strain field approximation is calculated by the strain in the reference medium. Therefore, on the following assumptions, the equivalent Mori–Tanaka properties (MTP) are represented as (Arora and Pathak 2020b):

$$C^{MTP} = \sum_{X=0}^N v_X c^X \mathbf{A}^X = \left(v_0 c^0 + \sum_{X=1}^N v_X c^X \mathbf{a}^X \right) : \mathbf{A}^0 \quad (5.24)$$

where \mathbf{A}^0 denotes the global strain concentration tensor of the matrix. The expression \mathbf{A}^0 is expanded as:

$$\mathbf{A}^0 = \mathbf{a}^0 : \langle \mathbf{a}^X \rangle^{-1} = \left(v_0 X + \sum_{X=1}^N v_X \mathbf{a}^X \right)^{-1} \quad (5.25)$$

5.3.1.6 Finite Element Method

In the micro-scale finite element analysis (FEA), the key method used is unit-volume homogenization to accomplish the macroscopic properties of the composites. With the assumption of the orthotropic nature of the unit volume, the

following constitutive relation for the evaluation of effective properties is used (Zhang et al. 2018). The small deformation to the unit volume is applied:

$$\overline{\sigma_{ij}} = E_{ijkl} \overline{\varepsilon_{kl}} \quad (5.26)$$

where E_{ijkl} is the effective stiffness tensor. In the unit volume, the average stresses, $\overline{\sigma_{ij}}$ and average strains, $\overline{\varepsilon_{kl}}$ are defined as follows (Zhang et al. 2018):

$$\overline{\sigma_{ij}} = \frac{1}{V} \int_V \sigma_{ij} dV \text{ and } \overline{\varepsilon_{kl}} = \frac{1}{V} \int_V \varepsilon_{kl} dV \quad (5.27)$$

where V is the volume of the unit cell.

In the cuboid unit-volume model, when employing periodic boundary conditions, if small displacement is applied, it means $\overline{\varepsilon_{kl}}$ is known and $\overline{\sigma_{ij}}$ can be determined by the following relation (Zhang et al. 2018):

$$\overline{\sigma_{ij}} = \frac{(F_i)_j}{S_j} \quad (5.28)$$

where $(F_i)_j$ is the i th resultant forces on the j th surface and S_j is the area of the j th surface.

The predicted stress-strain curves are then used to define the various strengths of the composites. Also, the linear range of the stress-strain curves can be used to determine the elastic moduli of the composites using the following relations (Zhang et al. 2018):

$$E_{ii} = \frac{\bar{\sigma}_{ii}}{\bar{\varepsilon}_{ii}}, \quad v_{ij} = \frac{-\bar{\varepsilon}_{jj}}{\bar{\varepsilon}_{ii}}, \quad G_{ij} = \frac{\bar{\sigma}_{ij}}{\bar{\varepsilon}_{ij}} \quad (i,j = 1,2,3) \quad (5.29)$$

The flow chart of Mori–Tanaka and FEM to determine the effective properties of the nanocomposites are presented in Figure 5.8.

5.3.2 MULTI-SCALE APPROACH

Multi-scale investigation to predict the mechanical and thermal properties of the composites is a well-known study for the structures (Arora and Pathak 2019a, 2020a; Padmanabhan et al. 2020; Bhatnagar et al. 2021). A generalized bottom-up multi-scale approach is shown in Figure 5.9 to study the composites. The micro-scale material properties, as defined in Section 3.1, can be obtained either using the popular Mori–Tanaka method or the finite element method. Further, the micro-scale properties would be used to study the structure at the macro-scale

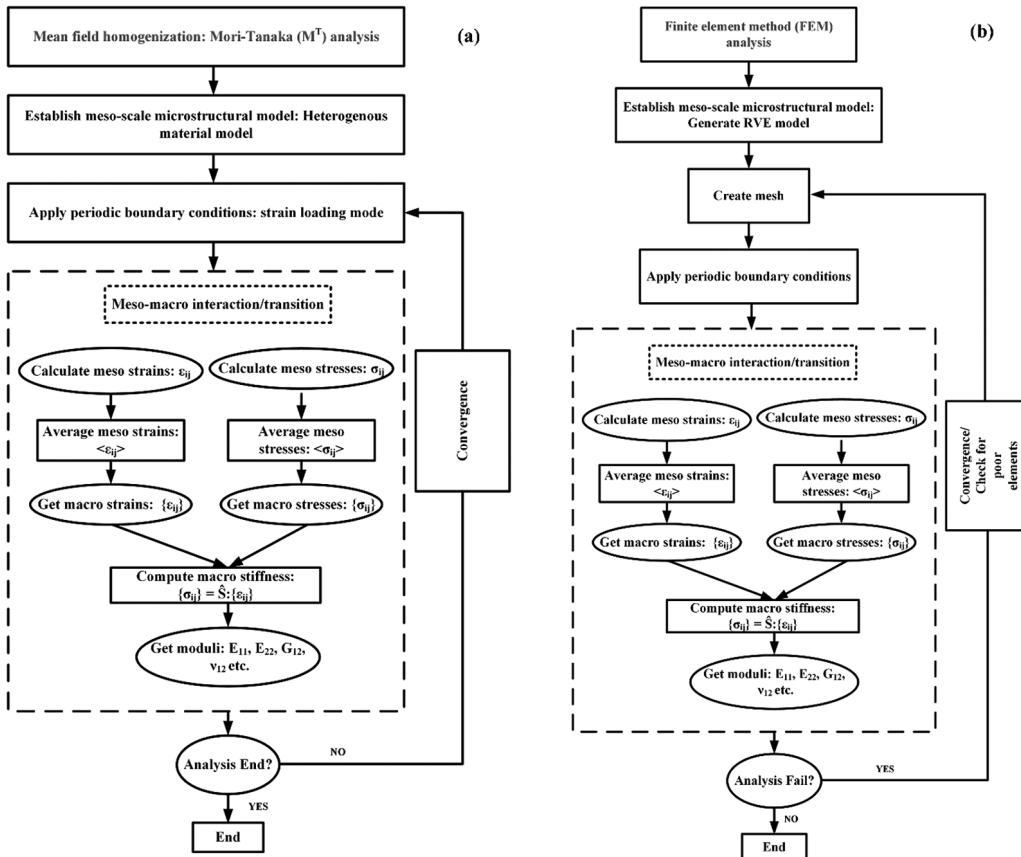


FIGURE 5.8 Flow work of Mori–Tanaka and FEM at a meso-scale to evaluate effective material properties (Arora and Pathak 2019b).

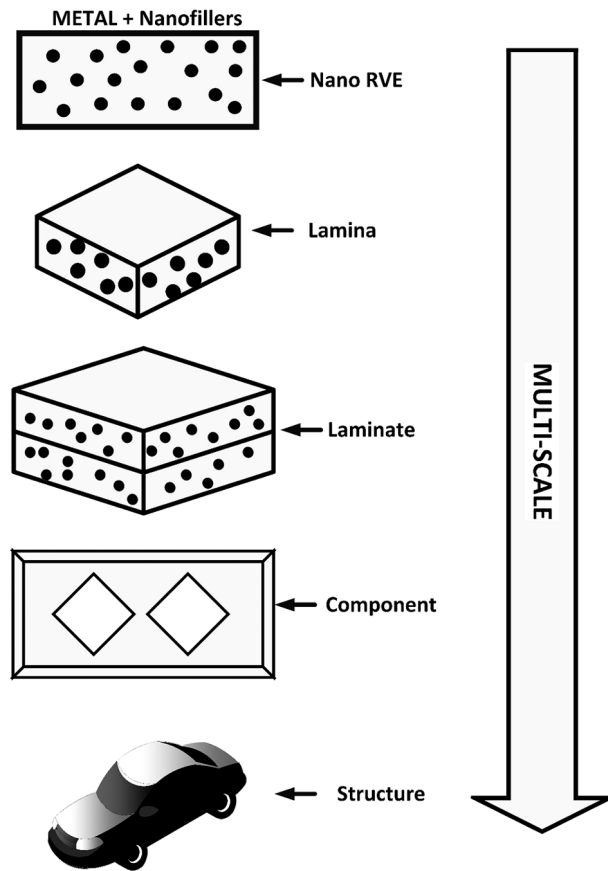


FIGURE 5.9 Multi-scale approach to study the computational mechanical testing of MMNCs.

level. Popularly tensile, fracture toughness, impact, compression, and fatigue are the macro-scale tests studied on the composites to define their basic mechanical properties. Experimentally, ASTM, ISO, JIS, or MPIF standards were followed to examine the composites.

The local and global numerical analysis is necessary to depict the elastic, elasto-plastic, and thermal material behavior of MMNCs. Multi-scale investigation helps predict the local damages, hot-spots, or stress-concentrations at micro-scale level and define the non-linear behavior of the MMNCs. Thus, the exact behavior of the MMNCs at the macro-scale level, considering the non-linear behavior depicted at the micro-scale, can be achieved by the multi-scale strategy. As shown in Figure 5.9, initially an RVE of metal and nanofillers is studied under different loading or environment. The material behavior at this

level is studied and called a continuum nano-mechanics approach. A single ply of the composite is called the lamina, which is the next level higher from RVE. The fiber orientation affects the overall properties of the lamina. Multiple plies of the composite are called laminate, which is the next level higher to the lamina. The orientation of plies affects the overall properties of the laminate. The levels of RVE–lamina–laminates are the multi-scale analysis to predict the properties of a small unit (RVE) at a relevant scale, homogenizing to express the constitutive models, and then to pass the information to simulate the large unit (laminate).

The virtual testing of the component to be used in the structure is carried out in three sequential steps. Within the framework of the FEM, the first step is computational micromechanics, which predicts the lamina's properties based on the information of the matrix and fillers. The manufacturer provides the basic information about the ply, such as the volume fraction of the constituents, the orientation of the fillers, interface conditions, mechanical and thermal properties of the constituents by thorough experimental characterization. Second, the computational meso-mechanics, using the properties of the homogenized lamina, lay-up sequence of the laminas, and interply behavior were used to determine the laminate's homogenized behavior. Lastly, this homogenized behavior of the laminate is utilized within the framework of computational mechanics until the component's failure.

5.4 EFFECTIVE MATERIAL PROPERTIES OF MMNCs

Computational research on the effective material properties of MMNCs has gained popularity due to the advancement of technology. Many commercial computational software packages have the capabilities to examine the behavior of the MMNCs virtually and thus save time and cost of manufacturing. Although the significant factors studied by many researchers that influences the behavior of MMNCs are as follows:

- Influence of volume fraction of the nanofillers
- Influence of orientation of the nanofillers
- Influence of interphase between the constituents
- Influence of aspect ratio of the nanofillers

Many nano-fillers have been used in the MMNCs in the form of particle and nanotubes. The higher elastic modulus, strength, and lower coefficient of thermal expansion (CTE) of these nano-fillers have been the critical criteria to tailor the mechanical properties of the MMNCs. We shall be discussing the effective material properties of three widely used nano-fillers, i.e., silicon carbide (SiC), graphene nanoplatelets (GNP), and carbon-nanotubes (CNTs) in MMNCs. Table 5.1 represents the elastic constants of these nanofillers.

TABLE 5.1
Elastic Constants of the Nanofillers

Nanofiller Type	Young's Modulus (GPa)	Poisson's ratio	CTE (10^{-6} K^{-1})
SiC (Mohammad K Hassanzadeh-Aghdam 2019; Hua and Gu 2013; Yuan et al. 2012)	410–450	0.17–0.19	4.3–4.8
Graphene nanoplatelets (Gao et al. 2017; Sun et al. 2021)	1000	0.17	4–6
Carbon nanotubes (Mohammad Kazem Hassanzadeh-Aghdam et al., 2018b)	800	0.469	-12

5.4.1 INFLUENCE OF VOLUME FRACTION OF THE NANOFILLERS

The volume fraction of nanofillers is one of the essential influencing factors which may enhance or deteriorate the properties of the MMNCs. It has been noticed that if a critical volume fraction either of nanoparticles or nanotubes in MMNCs is improving the mechanical properties, then it is decreasing the thermal properties. Therefore, researchers have to trade-off between the volume fraction of nanofillers and the desired properties of MMNCs.

Chawla et al. (Chawla et al. 2004) did the experimental and simulation analysis on the microstructure of SiC/Al nanocomposites. A three-dimensional model was studied using FEM to determine Young's modulus of the nanocomposites. A mismatch between the values has been found due to the difference in CTEs of the constituents. Hua et al. (Hua and Gu 2013) predicted the thermo-mechanical properties of the SiC/Al nanocomposites using the Mori-Tanaka theory in combination with FEM. The stiffness of SiC has increased the effective Young's modulus of the nanocomposites, whereas the effective Poisson's ratio and CTE have shown minimal sensitivity. An effective Young's modulus obtained by Mori-Tanaka, FEM, and experimentation are in good agreement. A higher sensitivity in Young's modulus was obtained after 10% addition of SiC particles. A 27.5% decrement has been observed in CTE as the volume fraction of SiC particles has increased from 0% to 30%.

Sun et al. (Sun et al. 2021) studied the elastic-plastic properties of the graphene reinforced nanocomposites, considering the hard and soft interface between the constituents. The micromechanics approach using Eshelby's inclusion model predicted that Young's modulus of the composites results in an increase in volume fraction (0% to 5%) of the graphene. On the other hand, the hard interphase has shown an increase in Young's modulus of the nanocomposites, but a decreasing pattern has been observed in the soft interphase case. With the increase in interfacial Poisson's ratio (from 0.1 to 0.4) an increase in Young's modulus with the rise in the volume fraction of graphene in case of hard interphase has been observed.

A minimal variation in Young's modulus has been observed in the soft interphase case along with Poisson's ratio of the interphase.

The micromechanical approach has been utilized by Hassanzadeh-Aghdam (Mohammad K Hassanzadeh-Aghdam 2019) to study the thermal properties of SiC/Al nanocomposites. The results predicted the increase in elastic modulus of the nanocomposites with the inclusion of the SiC particles with or without interphase. The CTE of the composites has decreased with the inclusion of the SiC particles. The interphase between the constituents has predicted lesser CTE than without interphase nanocomposites, although a linear relationship has been found between CTE and increment in volume fraction (0% to 15%) of SiC particles.

Yuan et al. (Yuan et al. 2012) use the finite element method to study the stress-strain distribution numerically in the Sic/Al nanocomposites. Young's modulus and tensile stress have been increased with an increase in volume fraction from 10% to 20%, whereas a decrement has been observed in modulus and strength of the composites from 30% to 40% volume fraction of the particles. The random distribution of the SiC particles decreased the mechanical properties as the volume fraction of the particles increased.

Hassanzadeh-Aghdam et al. (Mohammad Kazem Hassanzadeh-Aghdam et al., 2018b) used RVE micromechanical modeling to study the thermoelastic properties of the CNT/Al nanocomposites. The CTEs decreases with an increase in the volume fraction of the CNTs from 1% to 5%. Alfonzo et al. (Alfonso et al. 2015) predicted the effective Young's modulus of CNT/Al nanocomposites using FEM and compared the results with the rule of mixture. The work reveals that modulus has increased with an increase in the volume fraction of CNTs. Although, the cap ends of CNTs have less effective modulus compared to uncapped ends. M. K. Hassanzadeh-Aghdam et al. (M. K. Hassanzadeh-Aghdam and Mahmoodi 2017) modeled the CNT/AL nanocomposites using the analytical method to evaluate Young's modulus, yield strength, and ultimate strength of the nanocomposites. The work mainly focuses on the straight and wavy CNTs and a good agreement between the experimental and presented predictions. The three mechanical properties have found to be increasing with an increase in the volume fraction of CNTs. Also, it has been concluded that lower CTE CNTs can improve the strength of the nanocomposites.

Ansari et al. (Ansari et al. 2016) developed the 3D micromechanics-based analytical model for the investigation of Young's modulus and studying yield behavior under the biaxial loadings. The predicted results have shown good agreement with the experimental and molecular dynamic simulation results available in the literature. Both longitudinal and transverse Young's modulus was studied with or without interphase. Joshi et al. (Joshi and Upadhyay 2014a, 2014b) studied the multi-walled CNTs (MWCNTs) embedded in the Al matrix numerically using FEM by varying the stiffness of the interphase and volume fraction of the CNTs. The work reveals that the thick interphase and higher volume fraction increase Young's nanocomposites' modulus remarkably. Nouri et al. (Nouri et al. 2012) fabricated the MWCNTs and model the nanocomposites to determine Young's modulus. The predicted elastic modulus and hardness of the composites were in decent agreement with the experimental results.

TABLE 5.2**Effect of Volume Fraction on the Effective Material Properties of MMNCs**

Nanofiller (Volume Fraction, %)	Theory	Effective Young's Modulus (GPa)	Effective Poisson's Ratio	Effective CTE ($10^{-6}K^{-1}$)	Reference
SiC(20%)	3D-RVE	100–113	—	—	(Chawla et al. 2004)
SiC(0–30%)	Mori–Tanaka, FEM	75–115 (↑)	0.33–0.29(↓)	27–17 (↓)	(Hua and Gu 2013)
SiC(0–12%)	3D-RVE	73–94 (↑)	—	21–18.5 (↓)	(Mohammad K Hassanzadeh- Aghdam 2019)
SiC(0–10%)	Mori–Tanaka, FEM	85–450 (↑)	0.45–0.05(↓)	—	(Kursa et al. 2018)
GNP(0–5%)	Analytical modeling	76–114 (↑)	—	—	(Sun et al. 2021)
CNT(0–20%)	FEM	90–210 (↑)	—	—	(Alfonso et al. 2015)
CNT(0–5%)	Analytical modeling	70–135 (↑)	—	—	(M. K. Hassanzadeh- Aghdam and Mahmoodi 2017)
CNT(0–5%)	3D-RVE	74–118.4(↑)	—	—	(Ansari et al. 2016)
CNT(0–10%)	3D-RVE	—	—	24–12 (↓)	(Mohammad Kazem Hassanzadeh- Aghdam et al., 2018)
CNT (2%)	FEM	83.96 (average)	—	—	(Nouri et al. 2012)
CNT (3–9%)	FEM	138–178 (↑)	—	—	(Joshi and Upadhyay 2014b)

Note: (↑) represents an increase, (↓) represents decrease, and — represents data not available.

Therefore, based on the literature survey, Table 5.2 has been produced to visualize the effect of volume fraction on the nanocomposites' effective properties reinforced with SiC, GNP, and CNTs in the metal matrix.

5.4.2 INFLUENCE OF ORIENTATION OF THE NANOFILLERS

The second crucial influencing parameter is the orientation of the nanofillers. The research on orientation leads to different material behavior in another direction. Uni-directional, 2D, and 3D random orientation of nanofillers will be discussed in this section.

Hua et al. (Hua and Gu 2013) studied the aligned, 2D and 3D orientation of SiC particles in the Al matrix-reinforced nanocomposites for the evaluation of thermomechanical properties. Mori–Tanaka results in a different direction predicted that longitudinal and transverse Young's modulus is strongly dependent

on the orientation. A rise of 19.9% and 26.4% in the effective longitudinal modulus has been reported for the aligned case compared with 2D and 3D orientation cases. Transverse modulus reduced to 0.8% and 4.7% in the aligned case compared to 2D and 3D orientation cases. The longitudinal CTE in aligned, 2D, and 3D cases reduces to 49%, 35.6%, and 31%, respectively. Chawla et al. (Chawla et al. 2004) investigated the 20% volume reinforced SiC in the Al matrix experimentally and numerically. The 3D random distributed numerical model predicted Young's modulus perfectly with experimental results.

The micromechanical modeling of straight and wavy CNTs-reinforced Al MMNCs was studied to evaluate the effect of dispersion on the CTEs (Mohammad Kazem Hassanzadeh-Aghdam et al., 2018). Aligned and random distribution of straight and wavy CNTs have shown a strong influence on the CTEs. Aligned straight CNTs have shown a reduction in CTEs (10^{-6} K^{-1}) from 24 to 15. The randomly oriented straight and wavy CNTs have demonstrated a decrease of 19% and 21%, respectively. A similar study has been done on the CNTs reinforcing Al MMNCs (M. K. Hassanzadeh-Aghdam and Mahmoodi 2017). In this study, the effect of the aligned, 2D, and 3D random orientation of CNTs on the effective modulus, yield, and ultimate strength have been reported. In all three orientation cases, significant improvement in the properties has been reported in the aligned case, whereas a minimal difference has been achieved in the properties along the 2D and 3D random directions. An improvement of 34%, 12%, and 8% has been reported in modulus, yield, and ultimate strength, respectively, in the aligned MMNC compared to 3D random MMNC at 3% volume fraction of CNTs.

Micromechanical analysis on the thermal conductivity of CNT MMNCs was studied to determine the effect of aligned and random CNTs (C. Wang et al. 2019). A remarkable improvement in the thermal conductivity in the aligned MMNC compared to random MMNC have been reported. A gain of 141% in aligned MMNC compared to random MMNC, i.e., along the thermal loading direction, may provide a benefit in the heat transfer applications. Also, the interfacial thermal resistance was studied. The aligned MMNCs showed improvement both with or without interfacial thermal resistance. Table 5.3 illustrates the orientation effect on the material properties.

5.4.3 INFLUENCE OF INTERPHASE BETWEEN THE CONSTITUENTS

Interphase plays an essential role in the evaluation of the effective material properties of MMNCs. It is evident from the literature that both interphase thickness and stiffness are vital for overall improvement in the material properties. Therefore, this section will be discussing the interphase effect on material properties. Table 5.4 shows some of the significant results available in the literature.

The thickness and stiffness of the interface effect on the material properties MWCNTs reinforced MMCs have been investigated (Joshi and Upadhyay 2014a). Interphase thickness 0.05, 0.1, 0.2, 0.34 nm was varied to check the effect on the elastic modulus of the nanocomposites. It has been observed that increasing the thickness from 0.05 nm to 0.34 nm has increased the normalized modulus,

TABLE 5.3
Effect of Orientation on the Effective Material Properties of MMNCs

Nanofiller(Volume Fraction, %)	Orientation	Effective Young's Modulus(GPa)	Effective Poisson's Ratio	Effective CTE(10^{-6} K $^{-1}$)	Thermal Conductivity (W/m-K)	Reference
SiC (20%)	Aligned	122	0.35	16	—	(Hua and Gu 2013)
SiC (20%)	2D random	105	0.297	19	—	(Hua and Gu 2013)
SiC (20%)	3D random	107.9 ± 0.7^e	—	—	—	(Chawla et al. 2004)
		107.4 ± 0.4^t	—	—	—	(Chawla et al. 2004)
		95	0.31	21	—	(Hua and Gu 2013)
CNT (5%)	Aligned	119	—	—	—	(M. K. Hassanzadeh-Aghdam and Mahmoodi 2017)
		—	—	15	—	(Mohammad Kazem Hassanzadeh-Aghdam et al., 2018)
CNT (5%)	2D Random	84	—	—	—	(M. K. Hassanzadeh-Aghdam and Mahmoodi 2017)
		—	—	20.3	—	(Mohammad Kazem Hassanzadeh-Aghdam et al., 2018b)
CNT (5%)	3D Random	73.5	—	—	—	(M. K. Hassanzadeh-Aghdam and Mahmoodi 2017)
		—	—	21.5	—	(Mohammad Kazem Hassanzadeh-Aghdam et al., 2018b)
CNT (5%)	Aligned (no resistance)	—	—	—	460	(C. Wang et al. 2019)
	Aligned (with resistance)	—	—	—	455	
CNT (5%)	Random (no resistance)	—	—	—	360	(C. Wang et al. 2019)
	Random (with resistance)	—	—	—	320	

Note: “e” represents experimental, “t” represents theoretical, and “—” means no data available.

TABLE 5.4**Effect of Interphase on the Effective Material Properties of MMNCs**

Nanofiller(Volume Fraction, %)	Interphase	Effective Young's Modulus(GPa)	Effective CTE($10^{-6}K^{-1}$)	Reference
SiC (10%)	With	95	19.5	(Mohammad K Hassanzadeh-Aghdam 2019)
	Without	90	17.5	
	Experimental	95	—	
CNT (10%)	With	—	5	(Mohammad Kazem Hassanzadeh-Aghdam et al., 2018b)
	Without	—	2.5	
CNT (9%)	Soft	173	—	(Joshi et al., 2014b)
	Hard	188	—	
CNT (5%)	With	167.3	—	(Ansari et al. 2016)
	Without	118.4	—	
GNP (5%)	Soft	114.4	—	(Sun et al. 2021)
	Hard	96.2	—	
CNT (10%)	With	162	—	(Haghgoo et al. 2019)
	Without	137	—	

Note: ‘—’ represents no data available

i.e., $\left(\frac{E_{\text{nanocomposite}}}{E_{\text{matrix}}} \right)$ remarkably. It was also noticed that stiff and soft interphase had increased the normalized modulus to 1.9 and 1.75, respectively, at a maximum volume fraction of the CNTs.

The representative volume element analysis on CNT nanocomposites with and without interphase between the constituents has been done (Ansari et al. 2016). The results of the study are compared with the rule of mixture. It has been observed that increasing the volume fraction of CNTs from 1% to 5% with interphase present between the constituents has increased the longitudinal Young's modulus to 41% compared to without interphase nanocomposites. Similarly, a 23% gain in elastic modulus along the transverse direction has been noticed with the interphase.

The thermal behavior of the nanocomposites using the RVE method has been investigated when reinforced with 0% to 10% CNTs (Mohammad Kazem Hassanzadeh-Aghdam et al., 2018). It has been observed that without interface and with the interface (thickness of 2.5 nm to 10 nm), the CTEs ($10^{-6} K^{-1}$) have reduced, with an increase in the volume fraction of the CNTs. This reveals that thermoelastic results are sensitive to interphase conditions. The effect of interphase thickness on longitudinal as well as transverse CTEs was negative.

An investigation into Al_2O_3 and SiC-embedded MMNCs has been done using the RVE micromechanical method (Mohammad K Hassanzadeh-Aghdam 2019). It was reported that reinforcing Al_2O_3 from 0% to 20% volume fraction in Mg

matrix without interphase has shown a minimal change in CTEs of the composites. But with interphase presence, CTEs have reduced from 28.5 to 25.5 with the increase in volume fraction from 0% to 20%, respectively. The model suggested in this study has shown good agreement with up to an 8% volume fraction of CNTs. In the same study, reinforcing SiC in the Al matrix from 0% to 50% have shown a decrement in CTEs from 27 to 14, respectively. The results of interface thickness varied from 0.25 μm to 0.75 μm hardly showed any significant change in the respective volume fraction of CNTs. Although, the pattern of results obtained from the RVE model and rule of the mixture was the same. The elastic modulus of 0% to 12% reinforced SiC particles in Al matrix without and with the interface has shown good agreement with the experimental results. An increment of 6.4% has been observed in the nanocomposites with interphase than without interphase nanocomposites at 12% volume fraction of the particles.

The elastoplastic behavior of CNTs-reinforced MMNCs using micromechanical modeling have been studied (Haghgoo et al. 2019). According to the micromechanical model, with and without interphase, the elastic modulus increases with the change in the volume fraction of the CNTs. The study on improving the thickness of the interface from 5 nm to 35 nm reveals that the yield stress of the MMNCs enhances. Also, increasing the stiffness of the interphase from 109 GPa to 409 GPa has increased the yield stress from 90 MPa to 132 MPa, respectively. The elastoplastic nature of the interphase also affects the yield stress of the nanocomposites. If the interphase yield stress is varied from 65 MPa to 260 MPa, then the nanocomposites yield stress changes from 30 MPa to 120 MPa, respectively, and the elastic range also increase from 0.02% to 0.1%, respectively.

GNP-reinforced MMNCs with soft and hard interphase have been investigated by the Mori–Tanaka method (Sun et al. 2021). It has been observed that with the increase in the volume fraction of GNPs from 0% to 10%, the hard interphase nanocomposites have shown an increase in the elastic modulus. Still, for the soft interphase nanocomposites, hardly any change has been noticed. Also, the Young's modulus increases if the interphase modulus is equal to or greater than the matrix modulus. A change in yield strength of the nanocomposites from 150 MPa to 320 MPa corresponding to 0% to 8% volume fraction with hard interphase has been observed. This change was in good agreement with the experimental data.

5.4.4 INFLUENCE OF ASPECT RATIO OF THE NANOFILLERS

Multi-scale modeling on Al-Ni-Y nanocomposites has been employed to predict Young's nanocomposites' modulus (Liu and Sun 2005). Elastoplastic behavior has been predicted by applying the uniaxial load computationally. The ceramic particles are aligned in the loading direction. To determine the effect of aspect ratio on the elastoplastic properties of the nanocomposites, the aspect ratio of the particles has changed during the simulation. As the aspect ratio increase from 1 to 2, the overall elastic modulus of the nanocomposites increases by 8.2%, whereas the overall yield stress of the nanocomposites increases to 10.3% with the increase in aspect ratio from 1 to 2.

The thermo-mechanical behavior of SiC/Al nanocomposites using Mori-Tanaka combined with FEM to study the effect of aspect ratio on the effective Young's modulus and CTEs have been done (Hua and Gu 2013). Effective Young's modulus has increased to 63%, and effective Poisson's ratio and CTEs has reduced to 10% and 32%, respectively, with an increase in volume fraction from 0% to 30% of SiC particles of aspect ratio 20. No effect on the effective properties has been observed at an aspect ratio greater than 20. In general, particles of a higher aspect ratio have an appreciable effect on the overall properties of the nanocomposites.

The Young's modulus of CNT/Al nanocomposites has been studied using the FEM model (Alfonso et al. 2015). The main focus of the study was to determine the effect of different interface thickness and volume fraction of CNTs of the same aspect ratio. It has been observed that long CNTs without caps on the ends have a significant effect on the Young' modulus at the same aspect ratio. FEM, FEM with caps and rule of the mixture has been used to determine the Young's modulus. No difference has been found between FEM and the rule of mixture in the axial direction. But with the hemispherical ends of CNTs, Young's modulus has decreased with an increase in volume fraction compared to other schemes. This may be due to more effective load transfer across the planar interface in nanocomposites with hemispherical ends.

Mean filed approaches have been utilized to study the elastoplastic behavior of Al-based nanocomposites. The nanoparticles used in this study are SiC, Al_2O_3 , and ZrO_2 of volume fraction varied from 0% to 40%. The aspect ratio, i.e., 0.67 of all the nanoparticles in this study, has been kept constant to study the variation of different approaches. It has been observed that finite element and self-consistent averaging schemes are in decent agreement with an increase in volume fraction and constant aspect ratio. Young's modulus, shear modulus, Poisson's ratio, and bulk modulus were evaluated. Unidirectional, shear and bulk modulus increases, but Poisson's ratio decreases when studied with the schemes.

Micromechanical modeling of CNT-reinforced Al nanocomposites to study the longitudinal and transverse CTEs have been accomplished using the RVE method. Two different material nature of CNTs have been used, i.e., isotropic and transversely isotropic. It has been observed that longitudinal CTEs decreased for both isotropic and transversely isotropic CNT composites. Although, a 64% decrease in longitudinal CTEs at 10% volume fraction of transversely isotropic CNT nanocomposites have been observed compared to isotropic CNT nanocomposites. Transverse CTEs of transversely CNT nanocomposites have increased to 16% in comparison to isotropic CNT nanocomposites. The effect of short, aligned CNT with aspect ratio varied from 0 to 5000 on longitudinal and transverse CTEs have been studied with the volume fraction of CNTs varied from 1% to 5%. Longitudinal CTEs decreases with an increase in volume fraction and aspect ratio of the CNTs, whereas transverse CTEs increase. The primary outcome of the study was that after 500 aspect ratio, the decrement and increment in longitudinal and transverse CTEs, respectively, was negligible. Table 5.5 provides detailed insight into the effect of aspect ratio on the effect properties.

TABLE 5.5
Effect of Aspect Ratio on the Effective Material Properties of MMNCs

Nanofiller (Volume Fraction, %)	Aspect Ratio (L/d)	Effective Young's Modulus (GPa)	Effective CTE (10^{-6} K^{-1})	Reference
Ni-Y (25%)	1	85.75	—	(Liu and Sun 2005)
	1.5	89.25	—	
	2	92.75	—	
SiC (25%)	1	105	19	(Hua and Gu 2013)
	5	107	18.3	
	10	110	17.8	
	15	110	1.8	
	20	110	17.8	
CNT (20%)	14	210	—	(Alfonso et al. 2015)
SiC (25%)	0.67	110	—	(Kursa et al. 2018)
Al ₂ O ₃ (25%)	0.67	105	—	
ZrO ₂ (2%)	0.67	85	—	
CNT (5%)	5	—	20	(Mohammad Kazem Hassanzadeh-Aghdam et al., 2018)
	50	—	14	
	500	—	11	

Note: ‘—’ represents no data available.

5.5 HYBRID METAL MATRIX NANOCOMPOSITES (HMMNCs)

Reinforcement of either nanotubes or nanoparticles in the metal matrix composites as the second phase is called hybrid metal matrix nanocomposites (HMMNCs). In other words, the nanocomposites containing two fillers (fiber and nanotubes or nanotubes and nanoparticles) in a metal matrix are called as HMMNCs, shown in Figure 5.10.

HMMNCs have become popular due to their extraordinary mechanical and thermal properties with second nano-inclusion in the metal matrix nanocomposites. Some of the extensively studied HMMNCs are hybrid Al matrix, hybrid Mg matrix, hybrid Cu matrix hybrid titanium matrix and hybrid Fe/steel and Ni-Cr matrix nanocomposites (Zhou et al. 2020). These hybrid nanocomposites have been manufactured by in-situ processing, ex-situ processing, and additive manufacturing techniques (Zhou et al. 2020). Some of the reported continuous fibers are carbon, SiC, Al₂O₃, boron, steel wire, and tungsten. Apart from this, the discontinuous fibers reported are B₄C, TiO₂, MgO, ZrB₂, Si₃N₄, AlNa, and ZrC. The short fibers, whiskers, and sheets reported in the literature are SiC, Al₂O₃, TiB, CNTs, and GNP. Based on the addition of these fibers, the HMMNCs are categorized into two sets, i.e., hybrid continuous and discontinuous reinforcement composites and hybrid discontinuous reinforcement composites. The latter have

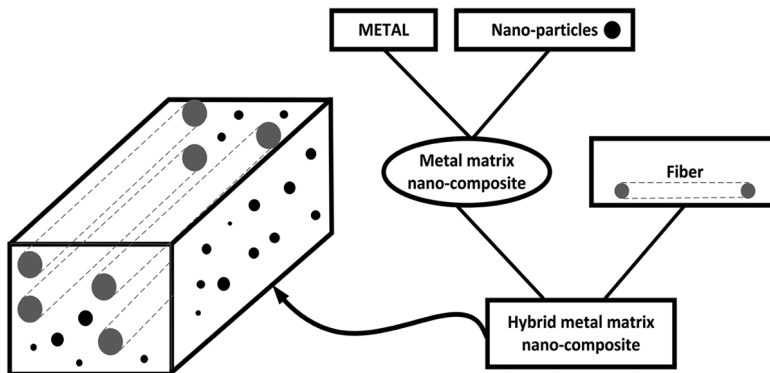


FIGURE 5.10 Pictorial example of HMMNCs.

further been sub-categorized into three different groups, i.e., hybrid micron discontinuous reinforcement composites, hybrid nano discontinuous reinforcement composites, and hybrid multi-scale discontinuous reinforcement composites.

These nanocomposites have been studied analytically with the extended simplified micromechanical approach with an RVE, the shear lag model with an RVE, and micromechanical approach based on the method of cell approach to determine the effective elastic properties, thermo-mechanical responses, and damage analysis in the literature (Chen et al. 2018; Hassanzadeh-Aghdam et al., 2018; Mohammad Kazem Hassanzadeh-Aghdam et al. 2019; Mahmoodi et al. 2018; Shi et al. 2019).

Al nanocomposites reinforced with SiC particles, and SiC whiskers have been studied analytically to determine the elastic properties of the hybrid nanocomposites (Chen et al. 2018). An extensive investigation into the effect of volume fraction, aspect ratio, dispersion, and agglomeration of the inclusions on the elastic modulus has been done. The results predicted that the aggregation of SiC particles has a negative effect on the elastic modulus of the nanocomposites. On the other hand, the factors which have enhanced the elastic modulus are increasing the volume fraction of SiC particles, the aspect ratio of SiC whiskers, decreasing the particle size, aligning the whiskers and uniform spatial distribution of the particles. Tables 5.6–5.10 illustrate the effect of various factors on the elastic modulus of the hybrid composites.

TABLE 5.6
Axial Young's Modulus (GPa) of Hybrid Nanocomposite Predicted with the Aligned Whiskers of Different Aspect Ratios (Chen et al. 2018)

Aspect Ratio, SiC Whiskers	Volume Fraction, SiC Particles	2%	4%	6%
10		120	137	148
100		147	155	165
1000		150	158	165

TABLE 5.7

Transverse Young's Modulus (GPa) of Hybrid Nanocomposite Predicted with the Aligned Whiskers of Different Aspect Ratios (Chen et al. 2018)

Aspect Ratio, SiC Whiskers	Volume Fraction, SiC Particles	2%	4%	6%
10		100	102	102
100		110	112	112
1000		120	122	122

TABLE 5.8

Young's Modulus (GPa) of Hybrid Nanocomposite Predicted with the Different Spatial Distribution of the Nanoparticles (Chen et al. 2018)

Distribution	Volume Fraction, SiC Particles	2%	4%	6%
Axial		145	155	160
Random		118	130	137
Transverse		100	110	120

TABLE 5.9

Young's Modulus (GPa) of Hybrid Nanocomposite Predicted with the Different Aggregation Degree of the Particles (Chen et al. 2018)

Aggregation Degree	Volume Fraction, SiC Particles	2%	4%	6%
1		115.5	128	134
0.8		115	120	128
0.6		114	117	120

TABLE 5.10

Young's Modulus (GPa) of Hybrid Nanocomposite Predicted with the Different Volume Fractions of SiC Whiskers (Chen et al. 2018)

Volume Fraction, SiC Whiskers	Volume Fraction, SiC Particles	2%	4%	6%
9%		95	105	130
18%		105	115	145
27%		115	130	155

Thermal and thermo-mechanical responses have been investigated by adding CNTs to the MMNCs as the second phase (Mohammad Kazem Hassanzadeh-Aghdam et al. 2019; Shi et al. 2019). The straight and wavy CNTs' effect on the responses has been investigated using micromechanical modeling with an RVE. It has been reported that the nanocomposites' overall thermal conductivity can be increased by adding significant and straight CNTs in the axial direction. The transverse thermal conductivity can be increased by adding the large diameter and wavy CNTs. Adding a large volume fraction of CNTs has increased the thermal conductivity considering the perfect bond condition between the CNTs and matrix. Tables 5.11–5.13 illustrate the effect of various factors on the thermal conductivity of the hybrid nanocomposites.

Ti-based hybrid nanocomposites with aligned SiC fibers and randomly distributed CNTs have been investigated to predict the overall thermo-mechanical response (Mohammad Kazem Hassanzadeh-Aghdam et al. 2019). The results reveal the effect of aspect ratio, off-axis angle, spatial distribution, and volume fraction of SiC, volume fraction, agglomeration, waviness, random distribution, and aspect ratio effect of CNTs on the CTEs elastic moduli of the hybrid nanocomposites. Tables 5.14–5.17 illustrate the effect of the volume fraction of CNTs and SiC fibers on the effective nanocomposite's properties. Other factors like the aspect ratio of CNTs (50, 133.3, and 200) have a negligible effect on the

TABLE 5.11
Axial and Transverse Thermal Conductivities of Hybrid MMNCs
(Shi et al. 2019)

Thermal Conductivity, W/mK	CNTs, Volume Fraction		
	2%	4%	6%
Axial	375	425	475
Transverse	335	345	350

TABLE 5.12
Axial and Transverse Thermal Conductivities of Hybrid MMNCs
Predicted with the Different Bonding Conditions (Shi et al. 2019)

Thermal Conductivity, W/mK	CNTs, Volume Fraction		
	2%	4%	6%
Axial (imperfect bonding)	325	326	327
Axial (perfect bonding)	375	430	495
Transverse (imperfect bonding)	290	270	245
Transverse (perfect bonding)	332	340	350

TABLE 5.13

Axial and Transverse Thermal Conductivities of Hybrid MMNCs with the Number of Waves (n) in CNTs and Aspect Ratio (Shi et al. 2019)

Thermal Conductivity, W/mK	CNTs, Aspect Ratio		
	0.1	0.3	0.5
Axial (n=1)	430	385	367
Axial (n=2)	403	362	354
Axial (n=3)	385	356	351
Transverse (n=1)	383	428	446
Transverse (n=2)	410	451	459
Transverse (n=3)	428	457	462

TABLE 5.14

Axial Young's Modulus (GPa) of Hybrid Nanocomposite Predicted with the Different Volume Fractions of SiC Fibers and CNTs (Mohammad Kazem Hassanzadeh-Aghdam et al. 2019)

Volume Fraction, SiC Fibers	Volume Fraction, CNTs	0%	3% (wavy)	5% (wavy)	5% (straight)
0%		105	120	130	140
10%		125	140	150	160
20%		160	180	185	200
30%		190	210	220	230
40%		220	230	245	260

TABLE 5.15

Transverse Young's Modulus (GPa) of Hybrid Nanocomposite Predicted with the Different Volume Fraction of SiC Fibers and CNTs (Mohammad Kazem Hassanzadeh-Aghdam et al. 2019)

Volume Fraction, SiC Fibers	Volume Fraction, CNTs	0%	3% (wavy)	5% (wavy)	5% (straight)
0%		105	115	130	140
10%		115	130	140	155
20%		130	145	160	175
30%		145	175	190	205
40%		175	190	215	235

TABLE 5.16

Axial and Transverse Poisson's Ratio of Hybrid Nanocomposite Predicted with the Different Volume Fraction of SiC Fibers and CNTs (Mohammad Kazem Hassanzadeh-Aghdam et al. 2019)

Volume Fraction, SiC Fibers	Volume Fraction, CNTs	0%	3% (wavy)	5% (wavy)	5% (straight)
Axial (0% to 40%)		0.30	0.29	0.28	0.27
Transverse (0%)		0.30	0.30	0.30	0.30
Transverse (10%)		0.314	0.308	0.306	0.304
Transverse (20%)		0.31	0.306	0.304	0.302
Transverse (30%)		0.30	0.298	0.296	0.294
Transverse (40%)		0.282	0.280	0.278	0.276

TABLE 5.17

Axial CTEs (10^{-6} K^{-1}) of Hybrid Nanocomposite Predicted with the Different Volume Fraction of SiC Fibers and CNTs (Mohammad Kazem Hassanzadeh-Aghdam et al. 2019)

Volume Fraction, SiC Fibers	Volume Fraction, CNTs	0%	3% (wavy)	5% (wavy)	5% (straight)
0%		10.5	7.5	6	6
10%		9	6.75	6.125	6.125
20%		7.75	6.25	4.75	4.75
30%		7.5	5.85	4.625	4.625
40%		6.75	5.65	4.55	4.55

axial and transverse Young's modulus and CTEs. CTEs of the nanocomposites have increased with the accumulation or aggregation of the CNTs, reducing the thermo-mechanical load transfer from the metal to the CNTs. On the other hand, increasing the aspect ratio of SiC fibers has increased the axial modulus, but no change in the transverse modulus has been observed by adding CNTs in the nanocomposites from 1% to 5% volume fraction.

REFERENCES

- Alfonso, I., Navarro, O., Vargas, J., Beltrán, A., Aguilar, C., González, G., & Figueroa, I. A. (2015). FEA evaluation of the Al4C3 formation effect on the Young's modulus of carbon nanotube reinforced aluminum matrix composites. *Composite Structures*, 127, 420–425. <https://doi.org/10.1016/j.compstruct.2015.03.032>

- Ansari, R., Hassanzadeh-Aghdam, M. K., & Darvizeh, A. (2016). On elastic modulus and biaxial initial yield surface of carbon nanotube-reinforced aluminum nanocomposites. *Mechanics of Materials*, 101, 14–26. <https://doi.org/10.1016/j.mechmat.2016.07.008>
- Arora, G., & Pathak, H. (2019a). Numerical study on the thermal behavior of polymer nano-composites. *Journal of Physics: Conference Series*, 1240(1). <https://doi.org/10.1088/1742-6596/1240/1/012050>
- Arora, G., & Pathak, H. (2019b). Modeling of transversely isotropic properties of CNT-polymer composites using meso-scale FEM approach. *Composites Part B: Engineering*, 166, 588–597. <https://doi.org/10.1016/J.COMPOSITESB.2019.02.061>
- Arora, G., & Pathak, H. (2020a). Experimental and numerical approach to study mechanical and fracture properties of high-density polyethylene carbon nanotubes composite. *Materials Today Communications*, 22, 100829. <https://doi.org/10.1016/j.mtcomm.2019.100829>
- Arora, G., & Pathak, H. (2020b). Multi-scale computational analysis of carbon-nanotube-polymer composite. In *Advances in Mechanical Engineering* (pp. 205–216). https://doi.org/10.1007/978-981-15-0124-1_19
- Arora, G., & Pathak, H. (2021). Nanoindentation characterization of polymer nano-composites for elastic and viscoelastic properties: experimental and mathematical approach. *Composites Part C: Open Access*, 4, 100103. <https://doi.org/10.1016/j.jcomc.2020.100103>
- Arora, G., Singh, M. K., Pathak, H., & Zafar, S. (2021). Micro-scale analysis of HA-PLLA bio-composites: effect of the interpenetration of voids on mechanical properties. *Materials Today Communications*, 28, 102568. <https://doi.org/10.1016/j.mtcomm.2021.102568>
- Bhatnagar, A. S., Gupta, A., Arora, G., Padmanabhan, S., & Burela, R. G. (2021). Mean-field homogenization coupled low-velocity impact analysis of nano fibre reinforced composites. *Materials Today Communications*, 26, 102089. <https://doi.org/10.1016/j.mtcomm.2021.102089>
- Chawla, N., Ganesh, V. V., & Wunsch, B. (2004). Three-dimensional (3D) microstructure visualization and finite element modeling of the mechanical behavior of SiC particle reinforced aluminum composites. *Scripta Materialia*, 51, 161–165. <https://doi.org/10.1016/j.scriptamat.2004.03.043>
- Chen, S., Hassanzadeh-Aghdam, M. K., & Ansari, R. (2018). An analytical model for elastic modulus calculation of SiC whisker-reinforced hybrid metal matrix nanocomposite containing SiC nanoparticles. *Journal of Alloys and Compounds*, 767, 632–641. <https://doi.org/10.1016/j.jallcom.2018.07.102>
- El-Kady, O., & Fathy, A. (2014). Effect of SiC particle size on the physical and mechanical properties of extruded Al matrix nanocomposites. *Materials and Design*, 54, 348–353. <https://doi.org/10.1016/j.matdes.2013.08.049>
- Gao, C., Zhan, B., Chen, L., & Li, X. (2017). A micromechanical model of graphene-reinforced metal matrix nanocomposites with consideration of graphene orientations. *Composites Science and Technology*, 152, 120–128. <https://doi.org/10.1016/j.compscitech.2017.09.010>
- Gupta, M., & Wong, W. L. E. (2015). Magnesium-based nanocomposites: lightweight materials of the future. *Materials Characterization*, 105, 30–46. <https://doi.org/10.1016/j.matchar.2015.04.015>
- Haghgoo, M., Ansari, R., Hassanzadeh-Aghdam, M. K., & Darvizeh, A. (2019). Elastoplastic behavior of the metal matrix nanocomposites containing carbon nanotubes: a micro-mechanics-based analysis. *Proceedings of the Institution of Mechanical Engineers, Part L: Journal of Materials: Design and Applications*, 233, 676–686. <https://doi.org/10.1177/1464420717700927>

- Hassanzadeh-Aghdam, M. K., Ansari, R., & Mahmoodi, M. J. (2018a). Micromechanical estimation of biaxial thermomechanical responses of hybrid fiber-reinforced metal matrix nanocomposites containing carbon nanotubes. *Mechanics of Materials*, 119, 1–15. <https://doi.org/10.1016/j.mechmat.2018.01.002>
- Hassanzadeh-Aghdam, M. K., & Mahmoodi, M. J. (2017). A comprehensive analysis of mechanical characteristics of carbon nanotube-metal matrix nanocomposites. *Materials Science and Engineering A*, 701, 34–44. <https://doi.org/10.1016/j.msea.2017.06.066>
- Hassanzadeh-Aghdam, M. K. (2019). Micromechanics-based thermal expansion characterization of SiC nanoparticle-reinforced metal matrix nanocomposites. <https://doi.org/10.1177/0954406218756447>
- Hassanzadeh-Aghdam, M. K., Ansari, R., & Mahmoodi, M. J. (2018b). Thermal expanding behavior of carbon nanotube-reinforced metal matrix nanocomposites-a micromechanical modeling. *Journal of Alloys and Compounds*, 744, 637–650. <https://doi.org/10.1016/j.jallcom.2018.02.100>
- Hassanzadeh-Aghdam, M. K., Mahmoodi, M. J., Ansari, R., & Mehdipour, H. (2019). Effects of adding CNTs on the thermo-mechanical characteristics of hybrid titanium nanocomposites. *Mechanics of Materials*, 131, 121–135. <https://doi.org/10.1016/j.mechmat.2019.01.022>
- Hong, S., & Myung, S. (2007). Nanotube electronics: a flexible approach to mobility. *Nature Nanotechnology*, 2(4), pp. 207–208. Nature Publishing Group. <https://doi.org/10.1038/nano.2007.89>
- Hu, M., & Yang, Z. (2021). Perspective on multi-scale simulation of thermal transport in solids and interfaces. *Physical Chemistry Chemical Physics*, 23(3), 1785–1801. <https://doi.org/10.1039/d0cp03372c>
- Hua, Y., & Gu, L. (2013). Prediction of the thermomechanical behavior of particle-reinforced metal matrix composites. *Composites Part B: Engineering*, 45(1), 1464–1470. <https://doi.org/10.1016/j.compositesb.2012.09.056>
- Iacobellis, V., & Behdinan, K. (2021). Multiscale methods for lightweight structure and material characterization. In *Advanced Multifunctional Lightweight Aerostructures; Design, Development, and Implementation* (pp. 43–66). Wiley. <https://doi.org/10.1002/9781119756743.ch3>
- Iijima, S., & Ichihashi, T. (1993). Single-shell carbon nanotubes of 1-nm diameter. *Nature*, 363(6430), 603–605. <https://doi.org/10.1038/363603a0>
- Joshi, P., & Upadhyay, S. H. (2014a). Evaluation of elastic properties of multi walled carbon nanotube reinforced composite. *Computational Materials Science*, 81, 332–338. <https://doi.org/10.1016/j.commatsci.2013.08.034>
- Joshi, P., & Upadhyay, S. H. (2014b). Effect of interphase on elastic behavior of multiwalled carbon nanotube reinforced composite. *Computational Materials Science*, 87, 267–273. <https://doi.org/10.1016/j.commatsci.2014.02.029>
- Kursa, M., Kowalczyk-Gajewska, K., Lewandowski, M. J., & Petryk, H. (2018). Elastic-plastic properties of metal matrix composites: validation of mean-field approaches. *European Journal of Mechanics, A/Solids*, 68, 53–66. <https://doi.org/10.1016/j.euromechsol.2017.11.001>
- Liu, H. T., & Sun, L. Z. (2005). Multi-scale modeling of elastoplastic deformation and strengthening mechanisms in aluminum-based amorphous nanocomposites. *Acta Materialia*, 53(9), 2693–2701. <https://doi.org/10.1016/j.actamat.2005.02.029>
- Mahmoodi, M. J., Hassanzadeh-Aghdam, M. K., Ansari, R., & Darvizeh, A. (2018). Damage analysis of unidirectional Ti hybrid nanocomposites containing nanoparticles. *Journal of Alloys and Compounds*, 769, 397–412. <https://doi.org/10.1016/j.jallcom.2018.07.345>

- Moradgholi, J., Monshi, A., Farmanesh, K., Toroghinejad, M. R., & Loghman-Estarki, M. R. (2017). Comparison of microstructure, toughness, mechanical properties and work hardening of titanium/TiO₂ and titanium/SiC composites manufactured by accumulative roll bonding (ARB) process. *Ceramics International*, 43(10), 7701–7709. <https://doi.org/10.1016/j.ceramint.2017.03.072>
- Muhammad, I. D., Awang, M., Mamat, O., & Shaari, K. Z. K. (2015). Estimating Young's modulus of single-walled zirconia nanotubes using nonlinear finite element modeling. *Journal of Nanomaterials*, 2015. <https://doi.org/10.1155/2015/157423>
- Noor, A. K., & Shah, R. S. (1993). Effective thermoelastic and thermal properties of unidirectional fiber-reinforced composites and their sensitivity coefficients. *Composite Structures*, 26(1–2), 7–23. [https://doi.org/10.1016/0263-8223\(93\)90040-W](https://doi.org/10.1016/0263-8223(93)90040-W)
- Nouri, N., Ziae Rad, S., Adibi, S., & Karimzadeh, F. (2012). Fabrication and mechanical property prediction of carbon nanotube reinforced Aluminum nanocomposites. *Materials and Design*, 34, 1–14. <https://doi.org/10.1016/j.matdes.2011.07.047>
- Padmanabhan, S., Gupta, A., Arora, G., Pathak, H., Burela, R. G., & Bhatnagar, A. S. (2020). Meso-macro-scale computational analysis of boron nitride nanotube-reinforced aluminium and epoxy nanocomposites: a case study on crack propagation. *Proceedings of the Institution of Mechanical Engineers, Part L: Journal of Materials: Design and Applications*, 0(0), 1–16. <https://doi.org/10.1177/1464420720961426>
- Pakseresht, M., Ansari, R., & Hassanzadeh-Aghdam, M. K. (2021). An efficient homogenization scheme for analyzing the elastic properties of hybrid nanocomposites filled with multiscale particles. *Journal of the Brazilian Society of Mechanical Sciences and Engineering*, 43(1), 3. <https://doi.org/10.1007/s40430-020-02709-4>
- Pop, E., Mann, D., Wang, Q., Goodson, K., & Dai, H. (2005). Thermal conductance of an individual single-wall carbon nanotube above room temperature. *Nano Letters*, 6(1), 96–100. <https://doi.org/10.1021/nl052145f>
- Pundhir, N., Arora, G., Pathak, H., & Zafar, S. (2020). Ballistic impact response of HDPE/UHMWPE polymer composite. In *Advances in Mechanical Engineering* (pp. 245–255). https://doi.org/10.1007/978-981-15-0124-1_23
- Qiu, C., Su, Y., Yang, J., Chen, B., Ouyang, Q., & Zhang, D. (2021). Structural modelling and mechanical behaviors of graphene/carbon nanotubes reinforced metal matrix composites via atomic-scale simulations: a review. *Composites Part C: Open Access*, 4, 100120. <https://doi.org/10.1016/j.jcomc.2021.100120>
- Reifsnider, K., Sendeckyj, G., Wang, S., Feng, W., Johnson, W., Stinchcomb, W., Pagano, N., Caruso, J., & Chamis, C. (1986). Assessment of simplified composite micro-mechanics using three-dimensional finite-element analysis. *Journal of Composites Technology and Research*, 8(3), 77. <https://doi.org/10.1520/CTR10326J>
- Salehi, M., Farnoush, H., & Mohandes, J. A. (2014). Fabrication and characterization of functionally graded Al-SiC nanocomposite by using a novel multistep friction stir processing. *Materials and Design*, 63, 419–426. <https://doi.org/10.1016/j.matdes.2014.06.013>
- Sawant, S., & Muliana, A. (2009). A multiscale framework for analyzing thermo-viscoelastic behavior of fiber metal laminates. *International Journal for Multiscale Computational Engineering*, 7(4), 351–370. <https://doi.org/10.1615/IntJMultCompEng.v7.i4.80>
- Shi, X., Gholamalizadeh, E., & Moheimani, R. (2019). Applying a micromechanics approach for predicting thermal conducting properties of carbon nanotube-metal nanocomposites. *Journal of Alloys and Compounds*, 789, 528–536. <https://doi.org/10.1016/j.jallcom.2019.03.064>
- Sun, Y., Hu, Y., & Liu, M. (2021). Elasto-plastic behavior of graphene reinforced nanocomposites with hard/soft interface effects. *Materials and Design*, 199, 109421. <https://doi.org/10.1016/j.matdes.2020.109421>

- Thilly, L., Petegem, S. Van, Renault, P. O., Lecouturier, F., Vidal, V., Schmitt, B., & Swygenhoven, H. Van. (2009). A new criterion for elasto-plastic transition in nanomaterials: application to size and composite effects on Cu-Nb nanocomposite wires. *Acta Materialia*, 57(11), 3157–3169. <https://doi.org/10.1016/j.actamat.2009.03.021>
- Wang, C., Sun, X., & Deng, J. (2019). Micromechanical estimation of effective thermal conductivities of metal matrix nanocomposites with local carbon nanotube agglomeration. *Journal of Alloys and Compounds*, 793, 191–201. <https://doi.org/10.1016/j.jallcom.2019.04.197>
- Wang, Y., Shang, L., Zhang, P., Yan, X., Zhang, K., Dou, S., Zhao, J., & Li, Y. (2020). Measurement of viscoelastic properties for polymers by nanoindentation. *Polymer Testing*, 83, 106353. <https://doi.org/10.1016/j.polymertesting.2020.106353>
- Watt, J. P. (1976). The elastic properties of composite materials. 14(4), 541–563.
- Xia, Z., Curtin, W. A., & Peters, P. W. M. (2001). Multiscale modeling of failure in metal matrix composites. *Acta Materialia*, 49(2), 273–287. [https://doi.org/10.1016/S1359-6454\(00\)00317-7](https://doi.org/10.1016/S1359-6454(00)00317-7)
- Yang, Z., & Lu, Z. (2013). Atomistic simulation of the mechanical behaviors of co-continuous Cu/SiC nanocomposites. *Composites Part B: Engineering*, 44(1), 453–457. <https://doi.org/10.1016/j.compositesb.2012.04.010>
- Yuan, M. N., Yang, Y. Q., Li, C., Heng, P. Y., & Li, L. Z. (2012). Numerical analysis of the stress-strain distributions in the particle reinforced metal matrix composite SiC/6064Al. *Materials and Design*, 38, 1–6. <https://doi.org/10.1016/j.matdes.2011.12.043>
- Zhang, C., Curiel-Sosa, J. L., & Bui, T. Q. (2018). Meso-scale finite element analysis of mechanical behavior of 3D braided composites subjected to biaxial tension loadings. *Applied Composite Materials*, 26, 139–157. <https://doi.org/10.1007/s10443-018-9686-0>
- Zhou, M. Y., Ren, L. B., Fan, L. L., Zhang, Y. W. X., Lu, T. H., Quan, G. F., & Gupta, M. (2020). Progress in research on hybrid metal matrix composites. *Journal of Alloys and Compounds*, 838, 155274. <https://doi.org/10.1016/j.jallcom.2020.155274>



Taylor & Francis

Taylor & Francis Group

<http://taylorandfrancis.com>

@seismicisolation
@seismicisolation

6 Impact of Coating Blends and Coating Techniques on Metal Matrix Composites

Jimmy Mehta and Prateek Mittal

Manav Rachna International Institute of Research and Studies, Faridabad, India

Sahil Mehta

Thapar Institute of Engineering and Technology (TIET), Patiala, India

CONTENTS

6.1	Introduction.....	118
6.1.1	Composite Materials.....	118
6.1.2	Coating.....	119
6.1.3	Coating Blend.....	120
6.1.4	Coating Technique	120
6.1.5	Metal Matrix Composite.....	120
6.2	Coating Techniques.....	121
6.2.1	Physical Vapor Deposition Process.....	121
6.2.2	Chemical Vapor Deposition Process.....	123
6.2.3	Thermal Spray Coatings	124
6.2.4	Detonation Gun.....	126
6.2.5	High-velocity Oxy Spray	127
6.2.6	Cold Spray	128
6.3	Background for Coating Techniques	128
6.4	Background for Metal Matrix Composite.....	129
6.4.1	Importance of Rare Earth.....	130
6.4.2	Summary.....	131
	References.....	131

6.1 INTRODUCTION

Tribology is interpreted as the science of studying comparative motion when two bodies are in contact. As the bodies interact, the three principles of surface engineering come into action i.e., wear, lubrication, and friction. These three principles are interrelated to each other and work in parallel. When two bodies rub against each other, material loss may occur and this is known as wear. If there is resistance amongst the bodies in contact, it is known as friction. To reduce this friction and enhance the smooth motion between bodies, we usually apply lubricant and the process is called lubrication. Tribology can be best understood by Figure 6.1 as shown below.

6.1.1 COMPOSITE MATERIALS

Usually defined as the blend of two or three materials with various physical and chemical properties. These are prepared using a desired combination of materials to achieve the required properties for a particular application. As compared to traditional elements and materials, composites are higher in strength and modulus-to-weight ratio. Matrix polymers play an integral role in composites, i.e., provide high chemical stability and corrosion resistance. Hence, they are much preferred in the transportation industry where lightweight and high-strength parts are required. Composites comprise many qualities like thermal insulators, freedom of architectural form, wear, and corrosion resistance, hence less or no requirement of lubrication, etc. Figure 6.2 shows the complete process followed for the preparation of composite. There are several methods available for preparation but the basic steps are the same. The few curing methods vary depending on the particular application they are being used for (McIlhagger et al. 2015).

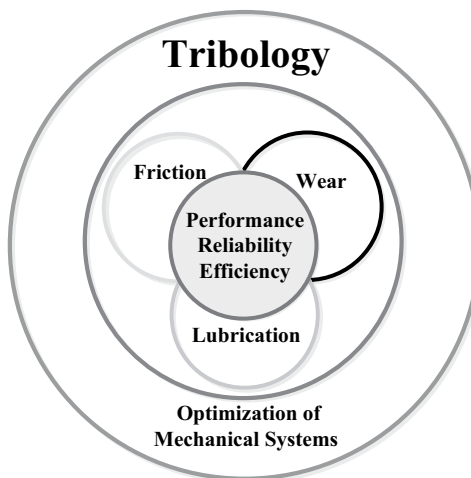


FIGURE 6.1 Tribology system.

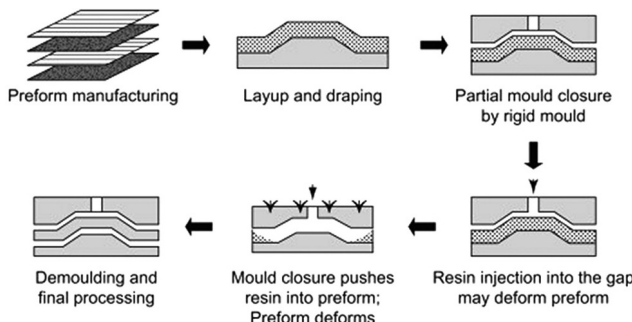


FIGURE 6.2 Process followed to prepare composite material (McIlhagger et al. 2015).

6.1.2 COATING

Coating layers, as shown in Figure 6.3, are generally applied on the surfaces that are in contact to avoid material degradation due to wear. This also reduces friction between contacting surfaces and regular flow of lubricant can be avoided. The purpose of coating may be decorative or functional, and maybe both. It is just like an envelope that covers the substrate material from variant environmental conditions (Kumar & Kumar 2018). These coating layers have several benefits but the most important is that it enhances the service life of a component by providing protection from the chemical environment, contamination, corrosion, etc. The coating is created by a process in which deposited material is heated or melted and impacted toward the substrate that forms a layer (Paredes et al. 2006).

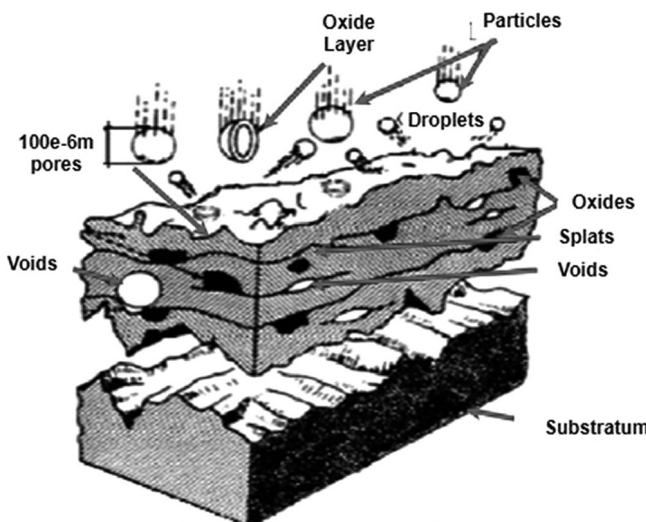


FIGURE 6.3 Schematics of coating layer formation (Paredes et al. 2006).

6.1.3 COATING BLEND

Coatings are the hard, densely packed layer applied on the top of a surface to protect it from external environmental conditions. These coating powders have different qualities and benefits. Besides, when blended, they work nicely and protect the specimen from chemicals and getting worn/corroded. For example, the most commonly used coating powder is Tungsten carbide with cobalt (WC-Co). The weight percentage of cobalt varies maybe 8%, 12%, 20%, etc. tungsten carbide is one of the best-known general wear and corrosion-resistant powders in literature. Similarly, when cobalt is added, the structure becomes more densely packed without any porosity. Chromium carbide (Cr_3C_2) is usually blended with nickel-chrome, having a weight percentage of 20–25%. But recently, it has been observed by many researchers through experiments that rare earth elements when added in coating mixture powder in measured quantity, they have given the expected and desired results. These researches have also been recognized by manufacturers and used in industries for enhancing the life of the component.

6.1.4 COATING TECHNIQUE

Techniques used for coating are not new and many new inventions/innovations have emerged over time. Recently, thermal spray coating processes are in fashion and many methodologies have been developed in it, like the D-Gun spray technique, plasma spray, high-velocity oxy-fuel, cold spray, etc. Earlier chemical spray and physical spray deposition techniques were also used and Table 6.1 below shows the differences between these.

6.1.5 METAL MATRIX COMPOSITE

This is composed of a metallic matrix and a reinforced material, which can be carbon fibers, glass, etc. These are good alternatives to traditional materials as they provide hardness, stiffness, wear, and corrosion resistance, and strength. However, with many advantages there are some disadvantages too, like the high cost of fabrication and machine tools required to serve one purpose, low ductility, etc. At present, MMCs are expected to give results that include two main characteristics: the first is high-performance composites prepared by expensive methods and reinforced with continuous fibers. The second is low performance, inexpensive composite reinforced with low-cost fibers. The first one is prepared by using expensive materials and techniques, hence when used in military services as it offers assurance of performance, whereas the second one is always doubted for performance. Stir casting and powder metallurgy methods are generally used for preparing MMCs (Jha et al. 2014; Rajkumar and Aravindan 2016; Singh et al. 2018a and Singh et al. 2018b). The only challenge faced during the fabrication of MMC is the production cost. It is expensive in most cases except stir casting (Hossain et al. 2020). Figure 6.4 below shows a few major applications of MMCs (Miracle 2005).

TABLE 6.1
Characteristics of Various Coating Methods

Characteristics	PVD	CVD	Thermal Spray
Coating geometry	Line of sight (visible to the operator)	Omni-directional	Line of sight (visible to the operator and in line with the torch)
Operating cost	Average medium to high	Average low to average medium	Very low to average medium
Coating materials	Metals, ceramics, alloys, polymers, compositions, carbides /nitrides/ silicide's	Metals, ceramics, silicon compounds, nitrate, and polymers	Polymers, metals, electric arc wire, oxy-fuel powder, plasma arc powder, and ceramics
Equipment cost	Average medium to very high	Low–medium to average medium	Very low to low medium
Process environment	Hard vacuum environment with fully seated outlets	Atmospheric to medium vacuum	Atmospheric to soft low-level vacuum
Surface finish	Very smooth to high gloss with a shiny finish	Smooth to glossy with a rough look	Uneven to a smooth finish with good quality.
Adherence	Restrained mechanical bond ranging to good and high-quality chemical bond	Good chemical bond ranging to admirable diffusion bonding of high-quality	Good mechanical bonding with high efficiency and quality
Coating thickness	Very thin to average medium	Thin to thick (ranging from 0.1 μm to 1mm)	Thick (ranging from 50 μm to 1cm)
Substrate temperature	Low	Average medium to very high	Average low to low medium

6.2 COATING TECHNIQUES

6.2.1 PHYSICAL VAPOR DEPOSITION PROCESS

In this method, metal vapors have been produced that deposit on electrically conductive material in a very thin layer. The vacuum chamber is created with a high vacuum of 10^{-6} torr so as to avoid any dirt and dust particle interaction during the deposition of the thin metal layer. Recent developments have proved this procedure to be more beneficial for the assembly of layers with required micro-structures and properties (Aliofkhazraei and Ali 2014). Figure 6.5 shows the schematic diagram of the deposition process. (Håkansson et al. 1991) used a physical vapor deposition technique for coating steel substrate using the TiN coating. Results have shown that coating was good when done with nano-size particles rather than micron-size particles.



FIGURE 6.4 Applications of metal matrix composites (Miracle 2005).

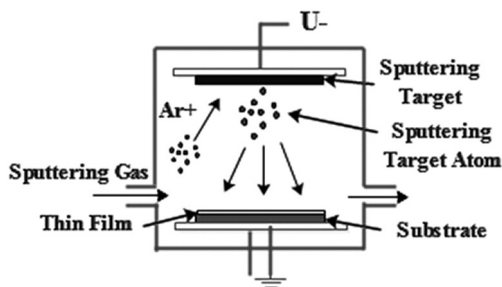


FIGURE 6.5 Pictorial diagram of the deposition process.

Advantages

- All types of inorganic and some organic materials can be used.
- Eco-friendly process
- Material properties are much improved compared with substrate material (Makhlof 2011)

Disadvantages

- Difficult to provide a thin layer to complex structures.
- High processing cost
- Low output (Naveen et al. 2016)

Applications: (Geng 2004; Helmersson et al. 2006; Uhlenbruck et al. 2011)

- Microelectronic devices
- Diffusion barriers
- Optical and conductive coating
- Battery and fuel cell electrodes
- Surface modification
- Interconnects

6.2.2 CHEMICAL VAPOR DEPOSITION PROCESS

In this process, gaseous precursors react to form a solid coating on a heated substrate. Thin films are produced by chemical reactions on the substrate surface using gaseous compounds (Xia 2021). Sometimes, deposition also occurs due to a reaction between elements of the substrate, and there is phase transfer from a gaseous state to solid, i.e., condensation (Chavez-Urbiola et al. 2016). The process is generally carried out at elevated temperatures to facilitate chemical reactions. It can also withstand extreme variant temperature conditions (SilcoTek2021). CVD has rapidly gained a market in the two major industries of semiconductors and the metallurgical coating industry, which includes cutting tools (Pierson 1999). Figure 6.6 depicts the schematic diagram of the deposition process. The success of the process depends on the processing conditions used. The temperature in this region ranges from 800°C to 2000°C. A coating thickness of up to 20 µm and good adherence can be achieved through this technique (Campbell et al. 1985; Carlsson and Martin 2010). Besides, Gupta et al. (2008) used polymeric nano-coating and observed a high aspect ratio of 80:1. They also observed that by using characterization techniques like SEM and XRD, the surface properties of pores could also be altered.

Advantages

- Reactants used are gases, therefore, the properties of gases can be used.
- Not a line-of-sight process (TWI 2021)
- High growth rate possible
- Can grow epitaxial films (Chavez-Urbiola et al. 2016)

Disadvantages

- Toxic and corrosive gases
- Complex process
- High temperature (Chavez-Urbiola et al. 2016)
- Size limited to reaction chamber capacity (SilcoTek 2021)

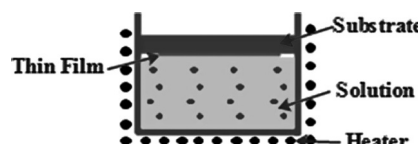


FIGURE 6.6 Schematic diagram of the CVD process.

Applications

- Coatings for wear and corrosion resistance
- Electronic and optoelectronic applications
- Refining and purification of metals (Creighton and Ho 2015)

6.2.3 THERMAL SPRAY COATINGS

The thermal spray coating is specifically imposed on the surface or material which has several properties, making it more robust. These properties include – robustness against decomposition, vaporization, sublimation, and even which does not dissociate on heating (Singh et al. 2013). This process includes metallic, ceramic, cermet, and in some cases the polymeric type of materials that are processed in either powder, wire, or rod form. The processing of the material is done in a torch-type gun structure where it is heated until its melting point is reached. This heating causes the molten part of the material to move toward the substrate material in full flow and form splats or layers, which is generally termed a coating. It is important to note that the lamellar structure formed due to solidification sticks well on the substrate material to enhance its base properties. This whole process of forming a coating on the material is called the thermal spray coating technique (Tucker, 2013a).

Thermal spray processes for wear and corrosion applications: An effective and attractive method to preserve and protect the material from outer environmental and experimental conditions to get the worn out, eroded, or corroded. Adhesion strength and protection rate are high when compared with other coating processes. Numerous materials and their different compositions are available for thermal spray, thus making it more beneficial for protecting the components and enhancing their performance (Kumar and Kumar 2018). Components are never exposed to a single environmental condition and a combination is present; for example, abrasive wear combined with high thermal stress (Metco 2017). This technique provides the maximum flexibility of coating among all the present techniques. This is due to the variety of spray processes involved and different types of spray materials. It has proven beneficial and economical, giving various options for components to be used. Figure 6.7 shows a detailed diagram of the formation of splats in the layer formation when molten metal is being deposited on the substrate material.

Applications: vary greatly for wear and corrosion resistance on a surface. Other applications include:

- Dimensional restoration
- Electromagnetic shielding
- Enhance/retard radiation
- Friction control
- Nuclear moderators
- Catalytic surfaces
- Crucibles and molds, etc. (Tucker, 2013b)

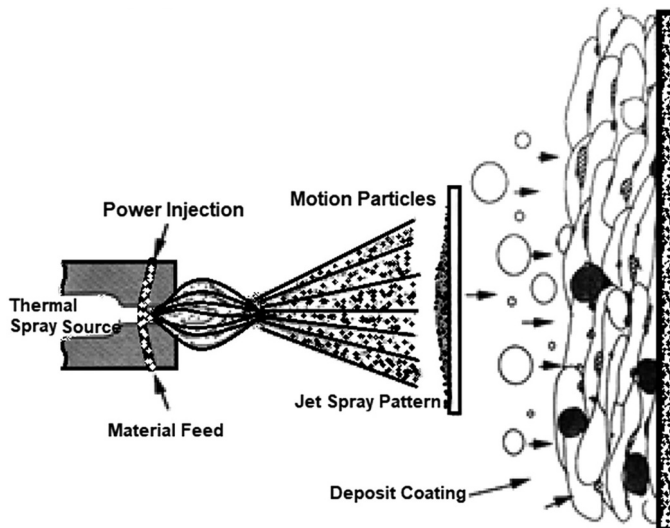


FIGURE 6.7 Schematic diagram of the thermal spray process (Lenling 2018).

Advantages

- Wide selection of materials: many materials are available that can be used for coating. It may include metals, ceramics, polymers in the form of wire, rod, or powder.
- Wide selection of base material: almost all materials can be coated and the lifespan of components made can be enhanced. Therefore, this technique finds applications in almost all manufacturing plants.
- Reduced cost: this method is used regularly by manufacturers on a daily basis; hence the coating and installation cost has been compensated by the reduced component failure and time loss.
- Rapid cooling of sprayed material on the substrate forms dense bond.
- Formation of lamellar splat shapes for a better surface finish.

Limitation of Coating

- Thermal residue stress, cracking, and distortion (Zavareh et al. 2017).
- Porosity: the process possess porosity and allows the passage for gases and/or liquids to flow through the coating/substrate interface. It may be controlled up to a certain limit.
- Anisotropic properties: coatings are generally anisotropic in the as-sprayed condition.
- Line-of-sight process: coatings are easy to apply on straight surfaces rather than complex geometrical shapes.
- Deviation from spraying normal to the surface can compromise coating properties (Tucker, 2013b).

TABLE 6.2
Comparison of Surface Modification Technologies

Method	Coating Materials	Substrate Materials	Degree of Adhesion
Thermal Spraying	Metals, alloys, ceramics, plastics, glass, cermet	Metals, ceramics, plastics, wood, paper products	Excellent
Plating	Metals, alloys	Materials that cannot be soaked in the plating solution	Good
CVD (Chemical Vapor Deposition)	Heat-resistant metals, ceramics, sulfides, selenium compounds, and others	Materials capable of withstanding 500°C – 2000°C and chemical corrosion by deposits	Good

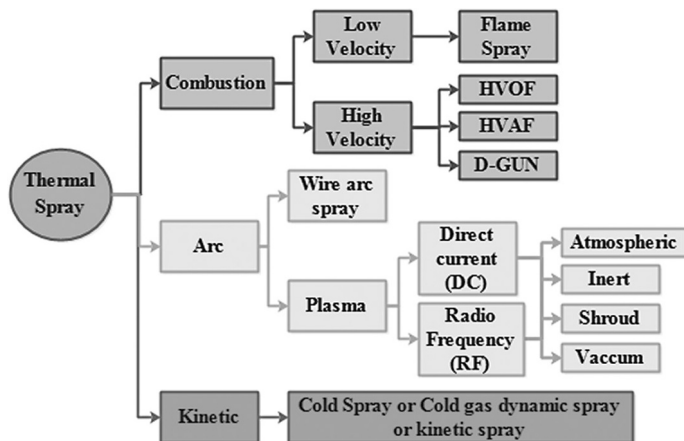


FIGURE 6.8 Classification of thermal spray techniques.

Table 6.2 shows the comparison of thermal spray, physical vapor deposition, and chemical vapor deposition process as per the substrate material selected.

Classification of thermal spray processes: this can be classified based on combustion, arc, and kinetics. Figure 6.8 shows the detailed classification. Among all these techniques, the detonation gun spray method, high-velocity oxy-fuel, and cold spray technique are mostly in fashion and used by manufacturers due to their advantages and cost-effectiveness.

6.2.4 DETONATION GUN

Widely used in the automobile and aeronautical, textile, and steel industries, the detonation gun method provides good adhesive strength, high density, better corrosion and wear resistance, high hardness with negligible oxidation, and a smooth

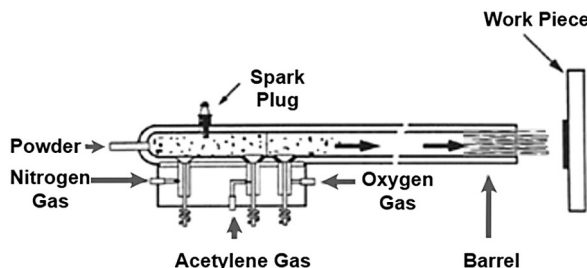


FIGURE 6.9 Schematic deposition process of D-Gun spray method (Singh et al. 2012).

surface (Kumar and Kumar 2018). In Figure 6.9, the schematic process shows the deposition of powdered spray on the work-piece. Powder in heated form is flowing through the barrel.

6.2.5 HIGH-VELOCITY OXY SPRAY

Developed in 1958, this technique has led to significant developments in thermal spray processes. The coatings produced are lamellar in structure embedded with solid particles, oxides, and inclusions (Zavareh et al. 2017). Majorly used in the oil and gas industry, power and mining industry, paper industry, petrochemicals, and aerospace as it provides very little porosity due to higher particle impact velocity and thickened coating due to less residual stress (Kumar and Kumar 2018). This process can deposit a dense coating with any modification in the phase composition of materials (Irvin et al. 1993). This technique consists of impact interaction between the substrate material and powdered particles in the flame stream. As shown in Figure 6.10, fuel gas and oxygen are supplied to the combustion chamber. The temperature of the flame chamber is about 3000°C. Flames flow out under high pressure through the nozzle. Powder composition is also supplied

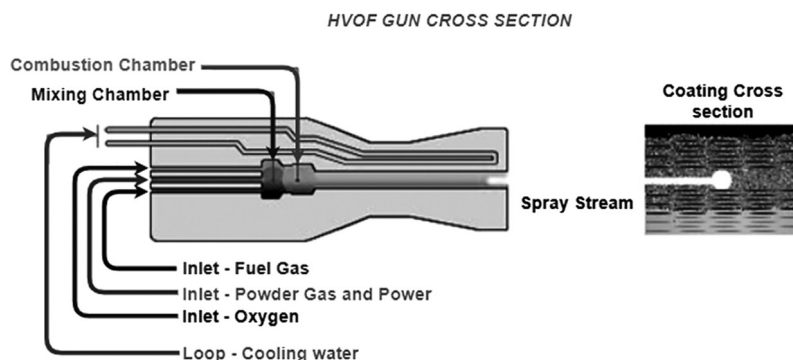


FIGURE 6.10 Schematic diagram of HVOF thermal spray (Kandeva et al. 2017).

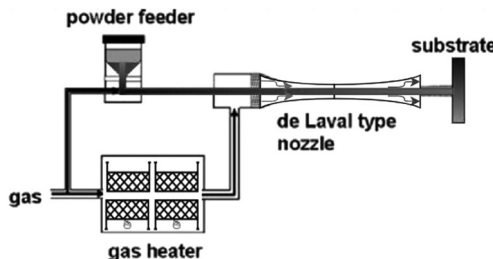


FIGURE 6.11 Schematic diagram of cold spray technique (Schmidt et al. 2009).

axially under high pressure to the combustion chamber. Powder compositions may be a mixture of alloys, metals, ceramics, polymers, etc. Particles then deposit on the substrate material in form of thin lamellas (Kandeva et al. 2017).

6.2.6 COLD SPRAY

The main benefit of this technique compared with others is that it works at low temperatures without any heat. Also, there is no oxide layer formation and high density, thermal and electrical conductivity, providing improved wear and corrosion resistance and high impact strength (Kumar and Kumar 2018). Compared with the other spray techniques, the cold spray technique possesses the major advantage of being easier to implement and less complex to understand. Figure 6.11 presents a brief schematic diagram explaining the cold spray process. As per the figure, the highly pressurized gas, which can be either helium or nitrogen, is preheated to a certain temperature and processed after being expanded in the converging/diverging nozzle. Further, through a separate pipeline, the fluidized and powdered feedstock is added to the main chamber, where it is accelerated by the pressurized gas at a de-Laval type nozzle. In the final stage, the powder impacts the substrate at high force and velocity, resulting in the completion of the coating process (Schmidt et al. 2009).

6.3 BACKGROUND FOR COATING TECHNIQUES

Wear (a component of tribology) and its intensity are the major reason for machine failure and component cost. The extraction of raw material from the natural environment is also connected with equilibrium in the eco-system (Stachowiak and Batchelor 2000; Kandeva et al. 2011; Vencl 2012; Petrov et al. 2016; Tashev et al. 2016; Dimitrova et al. 2017; Kandeva et al. 2018).

Coating layers are provided on the surface to protect the metallic component from getting oxidized or corroded (Hanuman and Goud 2016). Kumar and Kumar (2018) studied the oxidation behavior of T-22 boiler steel when used in uncoated and coated conditions. The detonation gun spray technique was used and WC-12Co and Ni-20Cr powders were employed. In the reference state of the art research, the experiment was performed at 900°C and for a total duration of

50 cycles, considering the silicon wire tube furnace experimental setup. Taking the number of cycles into account, each cyclic process included 60minutes of keeping the sample in the experimental setup, followed by 20minutes of cooling at room temperature (25–27°C ideally). Samples were characterized by dynamic structural equation modeling (DSEM) and it was found that Ni-20Cr was more effective to avoid oxidation.

Tijender and Shukla showed the successful implementation and application of Ni-20Cr on 304SS austenitic stainless steel using the D-Gun technique. From the microstructural characterization, the presence of un-melted/semi-melted particles and porosity could be observed (Tijender and Shukla 2020). Mehta et al. (2019) studied the effect of detonation gun sprayed chromium carbide nickel-chrome coating mixed with cerium oxide. Experiments were conducted for lubricated states and without lubrication states. It was revealed that coated samples have shown almost negligible wear rate loss and volume loss as compared to uncoated samples. It was also concluded that when rare-earth is added in increased amounts, there is less evidence of wear and corrosion. Arunnellaappan et al. (2021) deposited a cermet coating on AA5083 using the D-Gun technique. Three different powders were used (WC-Co, WC-Co-Cr, and Cr₃C₂-NiCr) and SEM, EDS, and XRD were used as analyzing techniques for morphology and characterization. It was observed that Cr₃C₂-NiCr provided a smooth compact and uniform lamellar structure coating, whereas WC-Co and WC-Co-Cr provided high thickness with surface defects. Mittal et al. (2019) used the detonation gun technique to coat SA213T91 boiler steel by Ni-Cr and Stellite-21. These were then oxidized in the presence of air and Na₂SO₄-60% V₂O₅ salt mixture at 900°C for 100 cycles (each cycle of one-hour heating in the furnace and then cooling in ambient air for 20 minutes). From the kinetics of oxidation, it was revealed that the D-Gun is a better thermal spray technique than other available methods. Singh and Mishra (2020) deposited WC-12Co, Stellite 6, and Stellite 21 using the D-Gun technique on SAE213-T12 boiler steel. SEM, optical microscope, and XRD were used to characterize the coating for solid particle erosion behavior at 30°C and 90°C. It was concluded that cobalt content played an important role. Eroded surface involved micro cracks and micro-ploughing.

6.4 BACKGROUND FOR METAL MATRIX COMPOSITE

Focusing on the background of metal matrix composites, several pieces of literature have been identified. As per the study, aluminum-based components have gained a lot of attention in recent times. This is because of the various fundamental and practical reasons along with several benefits (Ali et al. 2019). Besides, the hybrid composites have also been addressed by the researchers because of their high compressive strength in comparison to the single massive alloy-based material (Mohal 2017). This is due to the addition of reinforcement particles and their diffusion, which creates a rigid layer in the matrix alloys. Mittal et al. (2021a) presented study related to the structural wear and thermal behavior of Cu-Al₂O₃-graphite hybrid composite. The composite was experimentally prepared using the

stir casting method. In the detailed analysis of results, the parameters like density, micro-hardness, wear compressive strength have been considered and the investigation reveals that in the developed composite the Al_2O_3 particles were uniformly distributed. As per the discussions, the concluding remark can be put forth as increasing the percentage of reinforcement leads to an increase in the compressive strength and specific heat at a linear rate but that also results in a decrease in density as well as hardness (Mittal et al., 2021b). Rohit et al. (2017) used the stir casting process to fabricate magnesium metal matrix composite. The weight percentage of reinforcement was varied, and mechanical properties like hardness and tensile strength were checked. Alaneme et al. (2013) assessed the microstructure characteristics and mechanical properties of the aluminum hybrid composite prepared using bamboo leaf ash and silicon carbide in different weight percentages. It was revealed that tensile strength and hardness decrease with an increase in the reinforcement of bamboo leaf ash. Manikandan and Arjunan (2020) also analyzed the mechanical properties like hardness, compressive strength, and wear resistance of aluminum 6061 alloys. MgO reinforcements were used in varying weight percentages. Again, it was found that the mechanical properties also increased with an increased reinforcement percentage. Fibers are the most capable reinforcement. This is because they transfer their strength properties, which amplifies the physical and mechanical properties of the matrix. A study aimed at evaluating metal matrix alloy with the composition of Al-SiC-Mg and Al-B4C-Mg . These contained 5% and 10wt% by weight of SiC and B4C each and 1 wt% of Mg. All the other experimental parameters were kept constant and these composites were prepared using stir casting. Microstructural properties and mechanical properties like hardness and tensile strength were analyzed (Srivastava 2017). Jamwal, Vates and Gupta, et al. (2019) concluded that as reinforcement content is increased, wear rate also falls. The authors used the stir casting method to prepare $\text{Al}/\text{Al}_2\text{O}_3$ -TiC composites. Because of good interfacial bonding between mating materials, including Al_2O_3 and TiC, the compressive modulus of the composite increased to about 149.3 MPa. Jamwal et al. (2019) studied the effect of the addition of SiC-graphite reinforcement on the properties of copper. Composites were prepared by using stir casting. Microstructure analysis study shows that there is a uniform distribution of SiC in the Cu matrix, hence mechanical and corrosion properties were highly impacted by reinforcement. Mittal et al. (2021b) focused on the challenges faced during the synthesis of $\text{Cu-Al}_2\text{O}_3$ -C and Cu-ZrO_2 -C using the stir casting method. The method has a few limitations and disadvantages like agglomeration, non-uniform dispersion, and the authors have discussed them in detail. Pre-heating the mold and reinforcement using suitable reinforcement techniques were proposed solutions. For copper matrix, magnesium is generally used as a wetting agent (Mittal et al. 2021a).

6.4.1 IMPORTANCE OF RARE EARTH

Mehta et al. (2019) have used rare earth cerium oxide mixed with tungsten carbide cobalt powder and chromium carbide nickel chrome powder. Experiments

have shown that the accumulation of rare earth helps in enhancing the working life of the component and reduces wear rate but only when added in a limited quantity. If added in excess, it may lead to surface cracks and the microstructure gets disrupted (Mehta et al. 2018). Singh et al. (2015) concluded that rare earth has improved a coating's consistency and resistance against oxidation. Ce, La, Y, Zr, are usually used in coating blends. Ma and Tiefan (1994) observed the effect of rare earth oxides Y_2O_3 , Gd_2O_3 when deposited on M38G alloy for hot corrosion. NiAl coating was used and exposed to $\text{Na}_2\text{SO}_4 + 25\text{wt\%K}_2\text{SO}_4$ fused salt at a temperature of 850°C. It was concluded that the addition of rare earth oxide in the coating improves the resistance against and lessens the corrosion percentage of sulfides on the coating.

When composites are used with coatings: Metal matrix composites prepared using reinforcements are advantageous, but fatigue and failure issues still exist and hence need to be rectified. Therefore, these materials are also coated to enhance the working life of components. SEM and XRD are the generally preferred techniques for microstructure analysis and phase detection. These composites, when coated, blend with the powder and results majorly depend on the procedure used for applying the coating. Detonation gun, HVOF, and cold spray are the first preferences as they provide dense and hard layers with minimum porosity.

6.4.2 SUMMARY

From the above literature, the following points can be summarized as:

- Coatings and composites are not a new process in this modern era of manufacturing and production.
- A wide variety of composites are being prepared for various applications.
- New combinations of coating powders and techniques are being experimented with by scholars and researchers to provide beneficial combinations to industrialists.
- New composites are being prepared that are lightweight and cost-effective.
- Aluminum composites are more focused on aerospace industries because of their strength-to-weight ratio and corrosion resistance.
- Metal matrix composite materials may be prepared for desired compositions to get the required properties, but this may be expensive.
- Thermal spray processes are easy and the best available option to provide a coating to any material and enhance the working life of the component.
- D-Gun and HVOF spray techniques are generally preferred.

REFERENCES

- Alaneme, K.K., Ademilua, B.O., & Bodunrin, M.O. (2013). Mechanical properties and corrosion behaviour of aluminium hybrid composites reinforced with silicon carbide and bamboo leaf ash. *Tribol. Ind.* 35(1), 25–35.
- Ali, Z., et al. (2019). Characterization of aluminium-7075 reinforced with boron carbide (B4C) synthesized by stir casting. *Int. J. Eng. Res. Technol.* 8(6), 419–421.

- Aliofkhazraei, M. & Ali, N. (2014). PVD technology in fabrication of micro- and nano-structured coatings. *Comp. Mater. Process.* 7, 49–84.
- Arunnellaiappan, T., Baskaran, S., Arun, S., & Prithivirajan, R. (2021). Corrosion behaviour of detonation gun sprayed cermet coatings on AA5083. *Surf. Eng.* 37(2), 263–270.
- Campbell, B.A., Bryant, A., & Miller, N.E. (1985). Chemical vapor deposition. Process. U.S. Patent No. 4, 547, 404, Published Oct. 15, 1985.
- Carlsson, J.O. & Martin, P.M. (2010). Chemical vapor deposition. In: Martin, P.M. (ed.). *Handbook of Deposition Technologies for Films and Coatings*. Science Applications and Technology, Elsevier, 314–363.
- Chavez-Uribola, I.R., Willars-Rodriquez, F., & Vorobiey, Y.V. (2016). Basic principles of chemical vapor deposition technique at atmospheric pressure for synthesis of cadmium telluride and its implementation as diode. *China Semiconductor Technology International Conference*, 1–6.
- Creighton, J.R. & Ho, P. (2015). Chemical vapor deposition (CVD). *Handb. Thin-Film Technol. – ASM Int.*, Chapter 1, 225–252.
- Dimitrova, R., Kandeva, M., Kamburov, V., & Jordanov, M. (2017). Mechanical and tribological characteristics of hardfaced dispersive reinforced aluminium metal matrix layers. *J. Balk. Tribol. Assoc.* 23(4), 641–652.
- Geng, H. (2004). *Semiconductor Manufacturing Handbook*. New York: McGraw-Hill.
- Gupta, M., et al. (2008). Initiated chemical vapor deposition (iCVD) of conformal polymeric nano coatings for the surface modification of high-aspect-ratio pores. *Chem Mat.* 20(4), 1646–1651.
- Håkansson, G., et al. (1991). Microstructures of TiN films grown by various physical vapour deposition techniques. *Surf. Coat. Technology.* 48(1), 51–67.
- Hanuman, M. & Goud, C. (2016). A review on thermal barrier coatings on gas turbine engine. *Anveshna's Int. J. Res. Eng. Appl. Sci.* 1(3), 27–43.
- Helmersson, U., Lattemann, M., Bohlmark, J., Ehiasarian, A.P., & Gudmundsson, J.T. (2006). Ionized physical vapor deposition (IPVD): a review of technology and applications. *Thin Solid Films* 513(1), 1–24.
- Hossain, S., et al. (2020). Fabrication, microstructural and mechanical behavior of Al-Al₂O₃-SiC hybrid metal matrix composites. *Mater. Today Proc.* 21, 1458–1461.
- Irvinc, B., Knight, R., & Smith, R.W. (1993). The HVOF process – the hottest topic in the thermal spray industry. *Weld. J.* 1993, 25–30.
- Jamwal, A., Vates, U.K., Gupta, P., et al. (2019). Fabrication and characterization of Al₂O₃-TiC-reinforced aluminum matrix composites. In: Shanker, K., Shankar, R., & Sindhwan, R. (eds.). *Advances in Industrial and Production Engineering*. Singapore: Springer, pp. 349–356.
- Jamwal, A., et al. (2019). Microstructure, wear and corrosion characteristics of Cu matrix reinforced SiC-graphite hybrid composites. *J. Compos. Mater.*, 53(18), 2545–2553.
- Jha, P., Gupta, P., Kumar, D., & Parkash, O. (2014). Synthesis and characterization of Fe-ZrO₂ metal matrix composites. *J. Compos. Mater.*, 48(17), 2107–2115.
- Kandeva, M., Ivanova, B., Karastoyanov, D., Grozdanova, T., & Assenova, E. (2017). Abrasive wear of high velocity oxygen fuel (HVOF) superalloy coatings under vibration load. *IOP Conf. Ser. Mater. Sci. Eng.* 174(1).
- Kandeva, M., Peichev, I., Kostova, N., & Stoichkov, K. (2011). Complex study of surface layers and coatings. *J. Balk. Tribol. Assoc.* 17, 387–393.
- Kandeva, M., Penyashki, T., Kostadinov, G., Kalitchin, Z., & Kaleicheva, J. (2018). Wear of electroless nickel-phosphorus composite coatings with nanodiamond particles. *J. Environ. Prot. Ecol.* 19(3), 1200–1214.
- Kumar, A., Srivastava, V., & Mishra, N.K. (2018). Oxidation resistance of uncoated & detonation-gun sprayed WC-12Co and Ni-20Cr coatings on T-22 boiler steel at 900°C. *IOP Conf. Ser. Mater. Sci. Eng.* 377(1).

- Kumar, R. & Kumar, S. (2018). Thermal spray coating: a study. *Int. J. Eng. Sci. Res. Technol.* 7(3), 610–617.
- Lenling, B. (2018). Coating microstructures: understanding the science behind thermal spray coatings. Empowering pumps and equipment's. [Online]. Available: <https://empoweringpumps.com/tstcoatings-microstructures-science-thermal-spray-coatings/>. [Accessed: May 21, 2021].
- Ma, X., & Tiefan, Li. (1994). Influence of RE Oxide addition on hot corrosion behavior of NiAl Coatings. *Transactions of NFSOC*. 4, 83–88.
- Makhlouf, A.S.H. (2011). *Current and Advanced Coating Technologies for Industrial Applications*, Chapter 1, Cambridge: Woodhead Publishing Limited.
- Manikandan, R. & Arjunan, T.V. (2020). Mechanical and tribological behaviours of aluminium hybrid composites reinforced by CDA-B4C. *Mater. Res. Express.* 7(1), 1–18.
- McIlhagger, A., Archer, E., & McIlhagger, R. (2015). Manufacturing processes for composite materials and components for aerospace applications. *Polymer Composites in the Aerospace Industry*, 3, 53–75.
- Mehta, J., Grewal, J.S., & Gupta, P. (2018). Wear behavior of boron steel coated cerium oxide tungsten carbide cobalt coating. *J. Appl. Sci. Eng.* 21(4), 519–526.
- Mehta, J., Grewal, J.S., Sadasivuni, K.K., & Gupta, P. (2019). Analysis of wear behavior and surface properties of detonation gun-sprayed composite coating of Cr₃C₂–NiCr–CeO₂ on boron steel. *Proc. Inst. Mech. Eng. Part L J. Mater. Des. Appl.* 233(12), 2433–2443.
- Metco, S. (2017). An introduction to thermal spraying. *Corros. Manag.* 2017(140), 20–23.
- Miracle, D.B. (2005). Metal matrix composites – from science to technological significance. *Compos. Sci. Technol.* 65(16), 2526–2540.
- Mittal, P., et al. (2021a). Structural, wear and thermal behavior of copper metal matrix composites: a review, Lecture Notes in Mechanical Engineering. *Advances in Engineering Materials*. Singapore: Springer, 319–327.
- Mittal, P., et al. (2021b). Challenges and opportunities in synthesis of hybrid Cu-Al₂O₃-C and Cu-ZrO₂-C composites through stir casting route, Lecture Notes in Mechanical Engineering. *Advances in Engineering Materials*. Singapore: Springer, 1–9.
- Mittal, R., Singh, M., & Kumar, P. (2019). Characterization of detonation gun thermal spray coatings on SA213T91 in simulated boiler environment. *Mater. Today Proc.* 18, 4952–4962.
- Mohal, S. (2017). Microstructural investigation of aluminium- silicon carbide particulate metal matrix composite fabricated by stir casting. *IJIRST –International J. Innov. Res. Sci. Technol.* 3(11), 26–30.
- Naveen, A., et al. (2016). A review on thermal barrier coatings and its deposition techniques. *Int. J. Eng. Sci. Manag. Res.* 3(3), 1–9.
- Paredes, R.S.C., Amico, S.C., & d'Oliveira, A.S.C.M. (2006). The effect of roughness and pre-heating of the substrate on the morphology of aluminium coatings deposited by thermal spraying. *Surface and Coatings Technology*, 200(9), 3049–3055.
- Petrov, T., Tashev, P., & Kandeva, M. (2016). Wear resistance of surface layers modified with Al₂O₃ and TiCNnanopowders weld overlaid using TIG and ITIG methods. *J. Balk. Tribol. Assoc.* 22(1), 304–315.
- Pierson, H.O. (1999). *Handbook of Chemical Vapor Deposition (CVD) –Principles, Technology, and Applications*. New York: Noyes Publications and William Andrew Publishing, 51–80.
- Rajkumar, K., & Aravindan, S. (2016). Mechanical, electrical and tribological properties of copper-graphite composites. *Composite Materials: Processing, Applications, Characterizations*. Singapore: Springer, 433–455.

- Rohit, S., Rose, A.R., & Rakshit, B. (2017). Development of magnesium composite material by the method of stir casting for applications in automotive and aerospace industries. *Proc. 10th Int. Conf. Precision, Meso, Micro Nano Eng. (COPEN 10)*, pp. 28–31.
- Schmidt, T., et al. (2009). From particle acceleration to impact and bonding in cold spray-ing. *J. Therm. Spray Technology*. 18(6), 794–808.
- SilcoTek (2021). Chemical Vapor Deposition Explained. Its Benefits and Drawbacks. (2021). [Online]. Available: <https://www.silcotek.com/semi-coating-blog/chemical-vapor-deposition-explained.-its-benefits-and-drawbacks>. [Accessed: May 18, 2021].
- Singh, A., Chawla, V., & Singh, A. (2013). Combating hot corrosion of boiler tubes with detonation gun sprayed coatings: a review. *6th International Conference on Recent Trends in Engineering, Science, and Management: ICRTESM-17*, Chanigarh, India. 5762, 742–749.
- Singh, H., Chatha, S.S., & Sidhu, B.S. (2015). Role of rare earth elements in thermal spray coatings. *Latest Dev. Mater. Manuf. Qual. Control*. 2015, 294–297.
- Singh, L., Chawla, V., & Grewal, J.S. (2012). A review on detonation gun sprayed coatings. *J. Miner. Mater. Charact. Eng*. 11(3), 243–265.
- Singh, N., Parkash, O., & Kumar, D. (2018a). Phase evolution, mechanical and corrosion behavior of Fe(100-x) Ni(x) alloys synthesized by powder metallurgy. *J. Phys. Chem. Solids*. 114(October), 8–20.
- Singh, N., Parkash, O., & Kumar, D. (2018b). Wear behavior of ZrO₂ particle reinforced (Fe,Ni) matrix composite. *Proc. 7th Int. Conf. Fract. Fatigue Wear*, 682–690.
- Singh, P.K., & Mishra, S.B. (2020). Erosion performance of detonation gun deposited WC-12Co, Stellite 6 and Stellite 21 coatings on SAE213-T12 steel. *Tribol. Mater. Surfaces Interfaces*, 14, 229–239.
- Srivastava, A. (2017). Recent advances in metal matrix composites (MMCs): a review. *Biomed. J. Sci. Tech. Res.* 1(2), 520–522.
- Stachowiak, G. & Batchelor, A.W. (2000). *Engineering Tribology*. Boston, MA: Butterworth-Heinemann.
- Tashev, P., Lazarova, R., Kandeva, M., Petrov, R., & Manolov, V. (2016). Tungsten inert gas weld overlay using nano-sized TiN powder. *J. Balk. Tribol. Assoc.* 22(3), 2904–2920.
- Tijender & Shukla, V.N. (2020). Surface engineering analysis of D-Gun sprayed Ni-20Cr coating in aggressive environment. *Int. J. Eng. Res.* 9(4), 677–681.
- Tucker, R.C. (2013a). Thermal spray coatings. *ASM Handb. Surf. Eng.*, Chapter 5, 1446–1471.
- Tucker, R.C. (2013b). Introduction to coating design and processing. *ASM Handbook, Therm. Spray Technology*. 5, 76–88.
- TWI (2021). What is Chemical Vapour Deposition (CVD)? (2021). [Online]. Available: <https://www.twi-global.com/technical-knowledge/faqs/faq-what-is-chemical-vapour-deposition-cvd>. [Accessed: May 14, 2021].
- Uhlenbruck, S., Nédélec, R., Sebold, D., Buchkremer, H.P., & Stöver, D. (2011). Electrode and electrolyte layers for solid oxide fuel cells applied by physical vapor deposition (PVD). *J. Chem. Inf. Model.* 35(1), 2275–2282.
- Vencl, A. (2012). Optimization of the deposition parameters of thick atmospheric plasma spray coatings. *J. Balk. Tribol. Assoc.* 2012(18), 405–414.
- Xia, L. (2021). Importance of nanostructured surfaces. In: Osaka, A., and Narayan, R. (eds.). *Bioceramics: From Macro to Nanoscale*. Elsevier Series on Advanced Ceramic Materials, Chapter 2, pp. 5–24.
- Zavareh, M.A., et al. (2017). Fundamentals and applications of thermal spray coating fundamentals and applications of thermal spray coating. *Can. J. Basic Appl. Sci.* 5(1), 1–11.

7 Effects of Performance Measures of Non-conventional Joining Processes on Mechanical Properties of Metal Matrix Composites

Kamaljit Singh

CEC Landran, Mohali, Punjab, India

Suneev Anil Bansal

MAIT, Maharaja Agrasen University, HP, India

Bharat Institute of Engineering and Technology,

Mangalpally, Ibrahimpatnam, Hyderabad, Telangana, India

Virat Khanna

MAIT, Maharaja Agrasen University, HP, India

Satinder Singh

IIT Jammu, J&K, India

CONTENTS

7.1	Introduction.....	136
7.2	Friction Stir Welding.....	137
7.2.1	Analysis of Microstructure at the Weld Zone	138
7.2.2	Effect of Process Parameters on Mechanical Properties of FSW Joint.....	139
7.2.2.1	Micro-Hardness.....	139
7.2.2.2	Ultimate Tensile Strength (UTS)	144
7.2.3	Effect of Tool Profile on Mechanical Properties.....	145

7.3	Ultrasonic Processing of MMC	146
7.3.1	Effect of Friction and Ultrasonic Power	146
7.3.2	Mechanical Properties	147
7.3.2.1	Hardness.....	147
7.3.2.2	Shear Strength.....	147
7.3.3	Effect of Process Parameters	148
7.3.3.1	Normal Force/Weld Force (N)	148
7.3.3.2	Weld Speed (m/s).....	148
7.3.3.3	Oscillation Amplitude	148
7.4	Laser Welding	148
7.4.1	Microstructure Analysis.....	149
7.4.2	Major Defects in Laser Beam Welds	150
7.4.2.1	Porosity	150
7.4.2.2	Hot Cracking	151
7.4.3	Influence of Parameters on Mechanical Properties of MMC	151
7.4.3.1	Effect of Laser Parameters.....	151
7.4.3.2	Effect of Welding Speed	153
7.4.3.3	Effect of Shielding Gas	153
7.5	Electron Beam Welding	153
7.5.1	Microstructure Evolution.....	154
7.5.2	EBW Input Parameters	155
7.5.2.1	Effect of Beam Parameters on the Weld	156
7.5.2.2	Effect of Welding Speed	156
	References.....	157

7.1 INTRODUCTION

The joining of metal matrix composites (MMCs) is an imperative process of the manufacturing industry. Fastening the composite through bolts and rivets could deteriorate the composite surface while drilling and can induce stresses in them (Kalaiselvan et al., 2021). MMC's generally have better mechanical properties compared to monolithic materials and display better results in challenging conditions (Khanna et al., 2021b). Materials like aluminum, copper, and magnesium are often reinforced with several type of reinforcements such as ceramics, carbon nanotubes, grapheme, fullerene, and other metallic elements (Khanna et al., 2020, 2021a). Binding the metal matrix with the reinforcement generates numerous opportunities to enhance the characteristics of materials in different ways (Contreras Cuevas et al., 2018).

Despite the fact that MMC provides many advantages over single materials, they are quite hard to bring together with traditional techniques, due the issues associated with them such as oxidation and cracks (Kalaiselvan et al., 2021). It has been observed in previous studies that fusion welding techniques are unfavorable compared with the solid state welding techniques when it comes to the joining of MMCs (Fernández et al., 2017; Jayabalakrishnan & Balasubramanian, 2018). The adaptability potential of distinctive welding methods is shown in Table 7.1. In this study, more emphasis is made on the effect of parameters on the weldability of MMCs in both fusion (laser welding and electron beam welding) as

TABLE 7.1

Performance Chart for Various Welding Techniques (Contreras Cuevas et al., 2018)

Sr. No	Welding Technique	High Strength and Temperature	Complex Shapes	Application in Joining MMC
1.	Friction stir welding	A	C	A
2.	Ultrasonic additive Manufacturing	A	B	A
3.	Laser welding	A	A	C
4.	Electron beam welding	A	A	C
5	Diffusion bonding	B	C	B

Operational performance figures: A – Good, B – Fair, C – Poor

well as solid state welding techniques (friction stir welding and ultrasonic additive manufacturing), comprehensively.

7.2 FRICTION STIR WELDING

Since its invention in the late nineties, friction-stir-welding (FSW) has emerged as one of the most preferred metal joining processes. FSW has already been successfully applied in joining of different metals and their alloys such as aluminum, magnesium, and copper. Besides this, studies also depict that FSW has been implemented efficiently for the processing of Al, Mg, Ti, Cu and other metal-based composites. Due to numerous benefits, such as economical operational cost with fewer defects, FSW has found ample applications in fabricating aircraft, defense, and automobiles components (Mustafa et al., 2015). Figure 7.1 describes

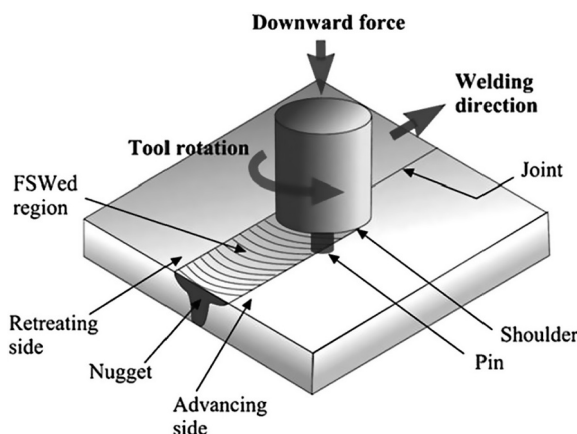


FIGURE 7.1 The principle of the FSW process (Gemme et al., 2010).

the different components of the FSW process. In this process, a cylindrical rotating tool with a profiled probe and shoulder is pressed axially and fed at a steady transverse rate along the joint line on the interface of work-plates (Nourani et al., 2015). The FSW welding is performed by generating frictional heat at the welding region but without melting or recasting the material (Tamjidy et al., 2017). The mechanical properties and microstructure of weld joints are highly influenced by FSW process parameters. Hence, optimum values of FSW parameters such as welding speed, rotational speed, tool tilt angle, axial pressure, and tool profile should be carefully chosen to facilitate sound welded joints (Padmanaban et al., 2015). Furthermore, FSW is regarded as a green process due to its high energy efficacy and eco-friendly characteristic as it does not require shield gases (Tamjidy et al., 2017).

7.2.1 ANALYSIS OF MICROSTRUCTURE AT THE WELD ZONE

At the weld region, frictional heat induced at the interface between the tool and the workpiece causes plastic deformation of the material. This frictional heat varies for different tool speeds. The quality of the joint depends enormously on this heat produced at the weld area. While adequate generated heat would result in defect-free joints, excessive or insufficient heat could degrade the microstructure and strength of the joint (Dolatkhah et al., 2012). Thus, it becomes indispensable to select parameters cautiously to obtain high-quality FSW joints. The joint is basically divided into distinctive zones for macrostructure analysis as shown in Figure 7.2. At these zones, due to variation in thermomechanical effect, the grains size and particles distribution could be distinct (Imam et al., 2017; Zolghadr et al., 2019) when the plastic flow of material is influenced by the properties of work-material, tool configuration, and welding parameters (Prater et al., 2013; Sahraeinejad et al., 2015).

Moreover, during welding, onion-shaped structure forms at the nugget zone due to material flow around the tool pin and differences in dislocation densities (Cavaliere et al., 2004; Ceschini et al., 2007). However, depending on the type of MMCs, recrystallization properties, and the cross-section of the work material, these onion rings can emerge partially or disappear completely (Chen et al., 2009; Ni et al., 2013; Salih et al., 2019; Wang et al., 2014b).

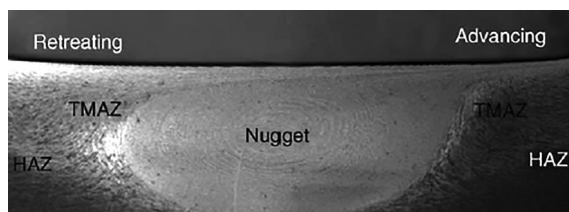


FIGURE 7.2 The macrostructure of a typical FSW joint (Kumar et al., 2019).

7.2.2 EFFECT OF PROCESS PARAMETERS ON MECHANICAL PROPERTIES OF FSW JOINT

The mechanical strength and hardness of FSW joints rely on several input parameters such as tool material, tool geometry, the rotational speed of the tool, and transverse speed. These performance measures not only control the joining operation but also produce highly efficient MMCs joints. Therefore, these parameters are optimized, while focusing to enhance the joint's mechanical properties.

7.2.2.1 Micro-Hardness

Micro-hardness across the welded joint describes the number of phases and reinforcement particles distribution. The reinforcement enhances the hardness in two distinct ways, by decreasing the grain size and forming clusters at ultra-hard zones (Ahn et al., 2012). The various input process parameters affect the joint hardness differently. Also, FSW input parameters such as tool rotational speed and welding speed influence the input heat significantly and govern the flow of material (Das et al., 2018).

It has been observed in a study that with an increase in the transverse speeds, the microhardness of the AA5182 joint without the incorporation of reinforcement material increases. In contrast, the hardness of the AA5182-WC nanocomposite decreases with an increase in welding speed. However, due to the incorporation of nanoparticles, it is still higher compared to unreinforced joints. Also, the improvements in grains size of Al alloy were restrained after a definite size by WC reinforcement particles due to reduced heat input causing a decrease in the hardness at a higher speed (Paidar et al., 2018).

Furthermore, various research has reported that hardness profiles obtained for FSW joints have two types. In the first type, the highest hardness value occurs at the center of the weld zone, that reduces gradually in the TMAZ and HAZ until it reaches the hardness value of the base material, as illustrated in Figure 7.3. The hardness increment at the weld zone is attributed to two reasons: homogenous distribution of reinforcement particles at nugget and grain refinement caused by recrystallization. These reasons congregate the conditions of the Hall pitch equation (hardness is inversely proportional with grain size) and Orowan mechanism of hardness (uniform distribution of finer particle enhance hardness) (Ceschini et al., 2007; PERIYASAMY et al., 2013).

Besides, at the offset from the weld zone due to the presence of coarse grains, the hardness value in the nugget zone begins to reduce. It can be observed from Figure 7.4 and Table 7.2 that the hardness of MMCs combined with FSW majorly increases with the addition of reinforcement at specific input parameters.

However, in a few studies, opposite results were originated. For example, there was nearly 8% drop in the hardness of $\text{Al}_1\text{O}_{75}\text{-O-SiC}$ composite as compared to joint without reinforcement, which had been attributed to induction of heat from earlier specimen by FSW (Bahrami et al., 2014b).

The second type of hardness profile have a "W"-shaped curve. This curve is highly dependent on the amount of dislocation densities and refinement of particles. It was observed in a study that the hardness of the AA7005/10 vol.% Al_2O_{3p}

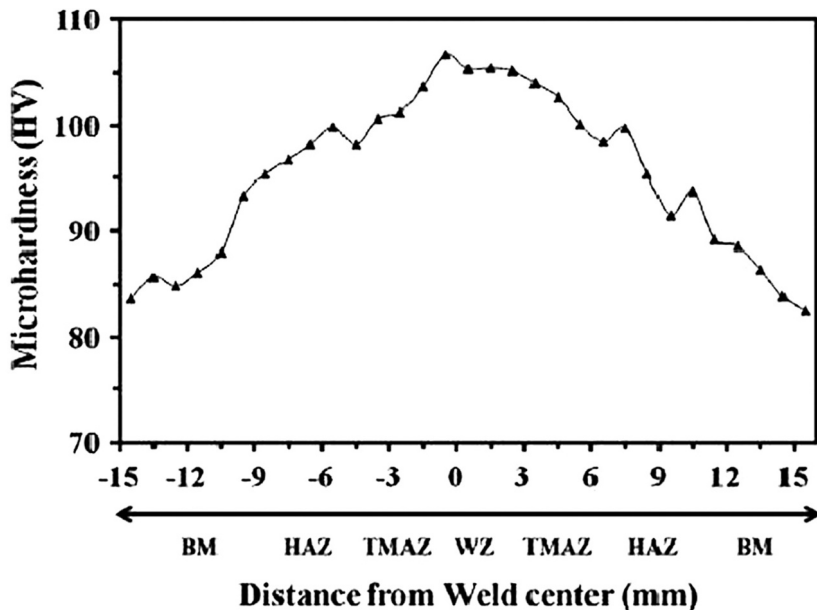


FIGURE 7.3 The effect of heat energy input on microhardness B4C – AA6060 at the weld zone (Kalaiselvan et al., 2014).

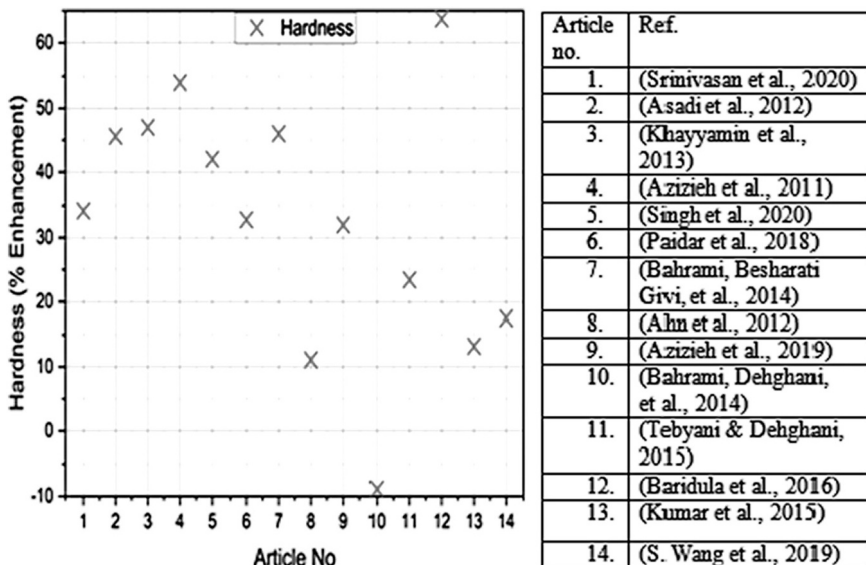


FIGURE 7.4 Percentage enhancement in hardness for MMCs joined by friction stir welding/processing.

TABLE 7.2
Effect of Parameters on Hardness and Tensile Strength of the FSW MMC Joint

S.No	Work Material	Technique	Material Thickness (mm)	Tool Pin Profile	Welding Speed (mm/min)	Rotational Speed (RPM)	Axial Load (kN)	Tensile Strength (MPa)	Hardness	Ref.
1.	AA6061-6wt%ZrO ₂ -2wt%C	Stir Casting	6	Square pin profile	48.3	852.82	5.11	190 from 73, improved by 61%	50 HRB	(Pandiyarajan et al., 2019)
2.	AA6063-6%ZrO ₂ +3% C	Stir Casting	6	Square pin	20	1100	7	123.67 from 92.18, 25.4%	79.18 HV from 52.11 HV, 34.18%	(Srinivasan et al., 2020)
3.	AZ91-SiC	Groove and FSW	5	Thread and without thread and flutes	63	710			115.9HV from 63 HV, 45.6%	(Asadi et al., 2012)
4.	AZ91-8vol%SiO ₂	Groove and FSW	8	Square pin	63	1250		192 MPa from 139, 27% more	124 Hv from 65 HV, 47% more	(Khayyamin et al., 2013)
5.	AZ31-Al ₂ O ₃	Groove and FSW	5	Threads, without threads and flutes	45	800			~92 HV from ~42 HV, 54%	(Azizieh et al., 2011)
6.	AA6061-T6-Al ₂ O ₃	Groove and FSW	2.5	Cylindrical pin	70	2000		~258 From ~290, decreased by 11%	~89 HV from ~51 HV, 42%	(Singh et al., 2020)

(Continued)

TABLE 7.2 (Continued)**Effect of Parameters on Hardness and Tensile Strength of the FSW MMC Joint**

S.No	Work Material	Technique	Material Thickness (mm)	Tool Pin Profile	Welding Speed (mm/min)	Rotational Speed (RPM)	Axial Load (kN)	Tensile Strength (MPa)	Hardness	Ref.
7.	Al2009-15vol%SiC _p	PM, Hot rolling and temperate	6	Conical pin	100	800		559 from 537, 3.9%		(Wang et al., 2014b)
8.	AA5182/WC	Groove and FSW	5	Cylindrical threaded pin	100	500		~310 From ~268, 13.5%	128 HV from 86 HV, 32.8%	(Paidar et al., 2018)
9.	AA7075	Groove	5	Four flute square pin	40	1250		268 from 230, 14.1%	122.3 from 66 HV, 46%	(Bahrami et al., 2014a)
10.	AA5083-SiC _p	Groove and FSW at 3° tilt angle	4		22	1800			90 HV from 80 HV, 11.1%	(Ahn et al., 2012)
11.	25vol.%SiC/2124Al	Powder metallurgy	8	un-threaded WC-Co	15	400	12	359 from 371, 3.2%		(Fernández et al., 2017)
12.	AC4A-30vol%SiC	Stir Casting	6	smooth pin	25	2000		309 from 123.8, 59%		(Liu et al., 2017)
13.	Al7075-10%SiC	Stir Casting		TiAlN coated tapered pin	20	1600		97.97 from 52.10, 46%		(Madhavarao et al., 2018)
14.	1100Al-Fe ₂ O ₃	Groove and FSW	10	Threaded pin	56	1000			78 from 53 HV, 32%	(Azizieh et al., 2019)

15.	Al 7075-O-SiC	Groove and FSW	5	Conical threaded pin	40	1250	270 from 190.7, 29.3%	111.4 from 113.9 HV 8.9%,	(Bahrami et al., 2014b)
16.	IF steel-SiC	FSW		WC tool with concave shoulder		1250	0.5	360 from 200, 44.4%	235HV from 180 HV, 23.4%
17.	AA5052-AA6063-Cu	Groove and FSW	6	Cylindrical Pin	200	1400	1.5	109.14 from 75.87, 30.4%	150.0 from 54.33 HV, 63.7%
18.	AA7075 T6-B ₄ C	Groove, FSP and FSW	8	Cylindrical and conical threaded tool	25	750			196 HV from 170 HV, 13.2%
19.	AA2014-GNS	Ring groove and refilledFrictionstir spot welding	2	Ring shaped tool		1500-1800		~148 from ~122, 17.5%	(Wang et al., 2019)
20.	AA6082-Al ₂ O ₃	Groove and FSW	2	Hexagonal pin tool	40	710	227.61 from 260.86, 12.7%	74HV from 54 HV, 27%	(Mohammed et al., 2019)

composite decreased to 170 HV in NZ from 185 HV at TMAZ. The reason for lower hardness in HAZ for both the AS and RS in comparison to the NZ for MMC joint is emergence of dislocations caused by the thermal expansion difference between reinforcement particles and the metal matrix (Bozkurt et al., 2011; Ceschin et al., 2007).

7.2.2.2 Ultimate Tensile Strength (UTS)

For most engineering practices, a material is required to have both high strength and high hardness. The tensile test results of FSW MMC joints carried out in different studies are shown in Figure 7.5 and Table 7.2. Heat generation at the workpiece tool interface, material softening, and the quality of joint formed much depends on various factors, such as FSW process parameters, tool design and presence of intermetallic compounds. FSW process parameters such as tool rotational speed, welding speed, and axial force are the dominating factors among others that influence the amount of frictional heat generation and intermixing process. Thus, the selection of optimal process parameters and their values becomes imperative to attain high-quality joints with superior strength. It can be observed from Table 7.1 that increasing the rotational speed to a certain limit enhances the UTS up to 60% for FSW joints. At a lower tool rotational speed, insufficient heat occurs at the weld joint, while at higher speed the heat is excessive. In both cases, not enough mixing occurs at the weld zone which limits the improvement of FWS joint UTS at the nugget zone (Eslami et al., 2019; Paidar et al., 2018).

Although tool travel speed has a trivial impact on the heat input in comparison to the tool rotation speed, it influences the FSW MMC joints strength (BOZKURT

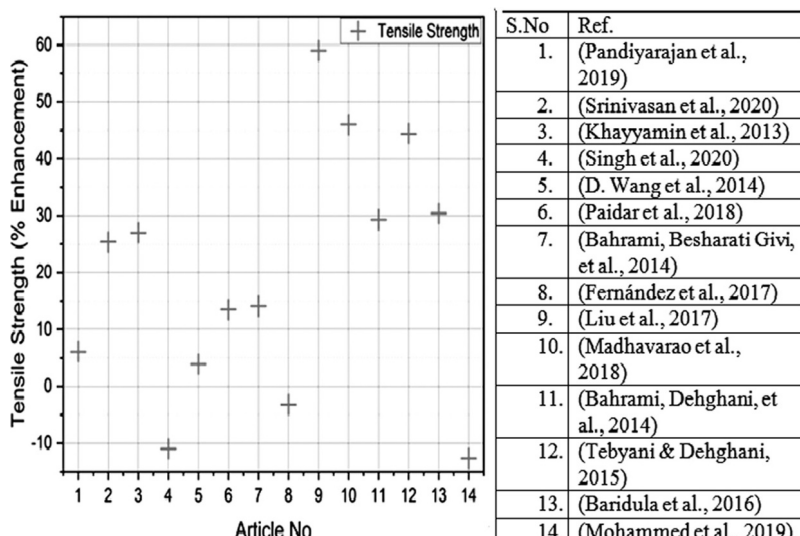


FIGURE 7.5 Percentage enhancement in tensile strength for MMCs joined by friction stir welding/processing.

et al., 2012). The rate at which heat transfers to the work material, and the rate at which the solidification of material occurs also depends on the transverse tool speed. It has been found that upon increasing the welding speed, the UTS increases but only up to a specific value; thereafter, it reduces with further increment in the speed. While heat generation relies on the tool rotation speed, the transfer rate of heat to the workpiece, together with the cooling of the workpiece, is affected by tool welding speed (Prabhu et al., 2017). At a particular rotational speed, low and high weld speeds produce tunnel defects due to improper cooling and improper stirring. Consequently, the UTS in both cases have lower values (Wang et al., 2014a).

Another important factor is axial load which governs the induction of heat between the workpiece and the rotating tool due to friction. For lower axial load, micro voids and tunnel defects emerge because of low heat generation. On the other hand, at higher axial force, wormholes, unnecessary flash, and thinning at the stir zone occurs (Arun Kumar Shettigar et al., 2017; Murugan & Ashok Kumar, 2013; Yigezu et al., 2014). Thus, the joint strength decreases when the axial force is applied other than at its optimal value for the FSW of MMCs.

7.2.3 EFFECT OF TOOL PROFILE ON MECHANICAL PROPERTIES

A tool's profile has a considerable effect on FSW joint strength. Distinct types of tool shapes have been employed by the researchers to identify their impact on hardness as well as on tensile strength, as shown in Table 7.2. For instance, in an investigation it was observed that square-shaped tool resulted in the highest tensile value and high joint efficiency of 99.47% due to its large volume ratio of 1.56 as compared to other profiles such as hexagonal and orthogonal with 1.21 and 1.11 volume ratios, respectively (Vijay & Murugan, 2010). Similarly, in another study it was found that conical threaded tools compared with straight cylindrical tool pins had shown higher joint efficiency due to better flow of softened material (Hassan et al., 2012). Moreover, tool materials also impact joint efficiency. As shown in Figure 7.6, welding performance of the AlTiN-coated tool increased by

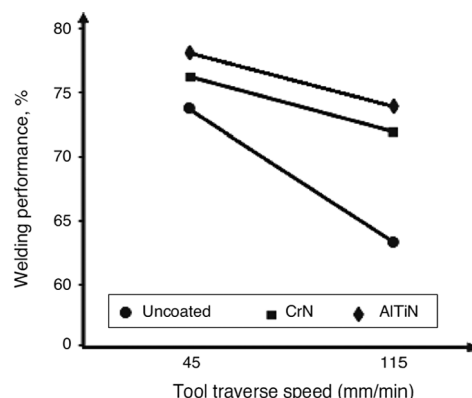


FIGURE 7.6 The impact of tool material on the welding performance of the MMC joint for different tool speeds (Bozkurt & Boumerzoug, 2018).

nearly 5% as compared to the uncoated tool, and tensile strength reached its peak value of 355.15 MPa. This was mainly because uncoated tool fractures occurred in the stir zone and local defects such as lower penetration and root flaws were observed (Bozkurt & Boumerzoug, 2018).

7.3 ULTRASONIC PROCESSING OF MMC

Ultrasonic additive manufacturing (UAM) is a modern technique based on the ultrasonic welding of metals. It holds the two distinct workpieces, sealed together under compression, which are vibrated relatively through an ultrasonic transducer mechanism, causing some frictional effect between them. Consequently, nascent surfaces appear due to a reduction in oxides and surface dissimilarities (Hahnlen & Dapino, 2014). A strong bond is formed due to applied compressive load on the clean opposing surfaces, joining the two surfaces altogether. The bond established by the UAM technique for dissimilar metals is a result of either frictional interlocking or metallurgical diffusion mechanism (Li, 2021).

7.3.1 EFFECT OF FRICTION AND ULTRASONIC POWER

Plastic flow is an indispensable element of UAM that redistributes the oxidation layer, surface interlocking, and reduces defects such as voids at the surface interfaces. Radically, it occurs due to the compressive stress and plastic deformation due to cyclic shearing. Friction and ultrasonic power are the foremost factors that affect the plastic flow and microstructure of the materials.

Friction is imperative for the ultrasonic joining of metals, as it removes the oxidation layer and produces clean mating surfaces. Surface roughness is crucial for the flow of plastic material during UAM. It has been observed that highly finished surfaces restrict plastic flow, and the layer of oxide film does not break successfully (Li, 2021). Moreover, when materials of different hardnesses are embedded together through UAM, plastic deformation increases for softer material, causing relatively poor bonding (Yang et al., 2009).

Generally, in the UAM process, the microstructural transformation occurs at the interfaces of the materials, while it remains intact for the rest of the bulk material (Li, 2021). However, it has been seen in an experimental work that at very high ultrasonic power, the microstructure, as well as the texture of the bulk material, could also transform. With the appliance of high power, the material recrystallizes dynamically and refines grains size, causing the materials to deform completely (Fujii et al., 2011). However, it has also been identified in studies that the material may plastically deform largely for soft materials such as aluminum, whereas for hard materials like titanium, this change is comparatively small (Wolcott & Dapino, n.d.).

7.3.2 MECHANICAL PROPERTIES

The mechanical properties of the materials joined together with UAM depend greatly on the quality and the attributes of the surface interfaces. To increase mechanical properties, it is of paramount importance to produce a strong interface bond between the materials (Levy et al., 2018). Through appropriate selection of UAM process parameters such as normal force, speed, amplitude and temperature, different levels of properties can be attained that depend on the type of material used, joining direction, heat treatment and presence of defects (Li, 2021).

7.3.2.1 Hardness

In an investigation, it has been observed that the hardness of the monolithic aluminum was near about 140 HV, while for amorphous material (Fe and Si/B) it was approximately 1300 HV. However, during ultrasonic processing under optimal parameters (weld speed 28 mm/s, amplitude 25 µm, and 190°C preheat temperature) the laminated composite exhibited hardness of 900 HV, which was much more than pure aluminum. This enhancement in the hardness of the composite was attributed to the absence of defects such as cracks at the indentation tip and combining together the highly hard material to the less hard aluminum (Liu et al., 2018).

Similar findings originated when the aluminum matrix was consolidated with carbon steel and iron to form laminated composites. The hardness of pure aluminum was 61 HV which after ultrasonic processing reached 152 HV for Al/carbon steel and 124 HV for Al/Fe composites, respectively. This is due to the fact that both carbon steel and iron layer had higher hardness (209 HV and 151 HV) compared to aluminum. This improvement has been a result of consolidation energy and increased temperature that caused hardening at the interface and increased plastic deformation. It has also been noted that the hardness gradient ameliorates with changes in the interfacial bond distance (Wang et al., 2020).

7.3.2.2 Shear Strength

To improve the strength of joints post-treatments are often incorporated with UAM process. Spark plasma sintered specimen of Al-Ti composites, tested under a normal load of 50-KN till failure resulted in higher shear strength. The ultimate shear strength of the SPS Al-Ti composite is enhanced by nearly 54% as compared to non-treated specimens. The outcomes clearly exhibited that built specimens showed brittle fractures, whereas the post-treated specimens had ductile fractures due to the occurrence of sliding movement while loading (Wolcott et al., 2016). Likewise, the Al-Ti composites fabricated after 4 hours of post-treatment at 480°C then cooled in the furnace illustrated similar results. Specimens produced using optimal parameter levels (i.e., 1500 N normal force, 30 µm amplitude, 42 mm/s weld speed, and 2 numbers of bilayers) had high shear strength of 64 MPa, which is comparable to solid 1100-O aluminum. This is also ascribed to the absence of voids due to the post-processing and ductile fracture of the composite, while at other levels of process parameters, the composite experienced brittle fracture due to poor interlocking (Hopkins et al., 2010).

7.3.3 EFFECT OF PROCESS PARAMETERS

7.3.3.1 Normal Force/Weld Force (N)

Normal force is applied onto the building materials through sonotrade in UAM. This applied load is responsible for close contact between the material surfaces and to ease the process of plastic flow (Yang et al., 2009). It has been observed that high pressure and a larger bond area lower the void volume, causing more stress and higher deformation (Friel & Harris, 2009; Yang et al., 2007). Conversely, lower applied force results in inadequate deformation and poor contact between the mating materials, forming a weak interfacial bonding (Hopkins et al., 2010). Hence, to reduce the number of voids and improve the weld quality, it is necessary to choose optimal normal force levels.

7.3.3.2 Weld Speed (m/s)

The speed of the sonotrode during the welding of the workpieces can range in between 1 mm/s to 100 mm/s (Li et al., 2015). It is the welding speed that defines the amount of energy the sonotrode exerts onto the workpiece during welding. Thus, the slow pace of the transducer's horn system onto the bilayers allows adequate pressure to be applied upon them. Thereby, increasing the total energy input into the layers ultimately improves the bond quality of the weld (Hopkins et al., 2010; Kong et al., 2003, 2004).

7.3.3.3 Oscillation Amplitude

In general, the mechanical behavior of MMC composites exhibits a linear relationship with oscillation amplitude. It has been observed that at high amplitude, higher energy induces into the building material, which improves the bond quality and enhances its ultimate shear strength. Also, higher amplification reduces the defects in the bilayers and produces improved surfaces (Hopkins et al., 2010; Kong et al., 2004). However, after a certain limit, a further increase in the amplitude could break the bond already formed during joining due to increased stresses.

7.4 LASER WELDING

Metal matrix composites are often reinforced with several ceramic materials such as oxides, carbides, and nitrides (Kalaiselvan et al., 2021). The components fabricated from such composites exhibit excellent properties, such as high stiffness, high specific strength, and low wear rate which are essential in aerospace, road and rail transport, and electronic packaging industries (Meng et al., 2013a; Wang et al., 2000). However, the MMCs joined through ARC welding and FSW show insufficient fusion, interface reactions, and segregation of reinforcements at the strengthening phase (Guo et al., 2012; Lei et al., 2017). Due to the numerous problems associated with such techniques, it becomes indispensable to weld MMCs through more advanced techniques such as laser welding (Kalaiselvan et al., 2021).

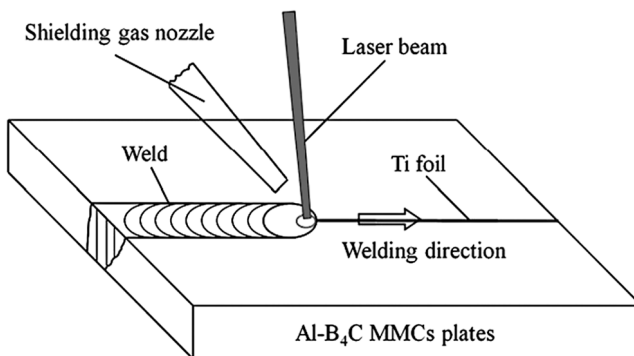


FIGURE 7.7 The principle of the laser welding technique (Guo et al. 2012b).

As shown in Figure 7.7, in laser beam welding, a laser is utilized to join different materials together through fusion. In this process, the mating surfaces of the materials are melted by the high intensity of the laser causing the molten metal to intermix and solidify after the removal of the heating source (Kalaiselvan et al., 2021). Laser beam welding can produce high-quality components due to its ability to generate controlled heat at a localized area. Moreover, the weld produced through laser beam welding has another advantage over arc welds, in that it changes mechanical properties at the weld to a limit and shows less deterioration on the workpiece. This is attributable to the fact that laser welding causes very small heat-affected zones due to its intense focused beam (Guo et al., 2012a). There is no direct physical contact between the head and workpiece, so the rapid welding process makes it even more effective (Banerjee et al., 2016; Dai et al., 2019).

7.4.1 MICROSTRUCTURE ANALYSIS

The melt pool of laser beam welds usually undergoes a rapid cooling rate and solidifies in just a few milliseconds, producing a meta-stable structure that seriously impacts its final mechanical properties. Hence, it is extremely important to understand the microstructural attributes of the weld (Fotovvati et al., 2018). While joining the A359/SiC MMCs in CO₂ laser welding, a small number of needle-like structures of Al₄C₃ were observed in the weld pool between the parent metal and bead due to controlled laser power. Moreover, the bead weld surface demonstrated a fine dendrite matrix with few interdendritically arranged eutectic structures and occasionally present SiC particles (Bassani et al., 2007).

Conversely, Figures 7.8a and b clearly indicate that reinforcement particles can be evenly distributed in the metal matrix and produces homogenous composites during electron beam welding (EBW). Besides, the presence of needle-like phases of Al-B-C and Al-B elemental compounds in the weld zone in large proportion could induce large stresses at the matrix and needle interface, affecting the

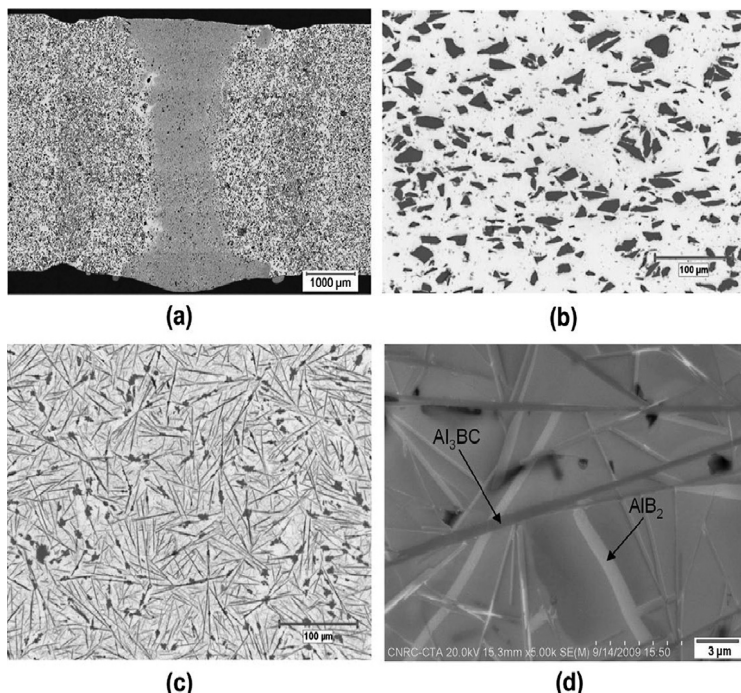


FIGURE 7.8 represents microstructural view of aluminum matrix with B_4C reinforcement: (a) laser joint, (b) parent material, (c) weld region in optical microscope, and (d) weld region under scanning electron microscopy (Guo et al., 2012b).

mechanical properties negatively. Thus, it is essential to reduce such phases in the weld zone. As suggested in many studies, this can be reduced by appropriate levels of laser energy. However, in this case, the results were unfavorable (Guo et al., 2012b).

7.4.2 MAJOR DEFECTS IN LASER BEAM WELDS

Laser beam welding has become quite attractive for manufacturing several components in the automotive as well as aerospace industries. However, sometimes due to the presence of geometrical and metallurgical defects, the quality of such components is compromised. In this section the main defects that arise while alloying workpieces shall be discussed.

7.4.2.1 Porosity

The formations of large and small voids or pores in the weld are termed as porosity, which usually takes place at the bottom and the surface of the welds. Often, the voids formed during the fabrication of MMCs are of small diameter, upto $100\mu m$ (Guo et al., 2012). This is generally affected by laser input parameters

such as power input, weld speed, and type of shield gas. This can be reduced to a large extent by selecting a suitable and optimal level of parameters (Chi et al., 2018).

7.4.2.2 Hot Cracking

Cracking is one of the most common defects in weld structures. The restriction caused during the free contraction of metals while cooling or solidification induces stresses that lead to the formation of cracks in the weld area (Cicală et al., 2005) (Figure 7.9).

Hot cracking is further divided in two groups, namely solidification cracking or liquation cracking. The phenomenon of solidification cracking at the fusion zone is relatively challenging. The factors, such as mechanical, thermal, and metallic metallurgy, altogether form hot solidification cracks (Cross, 2005).

Nevertheless, liquation crack occurs in the partially melted zone where less melted metal elements accumulate in the hot zone (Cooper et al., 2013). Novel techniques have been developed to understand and measure the susceptibility of hot cracking in laser beam welding. It has been observed that cracks formed in laser beam welds are comparatively less than ARC welds due to high rate of solidification (Bakir et al., 2019; Bakir et al., 2018; Chun et al., 2015).

7.4.3 INFLUENCE OF PARAMETERS ON MECHANICAL PROPERTIES OF MMC

Distinctive parameters affect the quality of the joint in a different way. Appropriate acknowledgment of these parameters would not only produce superior joints but also make the process more efficient. Figure 7.10 shows the prime laser welding input process parameters that affect the weld quality.

7.4.3.1 Effect of Laser Parameters

Laser parameters such as type of laser, power, beam radius or diameter, and beam irradiation angle play an important role in the quality of the MMC joint (Chun

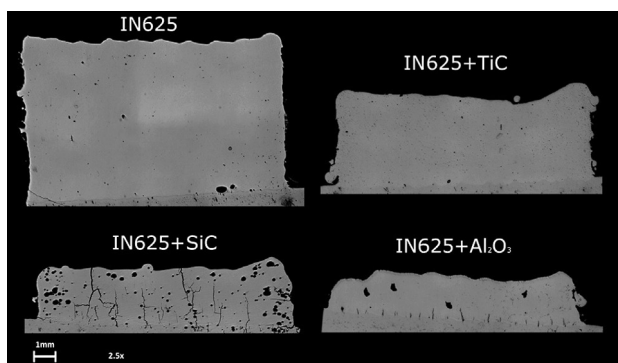


FIGURE 7.9 Porosity and cracks formed in the laser beam weld (Cooper et al., 2013).

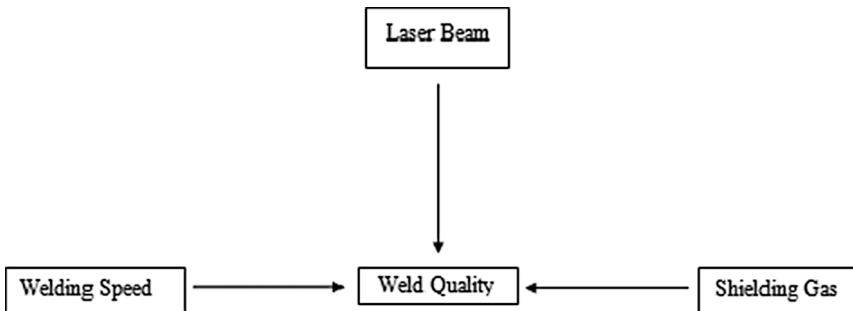


FIGURE 7.10 Major input parameters affecting the quality of laser welds.

et al., 2015; Hagenlocher et al., 2018). To produce MMCs with laser welding, it is extremely necessary to select optimal levels of these parameters.

7.4.3.1.1 *Laser Type*

The most important factor in laser welding is the type of laser. The most widely used laser materials are CO₂ and Nd: YAG (neodymium in yttrium aluminum garnet) (Dubey & Yadava, 2008; Jun et al., 2016). Since Nd: YAG laser produces a high-intensity beam at low power and shorter wavelength of 1.06 μm, it has become most attractive laser for welding of MMCs. Also, with a little or no HAZ, Nd: YAG produces welds with deep penetrations because of high laser focus and high intensity. Another major advantage of Nd: YAG over CO₂ is that the radiations are absorbed within the material much more strongly (Banerjee et al., 2016).

7.4.3.1.2 *Laser Power*

Laser power is a significant factor that defines the depth of penetration and welding speed for a specific material. The depth of penetration generally intensifies with increase in laser power and as soon as it reaches its full penetration level, it may cause defects such as undercut in the material due to poor viscosity of the molten material that causes cavities in the weld (Banerjee et al., 2017; David Raja Selvam et al., 2021; Harooni et al., 2013).

7.4.3.1.3 *Laser Dimensions*

The diameter or radius of the laser affects the dimensions of the molten pool in the joint. For example, in a study it was reported that when the power is low, and the ratio of surface tension gradient ($d\sigma/dT$, surface tension to temperature) is less than zero, convection takes place from the center to the pool surface edge causing melt to flow and reduces the diameter of depth. Meanwhile, the width of the pool increases. In other words, increasing the laser beam dimension in terms of diameter decreases the depth of the molten metal pool (Chi et al., 2018; Vaziri et al., 2009). Moreover, laser irradiation significantly affects the surface, microstructure, and mechanical behavior of the metal. Inadequate laser irradiation could result in the formation of craters (Yousaf et al., 2014).

7.4.3.2 Effect of Welding Speed

In particular, when it comes to producing deep welds, welding speed and thickness anticipate a reciprocal relationship, i.e., with an increase in the specimen thickness, the welding speed decreases. Likewise, the penetration depth decreases with an increase in the welding speed (Katayama, 2020). To demonstrate, in an experimental investigation, the effect of welding speed on welding penetration had been determined and observed that at low weld speeds (1 mm/s and 2 mm/s) the penetration has been over 1200 μm , while at high welding speed (12 mm/s) it plunged to nearly 750 μm . To obtain an appropriate and complete penetration, a suitable formulae had been applied: $fd = (3.6\text{--}5.4)v$, where f and d are the laser frequency and dimension and v is the welding speed (Jun et al., 2016).

7.4.3.3 Effect of Shielding Gas

Shielding gas selection should be made upon the basis of chemical and metallurgical phenomenon in between the gas and molten metal pool. A shielding gas can cause an adverse effect on the penetration, size, and efficiency of the weld. The fundamental purpose of shield gases is to ensure the weld area is well protected from oxidation, to maintain an accurate convection rate and to stabilize the plasma. Improper shielding can cause defects in the weld such as pores, undercut, and bead surface roughness, especially in the case of CO₂ laser welding (Cao et al., 2003). Several gases such as helium, nitrogen, CO₂, and argon have been used in different studies for this purpose. Gases which are dense like argon assist in penetration through mechanical exertion, whereas gases such as helium which are lighter have higher ionization potential and can absorb a large quantity of energy (Fotovvati et al., 2018). Moreover, the shielding gas distance and inclination angle from the laser material interface region also influence the occurrence of weld contamination (Meng et al., 2013b). Besides this, gas flow rate is another important aspect that results in improved weld properties. Shielding gas reduces the temperature of the workpiece during the welding operation. The CFD (computational fluid dynamics) analysis of laser welding process under the influence of shielding gas asserts that the cooling process during solidification improves when the gas flow rate is high. At low gas glow rate numerous defects such as spattering, irregularities in weld, and sagging could emerge on the weld bead surface (Bannour et al., 2012; Vyskoč et al., 2020).

7.5 ELECTRON BEAM WELDING

MMCs are often joined with different welding techniques to enhance their practicability in the manufacturing and processing industries. However, producing a weld without any defect has been a great challenge with conventional fusion welding processes. Presently, EBW has been used widely by industries to fabricate distinct welding structures, especially from thicker materials up to 12 inches. In such cases, the traditional methods can drip out the molten metal from the molten weld pool from the backside (Terentyev et al., 2015). Moreover, the electron beam, in comparison to laser beam, provides an extreme fusion process and

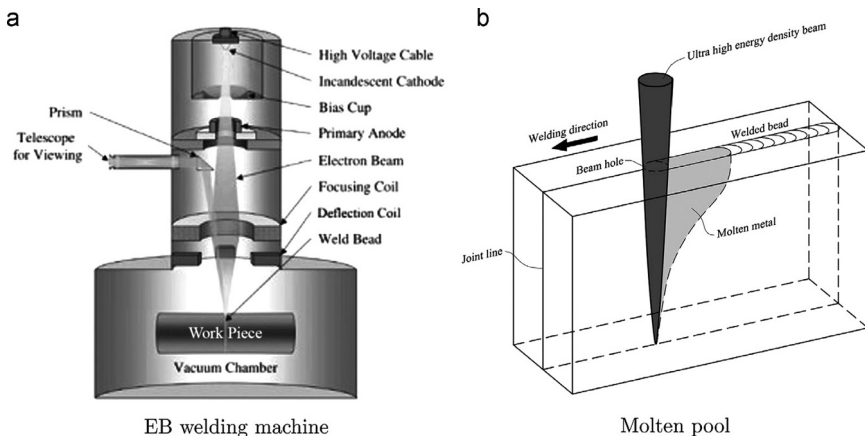


FIGURE 7.11 Operational illustration of EBW (Chiumenti et al., 2016).

produces a weld with narrow material distortion. Also, electron beam welding can be distinguished from other traditional joining methods in terms of the energy source it employs. As shown in Figures 7.11a and b, it utilizes a beam of highly pulsed electrons that impinges on the materials, and the associated kinetic energy transforms into thermal energy. Consequently, the edges of the metals get fused due to the heat generated and join the different metal surfaces together after solidification (Biermann & Aneziris, 2020; Kalaiselvan et al., 2021).

Highly deep and narrow penetrations can be evolved by using extremely high input voltages, i.e., up to about 150 kV (Singh, 2012) EBW is carried out in a closed vacuum chamber, reducing the porosity in the weld that otherwise occurs in other processes due to atmosphere and shield gases. The large pores can also be eliminated to an extent with extra stirring force from the controlled circular mode of the electron beam (Cui et al., 2010). Therefore, it can be observed that the MMC components welded in EBW exhibit few or no defects due to several reasons such as a highly energized focused beam and rapid welding process in vacuum and solidification (Wang et al., 2011). Although high vacuum designs are more promising in a welding joint with great weld attributes, partial vacuum and non-vacuum equipment are often used for mass production for rapid processing (Singh, 2012). Figure 7.12 demonstrates the impact of different welding methods on the metal surface while producing a butt joint.

7.5.1 MICROSTRUCTURE EVOLUTION

The mechanical behavior and weld appearance depend greatly on the microstructure of the joint produced in the EB process. For non-deviating welding of MMC, an uneven surface appears as the weld incorporates the reaction products of the matrix and reinforcement particles between the base material and the HAZ. This shows that considerable alterations occur in the structure of the composite during

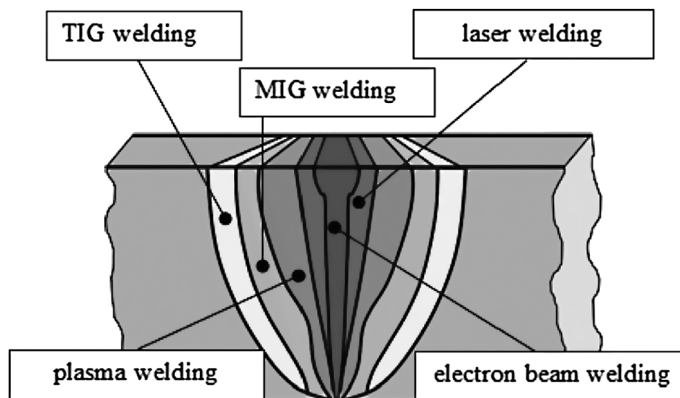


FIGURE 7.12 Fabrication of butt joint through different welding processes (Węglowski et al., 2016).

welding. The unwanted loss of material due to excessive heating produces a poor weld (Chen et al., 2015).

However, during the fabrication of WCp/NiBSi MMC through EBW, a highly dense structure was developed without defects such as porosity and cracking in vertical as well as in horizontal directions, respectively. Meanwhile, the matrix had a duplex microstructure composed mainly of gamma nickel along with Ni₃B and Ni Si participates. The reinforcement was able to maintain the spherical morphology. The fast cooling and solidification rate produced dendrites of γ Ni with little or no development of the interdendritic structure. Due to the presence of secondary phases, i.e., Ni₃B and Ni₃Si, the MMC became brittle. Also, except for hardness, other mechanical properties of the MMC produced unsatisfactory results (Peng et al., 2016).

As the microstructure of a weld seam and different base metals of an offset electron beam weld in molten AISI 304, dendrite cores with brown region dendrite develop. After cooling and solidification, the austenite changes from ferrite and becomes brown-colored after treating with a reagent. Also, in the transition area, the TWIP Mg-PSZ were completely embedded into the dendrites with color. Formation of zirconium oxides or magnesium oxides occurs in the cavities due to evaporation of TWIP metal matrix which may reduce the strength of the MMC (Halbauer et al., 2019).

7.5.2 EBW INPUT PARAMETERS

The most desirable parameters which influence the weld characteristics are beam power, beam current, voltage, energy input, beam offset, welding speed, the base metal's chemical composition, and required weld configurations (Borrman et al., 2019; Kurzynowski et al., 2019; Višniakov et al., 2018).

7.5.2.1 Effect of Beam Parameters on the Weld

The displacement of the beam depends on several influencing aspects of the process, such as the chemical composition of the material, welding speed, and laser beam energy input (Borrman et al., 2019). When the beam is not displaced or offset ($\Delta x = 0$), the TWIP MMC, the metal from the weld pool ejects periodically, resulting in loss of material. As a result, number of cavities emerges in the metal matrix. Increasing the beam displacement by few millimeters, material separation, error in the welding seam, underfill, and widening of seam can be observed. These errors in the weld seam can be attributed to the characteristic defect present in it. As soon as the beam offset is increased (0.4–0.6 mm), the dilution level decreases without considering the welding speed. Thus, the welds produced are defect-free with an ingress level of <10%. Thereby, due to small standard deviation for these offset values, the process becomes more stabilized (Halbauer et al., 2019).

7.5.2.2 Effect of Welding Speed

Many previous studies have found that the welding speed can resolve stability issues in the EB process. High welding speed assists in stabilizing the molten pool in the weld (Cui et al., 2010; Wang et al., 2011). Welding materials with thicker sections requires high speeds. As a result, the requirement for high beam power also increases. Under such conditions, maintaining the beam dimensions and electron beam angle aperture becomes a challenge, as the accurate settings could produce high-quality welds with plane-parallel walls (Dragunov et al., 2017). Thus, the minimum required welding speed to form a satisfactory weld becomes important to reduce the power requirement without compromising weld quality. The factors that affect the selection of minimum welding speed are material density, thickness of the weld, width of the weld, thermal and physical properties of a material. A distinct possible minimal welding speed for different materials based on the theoretical and the experimental results have been predicted in a study (Terentyev et al., 2015). However, MMCs may show different characteristics than single metal or an alloy. To obtain a weld of high quality, high welding speed should be selected to improve cooling rate, solidification and reduce defects, although at very high speeds, humping could take place (Biermann & Aneziris, 2020).

In summary, the overview that has been presented in this article is about the joining of MMCs through friction stir welding, ultrasonic additive manufacturing (solid state welding techniques), laser beam welding, and electron beam welding (fusion welding techniques). Both traditional and conventional methods have been successfully applied for fabricating MMC joints. However, their application produces different microstructure in the weld zone. The microstructure evolution at the weld zone has been comprehensively analyzed and the influences of the input parameters on the weld were investigated. Several factors, such as mechanical properties of the materials and the presence of defects influence the

MMCs' joining. Most of the MMCs were effectively bonded together under a solid state welding condition. On the other hand, reactions that occurred in the fusion welding techniques formed carbides and needle-like phases in-between the matrix and weld pool, which in turn reduced the strength and produces a brittle structure.

REFERENCES

- Ahn, B. W., Choi, D. H., Kim, Y. H., & Jung, S. B. (2012). Fabrication of SiCp/AA5083 composite via friction stir welding. *Transactions of Nonferrous Metals Society of China (English Edition)*, 22(Suppl.3), s634–s638. [https://doi.org/10.1016/S1003-6326\(12\)61777-4](https://doi.org/10.1016/S1003-6326(12)61777-4)
- Arun Kumar Shettigar, S. P., Rao, M., Shrikantha, R., & Herbert, M. (2017). Application of neural network for the prediction of tensile properties of friction stir welded composites. *Materials Science Forum*, 880, 128–131. <https://doi.org/10.4028/www.scientific.net/MSF.880.128>
- Asadi, P., Givi, M. K. B., Rastgoo, A., Akbari, M., Zakeri, V., & Rasouli, S. (2012). Predicting the grain size and hardness of AZ91/SiC nanocomposite by artificial neural networks. *International Journal of Advanced Manufacturing Technology*, 63(9–12), 1095–1107. <https://doi.org/10.1007/s00170-012-3972-z>
- Azizieh, M., Kokabi, A. H., & Abachi, P. (2011). Effect of rotational speed and probe profile on microstructure and hardness of AZ31/Al₂O₃ nanocomposites fabricated by friction stir processing. *Materials and Design*, 32(4), 2034–2041. <https://doi.org/10.1016/j.matdes.2010.11.055>
- Azizieh, M., Pourmodheji, R., Larki, A. N., Dezfuli, M. A. G., Rezaei, A., & Kim, H. S. (2019). Effect of multi-pass friction stir processing on the microstructure and hardness of AA1100/Al 13 Fe 4 in situ composites. *Materials Research Express*, 6(4), 046558. <https://doi.org/10.1088/2053-1591/aafe91>
- Bahrami, M., BesharatiGivi, M. K., Dehghani, K., & Parvin, N. (2014a). On the role of pin geometry in microstructure and mechanical properties of AA7075/SiC nanocomposite fabricated by friction stir welding technique. *Materials and Design*, 53, 519–527. <https://doi.org/10.1016/j.matdes.2013.07.049>
- Bahrami, M., Dehghani, K., & BesharatiGivi, M. K. (2014b). A novel approach to develop aluminum matrix nano-composite employing friction stir welding technique. *Materials and Design*, 53, 217–225. <https://doi.org/10.1016/j.matdes.2013.07.006>
- Bakir, N., Gumennyuk, A., & Rethmeier, M. (2018). Investigation of solidification cracking susceptibility during laser beam welding using an in-situ observation technique. *Science and Technology of Welding and Joining*, 23(3), 234–240. <https://doi.org/10.1080/13621718.2017.1367550>
- Bakir, N., Pavlov, V., Zavjalov, S., Volvenko, S., Gumennyuk, A., & Rethmeier, M. (2019). Development of a novel optical measurement technique to investigate the hot cracking susceptibility during laser beam welding. *Welding in the World*, 63(2), 435–441. <https://doi.org/10.1007/s40194-018-0665-8>
- Banerjee, A. J., Biswal, M. K., Lohar, A. K., Chattopadhyay, H., & Nagahanumaiah. (2016). Review on experimental study of Nd: YAG laser beam welding, with a focus on aluminium metal matrix composites. *International Journal of Engineering and Technology(UAE)*, 5(3), 92–101. <https://doi.org/10.14419/ijet.v5i3.5984>

- Banerjee, A. J., Roy, H., Biswal, M. K., Lohar, A. K., Chattopadhyay, H., & Hanumaiah, N. (2017). Investigation on tensile behaviour of laser welded Al–Mg–Sc–Zr in situ TiB₂ reinforced metal matrix composite. *Transactions of the Indian Institute of Metals*, 70(8), 2071–2077. <https://doi.org/10.1007/s12666-016-1028-z>
- Bannour, S., Abderrazak, K., Mhiri, H., & Le Palec, G. (2012). Effects of temperature-dependent material properties and shielding gas on molten pool formation during continuous laser welding of AZ91 magnesium alloy. *Optics and Laser Technology*, 44(8), 2459–2468. <https://doi.org/10.1016/j.optlastec.2012.03.034>
- Baridula, R. R., Ramaraju, R. V., Ibrahim, A. Bin, Faizal, M., & Che, B. (2016). Effect of nano particle deposition on mechanical properties of friction stir welded dissimilar aluminium alloys by Taguchi technique. *Transactions of the Indian Institute of Metals*. <https://doi.org/10.1007/s12666-016-0898-4>
- Bassani, P., Capello, E., Colombo, D., Previtali, B., & Vedani, M. (2007). Effect of process parameters on bead properties of A359/SiC MMCs welded by laser. *Composites Part A: Applied Science and Manufacturing*, 38(4), 1089–1098. <https://doi.org/10.1016/j.compositesa.2006.04.014>
- Biermann, H., & Aneziris, C. G. (2020). *Austenitic TRIP/TWIP Steels and Composites*. Springer.
- Borrmann, S., Asad, A., Halbauer, L., Buchwalder, A., Biermann, H., & Schwarze, R. (2019). Numerical simulation of the particle displacement during electron beam welding of a dissimilar weld joint with TRIP-matrix-composite. *Advanced Engineering Materials*, 21(5), 1–9. <https://doi.org/10.1002/adem.201800741>
- Bozkurt, Y., & Boumerzoug, Z. (2018). Tool material effect on the friction stir butt welding of AA2124-T4 Alloy Matrix MMC. *Journal of Materials Research and Technology*, 7(1), 29–38. <https://doi.org/10.1016/j.jmrt.2017.04.001>
- Bozkurt, Y., Kentll, A., Uzun, H., & Salman, S. (2012). Experimental investigation and prediction of mechanical properties of friction stir welded aluminium metal matrix composite plates. *Materials Science (MEDZIAGOTYRA)*, 18(4), 336–340. <https://doi.org/10.5755/j01.ms.18.4.3092>
- Bozkurt, Y., Uzun, H., and Salman, S. (2011). Microstructure and mechanical properties of friction stir welded particulate reinforced AA2124/SiC/25p-T4 composite. *Journal of Composite Materials*, 45(21), 2237–2245. <https://doi.org/10.1177/0021998311401067>
- Cao, X., Wallace, W., Poon, C., & Immarigeon, J. P. (2003). Research and progress in laser welding of wrought aluminum alloys. I. Laser welding processes. *Materials and Manufacturing Processes*, 18(1), 1–22. <https://doi.org/10.1081/AMP-120017586>
- Cavaliere, P., Cerri, E., Marzoli, L., & Dos Santos, J. (2004). Friction stir welding of ceramic particle reinforced aluminium based metal matrix composites. *Applied Composite Materials*, 11(4), 247–258. <https://doi.org/10.1023/B:ACMA.0000035478.71092.ec>
- Ceschini, L., Boromei, I., Minak, G., Morri, A., & Tarterini, F. (2007). Microstructure, tensile and fatigue properties of AA6061/20vol.%Al₂O₃p friction stir welded joints. *Composites Part A: Applied Science and Manufacturing*, 38(4), 1200–1210. <https://doi.org/10.1016/j.compositesa.2006.06.009>
- Chen, G. Q., Zhang, B. G., Liu, L. Y., & Feng, J. C. (2015). Electron beam welding of SiCp/Al composite to Ti-6Al-4V. *Materials Research Innovations*, 19(April), S51309–S51312. <https://doi.org/10.1179/1432891714Z.0000000001300>
- Chen, X.-G., da Silva, M., Gougeon, P., & St-Georges, L. (2009). Microstructure and mechanical properties of friction stir welded AA6063–B4C metal matrix composites. *Materials Science and Engineering: A*, 518(1–2), 174–184. <https://doi.org/10.1016/j.msea.2009.04.052>

- Chi, Y., Gu, G., Yu, H., & Chen, C. (2018). Laser surface alloying on aluminum and its alloys: A review. *Optics and Lasers in Engineering*, 100(July 2017), 23–37. <https://doi.org/10.1016/j.optlaseng.2017.07.006>
- Chiumenti, M., Cervera, M., Dialami, N., Wu, B., Jinwei, L., & Agelet de Saracibar, C. (2016). Numerical modeling of the electron beam welding and its experimental validation. *Finite Elements in Analysis and Design*, 121, 118–133. <https://doi.org/10.1016/j.finel.2016.07.003>
- Chun, E. J., Baba, H., Nishimoto, K., & Saida, K. (2015). Development of laser beam welding transverse-varestraint test for assessment of solidification cracking susceptibility in laser welds. *Metals and Materials International*, 21(3), 543–553. <https://doi.org/10.1007/s12540-015-4394-x>
- Cicală, E., Duffet, G., Andrzejewski, H., Grevey, D., & Ignat, S. (2005). Hot cracking in Al-Mg-Si alloy laser welding – Operating parameters and their effects. *Materials Science and Engineering A*, 395(1–2), 1–9. <https://doi.org/10.1016/j.msea.2004.11.026>
- Contreras Cuevas, A., BedollaBecerril, E., Martínez, M. S., & Lemus Ruiz, J. (2018). Joining of composites. In *Metal Matrix Composites* (pp. 187–226). Springer Nature Switzerland AG. https://doi.org/10.1007/978-3-319-91854-9_5
- Cooper, D. E., Blundell, N., Maggs, S., & Gibbons, G. J. (2013). Additive layer manufacture of Inconel 625 metal matrix composites, reinforcement material evaluation. *Journal of Materials Processing Technology*, 213(12), 2191–2200. <https://doi.org/10.1016/j.jmatprotec.2013.06.021>
- Cross, C. E. (2005). On the origin of weld solidification cracking. In *Hot Cracking Phenomena in Welds* (pp. 3–18). Springer Berlin Heidelberg. https://doi.org/10.1007/3-540-27460-X_1
- Cui, H. C., Lu, F. G., Peng, K., Tang, X. H., & Yao, S. (2010). Research on electron beam welding of in situ TiB₂p/ZL101 composite. *Journal of Shanghai Jiaotong University (Science)*, 15(4), 479–483. <https://doi.org/10.1007/s12204-010-1036-9>
- Dai, J., Yu, B., Jiang, W., Htun, H. M., & Liu, Z. (2019). Laser welding of dissimilar metal joint of 6061 Al alloy and Al matrix composite. *Advances in Materials Science and Engineering*, 2019. <https://doi.org/10.1155/2019/2359841>
- Das, H., Mondal, M., Hong, S.-T., Chun, D.-M., & Han, H. N. (2018). Joining and fabrication of metal matrix composites by friction stir welding/processing. *International Journal of Precision Engineering and Manufacturing-Green Technology*, 5(1), 151–172. <https://doi.org/10.1007/s40684-018-0016-7>
- David Raja Selvam, J., Dinaharan, I., & Mashinini, P. M. (2021). Microstructure and mechanical characterization of Nd:YAG laser beam welded AA6061/10 wt% ZrB₂ aluminum matrix composites. *Optics and Laser Technology*, 140(February), 107084. <https://doi.org/10.1016/j.optlastec.2021.107084>
- Dolatkhah, A., Golbabaei, P., BesharatiGivi, M. K., & MolaeiKiya, F. (2012). Investigating effects of process parameters on microstructural and mechanical properties of Al5052/SiC metal matrix composite fabricated via friction stir processing. *Materials and Design*, 37, 458–464. <https://doi.org/10.1016/j.matdes.2011.09.035>
- Dragunov, V. K., Terentev, E. V., Sliva, A. P., Goncharov, A. L., & Marchenkov, A. Y. (2017). Determination of welding speed in electron beam welding of thick components with continuous penetration. *Welding International*, 31(4), 307–311. <https://doi.org/10.1080/09507116.2016.1257243>
- Dubey, A. K., & Yadava, V. (2008). Experimental study of Nd:YAG laser beam machining-An overview. *Journal of Materials Processing Technology*, 195,(1–3), 15–26. <https://doi.org/10.1016/j.jmatprotec.2007.05.041>

- Eslami, N., Hischer, Y., Harms, A., Lauterbach, D., & Böhm, S. (2019). *Optimization of Process Parameters for Friction Stir Welding of Aluminum and Copper Using the Taguchi Method*. <https://doi.org/10.3390/met9010063>
- Fernández, R., Ibáñez, J., Cioffi, F., Verdera, D., & González-Doncel, G. (2017). Friction stir welding of 25%SiC/2124Al composite with optimal mechanical properties and minimal tool wear. *Science and Technology of Welding and Joining*, 22(6), 526–535. <https://doi.org/10.1080/13621718.2016.1268368>
- Fotovvati, B., Wayne, S. F., Lewis, G., & Asadi, E. (2018). A review on melt-pool characteristics in laser welding of metals. In *Advances in Materials Science and Engineering* (Vol. 2018). Hindawi Limited. <https://doi.org/10.1155/2018/4920718>
- Friel, R. J., & Harris, R. A. (2009). A nanometre-scale fibre-to-matrix interface characterization of an ultrasonically consolidated metal matrix composite. *Proceedings of the Institution of Mechanical Engineers, Part L: Journal of Materials: Design and Applications*, 224(1), 31–40. <https://doi.org/10.1243/14644207JMDA268>
- Fujii, H. T., Sriraman, M. R., & Babu, S. S. (2011). Quantitative evaluation of bulk and interface microstructures in Al-3003 alloy builds made by very high power ultrasonic additive manufacturing. *Metallurgical and Materials Transactions A*, 42(December), 4045–4055. <https://doi.org/10.1007/s11661-011-0805-x>
- Gemme, F., Verreman, Y., Dubourg, L., & Jahazi, M. (2010). Numerical analysis of the dwell phase in friction stir welding and comparison with experimental data. *Materials Science and Engineering: A*, 527(16–17), 4152–4160. <https://doi.org/10.1016/j.msea.2010.03.026>
- Guo, J., Gougeon, P., & Chen, X. G. (2012a). Study on laser welding of AA1100-16 vol.% B 4C metal-matrix composites. *Composites Part B: Engineering*, 43(5), 2400–2408. <https://doi.org/10.1016/j.compositesb.2011.11.044>
- Guo, J., Gougeon, P., & Chen, X. G. (2012b). Study on laser welding of AA1100-16 vol.% B 4C metal-matrix composites. *Composites Part B: Engineering*, 43(5), 2400–2408. <https://doi.org/10.1016/j.compositesb.2011.11.044>
- Guo, J., Gougeon, P., Nadeau, F., & Chen, X. G. (2012). Joining of AA1100-16 vol.-%B 4C metal matrix composite using laser welding and friction stir welding. *Canadian Metallurgical Quarterly*, 51(3), 277–283. <https://doi.org/10.1179/1879139512Y.0000000003>
- Hagenlocher, C., Seibold, M., Weber, R., & Graf, T. (2018). Modulation of the local grain structure in laser beam welds to inhibit the propagation of centerline hot cracks. *Procedia CIRP*, 74, 434–437. <https://doi.org/10.1016/j.procir.2018.08.164>
- Hahnlen, R., & Dapino, M. J. (2014). NiTi-Al interface strength in ultrasonic additive manufacturing composites. *Composites Part B*, 59, 101–108. <https://doi.org/10.1016/j.compositesb.2013.10.024>
- Halbauer, L., Laubstein, R., Radajewski, M., Buchwalder, A., Krüger, L., & Biermann, H. (2019). Electron beam welding and characterization of dissimilar joints with TWIP matrix composites. *Advanced Engineering Materials*, 21(5), 1–10. <https://doi.org/10.1002/adem.201800586>
- Harooni, M., Carlson, B., & Kovacevic, R. (2013). Effect of process parameters on the weld quality in laser welding of AZ31B magnesium alloy in lap joint configuration. *ICALEO 2013 - 32nd International Congress on Applications of Lasers and Electro-Optics*, 509–519. <https://doi.org/10.2351/1.5062923>
- Hassan, A. M., Qasim, T., Ghaithan, A., Hassan, A. M., Qasim, T., & Ghaithan, A. (2012). Effect of pin profile on friction stir welded aluminum matrix composites. *Materials and Manufacturing Processes*. October 2013, 37–41. <https://doi.org/10.1080/10426914.2012.663238>
- Hopkins, C. D., Dapino, M. J., & Fernandez, S. A. (2010). Statistical characterization of ultrasonic additive manufacturing Ti/Al composites. *Journal of Engineering Materials and Technology*, 132(4), 1–9. <https://doi.org/10.1115/1.4002073>

- Imam, M., Racherla, V., Biswas, K., Fujii, H., Chintapenta, V., Sun, Y., & Morisada, Y. (2017). Microstructure-property relation and evolution in friction stir welding of naturally aged 6063 aluminium alloy. *The International Journal of Advanced Manufacturing Technology*, 91(5–8), 1753–1769. <https://doi.org/10.1007/s00170-016-9865-9>
- Jayabalakrishnan, D., & Balasubramanian, M. (2018). Eccentric-weave FSW between Cu and AA 6061-T6 with reinforced graphene nanoparticles. *Materials and Manufacturing Processes*, 33(3), 333–342. <https://doi.org/10.1080/10426914.2017.1339323>
- Jun, D., Zheng, L., Li, Y., Yang, W., Chiyu, Z., & Yaocheng, Z. (2016). Research on pulsed laser welding of TiB₂-enhanced aluminum matrix composites. *The International Journal of Advanced Manufacturing Technology*, 85(1–4), 157–162. <https://doi.org/10.1007/s00170-015-7887-3>
- Kalaiselvan, K., Dinaharan, I., & Murugan, N. (2014). Characterization of friction stir welded boron carbide particulate reinforced AA6061 aluminum alloy stir cast composite. *Materials & Design*, 55, 176–182. <https://doi.org/10.1016/j.matdes.2013.09.067>
- Kalaiselvan, K., Dinaharan, I., & Murugan, N. (2021). Routes for the joining of metal matrix composite materials. In *Reference Module in Materials Science and Materials Engineering*. Elsevier. <https://doi.org/10.1016/b978-0-12-803581-8.11899-5>
- Katayama, S. (2020). *Fundamentals and Details of Laser Welding*. Springer. <https://www.springer.com/gp/book/9789811579325>
- Khanna, V., Kumar, V., & Bansal, S. A. (2020). Effect of carbonaceous nanomaterials' reinforcement on mechanical properties of aluminium metal-based nanocomposite: a review. *Materials Today: Proceedings*, 38, 289–295. <https://doi.org/10.1016/j.matpr.2020.07.221>
- Khanna, V., Kumar, V., & Bansal, S. A. (2021a). Aluminium-carbon fibre metal matrix composites: a review. *IOP Conference Series: Materials Science and Engineering*, 1033(1). <https://doi.org/10.1088/1757-899X/1033/1/012057>
- Khanna, V., Kumar, V., & Bansal, S. A. (2021b). Mechanical properties of aluminium-graphene/carbon nanotubes (CNTs) metal matrix composites: Advancement, opportunities and perspective. *Materials Research Bulletin*, 138(January). <https://doi.org/10.1016/j.materresbull.2021.111224>
- Khayyamin, D., Mostafapour, A., & Keshmiri, R. (2013). The effect of process parameters on microstructural characteristics of AZ91/SiO₂ composite fabricated by FSP. *Materials Science and Engineering A*, 559, 217–221. <https://doi.org/10.1016/j.msea.2012.08.084>
- Kong, C. Y., Soar, R. C., & Dickens, P. M. (2003). Characterisation of aluminium alloy 6061 for the ultrasonic consolidation process. *Materials Science and Engineering: A*, 363(1–2), 99–106. [https://doi.org/10.1016/S0921-5093\(03\)00590-2](https://doi.org/10.1016/S0921-5093(03)00590-2)
- Kong, C. Y., Soar, R. C., & Dickens, P. M. (2004). Optimum process parameters for consolidation of 3003 aluminum. *Journal of Materials Processing Technology*, 146(2), 181–187. <https://doi.org/10.1016/j.jmatprotec.2003.10.016>
- Kumar, N., Das, A., & Prasad, S. B. (2019). An analysis of friction stir welding (FSW) of metal matrix composites (MMCs). *Materials Today: Proceedings*, 26(xxxx), 2650–2656. <https://doi.org/10.1016/j.matpr.2020.02.558>
- Kumar, P. V., Reddy, G. M., & Rao, K. S. (2015). Microstructure and pitting corrosion of armor grade AA7075 aluminum alloy friction stir weld nugget zone e effect of post weld heat treatment and addition of boron carbide. *Defence Technology*, 2–9. <https://doi.org/10.1016/j.dt.2015.01.002>
- Kurzynowski, T., Madeja, M., Dziedzic, R., & Kobiela, K. (2019). The effect of EBM process parameters on porosity and microstructure of Ti-5Al-5Mo-5V-1Cr-1Fe alloy. *Scanning*, 2019. <https://doi.org/10.1155/2019/2903920>

- Lei, Z., Tian, Z., Li, P., Chen, Y., Zhang, H., & Chen, X. (2017). Joining of Sip/6063Al composite using additive manufacturing-based laser melting deposition. *Materials Letters*, 190, 191–194. <https://doi.org/10.1016/j.matlet.2017.01.016>
- Levy, A., Miriyev, A., Sridharan, N., Han, T., Tuval, E., Suresh, S., Dapino, M. J., & Frage, N. (2018). Ultrasonic additive manufacturing of steel : method, post-processing treatments and properties. *Journal of Materials Processing Tech.*, 256(January), 183–189. <https://doi.org/10.1016/j.jmatprotec.2018.02.001>
- Li, D. (2021). A review of microstructure evolution during ultrasonic additive manufacturing. *The International Journal of Advanced Manufacturing Technology*, 113, 1–19. <https://doi.org/10.1007/s00170-020-06439-8>
- Li, J., Monaghan, T., Masurtschak, S., Friel, R. J., & Harris, R. A. (2015). Exploring the mechanical strength of additively manufactured metal structures with embedded electrical materials. *Materials Science & Engineering A*, 639, 474–481. <https://doi.org/10.1016/j.msea.2015.05.019>
- Liu, B., Yang, Q., Liu, Y., & Wang, Y. (2018). Forming mechanism and bonding properties of Fe-Si-B amorphous strip/Al foil laminate composites by ultrasonic additive manufacturing (UAM). *Solid State Phenomenon*, 278, 39–47. <https://doi.org/10.4028/www.scientific.net/SSP.278.39>
- Liu, H., Hu, Y., Zhao, Y., & Fujii, H. (2017). Improving the particle distribution and mechanical properties of friction-stir-welded composites by using a smooth pin tool. *Mechanics of Composite Materials*, 53(4), 515–524. <https://doi.org/10.1007/s11029-017-9681-9>
- Madhavarao, S., Raju, C. R. B., & Kumar, G. S. V. S. (2018). Investigation of friction stir welding of metal matrix composites using a coated tool. *Materials Today: Proceedings*, 5(2), 7735–7742. <https://doi.org/10.1016/j.matpr.2017.11.450>
- Meng, C., Cui, H. C., Lu, F. G., & Tang, X. H. (2013a). Evolution behavior of TiB₂ particles during laser welding on aluminum metal matrix composites reinforced with particles. *Transactions of Nonferrous Metals Society of China (English Edition)*, 23(6), 1543–1548. [https://doi.org/10.1016/S1003-6326\(13\)62628-X](https://doi.org/10.1016/S1003-6326(13)62628-X)
- Meng, C., Cui, H. C., Lu, F. G., & Tang, X. H. (2013b). Evolution behavior of TiB₂ particles during laser welding on aluminum metal matrix composites reinforced with particles. *Transactions of Nonferrous Metals Society of China (English Edition)*, 23(6), 1543–1548. [https://doi.org/10.1016/S1003-6326\(13\)62628-X](https://doi.org/10.1016/S1003-6326(13)62628-X)
- Mohammed, S., Birru, A. K., Mohammed, S., & Birru, A. K. (2019). Friction stir welding of AA6082 thin aluminium alloy reinforced with Al₂O₃ nanoparticles. <https://doi.org/10.1080/0371750X.2019.1635046>
- Murugan, N., & Ashok Kumar, B. (2013). Prediction of tensile strength of friction stir welded stir cast AA6061-T6/AlNp composite. *Materials and Design*, 51, 998–1007. <https://doi.org/10.1016/j.matdes.2013.05.012>
- Mustafa, F. F., Kadhyam, A. H., & Yahya, H. H. (2015). Tool geometries optimization for friction stir welding of AA6061-T6 aluminum alloy T-joint using taguchi method to improve the mechanical behavior. *Journal of Manufacturing Science and Engineering*, 137, 1–8. <https://doi.org/10.1115/1.4029921>
- Ni, D. R., Chen, D. L., Wang, D., Xiao, B. L., & Ma, Z. Y. (2013). Influence of microstructural evolution on tensile properties of friction stir welded joint of rolled SiCp/AA2009-T351 sheet. *Materials & Design*, 51, 199–205. <https://doi.org/10.1016/j.matdes.2013.04.027>
- Nourani, M., Milani, A. S., & Yannacopoulos, S. (2015). On experimental optimization of friction stir welding of aluminum 6061: understanding processing-microstructure-property relations. *International Journal of Advanced Manufacturing and Technology*. <https://doi.org/10.1007/s00170-015-6932-6>

- Padmanaban, R., Muthukumaran, V., & Vighnesh, A. (2015). Parameter optimization for friction stir welding AA1100. *Applied Mechanics and Materials*, 813–814, 462–466. <https://doi.org/10.4028/www.scientific.net/AMM.813-814.462>
- Paidar, M., Asgari, A., Ojo, O. O., & Saberi, A. (2018). Mechanical properties and wear behavior of AA5182/WC nanocomposite fabricated by friction stir welding at different tool traverse speeds. *Journal of Materials Engineering and Performance*, 27(4), 1714–1724. <https://doi.org/10.1007/s11665-018-3297-7>
- Pandiyarajan, R., Maran, P., Murugan, N., Marimuthu, S., & Sornakumar, T. (2019). Friction stir welding of hybrid AA 6061-ZrO₂-C composites FSW process optimization using desirability approach. *Materials Research Express*, 6(6), 066553. <https://doi.org/10.1088/2053-1591/ab084e>
- Peng, H., Liu, C., Guo, H., Yuan, Y., Gong, S., & Xu, H. (2016). Fabrication of WCp/NiBSi metal matrix composite by electron beam melting. *Materials Science and Engineering A*, 666, 320–323. <https://doi.org/10.1016/j.msea.2016.04.079>
- Periyasamy, P., Mohan, B., Balasubramanian, V., Rajakumar, S., & Venugopal, S. (2013). Multi-objective optimization of friction stir welding parameters using desirability approach to join Al/SiCp metal matrix composites. *Transactions of Nonferrous Metals Society of China*, 23(4), 942–955. [https://doi.org/10.1016/S1003-6326\(13\)62551-0](https://doi.org/10.1016/S1003-6326(13)62551-0)
- Prabhu, S., Arun Kumar Shettigar, K. R., Rao, S., & Herbert, M. (2017). Influence of welding process parameters on microstructure and mechanical properties of friction stir welded aluminium matrix composite. *Materials Science Forum*, 880, 50–53. <https://doi.org/10.4028/www.scientific.net/MSF.880.50>
- Prater, T., Strauss, A., Cook, G., Gibson, B., & Cox, C. (2013). A comparative evaluation of the wear resistance of various tool materials in friction stir welding of metal matrix composites. *Journal of Materials Engineering and Performance*, 22(6), 1807–1813. <https://doi.org/10.1007/s11665-012-0468-9>
- Sahraeinejad, S., Izadi, H., Haghshenas, M., & Gerlich, A. P. (2015). Fabrication of metal matrix composites by friction stir processing with different particles and processing parameters. *Materials Science and Engineering: A*, 626, 505–513. <https://doi.org/10.1016/j.msea.2014.12.077>
- Salih, O. S., Ou, H., Wei, X., & Sun, W. (2019). Microstructure and mechanical properties of friction stir welded AA6092/SiC metal matrix composite. *Materials Science and Engineering: A*, 742, 78–88. <https://doi.org/10.1016/j.msea.2018.10.116>
- Singh, B. R. (2012). *A Hand Book on Friction Stir Welding* Issue (June). <https://doi.org/10.13140/RG.2.1.5088.6244>
- Singh, T., Tiwari, S. K., & Shukla, D. K. (2020). Mechanical and microstructural characterization of friction stir welded AA6061-T6 joints reinforced with nano-sized particles. *Materials Characterization*, 159, 110047. <https://doi.org/10.1016/j.matchar.2019.110047>
- Srinivasan, R., Vesvanth, M., Sivasuriya, K., Sanjay, S., & Madhu, M. J. V. (2020). Experimental investigation on the effect of tool rotation speed on stir cast friction stir welded aluminium hybrid metal matrix composite. *Materials Today: Proceedings*, 27(xxxx), 1787–1793. <https://doi.org/10.1016/j.matpr.2020.03.690>
- Tamjidy, M., Baharudin, B. T. H. T., Paslar, S., Matori, K. A., Sulaiman, S., & Fadaeifard, F. (2017). Multi-objective optimization of friction stir welding process parameters of AA6061-T6 and AA7075-T6 using a biogeography based. *Materials*, 10(533), 1–19. <https://doi.org/10.3390/ma10050533>
- Tebiyani, S. F., & Dehghani, K. (2015). Friction stir spot welding of interstitial free steel with incorporating silicon carbide nanopowders. *International Journal of Advanced Manufacturing Technology*, 79(1–4), 343–350. <https://doi.org/10.1007/s00170-015-6788-9>

- Terentyev, Y. V., Dragunov, V. K., Sliva, A. P., & Scherbakov, A. V. (2015). Effect of welding speed on weld formation in electron beam welding with continuous penetration. *Welding International*, 29(2), 150–154. <https://doi.org/10.1080/09507116.2014.897808>
- Vaziri, S. A., Shahverdi, H. R., Torkamany, M. J., & Shabestari, S. G. (2009). Effect of laser parameters on properties of surface-alloyed Al substrate with Ni. *Optics and Lasers in Engineering*, 47(9), 971–975. <https://doi.org/10.1016/j.optlaseng.2009.04.007>
- S.J. Vijay, & N. Murugan. (2010). Influence of tool pin profile on the metallurgical and mechanical properties of friction stir welded Al-10 wt.% TiB₂ metal matrix composite. *Materials and Design*, 31(7), 3585–3589. <https://doi.org/10.1016/j.matdes.2010.01.018>
- Višniakov, N., Mikalauskas, G., Černášejienė, R., Černášejus, O., & Škamat, J. (2018). Electron beam welding of copper-niobium microcomposites for pulsed power applications. *Materialwissenschaft Und Werkstofftechnik*, 49(5), 538–550. <https://doi.org/10.1002/mawe.201700240>
- Vyskoč, M., Sahul, M., Dománková, M., Jurčí, P., Sahul, M., Vyskočová, M., & Martinkovič, M. (2020). The effect of process parameters on the microstructure and mechanical properties of aw5083 aluminum laser weld joints. *Metals*, 10(11), 1–22. <https://doi.org/10.3390/met10111443>
- Wang, D., Wang, Q. Z., Xiao, B.L., & Ma, Z. Y. (2014a). Achieving friction stir welded SiCp/Al–Cu–Mg composite joint of nearly equal strength to base material at high welding speed. *Materials Science & Engineering A*, 589, 271–274. <https://doi.org/10.1016/j.msea.2013.09.096>
- Wang, D., Xiao, B. L., Wang, Q. Z., & Ma, Z. Y. (2014b). Evolution of the microstructure and strength in the nugget zone of friction stir welded SiCp/Al–Cu–Mg composite. *Journal of Materials Science & Technology*, 30(1), 54–60. <https://doi.org/10.1016/j.jmst.2013.09.018>
- Wang, H. M., Chen, Y. L., & Yu, L. G. (2000). ‘In-situ’ weld-alloying/laser beam welding of SiCp/6061Al MMC. 293, 1–6.
- Wang, S., Wei, X., Xu, J., Hong, J., Song, X., Yu, C., Chen, J., Chen, X., & Lu, H. (2019). Strengthening and toughening mechanisms in refilled friction stir spot welding of AA2014 aluminum alloy reinforced by graphene nanosheets. *Materials & Design*, 108212. <https://doi.org/10.1016/j.matdes.2019.108212>
- Wang, S. G., Ji, X. H., Zhao, X. Q., & Dong, N. N. (2011). Interfacial characteristics of electron beam welding joints of SiCp/Al composites. *Materials Science and Technology*, 27(1), 60–64. <https://doi.org/10.1179/174328409X412005>
- Wang, Y., Hou, F. M., Yang, Q., Fan, Z. Y., Pan, H. Y., & Xu, H. (2020). Microstructure and mechanical properties of Al/Fe micro-laminated composites fabricated by ultrasonic consolidation. *Journal of Physics: Conference Series*, 1507, 1–13. <https://doi.org/10.1088/1742-6596/1507/4/042002>
- Węglowski, M. S., Błacha, S., & Phillips, A. (2016). Electron beam welding - techniques and trends - review. *Vacuum*, 130, 72–92. <https://doi.org/10.1016/j.vacuum.2016.05.004>
- Wolcott, P.J., Sridharan, N., Babu, S. S., Miriyev, A., Frage, N., & Dapino, M. J. (2016). Characterisation of Al – Ti dissimilar material joints fabricated using ultrasonic additive manufacturing characterisation of Al-Ti dissimilar material joints fabricated using ultrasonic additive manufacturing. *Science and Technology of Welding and Joining*, 1718(21), 114–123. <https://doi.org/10.1179/1362171815Y.0000000072>
- Wolcott, Paul J., & Dapino, M. J. (n.d.). Ultrasonic additive manufacturing. In *Additive Manufacturing Handbook* (pp. 275–313). Taylor & Francis. <http://taylorandfrancis.com>

- Yang, Y., Ram, G. D. J., & Stucker, B. E. (2007). An experimental determination of optimum processing parameters for Al/SiC metal matrix composites made using ultrasonic consolidation. *Journal of Engineering Materials and Technology*, 129. <https://doi.org/10.1115/1.2744431>
- Yang, Y., Ram, G. D. J., & Stucker, B. E. (2009). Bond formation and fiber embedment during ultrasonic consolidation. *Journal of Materials Processing Technology*, 209, 4915–4924. <https://doi.org/10.1016/j.jmatprotec.2009.01.014>
- Yigezu, B. S., Venkateswarlu, D., Mahapatra, M.M., Jha, P.K., & Mandal, N.R. (2014). On friction stir butt welding of Al + 12Si/10 wt%TiC in situ composite. *Materials & Design*, 54, 1019–1027. <https://doi.org/10.1016/j.matdes.2013.09.034>
- Yousaf, D., Bashir, S., Akram, M., Kalsoom, U. I., & Ali, N. (2014). Laser irradiation effects on the surface, structural and mechanical properties of Al-Cu alloy 2024. *Radiation Effects and Defects in Solids*, 169(2), 144–156. <https://doi.org/10.1080/0420150.2013.834901>
- Zolghadr, P., Akbari, M., & Asadi, P. (2019). Formation of thermo-mechanically affected zone in friction stir welding. *Materials Research Express*, 6(8), 086558. <https://doi.org/10.1088/2053-1591/ab1d25>



Taylor & Francis

Taylor & Francis Group

<http://taylorandfrancis.com>

@seismicisolation
@seismicisolation

8 3D Printing of Metal Matrix Composites

A Review and Prospective

Gurdyal Singh and Gurpreet Singh

Chitkara University Institute of Engineering and Technology, Chitkara University, Punjab, India

Rajbir Bhatti

Mount Royal University, Calgary, Canada

Balkar Singh

IKG Punjab Technical University, Jalandhar, India

CONTENTS

8.1	Introduction.....	168
8.2	Metal Matrix Composites (MMCs)	170
8.3	Techniques of 3D Printing	171
8.3.1	Direct Metal Laser Sintering (DMLS).....	172
8.3.2	Selective Laser Melting (SLM)	174
8.3.3	Electron Beam Melting (EBM)	175
8.3.4	Binder Jetting (BJG) or 3DP.....	176
8.3.5	Directed Energy Deposition (DED).....	177
8.3.6	Laminated Object Manufacturing (LOM)	179
8.4	MMCs Processing by 3D Printing.....	180
8.4.1	Aluminum-based Composites.....	181
8.4.2	Nickel Matrix Composites.....	182
8.4.3	Titanium Matrix Composites	183
8.4.4	Copper Matrix Composites.....	184
8.4.5	Iron Matrix Composites.....	184
8.4.6	Zinc Matrix Composites	185
8.5	Applications of MMCs	185
8.5.1	Biomedical Industry.....	185
8.5.2	Aerospace Industry	188
8.5.3	Automotive Industry	188

8.5.4 Construction Industry	189
8.5.5 Personalized Item Industry	189
8.6 Challenges.....	190
8.7 Future Scopes.....	191
References.....	192

8.1 INTRODUCTION

As an additive manufacturing (AM) technique, 3D printing offers the fabrication of a variety of product structures ranging from simple to complex shapes of three-dimensional (3D) geometrical model by printing successive layers of chosen materials, sliced on top of each other (Ngo et al. 2018). In contrast, the conventional manufacturing technique involves material removal or material forming, processed by various cutting or forming tools by working on raw material, generating a lot of material wastage. Secondly, the raw material or semi-finished parts need to move through various stages, going from machine to machine, which involves logistics and energy consumption. Thirdly, the quality and precision of finished parts largely depends upon the machine capability and operator's skill (Shi and Wang 2020). On the other hand, 3D printing is capable of building fully functional parts in a single go at one station with no additional handling and minimum material wastage. Additionally, design engineers have the flexibility to create complex, realistic shapes, only possible by 3D printing (and not possible to manufacture with conventional manufacturing processes). The various industrial sectors have started to realize the paybacks of MMC products produced by 3D printing. Similarly, the rapid prototyping ability realized by 3D printing has drawn significant attention from research and development, as well as academia to design and develop new products. 3D printing has evolved itself as a sustainable manufacturing option. As per Wohler's report 2021, a 7.5% growth has been predicted in the 3D printing industry despite the COVID-19 pandemic (Wohlers and Caffrey 2021).

Composite materials are widely used in different industries for the fabrication of lightweight components and structures due to their benefits over monolithic counterparts (Mussatto et al. 2021). Composite materials are used extensively in the aviation industry to manufacture numerous aircraft components. Even in the automobile sector, composite materials are extensively used to reduce weight without compromising strength. The reduced weight helps in lowering the fuel consumption and consequently decreasing the pollution emission. Currently, composites are used for the fabrication of half of the airframe of aircraft, which contributes to reducing 20% of the weight of the aircraft (Hale 2012). Apart from this, composite materials are extensively used in other fields, like the automotive industry, construction, infrastructure, transportation, and sports because of their excellent mechanical properties, high strength-to-weight ratio, corrosion resistance, and low costs as compared to other traditional materials. Conventional methods of manufacturing the component from composite material are not able to fabricate the component with challenging lead time and may fail to cope with

demand in the coming future. So different fabrication techniques need to be developed to meet the huge requirement of composite materials. Moreover, it is quite difficult to handle the repair of composite materials with the usual manufacturing methods. So there is a dire need to explore new methods and machines to fabricate and repair the components of composite materials.

Earlier it was a challenging task to manufacture a customized product due to the high cost of production for tailored products. Many researchers are already putting their best efforts to develop new methods and machines for the fabrication of parts of composite materials. Additionally, 3D printing is capable of producing customized products at a low cost and in less time without the requirement of special tooling and dies. This is particularly constructive in the biomedical field to produce a wide range of medical implants, where totally different products are required according to the patient. It is also useful in the aerospace industry and in other industries for the manufacturing of parts which need to be replaced and are not readily available in the open market. 3D printing has gained wide acceptance as one of the popular techniques to develop parts to suit these applications. Currently, a wide variety of materials and their combinations are used for 3D printing, which are selected according to the suitability of applications, strength requirement, manufacturability, and environmental conditions. Composite materials involving metals and alloy-metals are preferred for 3D printing of the parts in the aerospace and automotive industries. MMCs involving ceramics are utilized in the manufacturing of the scaffolds and in construction of building parts using 3D printing.

The patent regulations and market strategies of the companies in the 3D printing field have created the need to use distinctive names for similar 3D printing processes. The various 3D printing techniques can be broadly classified into two categories. The first type of technique involves the melting of materials by highly focused thermal energy, as materials are being deposited and fused together layer-by-layer to form the requisite part. This technique is called directed energy deposition (DED), or laser engineered net shaping (LENS), or laser metal deposition (LMD). This technique is associated with flexibility in material powder composition, curved path deposition, and fast fabrication rate. The second technique uses thermal energy to directly heat or melt the material powder stored in the powder bed, and thus fuse the powder to build the part as per the directed path. This technique comes under powder-bed fusion (PBF) and processes based on this technique are known as selective laser sintering (SLS), direct metal laser sintering (DMLS), and selective laser melting (SLM). These techniques offered benefits in terms of improved mechanical properties, good surface quality, and high accuracy, notably ascribed as being due to fine microstructure and high resolution caused by the laser focusing on smaller spots on powders. However, anisotropic behavior and the lack of mechanical properties are the obstacles in the mass production of 3D printed parts. Additionally, 3D printing for parts fabrication is time-consuming, which is also a major hurdle in mass production. Nonetheless, better machine design can help in achieving better fabrication speed and it can also help in reducing cost.

This chapter provides a critical review of various 3D printing techniques commonly used for the fabrication of MMCs. Thereafter, research work on the adoption of various 3D printing technology for the processing of commonly used MMCs has been presented and their effect on performance enhancements have been analyzed. Further, the recent applications of 3D-printed MMCs products in various industries have been explored. Finally, the challenges in 3D printing of MMCs and future scopes are pointed out.

8.2 METAL MATRIX COMPOSITES (MMCs)

The composition of MMCs usually consists of a metallic matrix phase accompanied with one or more constituent phases for reinforcement. The matrix material acts as a continuous phase medium to hold the reinforcement together, to transfer the load and provide a protective environment, whereas reinforcement gives strength and stiffness to the composites. Composites can be classified on the basis of matrix material (polymers, ceramics, or metals) or on the basis of reinforcement types (fibers, particulates, platelet whiskers, or laminates). Figure 8.1 shows MMCs classification based on reinforcement types.

Over the years, numerous blends of matrix and reinforcement materials have been tried by various researchers. The effects of these combined with desirable properties have been explored to suit the particular application environment. Among these, iron, aluminum, copper-nickel, and titanium have been extensively used as metal matrices, whereas oxides, carbides, nitrides, etc. have been recommended as reinforcements for MMCs. Table 8.1 lists commonly used matrix materials along with reinforcements. The primary focus is to improve the various mechanical properties, such as strength, stiffness, and weight reduction, and make these economically feasible for mass production.

Among the various composite materials, MMCs have gained considerable focus over the last few decades due to developments in materials and improvements in manufacturing tools. The desired control and customization of key

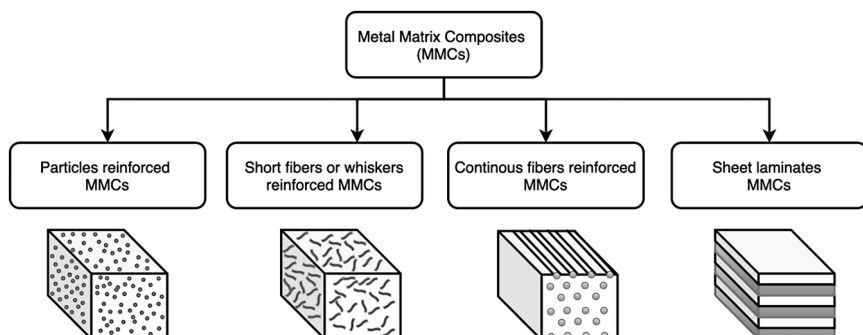


FIGURE 8.1 Types of MMCs as per reinforcement. (redrawn from Mistry and Gohil 2018).

TABLE 8.1
Commonly Used Matrix and Reinforcement Materials for MMCs

Matrix Materials	Metal Matrix Composites				
	Carbides	Oxides	Nitrides	Borides	Others
Aluminum	Ti ₃ SiC ₂	Al ₂ O ₃	TiN	TiB ₂	WS ₂
Nikel	TiC	TiO ₂	BN	ZrB ₂	Diamond
Titanium	SiC	SiO ₂	Si ₃ N ₄		
Iron	CNT	ZrO ₂			
Copper	B ₄ C	ZnO			
Zinc	Graphite				

(Adapted with Permission from Ramanathan et al. 2019)

physical, mechanical properties offered by MMCs have led for the extensive use of these in biomedical, automotive, aerospace, defense, and construction fields.

8.3 TECHNIQUES OF 3D PRINTING

3D printing involves the fabrication of products by adding material in layers and works on a constructive approach for parts building, compared to metal removal in conventional manufacturing processes. Thus, it acts as a promising technique to manufacture complicated geometries with ease and in less time. Design flexibility and minimum waste are the additional features that make 3D printing the first choice of engineers. As per need or function requirement, part specifications are generated by scanning already developed part or concept generation from a new idea. A CAD model is developed in any design software as per the inputs and the file is saved in STL format, and then this file is processed in the supported software package to generate codes compatible with 3D printing hardware. Then, the 3D printing machine manufactures the parts according to the designed geometrical shape. Thus, computer design is transferred to computer-aided manufacturing, where a machine (3D printer) develops a part by depositing the melted raw material layer by layer. The schematic diagram of product development for 3D printing is shown in Figure 8.2. The first commercial 3D technology was developed by Charles W. Hull in 1986 and it was followed by many other developments in this field, like powder bed fusion, inkjet printing, contour crafting, and fused deposition method. Nowadays, 3D printing in form of additive manufacturing has found applications in various industries, which include construction, biomedical, and defense.

Over the years, 3D printing techniques have evolved with the advancement of technologies, as per the market requirement to meet the growing demands. The necessity to build complex geometrical shapes with fine resolution, customized

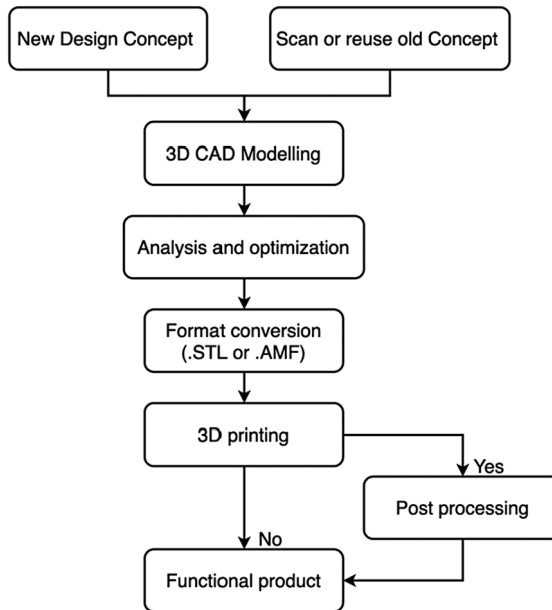


FIGURE 8.2 Schematic diagram of product development for 3D printing. (redrawn from Ho et al. 2015).

parts as per demand, light structures with improved properties, rapid tooling, repairs etc. acts as driving forces behind technological advancement in 3D printing field. The most appropriate and commercially viable 3D printing techniques associated with MMCs fabrication includes direct metal laser sintering (DMLS), selective laser melting (SLM), electron beam melting (EBM), binder jetting (BJG) or 3DP, directed energy deposition (DED), laminated object manufacturing (LOM) or UAM. The working principle of these techniques, along with their advantages and limitations, have been discussed in the next section.

8.3.1 DIRECT METAL LASER SINTERING (DMLS)

DMLS is a laser-based 3D printing technology, jointly developed by EOS GmbH, Munich, Germany in association with Rapid Product Innovations Rusko, Finland. Selective laser sintering (SLS) and DSLS are essentially the same technique. The term SLS is generally referred to for the processing of non-metals such as ceramics, plastics, glass etc., whereas DSLS terminology is referred to when associated with metals processing. This technique uses high-power lasers to diffuse and blend the metal powder in form of layers by tracing the path controlled by the 3D CAD data. The schematic diagram of the DMLS technique is shown in Figure 8.3. As a powder-bed process, it involves the spreading of closely packed thin layers of constituent powders on a platform. The laser is focused on the powder top layer by focusing optics and the exact pattern is traced as per the model geometry.

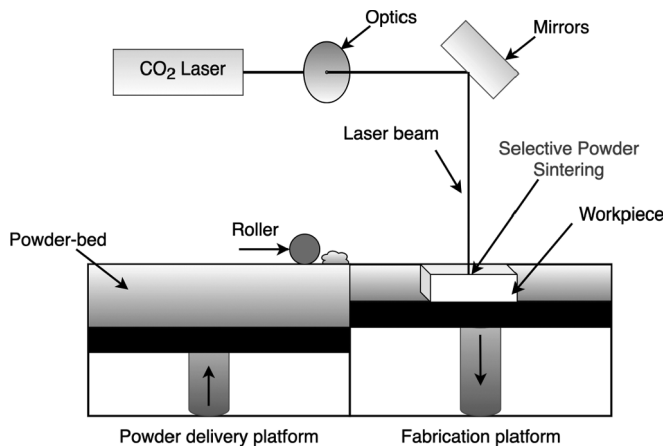


FIGURE 8.3 Schematic diagram of the DMLS technique. (redrawn from Gu and Shen 2006).

The part platform is lowered down after each layer and a fresh coat of powder is spread by re-coater blade or roller over the built part to create the next layer by laser beam sintering until the 3D part is built. The non-fused excess powder surrounding the built part is sucked by vacuum. The 3D printed part is then subjected to post-processing such as further sintering, coating etc. to improve surface characteristics. The powders used in DMLS consist of a high melting-point powder, usually part structural material mixed with low melting-point binder powder. The selective melting of low-melting-point binder powder by laser beam converts it into a liquid phase, which is driven into voids of non-melting structural powder through capillary action and helps fuse powders together to formulate the part with or without reinforcement particles. Thus, the involved sintering process does not fully melt the base powder, but just heats it to the point to enable fusing by binder material on a molecular level. The quality and strength of the DMLS 3D printed part in terms of density and porosity depends upon powder particle shape, size, packing, and binder (Utela et al. 2008). The laser processing parameters such as spot size, laser power, scan speed, and scan line spacing need to be optimized for efficient processing.

DMLS process offers the flexibility of using a blend of two or more structural powders to formulate multi-functional MMCs. The various combination of metallic powders such as iron, copper, tungsten, steel, nickel, cobalt, and their alloys are being explored by researchers worldwide under the DMLS process to formulate MMCs with tailored properties. The DMLS process is able to produce complex geometrical shapes due to flexible feeding of stocks or powder along with precise control over the laser path for pattern tracing which is otherwise impossible to manufacture by conventional means. The other associated benefits include better control of process parameters, structural flexibility, low setup time, and competitively economical 3D printing (Nandy et al. 2019).

8.3.2 SELECTIVE LASER MELTING (SLM)

Among the powder-bed fusion techniques, SLM is the most extensively used technique in the 3D printing field (Herzog et al. 2016). As compared to DMLS, SLM utilizes the laser beam to fully melt the metal powder and fuse them together, resulting in homogenous and denser parts. The process involves spreading of thin uniform layer over the substrate plate with help of a roller, followed by a laser which selectively traces the pattern as per the CAD model, melts the powder, and fuses it together layer by layer until the part is completed (Gokuldoss Prashanth et al. 2016). The whole SLM process occurred in a pressurized compartment filled with nitrogen or argon inert gas to avoid oxygen contamination during powder melting and later solidification. Sometimes the substrate plate is heated (200–500 °C) to control the cooling rate of brittle or high melting point materials to avoid possible cracking during solidification (Prashanth et al. 2015). The SLM process is governed by several process parameters, viz., layer thickness, hatch distance, laser power, scanning speed, hatch style, etc., which are required to be optimized as per the model along with the right material selection to control the properties and build the defect-free parts (Laakso et al. 2016). The schematic diagram of the SLM technique is shown in Figure 8.4.

SLM has established itself as the most versatile technique due to its suitability to process a wide range of materials, including Cu-based alloys, Ti-based alloys, Fe-based alloys, Ni-based alloys, Al-based alloys, and composite, as well as amorphous materials. The microstructure and mechanical properties of a fabricated part can be tailored to suit particular applications by selecting suitable parameters such as laser parameters, hatch-style variations, internal structure heating, base-plate heating, etc. (Prashanth et al. 2015). SLM offers the

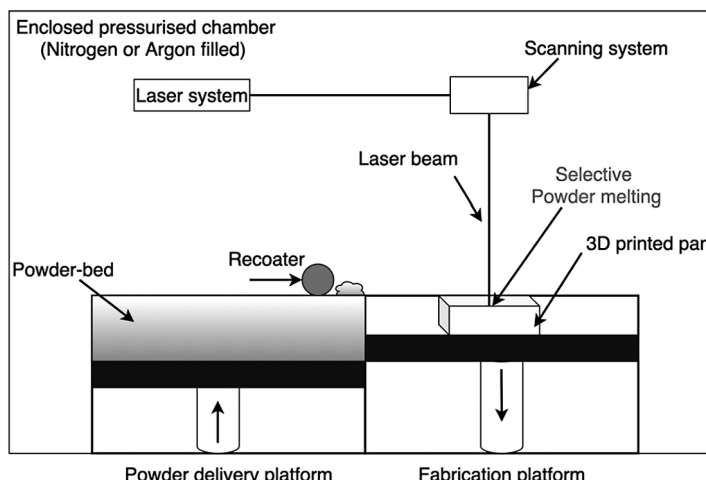


FIGURE 8.4 Schematic diagram of the SLM technique. (redrawn from Jiao et al. 2018).

advantages such as competence to process a wide variety of materials, reusability of powders, high cooling rate, flexibility in parameters selection to control the properties, relatively low cost, and ready-to-use functional parts (Ardila et al. 2014). Contrary, the SLM has some inherent limitations such as relatively slow process, part-size constraints, excessive power requirement, high initial investment, time-consuming process-parameters optimization, and rough surfaces of produced parts. Also, cracking problems sometimes occurred as is associated with brittle and high melting materials, which require substrate plate heating to control the cooling and internal stress generation. Researchers have explored the application of SLM to optimize the laser energy and scanning speed to fabricate fully dense composite parts. The results indicated a positive relationship between laser power and surface characteristics, whereas the relation with material density depends upon the reinforcement weight percentage in composite material (Han et al. 2017).

8.3.3 ELECTRON BEAM MELTING (EBM)

EBM is another technique quite similar in operation to the SLM process that works on layer-by-layer formation by melting and fusing the metal powder to build the part as per CAD geometry. Compared with the lasers used in the SLM technique, EBM uses electron beam as energy source for powder melting along with powder bed maintained at high temperatures in vacuum atmosphere and further required extended cooling period to cool the job after fabrication. The mechanism of powder feeding, path tracing, and platform movement is similar to other powder-bed processes. But the use of electron beam in EBM process is associated with more process parameters to control and optimized viz. beam focus, beam power, beam diameter, beam scanning velocity, temperature and heating inside build chamber. The schematic diagram of the EBM technique is shown in Figure 8.5.

The advantages of EBM include non-oxidation of fabricated parts due to vacuum operation, non-porous, or dense microstructure, the ability to process brittle intermetallic materials due to slow cooling rate, and crack-free structure due to the absence of internal stresses generated during solidification. On the other hand, the involvement of a number of process parameters associated with EBM makes their optimization quite difficult as compared to the SLM process and hence its use is limited to selected materials only, such as Ti grade-2, Ti-6Al-4V, Inconel-718, and Co-Cr-Mo alloy. As the electron beam is selectively used several times on each layer for heating and melting powders, it takes a much greater time to process each layer as compared to the SLM process and also the raised temperature inside the chamber makes it very hot which required an extended time, usually overnight, to cool the chamber and substrate plate before removing the built part. The other limitations include expansive fabrication of parts due to slowness or time-consuming process, size limitations on parts building, vacuum requirement during process, and non-suitability to process alloy material with volatile constituents such as Bi, Mg, Zn, Pb, etc.

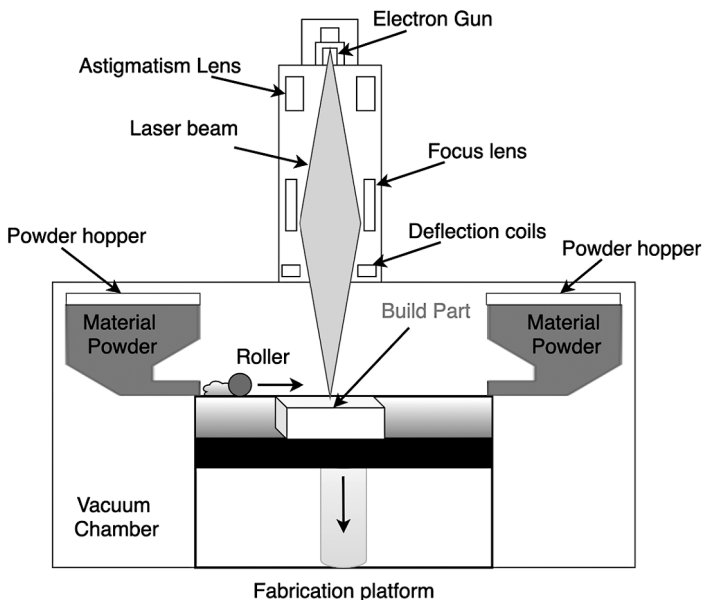


FIGURE 8.5 Schematic diagram of the EBM technique. (redrawn from Ameen et al. 2019).

8.3.4 BINDER JETTING (BJG) OR 3DP

The BJG is another process based on powder-bed methodology and formation of parts in layers by adhesive action of binder on powder by following the CAD part geometry. The process is also known as the 3DP process, as it primarily uses material in powder form and a liquid binder is fed selectively from a nozzle, which builds the part by adhesion of powder material (Utela et al. 2008). The powder material contributes majorly to the overall weight of the built part. The schematic diagram of the BJG technique is shown in Figure 8.6.

The part fabrication process consists of a build platform over which the base metal powder is spread by the roller in form of a thin layer. A print jet loaded with binding liquid traces the geometry pattern on the horizontal plane and deposits the binder to bind the material powder in the top layer. The build platform is lowered down, and a fresh coat of powder is spread to repeat the process of layer formation. The surrounding unbound powder acts as support during 3D printing and is removed/reused after object completion. The appropriate heating of the build chamber helps to increase printing speed by influencing the viscosity of binder liquid. The selection of the right processing parameters, viz. powder layer thickness, powder spreading speed, cabin heating, binder properties, rate of drying, etc., influences the quality of the final printed part (Snelling et al. 2017).

BJG has proved its ability to process a range of materials, including metals (stainless-steel), ceramics (glass), polymers (PA, ABS) and composites, along

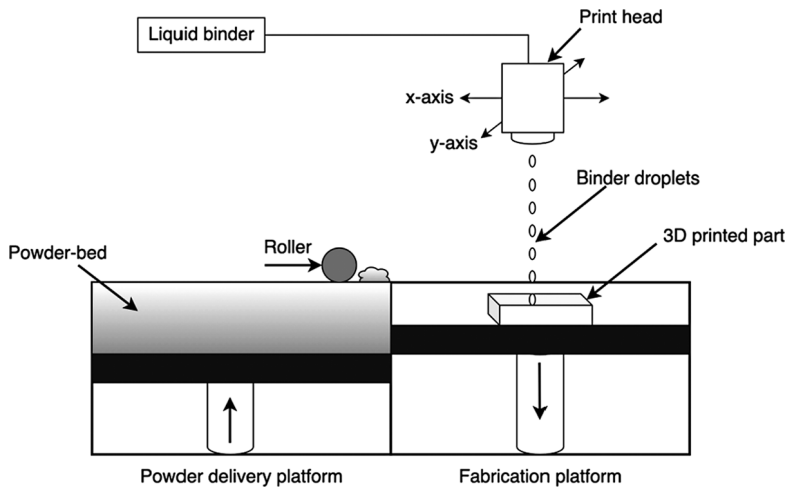


FIGURE 8.6 Schematic diagram of the BJG technique. (redrawn from Trenfield et al. 2018).

with color printing. Other advantages include a relatively high speed of printing, the flexibility of employing several binder print heads for different binder–powder combinations as per internal part structure quality requirements. The limitations associated with BJG include poor characteristics of fabricated parts due to the binding process, powder characteristics, and the requirement of additional post-processing increases overall build-up time (Gibson et al. 2010). Lores et al. (2019) reviewed the technological developments in BJG with a focus on materials and process characteristics. They found its suitability for different kinds of materials with a wide range of particle sizes. The choice of binding liquid, jetting parameters, materials with high flowability, and parts sintering are governing factors to make homogenous and denser 3D printed parts.

8.3.5 DIRECTED ENERGY DEPOSITION (DED)

The DED technique employs laser or electron beams as an energy source to melt and direct the feedstock (powder or wire) and deposit it directly on CAD controlled path on substrate. The processing is done within a controlled chamber with reduced oxygen levels. Figure 8.7 shows the schematic of the DED system employing laser with powder feedstock (Figure 8.7a) and electron beam with wire feedstock (Figure 8.7b) (Sing et al. 2019). This technique is known by several names as per technology, viz.,laser metal deposition (LMD), laser engineered net shaping (LENS), laser solid forming (LSF), directed light fabrication (DLF), 3D laser cladding, and Wire+Arc AM (WAAM) (Hong et al. 2015; Ngo et al. 2018). The DED process differs from other 3D printing processes in terms of the nonrequirement of a powder bed. The feedstock in form of wire or powder is fed

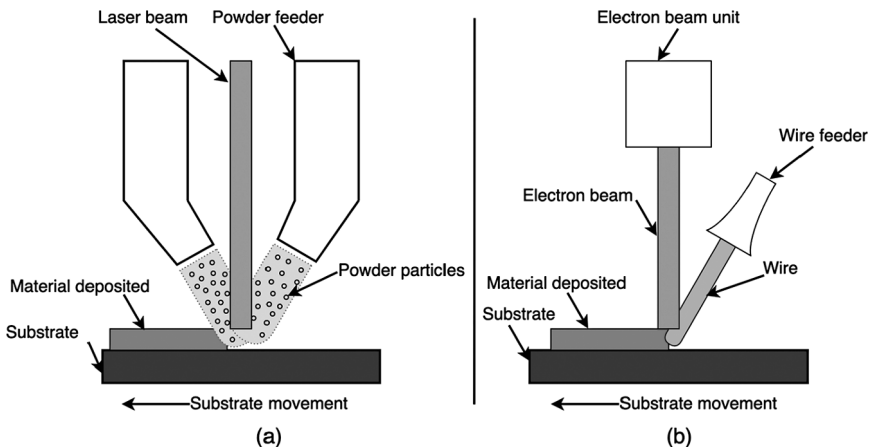


FIGURE 8.7 Schematic of DED system employing (a) laser with powder feedstock; (b) electron beam with wire feedstock. (redrawn from Sing et al. 2019).

from the overhead nozzle and is melted with an extremely high amount of energy, while depositing in layers on the substrate and getting solidified (Gibson et al. 2015b). The use of wire as feedstock material over powder-form is not preferred due to its pre-formed shape, but on the other hand, is considered more material-efficient over powder use. (Gibson et al. 2010). The complexity of equipment and its operation restricts the use of the DED process for repair or material addition to an existing structure and for manufacturing of high-performance super-alloy. It has proved to be very useful for filling cracks in already built parts or retrofitting manufactured parts.

This method offers the flexibility for multi-axis metal deposition employing four or five axis movements of feed-head for different materials simultaneously. This helps to deposit material at different angle in contrast to vertical-only deposition in other 3D printing techniques. This process can be used with polymers and ceramics, but is typically used with metals. Also, DED can be used in conjunction with conventional subtractive processes to manufacture the parts. DED offers advantages in terms of high fabrication speed, excellent mechanical properties, well-ordered grain structure, precise composition control, sizeable work envelope, reduced manufacturing time and associated cost, and 0.25 mm–0.5 mm the typical thicknesses of layers (Gibson et al. 2010). However, it is associated with building simple geometrical parts, low accuracy (0.25 mm), and poor surface when compared to DSLS or SLM (Gibson et al. 2015b). Hence, DED is generally preferred to fabricate large size components with less geometrical complexity and for repairing large components. This technique is most suitable for working with stainless steel, titanium, aluminum, Inconel, their alloys and composites in a range of applications, varying from the repair of turbine blades to other high-end component fabrication for the aerospace and automobile field.

8.3.6 LAMINATED OBJECT MANUFACTURING (LOM)

Laminated object manufacturing (LOM) or sheet lamination involves the cutting and bonding of material sheets or rolls in layers. It is one of the first commercially available AM methods. The part profiles or contours as per the CAD model are cut precisely using a laser beam or mechanical cutter, with successive layers bonded together using the form-then-bond or bond-then-form method. The form-then-bond method of LOM involves cutting the form or shape first and then bonding together in layers. This method removes the material pocket or extra material before bonding, thus helping to capture internal part features. This extra material left after cutting acts as support and is removed after part completion and further recycled (Gibson et al. 2015a). A variety of materials ranging from metals and metal-filled tapes, polymers, ceramics, and composites can be processed by the LOM technique. The type of material used and the desired properties requirement may demand for the post-processing of build parts, such as high-temperature treatment. Figure 8.8 shows the schematic diagram of the LOM (Figure 8.8a) and UAM technique (Figure 8.8b).

Ultrasonic additive manufacturing (UAM) is a new sub-class under LOM. UAM uses ultrasonic seam-welding to bind the sheets or ribbons of metal and is assisted with further machining by CNC to remove extra unbound sheets to finish the part. Thus, UAM employs the processes of ultrasonic seam-welding and CNC milling combined together, for the fabrication of 3D printed parts by lamination process (Li et al. 2017). The unique feature of the UAM process is its ability to bond different metals without the need to melt the metals involving high energy. Instead, this process utilizes ultrasonic frequency and low pressure to bond the sheets together. UAM is the only 3D printing technique, efficient in the building of metal structures at low temperatures (Hahnlen and Dapino 2014; Hehr and

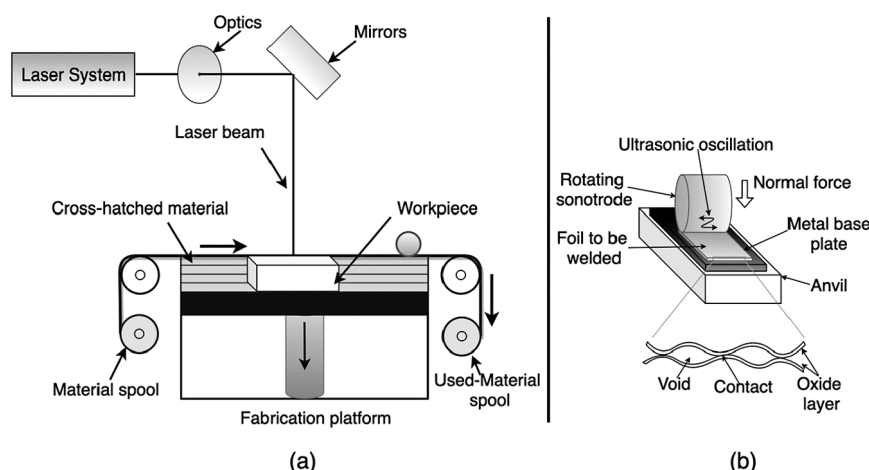


FIGURE 8.8 Schematic diagram of the (a) LOM and (b) UAM technique. (adapted with permission from Li et al. 2017).

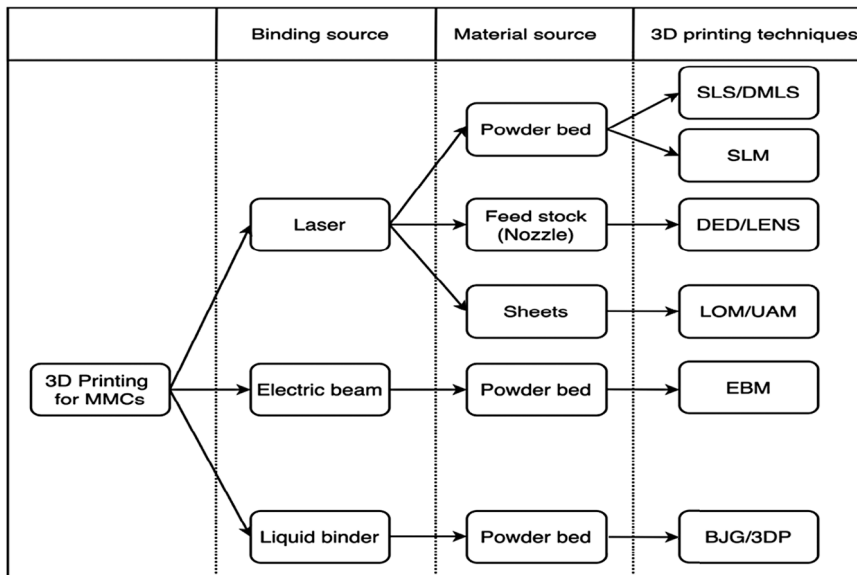


FIGURE 8.9 Summary of 3D printing techniques used for MMCs processing.

Dapino 2015). The use of LOM resulted in considerable savings of manufacturing time, and reduced tool cost, and is thus considered one of the prominent 3D printing techniques for building large components. It has found applications in a number of fields such as foundry industries, electronics, paper manufacturing, and automation. UAM direct write technologies can be used to fabricate smart structures embedded or printed with electronic integrated circuits, sensors, pipes, and other features using UAM for sensing, actuation, and feedback (Gibson et al. 2015a). Nonetheless, LOM-fabricated parts are associated with poorer dimensional accuracy as compared with powder-bed methods and inferior surface quality, which may require post-processing. Also, additional time is required to remove the excess parts of laminates after part fabrication and hence is not recommended for complex shapes.

The summary of various 3D printing techniques used for MMCs processing is shown in Figure 8.9. The selection of any 3D printing techniques depends on energy source/binder, type of material and their feeding mechanism, processing environment, etc., which ultimately affects the quality of fabricated parts.

8.4 MMCs PROCESSING BY 3D PRINTING

The right blend of metal matrix and reinforcement and proper 3D printing technique enables design and development of the applicable MMCs with desirable properties. This section reviewed the work done on some commonly used MMCs and 3D printing techniques used to process these composites to obtain products with desirable properties.

8.4.1 ALUMINUM-BASED COMPOSITES

Aluminum (Al)-based alloys are the most commonly used materials for general applications due to their lighter weight (Hu et al. 2018). But these alloys suffer from low hardness and poor wear characteristics, limiting their use in high-temperature surface engineering applications. These limitations can be addressed and material with improved properties, viz., higher stiffness, lighter weight, corrosion resistance, and better thermal conductivity can be developed by the inclusion of hard precipitates such as TiB_2 , SiC, Al_2O_3 into Al matrix. Al matrix composites have proved their utilization in the automotive, aerospace, and other industries. Aluminum MMCs 6061 reinforced with 25 vol% SiC have been used in aerospace products. 3D printing technology helped produce tailored, fully dense 3D parts by providing processing flexibility and offering uniform distribution of reinforcement with better in-situ reactions between powder layers, resulting in superior mechanical properties (Dadbakhsh and Hao 2012).

Al MMCs are the most explored composites due to their suitability and ease of manufacturing. SLM was explored by Dadbakhsh et al. (2012) to process the mixture of Al and Fe_2O_3 within the Al matrix to produce aluminum matrix composites. The use of inexpensive reinforcement Fe_2O_3 released extra heat that not only helped in consolidation of the composite powders, but also reduced the energy requirement to melt the powders during SLM processing (Dadbakhsh et al. 2012). Chang et al. (2015) used the SLM process to process Al matrix composites with Al_4SiC_4 and SiC as reinforcement and investigated the influence of reinforcement on the in-situ reaction, densification, microstructural, and tribological characteristics of MMCs. It was observed that finer SiC particles enhanced microhardness as well as wear performance due to homogenous microstructure and higher density of end product. Aluminum metal matrix composites reinforced with silicon carbide and/or alumina have exhibited superior properties such as lighter weight, higher strength, better thermal conductivity, enhanced wear resistance, and good stiffness. Ghosh et al. (2010) successfully fabricated Al-4.5Cu-3Mg MMCs, reinforced with various combinations of volume fraction and size of SiC particles by using the DMLS method with optimized processing parameters. The resulted composite developed good bonding between aluminum alloy matrix and SiC particles along with the best density achieved by 300 mesh size particles, whereas optimal microhardness was achieved with 1200 mesh size particles. In another study with the same material under the DMLS process, Ghosh and Saha (2011) discovered that wear resistance decreased with an increase in reinforcement particle size, whereas crack density increased with a particles' volume percentage beyond 15%. Similarly, Manfredi et al. (2014) explored the DMLS process by formulating Al-7Si-0.3Mg MMCs with two ceramic reinforcement particles of nano-sized $MgAl_2O_4$ (1 wt%) and SiC (10 wt%). The different processing parameters were optimized for both reinforcements during DMLS processing. The resultant composite reinforced with SiC showed a 70% increase in hardness, attributed mainly to aluminum carbides formulated due to reaction between well dispersed SiC particles and metal matrix, whereas

composite reinforced with MgAl_2O_4 nanoparticles exhibited an 11% decrease in hardness. The reduction in hardness due to the inclusion of MgAl_2O_4 reinforcement is caused by residual porosity and the non-uniform distribution of reinforcement particles. The SLM method was explored by Han et al. (2017) and it was observed that the addition of 4 vol% Al_2O_3 into Al considerably improves the yield strength and hardness of composite parts. Wang et al. (2018) employed SLM to synthesize $\text{AlSi}_{10}\text{Mg}$ composites reinforced with 0.5 wt% graphene nanoparticles. The inclusion of graphene resulted in increased porosity in addition to the strengthening effect of over 60 MPa. UAM process was used by Li et al. (2017) to fabricate MMC structures featuring embedded printed electrical materials. The interlaminar regions of Al matrices were successfully embedded with conductive and insulating properties to formulate the printed electrical circuit parts with multifunctional capabilities. Yang et al. (2010) applied the UAM for the fabrication of SiC fiber-reinforced Al 3003 MMC. Microstructural studies revealed no chemical reaction between matrix and fiber materials with a clear fiber-matrix interface as desired from UAM. Mechanical testing showed a significant enhancement in tensile strength as well as peel strength, whereas the shear strength of resulting MMCs deteriorates due to the inclusion of fibers.

8.4.2 NICKEL MATRIX COMPOSITES

Nickel (Ni) and Ni based super-alloys exhibited excellent corrosion resistance, fatigue resistance and low thermal expansion, thus are extensively preferred for use in aircraft jet engines, petro-chemical, nuclear energy sector, and turbines. As Ni possessed good ductility and toughness, whereas TiC exhibit high strength, hardness, and brittleness, thus combining TiC or other reinforcement in Ni matrix resulted into a balance MMC composite suitable for high temperature refractory, structural, and surface applications (de Liu et al. 2010). Furthermore, inclusion of graphitic phase in Ni-TiC-C composites acts as lubricant during friction and displays exceptional wear resistance.

The fabrication of Ni MMCs has been studied by a number of researchers using 3D printing techniques. Li et al. (2009) explored the direct laser fabrication (DLF) or DED process to fabricate Ni-TiC MMCs by reinforcing TiC particulates (20, 40, and 60 vol%) in Ni matrix. The results showed a gradual increase in wear-resistance and microhardness with an increase of TiC volume-fraction. EBM was investigated by Liu et al. (2019) to determine microstructure, mechanical, and corrosion properties of EBM-processed WC_p/NiBSi MMCs against traditional plasma transferred arc welding. The results demonstrated as par assessment of these properties by 3D technology were compared with the conventional method of fabrication. LENS 3D printing technology has shown the potential to produce Ni-Ti-C MMCs that combine the high fracture toughness of nickel, the high hardness of TiC, and solid lubrication of graphite by homogeneously distributing TiC and graphite reinforcement inside the Ni matrix in proper proportions to tailor the desirable properties of MMC (Borkar et al. 2014). Gopagni et al. (2011) used LENS 3D printing to laser deposit nickel, titanium, and carbon (graphite) powders

to formulate TiC-reinforced nickel MMC. Further, mechanical and tribological analysis of composite revealed improved hardness and steady-state friction-coefficient over the pure Ni material.

8.4.3 TITANIUM MATRIX COMPOSITES

Titanium (Ti) alloys have established their potential in widespread applications ranging from biomaterials implants to structural products in aerospace, marine and automotive fields owing to outstanding strength to weight ratio, biocompatibility, corrosion resistance, ductility, and formability. However, Ti alloys were deprived of tribological properties, such as surface hardness and wear resistance. These surface properties, along with toughness, can be improved either by surface nitriding or by reinforcement of the soft matrix with hard particles such as titanium nitrides, carbides, borides, etc., resulting in Ti-based MMC.

The feasibility of different 3D printing techniques to fabricate Ti-based MMCs has been investigated by various researchers. SLM was used by Attar et al. (2014) to produce Ti-TiB composites by using milled Ti-TiB₂ powders. The resulting composite showed a substantial improvement in mechanical properties such as compressive yield strength and microhardness as compared to pure-Ti. These improvements can be attributed to α -Ti matrix-led grain refinement, and strengthening, hardening effects caused by TiB particles. Sahasrabudhe et al. (2016) used the LENS 3D printing technique under a nitrogen environment for depositing TiN-Ti coatings on Ti alloys. They discovered a substantial enhancement in surface properties such as hardness and wear-resistance in comparison to pure-Ti substrate along with reduced friction due to surface nitridation. Das et al. (2012) employed the LENS process to deposit MMC coatings of Ti-6Al-4V and hexagonal-boron-nitride (h-BN) powders reinforced with TiB+TiN. It was observed that Young's modulus and surface hardness improved with the increase of BN content. Banerjee et al. (2002) fabricated Ti/TiB MMCs through the LENS process and achieved a fine, homogeneous dispersion of TiB precipitates which helped in enhancing the wear-resistance and other mechanical properties subjected to high temperatures such as creep. DED technique was successfully applied by Shishkovsky et al. (2018) for the fabrication of Ni-Cr-Al inter-metallic MMC structures. The formation of heterogeneous phases and an increase in microhardness was observed in fabricated parts. Farayibi et al. (2019) fabricated Ti-6Al-4V/TiB₂ MMCs by DED printing process. TiB₂ powder was satellited onto Ti-6Al-4V particles by using a modified feedstock in DED. The uniform dispersion and random orientation of eutectic TiB needles were observed inside the Ti-matrix in the microstructure study, which helped in achieving increased hardness in the resultant MMCs. Thus, this advocates the potential of DED to develop parts or coatings with uniform microstructure and customized properties. Murr et al. (2010) used the EBM technique to process titanium aluminide and demonstrated the potential of EBM to fabricate titanium aluminide MMCs directly in near net-shape with complex geometry.

8.4.4 COPPER MATRIX COMPOSITES

Copper (Cu) has been commonly used in applications involving high electrical and thermal conductivity such as electrodes, heat sinks, microchips, electrical switches, microwave magnetrons, etc. However, a dearth of sufficient mechanical and wear resistance properties limits their usage in structural and friction-bearing applications. These properties of Cu can be improved by reinforcing the metal powders with other metals, ceramics, carbon nanotubes, and graphite, etc.

The fabrication of Cu-based MMCs has been explored under the 3D printing domain by using various combinations. Gu and Shen (2006) fabricated Cu MMCs reinforced with tungsten-carbide cobalt (WC-Co) by the DMLS process. DMLS system delivered the metal powder automatically under computer process control, under room temperature in air atmosphere and employed CO₂ laser with continuous-wave signature for heating and sintering of rectangular size specimens of size 50×10×6 mm. It was discovered that a high level of WC-Co reinforcement resulted in agglomeration of the WC particles, whereas a low level was found insufficient to contribute toward structural modification. The 30 wt% of WC-Co content resulted in a homogeneous structure with high product hardness due to appropriate bonding at the matrix-reinforcement interface. Similarly, the DMLS method was used by Gu et al. (2009) to fabricate Cu-alloy MMC reinforced with Ni particles by operating laser with optimized parameters. The resultant MMC solidified with a coherent matrix particles interface made possible due to bonding between completely melted Cu matrix alloy and partially melted Ni particles under high temperature due to laser. The DMLS process sintering helped in achieving a high densification response of 95.2% of theoretical density. Baitimerov and Bykov (2021) successfully processed copper-alumina MMCs with 5% weight of alumina using SLM. The raw Cu powder was produced by gas atomization, whereas alumina powder was processed on an electrostatic filter by condensation. The produced Cu-alumina MMCs showed superior hardness as compared to cast-copper. Sing et al. (2019) successfully fabricated the copper-graphene (Cu-Gn) MMCs with varying concentrations of graphene (0.25, 0.5, 1, and 1.5 wt%) by 3D printing and ultrasonic-assisted pressure-less sintering (UAPS). The processed MMCs exhibited a homogeneous mixture of Cu-particles and graphene, resulting in improved properties such as hardness, wear rate, density, electrical conductivity, coefficient of friction, etc.

8.4.5 IRON MATRIX COMPOSITES

Recently, iron (Fe)-based MMCs have gained considerable attention from researchers due to their low cost and good mechanical properties (Dammak et al. 2014). Gaard et al. (2006) prepared MMC materials of Fe-Ni alloy, reinforced with TiC particles using the DMLS method and analyzed its effect along with material powders on the microstructural, mechanical, and tribological properties. The results showed cracking of specimen due to dissolution of TiC particles

and transition of the matrix phase from FCC to BCC at higher TiC proportions. The low level of TiC upto 30% affected the hardness, bending strength, and wear resistance to a level inferior to conventional manufactured components. Ramesh et al. (2009) used the DMLS technique to produce the Fe MMCs reinforced with Ni-coated SiC particles at optimized parameters for their processing. It was discovered that microhardness and wear resistance improved significantly, whereas density decreased with a high level of SiC content. In another study, Ramesh et al. (2009) concluded that scan speed negatively affects the hardness of printed parts, whereas the coefficient of friction gradually improved with SiC content. Likewise, SLM was explored by Almangour et al. (2016) using 316L stainless-steel reinforced with TiB₂ nanoparticles and discovered that the composite exhibits higher microhardness and yield strengths as compared to unreinforced steel. Also wear rate was significantly reduced at 15 vol% of reinforced particles.

8.4.6 ZINC MATRIX COMPOSITES

Despite zinc (Zn) being a comparatively heavier material than Al, it is used in MMCs because of its liquidity for casting, low liquidus temperature, and comparable mechanical properties with Al. BJJG was explored by Snelling et al. (2017) using zinc alloy as the metal matrix and ceramic as the reinforcing material to fabricate Zn MMCs. The resulted products exhibited reduced strength of the MMCs as compared pure matrix material along with cracks formation in MMC parts. He concluded that the geometrical shape of a part, as well as post-processing methods play a vital role in obtaining a quality product from BJJG 3D printing.

The choice of suitable 3D printing technique to process the MMCs depends upon base metal matrix materials, reinforcement materials, their forms for feeding, processing environment and desirable properties requirement. Table 8.2 summarize commonly used 3D techniques and associated benefits for processing commonly used MMCs.

8.5 APPLICATIONS OF MMCs

3D printing as an AM tool has proved its potential to excel in a range of applications. Its domain is now not limited to high-end products used in the aerospace or automotive industries but has also expanded to other fields like biomedical, electronic, consumer, construction industry, rapid tooling, etc. to deliver customized parts with desirable properties (Pinkerton 2016). This section discusses the usefulness of 3D-printed MMCs in various applied fields.

8.5.1 BIOMEDICAL INDUSTRY

As the biomedical industry requires highly customized parts as per the patient size, variation is in very low quantity, and their production via conventional means is not economical. 3D printing has proven its ability to produce and deliver

TABLE 8.2**Summary of 3D Techniques Used for Processing Commonly Used MMCs and Associated Benefits**

3D Technique	Base Metal Matrix	Reinforcement	Results	References
DMLS	Cu	WC-10%Co	Homogeneous structure with high product hardness due to appropriate bonding at matrix-reinforcement interface at 30 wt% of WC-Co.	(Gu and Shen 2006)
DMLS	Al-7Si-0.3Mg	SiC, MgAl ₂ O ₄	SiC showed 70% increase in hardness whereas composite reinforced with MgAl ₂ O ₄ nanoparticles exhibited 11% decrease in hardness.	(Manfredi et al. 2014)
DMLS	Al-4.5Cu-3Mg	SiC	Wear-resistance decreased with increase of reinforcement particle size whereas crack-density increased with the increase of particles volume beyond 15%.	(Ghosh et al. 2010; Ghosh and Saha 2011)
DMLS	Cu-10Sn, Cu-8.4P	Ni	Sintering helped in achieving part with high densification response of 95.2% of theoretical density.	(Gu et al. 2009)
DMLS	Fe+Ni (Invar36)	TiC	Homogeneous distributions of TiC particles. Thermal cracking and porosity of produced parts at higher TiC content.	(Gaard et al. 2006)
DMLS	Fe	SiC	Increase in micro-hardness, abrasive wear-resistance, and a reduction in density with increased SiC content.	(Ramesh and Srinivas 2009)
SLM	Al	Al ₂ O ₃	Addition of 4 vol% Al ₂ O ₃ considerably improves the yield strength and hardness of composite parts.	(Han et al. 2017)
SLM	Al	Fe ₂ O ₃	Reduced energy requirement to melt the powders during SLM processing due to Fe ₂ O ₃ .	(Dadbakhsh et al. 2012)
SLM	Al	Al ₄ SiC ₄ , SiC	Superior properties such as lighter weight, higher strength, better thermal conductivity, enhanced wear resistance, and good stiffness.	(Chang et al. 2015)
SLM	316L Steel	TiB ₂	Higher microhardness and yield strengths as compared to unreinforced steel. Also wear rate significantly reduced.	(Almangour et al. 2016)

(Continued)

TABLE 8.2 (Continued)

3D Technique	Base Metal Matrix	Reinforcement	Results	References
SLM	AlSi10Mg	Gn	Increased porosity in addition to strengthening effect.	(Wang et al. 2018)
SLM	Ti	TiB	Improvement in compressive yield strength as well as microhardness.	(Attar et al. 2014)
SLM	Cu	Al ₂ O ₃	Increase in hardness, in comparison with pure cast copper.	(Baitimerov and Bykov 2021)
EBM	WC _p	NiBSi	At par assessment mechanical and corrosion properties by printed parts with traditional plasma transferred arc-welding.	(Liu et al. 2019)
BIG	Zn-4Al-0.4Mg	Al ₂ O ₃ , SiO ₂ , MgO	Reduced strength of the MMC as compared pure matrix material and cracks formation in MMC parts.	(Snelling et al. 2017)
DED	Ni	TiC	Gradual increase in wear resistance and microhardness with the increasing of TiC volume fraction	(Li et al. 2009)
DED	Ti and Ni	Me-Al	The formation of heterogeneous phases and increase in microhardness was observed.	(Shishkovsky et al. 2018)
DED	Ti-6Al-4V	TiB ₂	Uniform dispersion and random orientation of eutectic TiB needles helped in achieving increased hardness.	(Farayibi et al. 2019)
DED/LENS	Ni	TiC	Improvement in hardness and steady-state friction coefficient over the pure Ni.	(Gopagni et al. 2011)
DED/LENS	Ti-6Al-4V	BN	Young's modulus and surface hardness increased with the increase of BN content.	(Das et al. 2012)
DED/LENS	Ti	TiB	Fine dispersion of TiB precipitates resulting into enhanced creep and wear resistance properties.	(Banerjee et al. 2002)
UAM	Al	Ti-6Al-4V foil	The conductive and insulating materials were successfully embedded for multifunctional capabilities.	(Li et al. 2017)
UAPS	Cu	Gn	Homogeneous mixing of metal particles and graphene resulting into better mechanical properties.	(Singh and Pandey 2020)
UAM	Al-1.2Mn-0.12Cu	SiC fibers	Improvement in peel strength, tensile strength, and deterioration in the shear strength.	(Yang et al. 2010)

highly customized components to meet demands in tissue engineering and other biomedical applications. It has shown its potential to artificially fabricate a variety of bio-parts ranging from bones, ears, windpipes, eyeglasses, blood vessels, and various tissues and organs. MMCs from 3D printing are currently employed in making artificial joints and limbs as per musco-skeleton requirements (Ho et al. 2015). The BJG process is being used in the pharmaceutical field to 3D print tablets with multi-salts, as well as other drug delivery forms (Trenfield et al. 2018). Despite current biomedical industry share being low, the contribution by 3D printing to the biomedical field is expected to grow by 21% before 2030 (Schubert et al. 2014).

8.5.2 AEROSPACE INDUSTRY

The primary requirement in the aerospace industry is complex geometrical shapes with lightweight structure and good mechanical properties. This suits MMC with 3D printing, as it is a very effective method to produce the parts required by aircraft and spacecraft companies (Singamneni et al. 2019). Also, aerospace engineering generally required parts in small lot size, which are not justified by conventional tooling and can be economically produced by 3D printing technologies (Wong and Hernandez 2012). The commonly used 3D printing technologies for the aerospace industry includes SLS, SLM, EBM, and DED (Dey 2014). Thus, 3D printing has been effectively employed for the production of complicated shapes with lightweight structures, low quantity, specialized parts, on-demand parts, as well as the repair and replacement of jet engine turbines, rotor-vanes, plates, aircraft wings, fuselage, and other structural parts (Manfredi et al. 2014). In 2015, the market size for composite materials was \$68.1 billion globally in all sectors and \$11.5 billion in the aerospace sector alone across the world. The global market of composite materials is growing, with a compound annual growth rate (CAGR) of 6.5% overall and with CAGR 9.1% for the aerospace industry, and is expected to be a market of \$105.8 billion and \$24.8 billion, respectively, by 2025. The aviation industry had a share of 16.88% of composite materials in the global market in 2015 and is expected to contribute 23.4% by 2025 (Aerospace Technology Institute (ATI) 2018).

8.5.3 AUTOMOTIVE INDUSTRY

3D printing has found many applications in the automotive industry (Ghosh et al. 2010; Frazier 2014). The applications of metallic composite parts include special tooling for injection molding, die-casting, prototype building, and patterns for casting (Gu et al. 2009). Among the reinforcement, SiC-based MMCs parts are nowadays extensively being used in several automotive components, ranging from cylinder liners to brake drums in automobiles (Manfredi et al.

2014). Toyota has used aluminum MMCs reinforced with fibers for their diesel engine piston (Mussatto et al. 2021). 3D printing enables the parts production to be in-house as per demand, thus permitting low size inventory, and reduced materials and shipping costs. This will help keep the automotive dealers equipped with updated parts as per demand and be able to reduce the associated expanses related with inventory (Beyer 2014). Also, 3D printing with MMCs has the ability to produce complex geometrical shapes with reduced weight while maintaining strength by optimizing the contour profiles, thus making it extremely beneficial for automotive companies (Biamino et al. 2014; Cooper et al. 2015).

8.5.4 CONSTRUCTION INDUSTRY

In recent times, 3D printing has gained growing interest in the construction industry as well to reduce overall build-up time. 3D printing has helped in bringing automation to construction processes and can contribute toward reducing laborious work or labor-related problems, construction time, material wastage, risk management for humans, etc. (Hossain et al. 2020).ApisCor in Dubai has constructed an office building with a floor space of 640 square meters and rooms 9.5 meters high. This is on record (at the time of writing) as the biggest 3D-printed building to date, using half the number of workers than the conventional construction method and with 60% less wastage. The 3D printing of related parts was completed on-site within two weeks (Bravo 2020). Comprehensive research is being conducted for using 3D-printed MMCs structure for large-scale adoption of 3D printing in construction projects.

8.5.5 PERSONALIZED ITEM INDUSTRY

The artistic need to generate new design, shapes, and profiles to give uniqueness to a product has provided the opportunity for 3D printing to excel in consumer-driven personalized item industry. The essence of freeform design in CAD and latter fabrication by 3D printing has realized the designs, which were practically impossible to produce using conventional methods. This capability has been well utilized by the jewelry and watch-making industries working on precious metals as per customer demand. Also, the development in 3D printing technologies has resulted in the availability of 3D machines, which are small in size, less expensive, and require less controlling parameters as compared to those used in the aerospace or automotive industries (Milewski 2017).

There is no doubt that the potentials applications of 3D printing will increase tremendously in the coming future, expanding their base and acceptability. Table 8.3 summarizes the key attributes of integrating 3D printing and its associated benefits.

TABLE 8.3

**Key Attributes of Integrating 3D Printing within any Industry
(Redrawn from Singamneni et al. 2019)**

3D Printing Capabilities	Advantages	Applied Benefits	Results
Complex geometry	Optimization	Functionality, structure, lightweight	Performance, Fuel efficiency
	Part consolidation	Lightweight, reduce part counts	Fuel efficiency, Improve supply-chain
	Design flexibility	JIT production and repair	Improve supply-chain
Mixed materials	Customization	Product acceptance	Brand loyalty
Agile manufacturing	Tailored properties	Functionality	Performance
Process and energy efficiency, repair	Only need CAD, no tooling required	JIT production and repair	Improve supply-chain
	Easy deployment	Localized production	
	Low cost	Operating benefits	Sustainability

8.6 CHALLENGES

Since the inception of 3D printing technology about three decades, it is still considered in the infant stage. Despite a lot of potential for 3D printing MMCs in various sectors, there are some issues that need to be addressed before wide acceptance as a reliable technique to compete with conventional manufacturing methods. Presently, 3D printing is limited to selected applications and products only by a few 3D printing techniques. Some deficiencies such as limited 3D-printing-compatible materials, excessive machine set-up time, part size limitations, inadequate surface finish, low production rate, post-processing requirements, quality control, thermal cracks, and de-bonding of reinforcements have been observed while processing MMCs by 3D printing (Ramesh et al. 2009; Kim et al. 2015). Moreover, the difficulty in predicting desirable properties, dearth of fully dense parts, and non-isotropic behavior of fabricated parts have limited their acceptance at large. The companies dealing with 3D printing required multi-functional and high-performance materials, increased scale of production, larger build envelopes for parts and affordable production (Tibbits 2014). The aviation industries required parts with an accuracy level up to 10 µm but the current 3D techniques can provide accuracy of 30–40 µm only, thus necessitating the need for post-processing of parts.

Among the various production methods currently preferred for MMCs, powder metallurgy and casting have appeared to be among the leaders in 3D printing. The cost of production plays a significant role in deciding the production method, energy consumption to produce per unit mass, as well as production volume. Powder metallurgy uses the lowest energy to produce unit mass and offers the

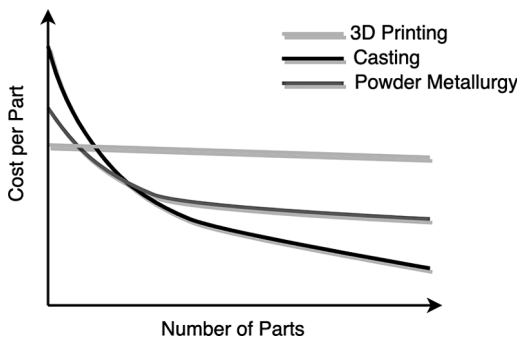


FIGURE 8.10 Cost per volume associated with different MMCs fabrication techniques. (redrawn from Mussatto et al. 2021).

highest raw material utilization, whereas in casting, the energy requirement is proportional to the mass used for melting (Mussatto et al. 2021). On the contrary, 3D printing consumes the highest energy to fabricate the parts with laser or beam, heaters, motors, pumps, computers, and some energy losses are among the major energy contributors. Thus, more energy used by 3D printing reduces its economic viability as compared to the other conventional methods. From the production volume point of view, powder metallurgy is the most cost-effective route to simple, small, and non-complex, large quantity (thousands per year) production, whereas casting justifies equipment and operational cost after a threshold production and thus is not economical for small volume production. Here, 3D printing is most suitable to produce small and complex geometry parts in small volume, wherein the costs associated with production volume moreover remain relatively constant with production volume as shown in Figure 8.10. Thus, improvements in technology, along with optimization of parameters associated with MMCs processing, would be required to reduce energy consumption and make 3D printing economically viable.

8.7 FUTURE SCOPES

The advancement of 3D printing technology and high-speed mass production will lead to the gradual decline of the associated costs and it will be more economically feasible to produce 3D printed parts. 3D printing will progressively dominate the markets involving product customization, complex geometrical shape, labor intensive, product assembly requirement, high transportation cost, inventory expenditure, and generate un-utilized wastes. Biomaterial, automotive, aerospace, industrial machinery, construction, and consumer markets have shown their potential for 3D-printed products and can offer lot of savings by offering mass production of products with a product quality comparable to conventional manufacturing methods.

To realize this, a lot of research would be required to optimize the various process parameters associated with 3D printing through research, modeling, and

simulation in combination with suitable materials to compete with the conventional manufacturing methods. Although the use of 3D printing technologies is most suitable to produce parts with a customized property profile as required by niche applications, it is essential for these fabrication methods to be cost-effective for expanding their applications and sustainable growth.

REFERENCES

- Aerospace Technology Institute (ATI) (2018). Composite material applications in aerospace. In *INSIGHT_09 Composite Materials*. <https://doi.org/10.1201/b12265>
- Almangour, B., Grzesiak, D., & Yang, J. M. (2016). Rapid fabrication of bulk-form TiB₂/316L stainless steel nanocomposites with novel reinforcement architecture and improved performance by selective laser melting. *Journal of Alloys and Compounds*, 680, 480–493. <https://doi.org/10.1016/j.jallcom.2016.04.156>
- Ameen, W., Al-Ahmari, A., & Mohammed, M. K. (2019). Self-supporting overhang structures produced by additive manufacturing through electron beam melting. *International Journal of Advanced Manufacturing Technology*, 104(5–8), 2215–2232. <https://doi.org/10.1007/s00170-019-04007-3>
- Ardila, L. C., Garciandia, F., González-Díaz, J. B., Álvarez, P., Echeverria, A., Petite, M. M., Deffley, R., & Ochoa, J. (2014). Effect of IN718 recycled powder reuse on properties of parts manufactured by means of selective laser melting. *Physics Procedia*, 56(C), 99–107. <https://doi.org/10.1016/j.phpro.2014.08.152>
- Attar, H., Bönisch, M., Calin, M., Zhang, L. C., Scudino, S., & Eckert, J. (2014). Selective laser melting of in situ titanium-titanium boride composites: processing, microstructure and mechanical properties. *Acta Materialia*, 76, 13–22. <https://doi.org/10.1016/j.actamat.2014.05.022>
- Baitimerov, R. M., & Bykov, V. A. (2021). Processing of alumina reinforced copper metal matrix composite by selective laser melting technology. *Solid State Phenomena*, 316(April), 175–180. <https://doi.org/doi.org/10.4028/www.scientific.net/SSP.316.175>
- Banerjee, R., Collins, P. C., & Fraser, H. L. (2002). Laser deposition of in situ Ti-TiB composites. *Advanced Engineering Materials*, 4(11), 847–851. [https://doi.org/10.1002/1527-2648\(20021105\)4:11<847::AID-ADEM847>3.0.CO;2-C](https://doi.org/10.1002/1527-2648(20021105)4:11<847::AID-ADEM847>3.0.CO;2-C)
- Beyer, C. (2014). Strategic implications of current trends in additive manufacturing. *Journal of Manufacturing Science and Engineering, Transactions of the ASME*, 136(6), 1–8. <https://doi.org/10.1115/1.4028599>
- Biamino, S., Klöden, B., Weißgärber, T., Kieback, B., & Ackelid, U. (2014). Properties of a TiAl turbocharger wheel produced by electron beam melting. *DDMC 2014 Fraunhofer Direct Digital Manufacturing Conference*, March, 1–4.
- Borkar, T., Sosa, J., Hwang, J. Y., Scharf, T. W., Tiley, J., Fraser, H., & Banerjee, R. (2014). Laser-deposited in situ TiC-reinforced nickel matrix composites: 3D microstructure and tribological properties. *Jom*, 66(6), 935–942. <https://doi.org/10.1007/s11837-014-0907-1>
- Bravo, E. (2020). *An administrative building in Dubai, the largest 3D printed structure in the world*. Available online: <https://www.smartcitylab.com/blog/digital-transformation/largest-3d-printed-building-in-the-world/> (accessed on 13 May 2021).
- Chang, F., Gu, D., Dai, D., & Yuan, P. (2015). Selective laser melting of in-situ Al₄SiC₄ + SiC hybrid reinforced Al matrix composites: Influence of starting SiC particle size. *Surface and Coatings Technology*, 272, 15–24. <https://doi.org/10.1016/j.surfcoat.2015.04.029>

- Cooper, D., Thornby, J., Blundell, N., Henrys, R., Williams, M. A., & Gibbons, G. (2015). Design and manufacture of high performance hollow engine valves by additive layer manufacturing. *Materials and Design*, 69, 44–55. <https://doi.org/10.1016/j.matdes.2014.11.017>
- Dadbakhsh, S. & Hao, L. (2012). In situ formation of particle reinforced Al matrix composite by selective laser melting of Al/Fe₂O₃ powder mixture. *Advanced Engineering Materials*, 14(1–2), 45–48. <https://doi.org/10.1002/adem.201100151>
- Dadbakhsh, S., Hao, L., Jerrard, P. G. E., & Zhang, D. Z. (2012). Experimental investigation on selective laser melting behaviour and processing windows of in situ reacted Al/Fe₂O₃ powder mixture. *Powder Technology*, 231, 112–121. <https://doi.org/10.1016/j.powtec.2012.07.061>
- Dammak, M., Gaspérini, M., & Barbier, D. (2014). Microstructural evolution of iron based metal-matrix composites submitted to simple shear. *Materials Science and Engineering A*, 616, 123–131. <https://doi.org/10.1016/j.msea.2014.08.004>
- Das, M., Balla, V. K., Basu, D., Manna, I., Sampath Kumar, T. S., & Bandyopadhyay, A. (2012). Laser processing of in situ synthesized TiB-TiN-reinforced Ti₆Al₄V alloy coatings. *Scripta Materialia*, 66(8), 578–581. <https://doi.org/10.1016/j.scriptamat.2012.01.010>
- de Liu, Z., Tian, J., Li, B., & Zhao, L. (2010). Microstructure and mechanical behaviors of in situ TiC particulates reinforced Ni matrix composites. *Materials Science and Engineering A*, 527(16–17), 3898–3903. <https://doi.org/10.1016/j.msea.2010.02.061>
- Dey, N. K. (2014). *Additive manufacturing laser deposition of Ti-6Al-4V for aerospace repair application*. Masters Theses, 7295. Available online: https://scholarsmine.mst.edu/masters_theses/7295.
- Farayibi, P. K., Abioye, T. E., Kennedy, A., & Clare, A. T. (2019). Development of metal matrix composites by direct energy deposition of ‘satellited’ powders. *Journal of Manufacturing Processes*, 45, 429–437. <https://doi.org/10.1016/j.jmapro.2019.07.029>
- Frazier, W. E. (2014). Metal additive manufacturing: a review. *Journal of Materials Engineering and Performance*, 23(6), 1917–1928. <https://doi.org/10.1007/s11665-014-0958-z>
- Gaard, A., Krakhmalev, P., & Bergström, J. (2006). Microstructural characterization and wear behavior of (Fe,Ni)-TiC MMC prepared by DMLS. *Journal of Alloys and Compounds*, 421(1–2), 166–171. <https://doi.org/10.1016/j.jallcom.2005.09.084>
- Ghosh, S. K., & Saha, P. (2011). Crack and wear behavior of SiC particulate reinforced aluminium based metal matrix composite fabricated by direct metal laser sintering process. *Materials and Design*, 32(1), 139–145. <https://doi.org/10.1016/j.matdes.2010.06.020>
- Ghosh, S. K., Saha, P., & Kishore, S. (2010). Influence of size and volume fraction of SiC particulates on properties of ex situ reinforced Al-4.5Cu-3Mg metal matrix composite prepared by direct metal laser sintering process. *Materials Science and Engineering A*, 527(18–19), 4694–4701. <https://doi.org/10.1016/j.msea.2010.03.108>
- Gibson, I., Rosen, D., & Stucker, B. (2015a). *Additive Manufacturing Technologies: 3D Printing, Rapid Prototyping, and Direct Digital Manufacturing*, Second Edition, 1991, 1–498. <https://doi.org/10.1007/978-1-4939-2113-3>
- Gibson, I., Rosen, D., & Stucker, B. (2015b). 3D printing, rapid prototyping, and direct digital manufacturing, second edition. In *Additive Manufacturing Technologies*(Second Edition), Elsevier Ltd, 1–498. <https://doi.org/10.1007/978-1-4939-2113-3>
- Gibson, I., Rosen, D. W., & Stucker, B. (2010). Rapid prototyping to direct digital manufacturing. In *Additive Manufacturing Technologies* (First Edition). Elsevier Ltd., 1–473. <https://doi.org/10.1007/978-1-4419-1120-9>.

- Gokuldoss Prashanth, K., Scudino, S., & Eckert, J. (2016). Tensile properties of Al-12Si fabricated via selective laser melting (SLM) at different temperatures. *Technologies*, 4(4), 38. <https://doi.org/10.3390/technologies4040038>
- Gopagoni, S., Hwang, J. Y., Singh, A. R. P., Mensah, B. A., Bunce, N., Tiley, J., Scharf, T. W., & Banerjee, R. (2011). Microstructural evolution in laser deposited nickel-titanium-carbon in situ metal matrix composites. *Journal of Alloys and Compounds*, 509(4), 1255–1260. <https://doi.org/10.1016/j.jallcom.2010.09.208>
- Gu, D., & Shen, Y. (2006). WC-Co particulate reinforcing Cu matrix composites produced by direct laser sintering. *Materials Letters*, 60(29–30), 3664–3668. <https://doi.org/10.1016/j.matlet.2006.03.103>
- Gu, D., Shen, Y., & Lu, Z. (2009). Microstructural characteristics and formation mechanism of direct laser-sintered Cu-based alloys reinforced with Ni particles. *Materials and Design*, 30(6), 2099–2107. <https://doi.org/10.1016/j.matdes.2008.08.036>
- Hahnlen, R., & Dapino, M. J. (2014). NiTi-Al interface strength in ultrasonic additive manufacturing composites. *Composites Part B: Engineering*, 59, 101–108. <https://doi.org/10.1016/j.compositesb.2013.10.024>
- Hale, J. (2012). Boeing 787 from ground up. *Boeing Comercial Aeromagazine*, 9. http://www.boeing.com/commercial/aeromagazine/articles/qtr_4_06/article_04_1.html
- Han, Q., Setchi, R., Lacan, F., Gu, D., & Evans, S. L. (2017). Selective laser melting of advanced Al-Al₂O₃ nanocomposites: simulation, microstructure and mechanical properties. *Materials Science and Engineering A*, 698(May), 162–173. <https://doi.org/10.1016/j.msea.2017.05.061>
- Hehr, A., & Dapino, M. J. (2015). Interfacial shear strength estimates of NiTi-Al matrix composites fabricated via ultrasonic additive manufacturing. *Composites Part B: Engineering*, 77, 199–208. <https://doi.org/10.1016/j.compositesb.2015.03.005>
- Herzog, D., Seyda, V., Wycisk, E., & Emmelmann, C. (2016). Additive manufacturing of metals. *Acta Materialia*, 117, 371–392. <https://doi.org/10.1016/j.actamat.2016.07.019>
- Ho, C. M. B., Ng, S. H., & Yoon, Y. J. (2015). A review on 3D printed bioimplants. *International Journal of Precision Engineering and Manufacturing*, 16(5), 1035–1046. <https://doi.org/10.1007/s12541-015-0134-x>
- Hong, C., Gu, D., Dai, D., Alkhayat, M., Urban, W., Yuan, P., Cao, S., Gasser, A., Weisheit, A., Kelbassa, I., Zhong, M., & Poprawe, R. (2015). Laser additive manufacturing of ultrafine TiC particle reinforced Inconel 625 based composite parts: tailored microstructures and enhanced performance. *Materials Science and Engineering A*, 635, 118–128. <https://doi.org/10.1016/j.msea.2015.03.043>
- Hossain, M. A., Zhumabekova, A., Paul, S. C., & Kim, J. R. (2020). A review of 3D printing in construction and its impact on the labor market. *Sustainability (Switzerland)*, 12(20), 1–21. <https://doi.org/10.3390/su122008492>
- Hu, Z., Chen, F., Xu, J., Nian, Q., Lin, D., Chen, C., Zhu, X., Chen, Y., & Zhang, M. (2018). 3D printing graphene-aluminum nanocomposites. *Journal of Alloys and Compounds*, 746, 269–276. <https://doi.org/10.1016/j.jallcom.2018.02.272>
- Jiao, L., Chua, Z. Y., Moon, S. K., Song, J., Bi, G., & Zheng, H. (2018). Femtosecond laser produced hydrophobic hierarchical structures on additive manufacturing parts. *Nanomaterials*, 8(8). <https://doi.org/10.3390/nano8080601>
- Kim, D. B., Witherell, P., Lipman, R., & Feng, S. C. (2015). Streamlining the additive manufacturing digital spectrum: a systems approach. *Additive Manufacturing*, 5, 20–30. <https://doi.org/10.1016/j.addma.2014.10.004>
- Laakso, P., Riipinen, T., Laukkanen, A., Andersson, T., Jokinen, A., Revuelta, A., & Ruusuvuori, K. (2016). Optimization and simulation of SLM process for high density H13 tool steel parts. *Physics Procedia*, 83, 26–35. <https://doi.org/10.1016/j.phpro.2016.08.004>

- Li, J., Monaghan, T., Nguyen, T. T., Kay, R. W., Friel, R. J., & Harris, R. A. (2017). Multifunctional metal matrix composites with embedded printed electrical materials fabricated by ultrasonic additive manufacturing. *Composites Part B: Engineering*, 113, 342–354. <https://doi.org/10.1016/j.compositesb.2017.01.013>
- Li, Y., Bai, P., Wang, Y., Hu, J., & Guo, Z. (2009). Effect of TiC content on Ni/TiC composites by direct laser fabrication. *Materials and Design*, 30(4), 1409–1412. <https://doi.org/10.1016/j.matdes.2008.06.046>
- Liu, C., Peng, H., Zhao, Y., Yuan, Y., Guo, H. B., & Xu, H. B. (2019). Microstructure, mechanical and corrosion properties of electron-beam-melted and plasma-transferred arc-welded WCP/NiBSi metal matrix composites. *Rare Metals*, 38(9), 814–823. <https://doi.org/10.1007/s12598-018-1096-9>
- Lores, A., Azurmendi, N., Agote, I., & Zuza, E. (2019). A review on recent developments in binder jetting metal additive manufacturing: materials and process characteristics. *Powder Metallurgy*, 62(5), 267–296. <https://doi.org/10.1080/00325899.2019.1669299>
- Manfredi, D., Calignano, F., Krishnan, M., Canali, R., Ambrosio, E. P., Biamino, S., Ugues, D., Pavese, M., & Fino, P. (2014). Additive manufacturing of Al alloys and Aluminium Matrix Composites (AMCs). *Light Metal Alloys Applications*, 3–34. <https://doi.org/10.5772/57069>
- Milewski, J. O. (2017). Additive manufacturing of metals. In *NDT in Progress 2017 - 9th International Workshop NDT in Progress, Proceedings* (Vols. 2017-Octob).
- Mistry, J. M., & Gohil, P. P. (2018). Research review of diversified reinforcement on aluminum metal matrix composites: Fabrication processes and mechanical characterization. *Science and Engineering of Composite Materials*, 25(4), 633–647. <https://doi.org/10.1515/secm-2016-0278>
- Murr, L. E., Gaytan, S. M., Ceylan, A., Martinez, E., Martinez, J. L., Hernandez, D. H., Machado, B. I., Ramirez, D. A., Medina, F., Collins, S., & Wicker, R. B. (2010). Characterization of titanium aluminide alloy components fabricated by additive manufacturing using electron beam melting. *Acta Materialia*, 58(5), 1887–1894. <https://doi.org/10.1016/j.actamat.2009.11.032>
- Mussatto, A., Ahad, I. U., Mousavian, R. T., Delaure, Y., & Brabazon, D. (2021). Advanced production routes for metal matrix composites. *Engineering Reports*, 3(5), 1–25. <https://doi.org/10.1002/eng2.12330>
- Nandy, J., Sarangi, H., & Sahoo, S. (2019). A review on direct metal laser sintering: process features and microstructure modeling. In *Lasers in Manufacturing and Materials Processing* (Vol. 6, Issue 3). <https://doi.org/10.1007/s40516-019-00094-y>
- Ngo, T. D., Kashani, A., Imbalzano, G., Nguyen, K. T. Q., & Hui, D. (2018). Additive manufacturing (3D printing): a review of materials, methods, applications and challenges. *Composites Part B: Engineering*, 143, 172–196. <https://doi.org/10.1016/j.compositesb.2018.02.012>
- Pinkerton, A. J. (2016). Lasers in additive manufacturing. *Optics and Laser Technology*, 78, 25–32. <https://doi.org/10.1016/j.optlastec.2015.09.025>
- Prashanth, K. G., Shakur Shahabi, H., Attar, H., Srivastava, V. C., Ellendt, N., Uhlenwinkel, V., Eckert, J., & Scudino, S. (2015). Production of high strength Al₈₅ Nd 8 Ni 5 Co 2 alloy by selective laser melting. *Additive Manufacturing*, 6, 1–5. <https://doi.org/10.1016/j.addma.2015.01.001>
- Ramanathan, A., Krishnan, P. K., & Muraliraja, R. (2019). A review on the production of metal matrix composites through stir casting – furnace design, properties, challenges, and research opportunities. *Journal of Manufacturing Processes*, 42, 213–245. <https://doi.org/10.1016/j.jmapro.2019.04.017>
- Ramesh, C. S., & Srinivas, C. K. (2009). Friction and wear behavior of laser-sintered iron-silicon carbide composites. *Journal of Materials Processing Technology*, 209(14), 5429–5436. <https://doi.org/10.1016/j.jmatprotec.2009.04.018>

- Ramesh, C. S., Srinivas, C. K., & Channabasappa, B. H. (2009). Abrasive wear behaviour of laser sintered iron-SiC composites. *Wear*, 267(11), 1777–1783. <https://doi.org/10.1016/j.wear.2008.12.026>
- Sahasrabudhe, H., Soderlind, J., & Bandyopadhyay, A. (2016). Laser processing of in situ TiN/Ti composite coating on titanium. *Journal of the Mechanical Behavior of Biomedical Materials*, 53, 239–249. <https://doi.org/10.1016/j.jmbbm.2015.08.013>
- Schubert, C., Van Langeveld, M. C., & Donoso, L. A. (2014). Innovations in 3D printing: a 3D overview from optics to organs. *British Journal of Ophthalmology*, 98(2), 159–161. <https://doi.org/10.1136/bjophthalmol-2013-304446>
- Shi, J., & Wang, Y. (2020). Development of metal matrix composites by laser-assisted additive manufacturing technologies: a review. *Journal of Materials Science*, 55(23), 9883–9917. <https://doi.org/10.1007/s10853-020-04730-3>
- Shishkovsky, I., Missemmer, F., & Smurov, I. (2018). Metal matrix composites with ternary intermetallic inclusions fabricated by laser direct energy deposition. *Composite Structures*, 183(1), 663–670. <https://doi.org/10.1016/j.compstruct.2017.09.004>
- Sing, S. L., Tey, C. F., Tan, J. H. K., Huang, S., & Yeong, W. Y. (2019). 3D printing of metals in rapid prototyping of biomaterials: Techniques in additive manufacturing. In *Rapid Prototyping of Biomaterials: Techniques in Additive Manufacturing* (Second Edition). Elsevier Ltd. <https://doi.org/10.1016/B978-0-08-102663-2.00002-2>
- Singamneni, S., Yifan, L. V., Hewitt, A., Chalk, R., Thomas, W., & Jordison, D. (2019). Additive manufacturing for the aircraft industry: a review. *Journal of Aeronautics & Aerospace Engineering*, 8(1). <https://doi.org/10.35248/2168-9792.19.8.215>
- Singh, G., & Pandey, P. M. (2020). Rapid manufacturing of copper-graphene composites using a novel rapid tooling technique. *Rapid Prototyping Journal*, 26(4), 765–776. <https://doi.org/10.1108/RPJ-10-2019-0258>
- Snelling, D. A., Williams, C. B., Suchicital, C. T. A., & Druschitz, A. P. (2017). Binder jetting advanced ceramics for metal-ceramic composite structures. *International Journal of Advanced Manufacturing Technology*, 92(1–4), 531–545. <https://doi.org/10.1007/s00170-017-0139-y>
- Tibbits, S. (2014). 4D printing: multi-material shape change. *Architectural Design*, 84(1), 116–121. <https://doi.org/10.1002/ad.1710>
- Trenfield, S. J., Madla, C. M., Basit, A. W., & Gaisford, S. (2018). Binder jet printing in pharmaceutical manufacturing. *AAPS Advances in the Pharmaceutical Sciences Series*, 31, 41–54. https://doi.org/10.1007/978-3-319-90755-0_3
- Utela, B., Storti, D., Anderson, R., & Ganter, M. (2008). A review of process development steps for new material systems in three dimensional printing (3DP). *Journal of Manufacturing Processes*, 10(2), 96–104. <https://doi.org/10.1016/j.jmapro.2009.03.002>
- Wang, Y., Shi, J., Lu, S., & Xiao, W. (2018). Investigation of porosity and mechanical properties of graphene nanoplatelets-reinforced AlSi10 Mg by selective laser melting. *Journal of Micro and Nano-Manufacturing*, 6(1). <https://doi.org/10.1115/1.4038454>
- Wohlers, T., & Caffrey, T. (2021). *Wohlers Report 2021-3D Printing and Additive Manufacturing State of the Industry*. Wohlers Associates. <https://wohlersassociates.com/press83.html>
- Wong, K. V., & Hernandez, A. (2012). A review of additive manufacturing. *ISRN Mechanical Engineering*, 2012, 1–10. <https://doi.org/10.5402/2012/208760>
- Yang, Y., Stucker, B. E., & Janaki Ram, G. D. (2010). Mechanical properties and microstructures of SiC fiber-reinforced metal matrix composites made using ultrasonic consolidation. *Journal of Composite Materials*, 44(26), 3179–3194. <https://doi.org/10.1177/0021998310371528>

9 Conventional and 3D Printing Technology for the Manufacturing of Metal-Matrix Composite *A Study*

Rakesh Kumar

Department of Regulatory Affairs Auxein Medical Private Limited, Sonipat, India

Santosh Kumar

Department of Mechanical Engineering, Chandigarh Group of Colleges, Landran, Mohali, India

Mohit Kumar and Gaurav Luthra

Department of Regulatory Affairs, Auxein Medical Private Limited, Sonipat, India

CONTENTS

9.1	Summary	198
9.2	Introduction.....	198
9.2.1	What are MMCs?.....	199
9.2.1.1	Classification of Composites.....	200
9.2.1.2	Comparison of Metal Matrix Composites (MMCs) with Polymer Matrix Composites (PMCs) and Ceramic Matrix Composites (CMCs).....	203
9.2.1.3	Models for the Determination of Behavior and Properties of MMCs.....	203
9.2.2	Fabrication of MMCs Using Convention Methods.....	203
9.2.2.1	Solid State Processing.....	204
9.2.2.2	Liquid State Processing.....	206
9.2.2.3	In-situ MMCs Processing	210

9.2.3	Critical Issues Using MMCs.....	210
9.2.4	Fabrication by Using 3D Printing.....	210
9.2.4.1	Fusion Deposition Modeling (FDM)	211
9.2.4.2	Stereo Lithography (SLA)	212
9.2.4.3	Ink Jet Printing (IJP)	213
9.2.4.4	Selective Laser-Sintering (SLS).....	214
9.2.4.5	Selective Laser Melting (SLM).....	214
9.2.4.6	Electron Beam Melting (EBM).....	215
9.2.5	Process Capability Analysis of a 3D Printing Process.....	216
9.2.6	Conclusion	217
9.2.7	Future Scope and Challenges of MMCs Fabrication Using 3D Printing	217
	References.....	218

9.1 SUMMARY

Metal matrix composites (MMCs) usually consist of a low-density metal in which one or more materials are added to a metal to achieve specific property enhancements for a particular application. The fabrication of MMCs involves various traditional methods such as solid state processing, liquid state processing, and in-situ MMCs processing. However, there are some critical issues with conventional MMCs' processing routes, such as limited shape and feature, no complex shape, non-uniform distribution, limited part size, etc. To overcome these issues, 3D printing manufacturing techniques are identified as better alternatives for processing MMCs. This process allows the customization of each component, components with internal structures, and fabrication of components in small production runs at a very low cost. In addition, the layer-by-layer additive material consolidation eliminates the need for complex intermediate tooling and reduces manufacturing lead times, producing more complex shapes with the freedom to design.

9.2 INTRODUCTION

Metal matrix composites (MMCs) are high-performance lightweight materials with higher wear resistance and superior mechanical properties. These materials are made of two or more than two materials that are very cumbersome to obtain from a single material. In these material combinations, one works as a reinforcement and the other is a matrix. The reinforcement can be a discontinuous or continuous type and is utilized to alter the physical characteristics (thermal conductivity, resistance against wear, friction coefficient, etc.) (Callister 2001). The matrix is a monolithic and completely continuous material that distributes the stress utilized over it to the reinforcement constituents. It is a lightweight metal (Ti, Al, etc.) that exhibits a flexible base for reinforcement in structural use. Marsh, G. reported that currently the automobile industry is facing pressure to develop pollution-free and fuel-efficient motor vehicles. So, the industry has switched

over to fiber-reinforced composites from costlier alloy materials to make its items lightweight and eco-friendly. The composition materials (composite material) are made from two (or more than two) combining materials and matrix of (Mg, Al, etc.), and are the principally accepted material for composites – although for high-temperature applications, Ti is also used as a matrix (Marsh 2003). Some authors reported that metal matrix composites provide many attractive advantages (higher strength, high stiffness, good wear resistance, and lightweight properties) over monolithic materials (Surappa 2003; Matthews and Rawlings 1994; Waku and Nagasawa 1994). Despite these, the toughness of MMCs is inferior as compared to monolithic metals and high cost. Conventional monolithic materials have drawbacks in attaining good combination of toughness, stiffness, strength, and density. To compensate these difficulties and to fulfill the increasing demand of present-day technology, composites are most encouraging materials of recent interest. Generally, MMCs give significantly enhanced properties such as high strength and high specific and better resistance against wear than to unreinforced alloys.

9.2.1 WHAT ARE MMCs?

Metal matrix composites (MMCs) are lightweight structural materials mostly used in spacecraft, helicopters, etc. The matrix of MMCs is generally a low-density metal alloy. For high-temperature applications, Ni super alloy is used as the matrix phase in metal matrix composites. The applications of metal oxide or ceramics in the form of whiskers, continuous fibers, or particles help to strengthen the metal matrix phase. Silicon carbide, boron and carbon are generally used as continuous fiber reinforcement whereas; boron carbide, Silicon carbide and alumina are particle reinforcements. In MMCs the reinforcement maximum volume content is usually <30%, which is lesser compared to the timbre content in the case of aerospace carbon epoxy composites (up to 65%) (Kang and Kang 2006). The processing difficulties, material removal, and shaping of metal matrix composite developed low ductility and more hardness, hence reinforcement content of >30% is not preferred (Shirvanimoghaddam et al. 2017).

In the 1970s, composite materials were called the materials of the future when they were first introduced in distinct engineering applications. These innovative materials help to meet the demand of specific designs, as well as function. Composites are generally made of two or more materials (metals, reinforced plastics, and ceramics). The reinforcements may be in particles, fibers, whiskers, or lamellae form. The composite is also called hybrid composite when a minimum of three materials are present. Typically, the characteristics of a composite are good to those of its individual constituents owing to light in weight, better resistance against wear, high value of modulus of elasticity, high electrical and thermal properties, cast able, high strength to wt. ratio, etc. The distribution, shape, type, position reinforcement arrangement, and size will influence the anisotropy and properties of the composite material (Kumar and Kumar 2018a, 2018b).

9.2.1.1 Classification of Composites

(a) On the basis of matrix materials and their structure

The composites are grouped into distinct categories, as illustrated in Figure 9.1 (Callister Jr and Rethwisch 2012; Kumar and Kumar 2018a).

Metal Matrix Composites: A composite material with minimum of two constituent components, one being a metal. The other material may be a distinct metal or another material ceramic (organic or compound). This composite is extensively used in engineering applications in the temperature range of 250°C to 750°C. The selection of matrix can be done on the basis of corrosion resistance, oxidation, or other characteristics (Taya and Arsenault 1989). Generally, the materials such as Ti, Mg, Cu, Fe, Al, Ni, Pb, Ag, Sn, Si and Zn are used as the matrix material. However, Mg, Ti, Al, etc. are mostly used. The continually increasing requirement for high thermal resistance, strength, and wear resistance etc. has driven the search for new materials. MMCs have combined the metallic characteristics of matrix alloys (high toughness and ductility) with the ceramic characteristics of reinforcements of superior modulus and strength dominant to more strength compression, in shear and higher service temperature capabilities. Metal matrix composites are attaining importance because of their attractive properties (lightweight, fire resistance, better specific strength, no moisture absorption; wear resistance, good radiation resistance, resistance against corrosion and high elastic modulus, etc.). The demerits of MMCs over PMC sand monolithic metals are the higher cost of material, and complicated fabrication techniques for fiber-reinforced systems (except for casting) (Sankhla 2015; Bedi et al. 2019). Depending upon the reinforcement type or material structure and shape of metal matrix composites, it can be subdivided as fiber-reinforced, particle reinforced, and layer composite. However, processing methods are decided according to the reinforcement shape, composite shape, and matrix material (Clyne and Withers 1993).

Polymer Matrix Composites (PMCs): Polymer is a large molecule consisting of repeating structural units generally connected by covalent chemical bonds, e.g.,

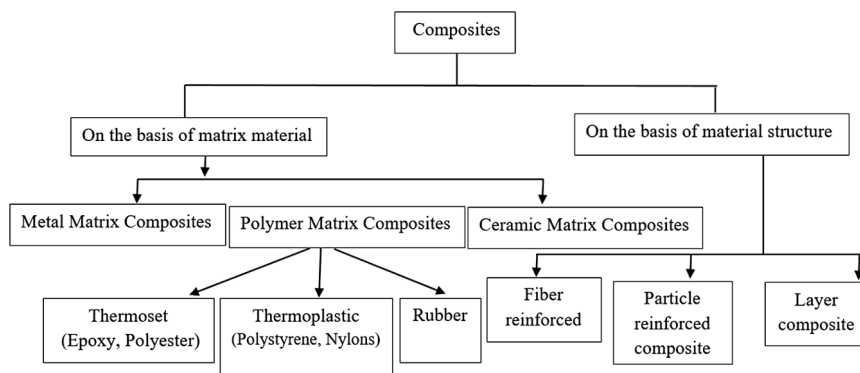


FIGURE 9.1 Classification of composites material.

polyethylene, polypropylene, polyvinyl chloride, etc. Polymers are classified into four distinct categories such as linear polymer, thermosetting polymers, elastomers, and thermoplastic polymers. Among all thermosetting resins, polymer is extensively used in PMCs, because of its light weight, creep resistance, high thermal, insulating properties, and high rigidity etc. PMCs are composed of a polymer matrix composed of a fibrous reinforcing dispersed phase. These composites are very famous owing to their simplicity, cost-effectiveness (fabrication and raw material cost), more stiffness and higher specific tensile strength properties (McDaniels et al. 1986; Lee and Mykkanen 1987). Ceramics matrix composites (CMCs) are solid ceramics that can be characterized as solid materials, which indicate strong ionic bonding and covalent bonding. CMCs are materials that exhibit physically or chemically different phases in great proportion greater than 5% dispersed in continuous matrix. These types of composites are extensively used in the aerospace and energy sectors. These applications require either temporary or permanent joint between CMC parts and surrounding materials (Razzell et al. 2016). They possess the following merits, such as high resistance against corrosion, greater compressive strength, stability at high temperatures, high melting point, etc. This type of composite is largely used in engineering applications in the temperature range of 800°C to 1650°C. Depending upon the material structure, composites are classified into three major groups, namely fiber-reinforced, particle-reinforced, and layer composite. Fiber-reinforced polymer is a composite material made up of fibers with polymer matrix reinforced. Generally, fibers are glass, aramid, or carbon, although other fibers (wood, asbestos, or paper) have been sometimes used (Erden and Ho 2017).

The condition of fiber-reinforced metal matrix composite greatly depends upon on the following:

- (i) Fiber position
- (ii) Fibers' aspect ratio
- (iii) Mechanical strength of matrix and fibers, etc. The fiber-reinforced composites (FRCs) have several advantages compared to particle-reinforced. Due to the flaw propagation, most of the high-stiffness and high-strength materials fail. These reinforced MMCs can be easily fabricated by either the vortex, compo, or squeeze casting method. Among all casting methods, the squeeze casting technique is greatly compatible for a distinct volume of fibers and matrix reinforcement combinations (Seshan et al. 1996). FRCs are stiff and strong but lack ductile fibers and can be integrated into a more ductile and softer matrix. This provides a good strength-to-weight ratio and enhances the other mechanical characteristics. Although, in particle-reinforced composites (PRCs) the microstructure of ceramics composites and metal which exhibit particles of one phase are strewn in the other. PRCs are less useful in terms of strengthening as compared to fiber reinforcement. These composites gain in stiffness primarily, but also can achieve enhancement in toughness and strength. The particle-matrix interaction is considered at the macroscopic level (1–50 µm particle size). PRCs materials are extensively used because of their low cost and ease of availability. Based on strengthening mechanism

and reinforcement, PRCs are subdivided into two groups known as large particle composites or particulate-reinforced and dispersion-strengthened. The dispersion-strengthened composite consists of dislocated interactions between the matrix and the particles. In addition, the particle size lies in the range of 0.01–0.1 μm , which is much smaller, although particulate-reinforced composites have comparatively coarse particles in greater amounts. Concrete is a large-particle composite, consisting of cement, gravel (particulates for reinforcement), and sand (Ahmed and Jones 1990).

Laminar/layer composites are constructed in several combinations of a number of materials. It is characterized as materials consisting of layers of materials bonded together. These may be two (or more than two) metal materials arising alternately (Skorokhod 2003).

(b) Classification of composites on the basis of reinforcement

Reinforcement is also called the reinforcing phase owing to the stronger phase as compared to the matrix. The major properties of reinforcement include: high elastic modulus; high compression strength; good mechanical compatibility; superior tensile strength; and high processing ability. There are distinct categories of reinforcement; among these, reinforcement of the continuous and aligned fibers is the most extensively used for high-performance applications (Chawla 2012). However, according to the reinforcement phases, the composites are categorized into the following distinct types as given in Figure 9.2.

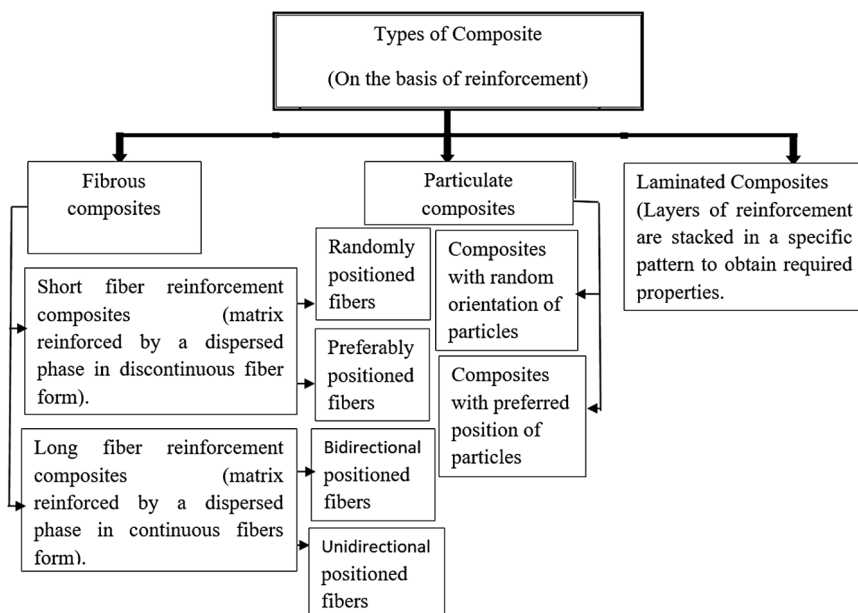


FIGURE 9.2 Classification of composites according to reinforcement phases (Singh et al. 2014).

9.2.1.2 Comparison of Metal Matrix Composites (MMCs) with Polymer Matrix Composites (PMCs) and Ceramic Matrix Composites (CMCs)

The comparison of MMCs, PMCs and CMCs are shown in Table 9.1.

TABLE 9.1

Comparison Study of Distinct Composites Processing Techniques and their Properties (Chawla 2012; Singh et al. 2014)

Properties/ Parameters	MMCs	PMCs	CMCs
Fabrication techniques	<ul style="list-style-type: none"> ➢ Powder metallurgy ➢ Foil deposition bonding ➢ Squeeze casting ➢ Stir casting ➢ Spray deposition ➢ Physical Vapor 	<ul style="list-style-type: none"> ➢ Injection molding ➢ Pultrusion ➢ Thermal forming ➢ Sheet molding 	<ul style="list-style-type: none"> ➢ Chemical vapor infiltration ➢ Cold processing and sintering ➢ Polymer infiltration and pyrolysis ➢ Reactive liquid Infiltration
Density (ρ)	Low	Moderate	Moderate
Young's modulus (Y)	Moderate	High	High
Cost	Low	Moderate	High
Fabrication	Easy	Complicated	Moderate
Tensile strength (P_t)	Very high	High	Moderate
Fatigue strength	High	Moderate	Low

9.2.1.3 Models for the Determination of Behavior and Properties of MMCs

There are distinct types of analytical models that comprises: the Eshelby model, self-consistent model, unit-cell models, composite cylinder model, etc. (Aghdam et al. 2000). These models can be utilized to determine the properties as well as behavior of MMCs, as shown in Figure 9.3.

9.2.2 FABRICATION OF MMCs USING CONVENTION METHODS

In the last ten years, new fabrication techniques of metal matrix composites have been developed. It is the primary processing way of its production which enhanced the processing leads to a near net shape composite part in an economic manner. Despite these distinct methods being available for the fabrication of MMCs, there is no independence in this respect. These methods mainly depend upon the selection of reinforcement and matrix materials. The main threat in the processing of composites is to uniformly distribute the reinforcement stages to attain a defect-free microstructure. MMCs are manufactured by using one of the following three methods – solid state, liquid state, and in-situ manufacturing – as given in Figure 9.4 (Ramu and Bauri 2009; Sahu and Banchhor 2016).

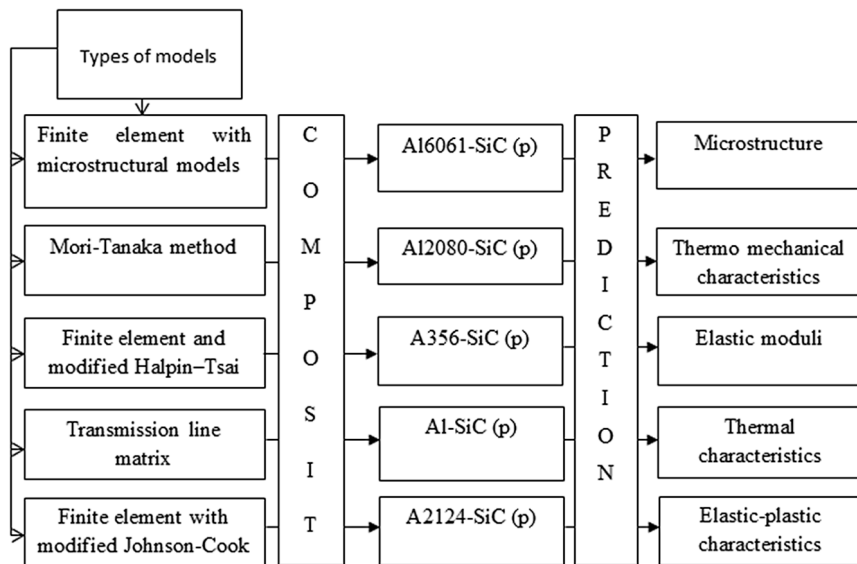


FIGURE 9.3 Distinct types of models and theories that have been used to determine the behavior and properties of MMCs (Shoukry et al. 2007; Hua and Gu 2013; Alfonso et al. 2016; Hocine et al. 2013; York Duran et al. 2017).

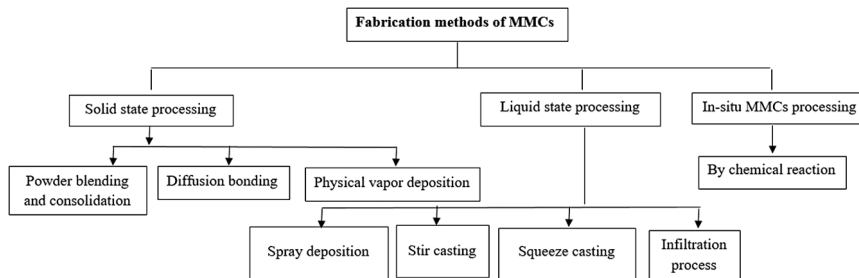


FIGURE 9.4 Fabrication methods of MMCs.

9.2.2.1 Solid State Processing

The primary fabrication techniques for solid state processing of MMCs are as below:

9.2.2.1.1 Powder Mixing and Consolidation

This is one of the important methods used for the fabrication of MMCs. Powder metallurgy (P/M) is capable of manufacturing high-strength Al alloys and reinforced nanoparticles. In this fabrication method, the blend of reinforcement and powdered matrix material are supplied into a mold of the desired shape and

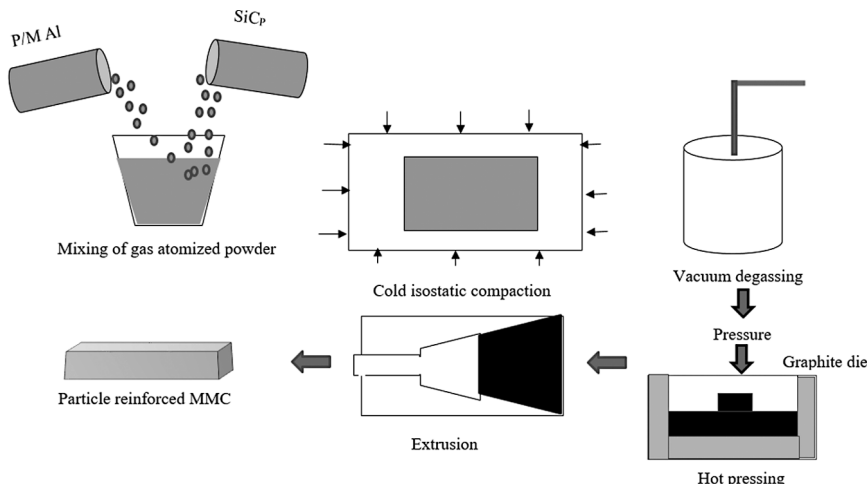


FIGURE 9.5 Schematic illustration of powder metallurgy processing method (Borgonovo and Apelian 2011).

compressed under high pressure, a process also known as cold pressing. After that, the compact is heated at an evaluated temperature to generate solid state diffusion to develop the bonding in the powdered particles. The compressed mixture may be directly pressed by hot pressing, which helps to improve the composite strength. The consolidated product is used as metal matrix composites after a few secondary operations (Leparoux et al. 2018). The schematic diagram of P/M processing scheme as given in Figure 9.5

9.2.2.1.2 Diffusion Bonding

Diffusion bonding is also termed as the foil-fiber-foil technique and this can be accomplished by depositing thick layers of matrix material onto the fibers (Nicolaou et al. 1995). This attractive fabrication technique is used mostly for aerospace applications, where mechanical characteristics in the sound metallurgical bond and bond area are most important (Lee 2012, Mouritz, 2012). MMCs with sheets or foils of matrix are fabricated by diffusion bonding. It comprises of the surface treatment of the metal using chemicals in the form of reinforcing material fibers and sheets for adequate interdiffusion. The bonding creates high pressure between the fibers and metal matrix of the metallic surfaces. This fabrication technique is broadly utilized for Mg and Al MMCs reinforced with discontinuous or continuous fibers. The bonding strength prior to diffusion bonding can be enhanced by coating the reinforcement via the ion deposition method. The use of temperature or pressure either by hot rolling or cold pressing provides a good bonding between the fiber matrix in the preform. Vacuum currently shows excellent diffusion bonding than other conditions (Muratoğlu, et al. 2006; Kandpal et al. 2014; Kumar and Kumar 2018a, 2018b, 2018c).

9.2.2.1.3 Physical Vapor Deposition (PVD)

This is an important fabrication method of MMCs that utilizes a distinct range of matrix composition. In this technique the fibers are regularly passed through a box filled with vapors of the matrix material and when condensation takes place upon the fiber, a thick coating are produced (Kumar and Kumar 2018b, 2018c). Further, vapor can be developed by electron beams of high intensity. The deposition rate lies in the range of 5–10 $\mu\text{m}/\text{min}$. Finally, it can be manufactured by assembling the coated fibers into bundles, consolidated by hot isostatic pressing or the hot-pressing technique. There are several studies in which the matrix is deposited by using distinct deposition, chemical vapor, physical vapor deposition, and plasma spraying process (Choy 2003). Recently, a new processing route called friction stir processing (FSP) is developed that allows the fabrication of MMCs (Lin and Hon 2008). Schematic diagrams of vapor deposition techniques to fabricate surface metal matrix composites CVD and PVD are given in Figure 9.6 and Figure 9.7, respectively.

9.2.2.2 Liquid State Processing

Most MMCs are manufactured by the liquid state fabrication process, owing to less cost for obtaining liquid metals than metal powder and the possibility of fabricating different complex shapes using liquid metals. However, this process technique has many demerits that consist of undesirable chemical reactions (reinforcement and liquid metal interface) and lack of reproducibility. The liquid composite slurry is eventually cast into different shapes using conventional/traditional casting methods (Cayron et al. 1999; Gopalakrishnan and Murugan 2012; Kevorkian 2004; Sansoucy et al. 2008).

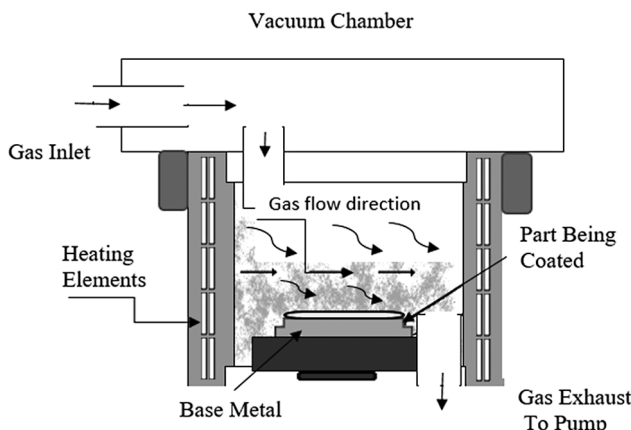


FIGURE 9.6 Schematic representation of the CVD method (Sunil 2015; Tither et al. 1995).

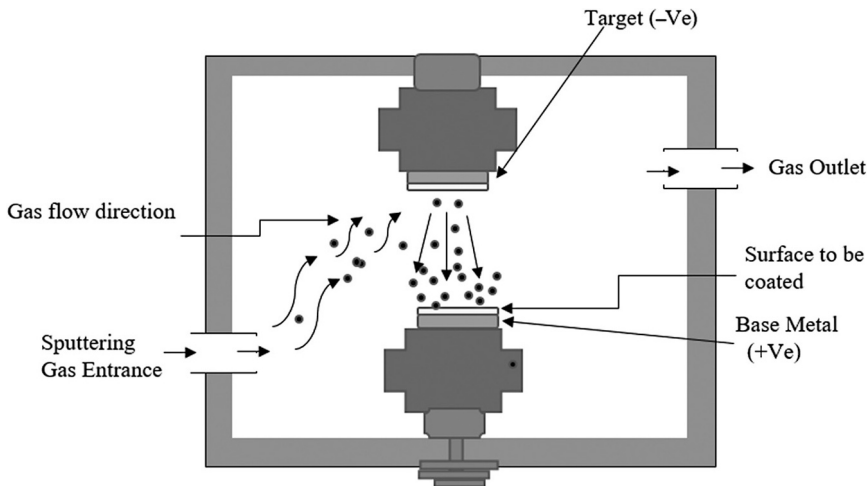


FIGURE 9.7 Schematic illustration of the PVD method (Sunil 2015).

9.2.2.2.1 *Stir Casting*

Stir casting is one of the important and most extensively used casting techniques for the manufacturing of MMCs owing to the advantages of flexible nature, simplicity, etc. This technique is also called slurry or combo casting and is initially improved by “Rohatgi” for Al matrix composites. The main merits of Al-based MMCs compared to unreinforced materials include high stiffness, high wear resistance, high strength, high damping capabilities, and enhancement in high-temperature characteristics (Wood and Ward-Close 1995). Al-(10–15%) B4C MMCs is an example of such a method that incorporates the following components such as motor, stirrer, heating furnace, crucible, and molten metal. Stir casting enhances mechanical properties and decreases porosity when it is compared with the conventional casting method. In this fabrication process, the particulate reinforcements are blended with solid ceramic particles and then allowed to solidify. The main characteristics of this method are the relatively economic, simple, limited dispersed phase contents and non-uniform dispersed phase distribution in the matrix. The application of stir casting in distinct sectors are automotive (engines, driveshaft, suspension, brake), aerospace and military (aircraft electrical AC doors, wing panel, missile fins, jet engine blade, precision components, struts); electronics (current collectors, electronic packaging); commercial (computer hard disk drives), sports (bicycle frame, tennis racket skis, wheel rims, etc. (Hashmi 2014; Sahu and Sahu 2018). However, another variant of this method is known as combo casting. In this process method the ceramic particles in semisolid state are added into the matrix alloy (Kumar et al. 2015; Chadwick 1991). The setup of the stir casting fabrication method is represented in Figure 9.8.

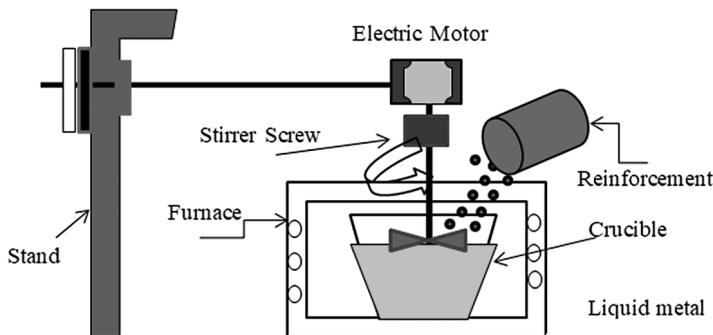


FIGURE 9.8 Schematic illustration of the stir casting process (Thandalam et al. 2015).

9.2.2.2.2 Squeeze Casting

This is one of the liquid metal routes for effective and efficient fabrication of MMCs utilizing ceramic preforms. In this method, the metal in molten state is filled into the open type die cavity under pressure (hydraulically ram) and subsequently the die is closed. As the molten metal is coming into contact with the die surface, it cools and the heat is transferred from the hot metal to the die surface. The result is free from porosity and fine grain casting developed (Chadwick 1991; Thandalam et al. 2015; Kaprinos et al. 2014; Souissi et al. 2019; Li et al. 2017; Moosa 2010). The schematic diagram of squeeze casting is shown in Figure 9.9.

In addition, some important characteristics of squeeze casting that make it more suitable for commercial use include:

- (a) Competence of mass production
- (b) Only selected component sectors are reinforced
- (c) Superior squeeze casting

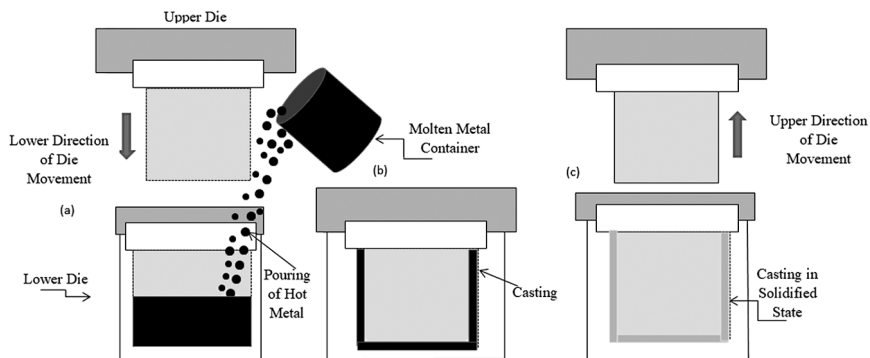


FIGURE 9.9 Schematic illustration of the squeeze casting process and its steps: (a) pouring liquid metal into the pre-heated die; (b) squeeze pressure utilization; (c) casting in solidified condition (Michaud and Mortensen 2001).

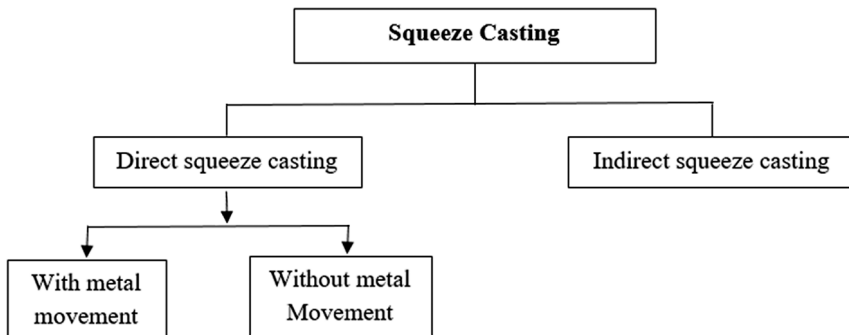


FIGURE 9.10 Classification of squeeze casting.

The classification of squeeze casting is shown in Figure 9.10.

In “direct squeeze casting,” pressure for infiltration of the pre-manufactured preform is utilized directly to the melt; whereas in indirect squeeze casting, the metal is sprayed into the die cavity using pistons of small diameter and a runner is used to transmit the pressure (hydraulic system to cavity) (Assar 1999).

9.2.2.2.3 Infiltration Process

Reinforcement is first assembled to permit a porous preform in this process. Further, the preform is infiltrated with heated metal to fill/complete the pores to form the composite (Kozack et al. 1993). Thus, when the metal in liquid state is injected or sprayed by a hydraulic or mechanically operated mechanism, then it is known as squeeze infiltration. The infiltration process of molten metal can be completed either by the use of pressure or not. The near-net-shape parts fabrication is the main merit of this process. PRIMEX and Lanxide use a pressureless infiltration process (Manu et al. 2016; Rao and Jayaram 2001; S-de-la-Muela et al. 2020).

9.2.2.2.4 Spray Deposition

This process uses droplet stream, which is generated from a molten bath and cold metal feeding into a region of rapid heat injection. The spray deposition method is categorized into two groups, namely the thermal spray process and as-sprayed process. In case of the Osprey process, the inert gas jet is used to melt and atomize the matrix alloy. Subsequently, reinforcement particles are allowed to enter this molten stream and small droplets are provided to spray onto a base metal (Clyne 2001; Lavernia and Grant 1988). In addition, droplet velocities of 20–40 m/s and a porosity level of 5–10% were found in the as-sprayed state. However, in thermal spraying the process deposition rate is approx. 1 g s^{-1} , which is slower and particle velocity is in the range of 50–400 m/s which is greater. The thermal spray process also enhances mechanical properties, and increases homogeneity (Aussavy et al. 2014).

9.2.2.3 In-situ MMCs Processing

This consists of a chemical reaction resulting in the formation of dispersed or reinforcing phase within a metal matrix. With in-situ MMCs processing, the constituent powders are blended and ignited to develop the reinforcement through a chemical reaction. Uniform distribution of particles, clean interface and fine particle size, and superior bonding between particles are the merits of this technique. However, the selection of materials system is limited. The XD process is an example of this technique (Lu et al. 1997; Kumar et al. 2008). Distinct categories of MMCs may be produced by in situ manufacturing methods such as particulate in situ metal matrix composite, and long and short fiber reinforced in situ metal matrix composite. Cu can be added to Al to form an *in-situ* metal matrix composite owing to greater wear resistance and less cost (Dubourg et al. 2002; Kumar et al. 2008). A comparison of distinct process methods for discontinuously reinforced MMCs manufacturing is shown in Table 9.2.

9.2.3 CRITICAL ISSUES USING MMCs

The distinct type of MMCs processing techniques (solid, liquid, and in-situ MMCs), reinforcement (whiskers, continuous fibers, particulates, wires, discontinuous fibers), and matrix composition utilized are not dependent on one another. But, in the case of molten material processing, they are connected in terms of the distinct interactions between reinforcement and the matrix. However, MMCs require optimum processing and recycling, etc. Thus, MMCs processing methods are the critical issues found with each of them are illustrated in Figure 9.11. Therefore, the distinct 3D printing techniques are relatively recent developments which help to eliminate all these issues (Behera et al. 2019).

9.2.4 FABRICATION BY USING 3D PRINTING

3D printing is a layered manufacturing method used to fabricate complicated shape with very less wastage which is not possible by conventional methods. The

TABLE 9.2

A Comparative Study of the Distinct Process Techniques for Discontinuously Reinforced MMCs Fabricating (Lavernia and Grant 1988)

Technique	Shape & Size	Cost	Volume Range	Damage to Reinforcement
Squeeze casting	Limited shape, max. 2 cm height	Moderately expensive	Max. 0.45	Severe damage
Spray casting	Limited shape, large size	Costlier	0.3–0.7	—
Powder metallurgy (P/M)	Wide range restricted size	Costlier	—	Reinforcement fracture
Stir casting	Small to large shapes	Less costlier	Max 0.3	No damage

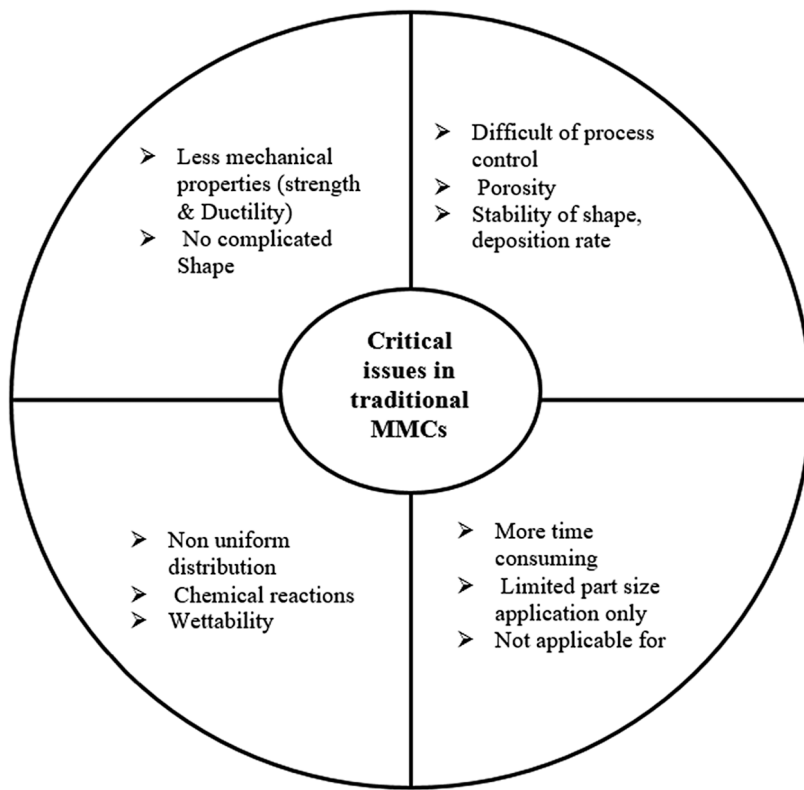


FIGURE 9.11 The distinct critical issues associated with traditional metal matrix composites (Diehl and Stöver 1990).

history of additive manufacturing is started by Charles Hull in 1980 called stereo lithography, after that there is a further enhancement in additive manufacturing in distinct field. Generally, this technology based upon three steps (modeling, printing, and finishing) (Hashim et al. 1999; Tagore et al. 2007). The distinct 3D printing methods, such as FDM, SLA, IJP, SLS, SLM, EBM, etc. are used for the fabrication of 3D components, are explained in the section below.

9.2.4.1 Fusion Deposition Modeling (FDM)

Scott Crump in 1988 developed a new technique that was commercialized by Stratasys. In this method first the plastic filament in the form of wire ($\varnothing 1.75$ and 3 mm) is supplied from the spool to the melter. The heat of the melter melts the filament. The distinct kind of thermoplastic materials such as ABS, poly-lactic acid, etc. can be used. Subsequently, the melted filament can then flow to the extrusion nozzle. The nozzle can move horizontally and the platform can move up and down vertically. In this way, the nozzle deposits a material on to a build platform and fabricates a model as per customer requirement in a layered fashion. The major

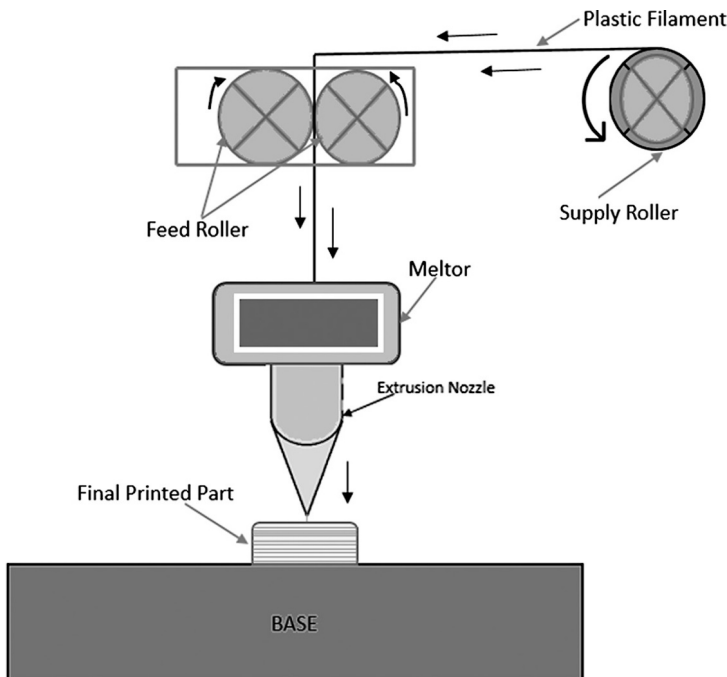


FIGURE 9.12 Line diagram of the fusion filament fabrication process (Mohamed and Masood 2015).

advantage of this process is the low printing and material costs compared with other 3D printing techniques. However, poor surface finish is the main drawback of this process. The factors that affect the mechanical characteristics of the FFF/FDM parts are the operator, material, measurement, environment, machine, and method (Masood 2014). A schematics diagram is depicted in Figure 9.12 (Hashim et al. 1999; Tagore et al. 2007; Mohamed and Masood 2015; Bernard and Fischer 2002; Mohamed and Masood 2015; Montero et al. 2001).

9.2.4.2 Stereo Lithography (SLA)

This is the first type of accurate and fast 3D printing technique that consists of a horizontally movable ultraviolet light and vertically movable vat. Instead of ink, the vat is completely filled with a type of photopolymer or resin that becomes hard. These photopolymers are photosensitive under a UV source; the resins are then solidified and design a required 3D model in layer fashion. Finally, the process is repeated again and again until the final part is not fully complicated. In this process method, a supporting structure is also required (Kumar 2014). The schematic diagram of SLS is given in Figure 9.13.

The merits of this method are that it's less costly, high-quality component printing, which can be done in a single stage, and without material wastage (Melchels et al. 2010).

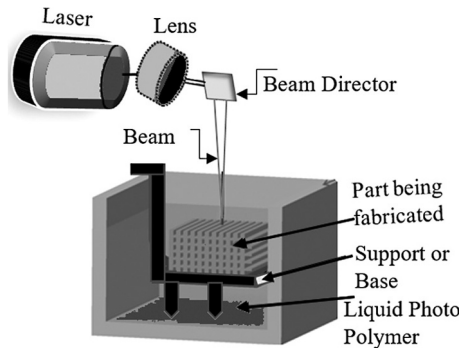


FIGURE 9.13 Schematic representation of the SLS fabrication method (Kumar et al. 2020a, 2020b).

9.2.4.3 Ink Jet Printing (IJP)

This is a non-contact, accurate method for the fabrication of distinct materials such as metal, composites, etc. (Barbulovic-Nad et al. 2006). In this technique, the print head is positioned above the build base. Initially, supporting materials known as wax and build material thermoplastic are held in molten state form inside two heated reservoirs. Both materials (supporting material and build material) are supplied through the IJP head and shoot droplets to the desired region, so as to form a single layer of the parts. Subsequently, these materials are solidified using UV rays to create a layer. If we compare this process method to other types of AM method, no post processing is needed (Derby 2010; Palermo and Innocenti 2019). The schematic representation of IJP is shown in Figure 9.14.

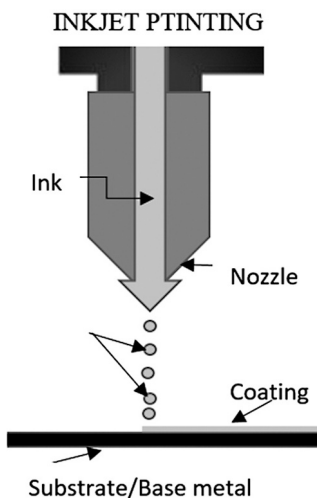


FIGURE 9.14 A schematic illustration of IJP (Kumar and Kumar 2020, Kumar et al. 2020a, 2020b).

9.2.4.4 Selective Laser-Sintering (SLS)

This 3D printing process is proposed by Carl Deckard in mid-1980s at the Univ. of Texas. This technique used CO₂ laser to sinter the powder materials (metals, ceramics, polymers) which are sprinkled on the platform bed in a layered fashion using a leveling roller (Ligon et al. 2017; Rajesh et al. 2015). Subsequently, the piston is down corresponding to a layer thickness (<0.1 mm) and focus the high power that fuses the powder particles to create a 3D object as shown in Figure 9.15. This technology has many advantages such as good adhesion strength, better mechanical characteristics, no use of support material etc. Although internal porosity is the major limitation, hence post-processing is needed (Kumar and Kumar 2020; Eshraghi and Das 2010; Kolan et al. 2012).

9.2.4.5 Selective Laser Melting (SLM)

This technology is started in 1995, a powder based fusion process, utilized to build 3D objects. This technique utilized distinct materials such as polymers, acrylonitrile butadiene styrene, wax, and powdered plastics, etc. (Kumar 2014). SLM uses high potential density laser to melt the metallic material and the laser beam moves away from the melt pool, the liquid metal is cooled, establishing a dense structure. Finally, the powder material is then injected and the part is completed by providing layer onto the previously build layer. In addition, the material particles remain loose but neither melted nor fused. This technique utilized support material hence, post-processing is needed as shown in Figure 9.16. (Yap et al. 2015; Gokuldoss et al. 2017; Kumar 2014; Santos et al. 2004; and Wang et al. 2017).

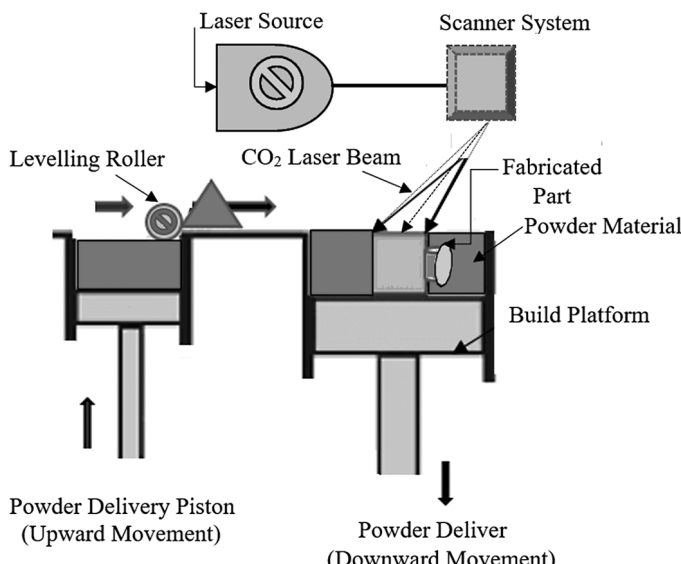


FIGURE 9.15 Schematic diagram of SLS method (Roy et al. 2019).

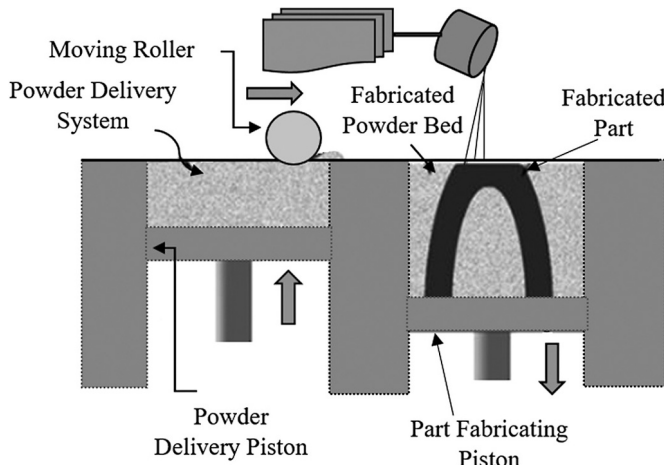


FIGURE 9.16 Schematic diagram of SLM method (Dobrzanski et al. 2017).

9.2.4.6 Electron Beam Melting (EBM)

It is first commercialized by Arcam in Sweden, considered a faster and more cost-effective technique than conventional methods (forging, casting, and machining). It is a powder-based manufacturing technique that uses metals (Cr, Co, Ti) to create a 3D object directly from metal powder (Gong et al. 2014; Nasr et al. 2014). EBM utilizes an electron beam (power source) for melting powder materials and fuses them together on the building bed. The electron gun extracts the electron from tungsten filaments under vacuum and projects it to the building bed. Finally, the laser fuses the material and produces the layer of an object, one over the other, until the part is fully completed (Heinl et al. 2007; Murr et al. 2012; Parthasarathy et al. 2010; Rafi et al. 2013). However, some post-processing techniques (surface smoothing, polishing, etc.) are used to enhance its strength and remove unwanted material, as shown in Figure 9.17.

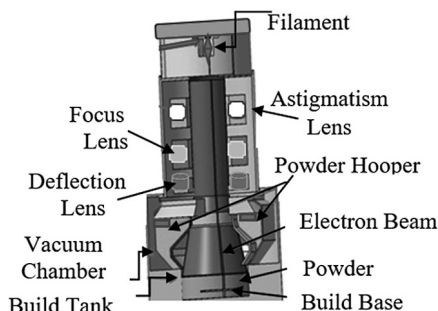


FIGURE 9.17 Schematic illustration of EBM technique (Azam et al. 2017).

TABLE 9.3

Comparison of Distinct AM Materials, Process Method, Cost, and their Applications (Kruth 1991; Hopkinson and Dicknes 2003)

Material	Method	Material Cost/Part (euro)	Machine Cost/Part (euro)	Application
➢ Ceramic suspension	Stereo	1.29	3.92	➢ Biomedical
➢ Curable resin	lithography (SLA)	—	—	➢ Prototypes
➢ Paper	Laminated	—	—	➢ Casting patterns
➢ Plastic	object manufacturing (LOM)	—	—	➢ Paper industry
➢ Thermoplastics (PLA, ABS etc.).	Fusion deposition modeling (FDM)	1.75	2.64	➢ Casting models
➢ Waxes	—	—	—	➢ Prototypes
➢ Thermoplastics	Selective laser sintering (SLS)	1.63	0.52	➢ Foundry industries
➢ Metal powder etc.	—	—	—	➢ Architectural designs
➢ Metals	Electron beam melting (EBM)	—	—	➢ Toys
➢ Ceramic powder	—	—	—	➢ Prototypes
➢ Metal powder etc.	—	—	—	➢ Casting patterns
➢ Metals	—	—	—	➢ Military
➢ Metals	—	—	—	➢ Casting models
➢ Metals	—	—	—	➢ Biomedical
➢ Metals	—	—	—	➢ Medical
➢ Metals	—	—	—	➢ Functional parts
➢ Metals	—	—	—	➢ Aeronautics industries.

In addition, the comparison between distinct 3D printing process techniques in terms of cost, types of materials used, and application in a distinct field is summarized in Table 9.3.

9.2.5 PROCESS CAPABILITY ANALYSIS OF A 3D PRINTING PROCESS

Digital manufacturing is gaining larger applications, especially in medical, socio-cultural, as well as manufacturing fields (Kumar et al. 2020a). This is due to the involvement of distinct uncontrollable and controllable factors. Nowadays, several threats are faced, such as part dimensions and shape, etc. Thus, in order to maintain quality, performance capability analysis is generally utilized as a prominent statistical tool in additive manufacturing to ascertain how well the 3D printing process meets a set of specification limits. The schematics illustration of process capability is shown in Figure 9.18.

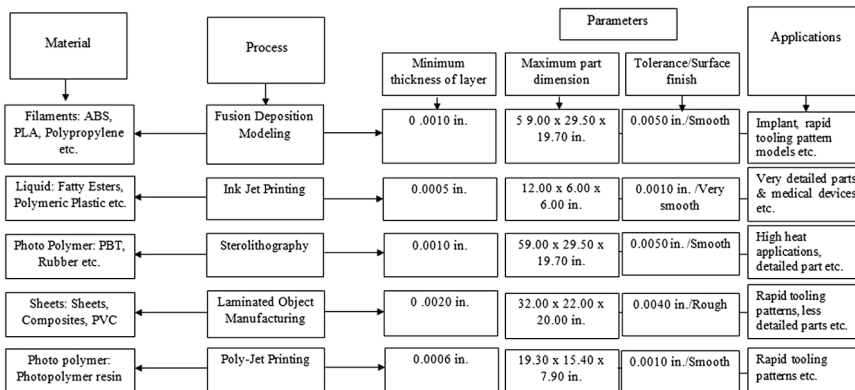


FIGURE 9.18 Schematic diagram of 3D printing process, parameters, material, and their applications in distinct fields (Ramya and Vanapalli 2016).

9.2.6 CONCLUSION

Over the past years, several challenges have been faced by the manufacturing industries during MMCs fabrication using conventional techniques. But with the advancement in technology, industry has made development in enhancing the production speed and reducing the manufacturing cost. Conventional fabrication techniques have not been able to address issues that include customized production of a small number of components at extremely low cost. To overcome these issues, 3D printing manufacturing techniques are deemed better alternatives for processing MMCs. The process methods enable the customization of each component, components with internal structures, and fabrication of components in small production runs at a very low cost.

9.2.7 FUTURE SCOPE AND CHALLENGES OF MMCs FABRICATION USING 3D PRINTING

3D printing plays a major role in distinct applications. Other applications, including human organ printing, are yet to be explored. Although 3D printing provides several advantages to manufacturers (cost savings, customization, fast design, product optimization of design, and the ability to manufacture complex geometrical shapes, etc.). However, there are still some threats to adopting 3D printing (high printing machine cost, sustainability, availability, and material cost). Hence a lot of research is needed on its processes, materials, and use of 3D printing.

REFERENCES

- Aghdam, M. M., Smith, D. J., and Pavier, M. J. (2000). Finite element micromechanical modelling of yield and collapse behaviour of metal matrix composites. *J Mech Phys Solids*, 48(3), 499–528.
- Ahmed, S., and Jones, F. R. (1990). A review of particulate reinforcement theories for polymer composites. *Journal of Materials Science*, 25(12), 4933–4942. doi:10.1007/BF00580110
- Alfonso, I., Figueroa, I.A., Rodriguez-Iglesias, V., et al. (2016). Estimation of elastic moduli of particulate-reinforced composites using finite element and modified Halpin-Tsai models. *J Braz Soc MechSci Eng.*, 38(4), 1317–1324.
- Assar, A.-E. M. (1999). Fabrication of metal matrix composite by infiltration process—part 2: experimental study. *Journal of Materials Processing Technology*, 86(1–3), 152–158. doi:10.1016/S0924-0136(98)00304-5
- Aussavy, D., Costil, S., El Kedim, O. et al. (2014). Metal matrix composite coatings manufactured by thermal spraying: influence of the powder preparation on the coating properties. *J. Thermal Spray Technology*, 23, 190–196. doi:10.1007/s11666-013-9999-3
- Azam, F. I., Abdul Rani, A. M., Altaf, K. et al. (2017). An in depth review on direct additive manufacturing of metals. *IOP Conference Series: Material Science & Engineering*, 328, 1–8. doi:10.1088/1757-899X/328/1/012005
- Barbulovic-Nad, I., Lucente, M., Sun, Y., Zhang, M., Wheeler, A. R., and Bussmann, M. (2006). Bio-microarray fabrication techniques—a review. *Crit Rev Biotechnol.*, 26(4), 237–259. doi:10.1080/07388550600978358. PMID: 17095434
- Bedi, T. S., Kumar S., and Kumar, R. (2019). Corrosion performance of hydroxyapatite and hydroxyapatite/titania bond coating for biomedical applications, *Materials Research Express*, 7, 015402, doi:10.1088/2053-1591/ab5cc5
- Behera, M. P., Dougherty, T., and Singamneni, S. (2019). Conventional and additive manufacturing with a metal matrix composite: a perspective. *Procedia Manufacturing*, 30, 159–166.
- Bernard A., and Fischer, A. (2002). New trends in rapid product development. *CIRP Ann Manuf Technol*, 51(2), 635–652.
- Borgonovo, C., and Apelian, D. (2011). Manufacture of aluminum nanocomposites: a critical review. *Materials Science Forum*, 678, 1–22. doi:10.4028/www.scientific.net/MSF.678.1
- Callister, W. D. (2001). *Fundamentals of materials science and engineering*, Wiley: New York.
- Callister, W. Jr, and Rethwisch, D. (2012). *Fundamentals of materials science and engineering: an integrated approach*. (4th edition) John Wiley & Sons, Inc.: Hoboken.
- Cayron, C., Buffat, P. A., Hausmann, C., and Beffort, O. (1999). About the epitaxial growth of Mg subgrains on Al₂MgC₂ interfacial carbides in a squeeze cast Mg-4Al/T300 metal matrix composite. *Journal of Materials Science Letters*, 18(20), 1671–1674.
- Chadwick, G. (1991). Squeeze casting of metal matrix composites using short fiber performs. *Materials Science and Engineering: A*, 135, 23–28. doi:10.1016/0921-5093(91)90530-z
- Chawla, Krishan K. (2012). *Composite Materials: Science and Engineering*. Springer-Verlag: New York, 542. doi:10.1007/978-0-387-74365-3
- Choy, K. L. (2003). Chemical vapour deposition of coatings. *Progress in Materials Science*, 48, 57–170.
- Clyne, T. W. (2001). *Composites: Interfaces. Encyclopedia of Materials: Science and Technology*, 1382–1391. doi:10.1016/b0-08-043152-6/00257-6
- Clyne, T. W., and Withers, P. J. (1993). *An introduction to metal matrix composites*. Cambridge University Press, 456–459. doi:10.1017/CBO9780511623080

- Derby, B. (2010) Inkjet printing of functional and structural materials: fluid property requirements, feature stability, and resolution. *Annu Rev Mater Res.*, 40, 395–414.
- Diehl, W., and Stöver, D. (1990). Injection moulding of superalloys and intermetallic phases. *Metal Powder Report*, 45(5), 333–338.
- Dobrzanski, L. A., Dobrzanska-Danikiewicz, A. D., and Dobrzanski, L. B. (2017). Porous selective laser melted Ti and Ti-6Al-4V material for medical application. In *Powder Metallurgy - Fundamentals and Case Studies*. doi:10.5772/65375
- Dubourg, L., Hiawka, F., and Cornet, A. (2002). Study of aluminum–copper–iron alloys: application for laser cladding. *Surf. Coat. Technol.*, 151, 329–332. doi:10.1016/S0257-8972(01)01591-2
- Erden, S., and Ho, K. (2017). Fiber reinforced composites. *Fiber Technology for Fiber-Reinforced Composites*, 51–79. doi:10.1016/b978-0-08-101871-2.00003-5
- Eshraghi, S., and Das, S. (2010). Mechanical and microstructural properties of olycaprolactone scaffolds with one-dimensional, two-dimensional, and three-dimensional orthogonally oriented porous architectures produced by selective laser sintering. *Acta Biomater.*, 6(7), 2467–2476. doi:10.1016/j.actbio.2010.02.002
- Gokuldoss, P. K., Kolla, S., and Eckert, J. (2017). Additive manufacturing processes: selective laser melting, electron beam melting and binder jetting-selection guidelines. *MDPI*, 10(6), 1–12. doi:10.3390/ma10060672
- Gong, X., Anderson, T., and Chou, K. (2014). Review on powder-based electron beam additive manufacturing technology. *Manufacturing Review*, 1–12. doi:10.1051/mfreview/2014001
- Gopalakrishnan, S., and Murugan, N. (2012). Production and wear characterization of AA 6061 matrix titanium carbide particulate reinforced composite by enhanced stir casting method. *Composites: Part B*, 43(2), 302–308.
- Hashim, J., Looney, L., and Hashmi, M. S. J. (1999). Metal matrix composites: production by the stir casting method. *Journal of Materials Processing Technology*, 92–93, 1–7.
- Hashmi, T. Q. (2014). Liquid state methods of producing metal matrix composites: a review article. *IJRMET*, 5, 103–106.
- Heinl, P., Rottmair, A., Korner, C., and Singer, R. F. (2007). Cellular titanium by selective electron beam melting. *Advance Engineering Materials*, 9(5), 360–364. doi:10.1002/adem.200700025
- Hocine, R., Boudjemai, A., Boukortt, A., and Belkacemi, K. (2013). 3D TLM formulation for thermal modelling of metal matrix composite materials for space electronics system, *International Conference on Recent Advances in Space Technologies*, Istanbul, Turkey. doi:10.1109/RAST.2013.6581254
- Hopkinson, N., and Dicknes, P. (2003). Analysis of rapid manufacturing—using layer manufacturing processes for production. *Proceedings of the Institution of Mechanical Engineers, Part C: Journal of Mechanical Engineering Science*, 217(1), 31–39. doi:10.1243/095440603762554596
- Hua, Y., and Gu, L. (2013). Prediction of the thermomechanical behavior of particle-reinforced metal matrix composites. *Compos Part B Eng.*, 45(1), 1464–1470.
- Kandpal, B., Kumar, and Singh. (2014). Production technologies of metal matrix composite, a review. *International Journal of Research in Mechanical Engineering & Technology*, 4(2), 27–32. <http://www.ijrmet.com/vol4issue2/spl2/4-Bhaskar-Chandra-Kandpal.pdf>
- Kang, H. K., and Kang, S. B. (2006). Thermal decomposition of silicon carbide in a plasma sprayed Cu/SiC composite deposit. *Materials Science and Engineering*, 428, (1–2), 336–345.

- Kapranos, P., Carney, C., Pola, A., and Jolly, M. (2014). Advanced casting methodologies: investment casting, centrifugal casting, squeeze casting, metal spinning, and batch casting, 39–67. doi:10.1016/B978-0-08-096532-1.00539-2
- Kevorkijan, V. (2004). Mg AZ80/SiC composite bars fabricated by infiltration of porous ceramic preforms. *Metallurgical and Materials Transactions A*, 35(2), 707–715.
- Kolan, K. C. R., Leu, M. C., Hilmas, G. E., and Velez, M. (2012). Effect of material, process parameters, and simulated body fluids on mechanical properties of 13-93 bioactive glass porous constructs made by selective laser sintering, *J. Mech. Behav. Biomed. Mater.*, 13(14), 14–24.
- Kozack, M. J., Khatri, S. C., Allison, J. E., et al. (1993). *Fundamentals of metal matrix composites*, S. Suresh, A. Mortensen, and A. Needleman, eds., Butterworth-Heinemann: Stoneham, MA, p. 297.
- Kruth, J. P. (1991). Material inprocess manufacturing by rapid prototyping techniques. *CIRP Annals*, 40(2), 603–614. doi:10.1016/S0007-8506(07)61136-6
- Kumar, S. (2014). Selective laser sintering/melting. *Comprehensive Materials Processing*, 93–134. doi:10.1016/b978-0-08-096532-1.01003-7
- Kumar, R., and Kumar, S. (2018a). Fabrication process and classification of composite materials, A study. *Journal of Material Science and Manufacturing Technology*, 3(1), 1–15.
- Kumar, R., and Kumar, S. (2018b). Comparative parabolic rate constant and coating properties of nickel, cobalt, iron and metal oxide based coating: a review, *I-Manager's Journal on Material Science*, 6(1), 45–56. doi:10.26634/jms.6.1.14379
- Kumar, R., and Kumar, S., (2018c). Thermal spray coating process: a study, *International Journal of Engineering Science and Research Technology*, 7(3), 610–617.
- Kumar, R., and Kumar, S. (2020). Trending applications of 3D printing: a study. *Asian Journal of Engineering and Applied Technology*, 9(1), 1–12.
- Kumar, S., Chakraborty, M., Subramanya Sarma, V., and Murthy, B. S. (2008). Tensile and wear behaviour of in situ Al-7Si/TiB₂ particulate composites. *Wear*, 265, 134–142.
- Kumar, A., Kumar, S., and Garg, R. (2015). A review paper on stir casting of reinforced aluminum metal matrix composite. *International Journal of Advance Research Science and Technology*, 4(1), 63–73.
- Kumar, R., Kumar, M., and Singh J. (2020a). The role of additive manufacturing for medical applications: a critical review. *Journal of Manufacturing Process*. 64, 828–850.
- Kumar, R., Kumar, S., and Goyal, N. (2020b). Trending applications and mechanical properties of 3d printing: a review. *Asian Journal of Engineering and Applied Technology*, 9(1), 1–12.
- Lavernia, E. J., and Grant, N. J. (1988). Spray deposition of metals: a review. *Materials Science and Engineering*, 98, 381–394. doi:10.1016/0025-5416(88)90191-7
- Lee, H.-S. (2012). Diffusion bonding of metal alloys in aerospace and other applications. *Welding and Joining of Aerospace Materials*, 320–344. doi:10.1533/9780857095169.2.320
- Lee, J. A., and Mykkanen, D. L. (1987). Metal and polymer matrix composites. United States. <https://www.osti.gov/biblio/6229913>.
- Leparoux, M., Kollo, L., Kwon, H., Kallip, K., Babu, N. K., AlOgab, K., and Talari, M. K. (2018). Solid state processing of aluminum matrix composites reinforced with nanoparticulate materials. *Advanced Engineering Materials*, 1–18. doi:10.1002/adem.201800401
- Li, R., Liu, L., Zhang, L., et al. (2017). Effect of squeeze casting on microstructure and mechanical properties of hypereutectic Al-x Si alloys. *Journal of Materials Science and Technology*, 33(4), 404–410.
- Ligon, S. C., Liska, R., Stamp, J., Gurr, M., and Mühlaupt, R. (2017). Polymers for 3D printing and customized additive manufacturing. *Chem. Rev.*, 117, 10212–10290.

- Lin, T. C. and Hon, M. H. (2008). Synthesis and microstructure of the Ti_3SiC_2 in SiC matrix grown by chemical vapor deposition. *Ceramics International*, 34(3), 631–638.
- Lu, L., Lai, M. O., Chen, F. L. (1997). Al-4 wt% Cu composite reinforced with in-situ TiB₂ particles. *Acta Materialia*, 45(10), 4297–4309. doi:10.1016/S1359-6454(97)00075-X
- Manu, K. M. S., Raag, L. A., Rajan, T. P. D. and Gupta, M. et al. (2016). Liquid metal infiltration processing of metallic composites: a critical review, *Metallurgical and Materials Transactions B*, 5, <https://www.springerprofessional.de/en/liquid-metal-infiltration-processing-of-metallic-composites-a-cr/10500862>.
- Marsh, G. (2003). Next step for automotive materials. *Materials Today*, 6(4), 36–43.
- Masood, S. H. (2014). Advances in fused deposition modeling. *Comprehensive Materials Processing*, 10, 69–91. <http://dx.doi.org/10.1016/B978-0-08-0963521-1.01002-5>
- Matthews, F. L. and Rawlings, R. D. (1994). *Composite materials: engineering and science*. Wood Head Publishing Limited: Washington.
- McDanels, D. L., Serafini, T. T., and DiCarlo, J. A. (1986). Polymer, metal, and ceramic matrix composites for advanced aircraft engine applications. *JMES*, 8, 80–91. doi:10.1007/BF02833463
- Melchels, F. P., Feijen, J., and Grijpma, D. W. (2010). A review on stereo lithography and its applications in biomedical engineering. *Biomaterials*, 31, 6121–6130.
- Michaud, V., and Mortensen, A. (2001). Infiltration processing of fibre reinforced composites: governing phenomena, *Composites Part A, Applied Science and Manufacturing*, 32(8), 981–996. doi:10.1016/S1359-835X(01)00015-X
- Mohamed, O. A., and Masood, S. H. (2015). Optimization of fused deposition modeling process parameters: a review of current research and future prospects. *Adv. Manuf.*, 3, 42–4253. doi:10.1007/s40436-014-0097-7
- Montero, M., Roundy, S., Odell, D. et al. (2001). Material characterization of fused deposition modeling ABS by designed experiments. In: *Proceedings of Rapid Prototyping and Manufacturing Conference*. Cincinnati, OH, USA.
- Moosa, A. A. (2010). Microstructure and some properties of aluminum-silicon matrix composites reinforced by alumina or chromia. *Academic Scientific Journal*, 6, 57–68.
- Mouritz, A. P. (2012) Metal matrix, fibre–metal and ceramic matrix composites for aerospace applications. In *Introduction to Aerospace Materials*, Woodhead Publishing Limited, 394–410. doi:10.1533/9780857095152.394
- Muratoğlu, M., Yilmaz, O., and Aksoy, M. (2006). Investigation on diffusion bonding characteristics of aluminum metal matrix composites (Al/SiCp) with pure aluminum for different heat treatments. *Journal of Materials Processing Technology*, 178(1–3), 211–217. doi:10.1016/j.jmatprotec.2006.03.168
- Murr, L. E., Gaytan, S. M., Ramirez, D. A., Martinez, E., Hernandez, J., Amato, K. N., Shindo, P. W., Medina, F. R., and Wicker, B. R. (2012). Metal fabrication by additive manufacturing using laser and electron beam melting technologies. *Journal of Materials Science & Technology*, 28(1), 1–14. doi:10.1016/S1005-0302(12)60016-4
- Nasr, E. A., Ali, K., Al-Ahmari, A., Moiduddin, K. et al. (2014). In: *World Automation Congress*, TSI Press.
- Nicolaou, P. D., Piehler, H. R., and Semiatin, S. L. (1995). Fiber fracture during processing of continuous fiber, metal-matrix composites using the foil/fiber/foil technique. *Metall Mater Trans A*, 26, 1129–1139. doi:10.1007/BF02670610
- Palermo, A., and Innocenti, B. (2019). The role of 3D printing in medical applications: a state of the art. *Journal of Health Care Engineering*, doi:10.1155/2019/5340616
- Parthasarathy, J., Starly, B., Raman, S., and Christensen, A. (2010). Mechanical evaluation of porous titanium (Ti6Al4V) structures with electron beam melting (EBM). *Journal of the Mechanical Behavior of Biomedical Materials*, 3, 249–259. doi:10.1016/j.jmbbm.2009.10.006

- Rafi, H. K., Karthik, N. V., Gong, H., Starr, T. L., and Stucker, B. E. (2013). Microstructures and mechanical properties of Ti6Al4V parts fabricated by selective laser melting and electron beam melting. *Journal of Materials Engineering and Performance*, 22, 3872–3883. doi:10.1007/s11665-013-0658-0
- Rajesh, R., Sudheer, S., and Kulkarni Mithun, V. (2015). Selective laser sintering process –a review. *International Journal of Current Engineering and Scientific Research (IJCESR)*, 2(10), 91–100.
- Ramu, G., and Bauri, R. (2009). Effect of equal channel angular pressing (ECAP) on microstructure and properties of Al-SiCp composites. *Materials and Design*. 30(9), 3554–3559.
- Ramya, A., and Vanapalli, S. L. (2016). 3D printing technologies in various applications. *International Journal of Mechanical Engineering and Technology (IJMET)*, 7(3), 396–409.
- Rao, B. S., and Jayaram, V. (2001). New technique for pressureless infiltration of Al alloys into Al₂O₃ preforms. *Journal of Materials Research*, 16(10), 2906–2913.
- Razzell, A. G., Venkata Siva, S. B., and Rama Sreekanth, P. S. (2016). Joining and machining of ceramic matrix composites. *Reference Module in Materials Science and Materials Engineering*, 1–9. doi:10.1016/b978-0-12-803581-8.03915-1
- Roy, N. K., Behera, D., Dibua, O. G., et al. (2019). A novel microscale selective laser sintering (μ -SLS) process for the fabrication of microelectronic parts. *Microsyst Nanoeng*, 5, 64. doi:10.1038/s41378-019-0116-8
- Sahu, P. S., and Banchhor, R. (2016). Fabrication methods used to prepare Al metal matrix composites- a review. *International Research Journal of Engineering and Technology (IRJET)*, 3, 123–132.
- Sahu, M. K., and Sahu, R. K. (2018). Fabrication of aluminum matrix composites by stir casting technique and stirring process parameters optimization. Open access peer reviewed chapter. doi:10.5772/intechopen.7348
- Sankhla, A. (2015). On studies of powder metallurgy as an effective method for processing metal matrix composites. *Indian Journal of Applied Research*, 5, 43–45.
- Sansoucy, E., Marcoux, P., Ajdelztajn, L., and Jodoin, B. (2008). Properties of SiC-reinforced aluminium alloy coatings produced by the cold gas dynamic spraying process. *Surface and Coatings Technology*, 202(16), 3988–3996.
- Santos, E. C., Osakada, K., Shiomi, M., Kitamura, Y., and Abe, F. (2004). *Microstructure and mechanical properties of pure titanium models fabricated by selective laser melting*.
- S-de-la-Muela, S. M., Cambronero, L. E. G., and Ruiz-Román, J. M. (2020). Molten metal infiltration methods to process metal matrix syntactic foams. *Metals*, 10, 149. doi:10.3390/met10010149
- Seshan, S., Guruprasad, A., Prabha, M., and Sudhakar V. (1996). Fibre-reinforced metal matrix composites — a review. *J. Indian Inst. Sci.*, 76, 1–14.
- Shirvanimoghaddam, K., Hamim, S. U., Akbari, M. K., et al. (2017). Carbon fiber reinforced metal matrix composites: Fabrication processes and properties. *Composites Part A: Applied Science and Manufacturing*, 92, 70–96. doi:10.1016/j.compositesa.2016.10.032
- Shoukry, S. N., Prucz, J. C., Shankaranarayana, P. G., and William, G. W. (2007). Microstructure modeling of particulate reinforced metal matrix composites. *Mech Adv Mater Struct.*, 14(6), 499–510.
- Singh, N. B., Rai, S., and Agarwal, S. (2014). Polymernanocomposites and Cr(VI) removal from water. *Nanoscience and Technology*, 1(1), 1–10. doi:10.15226/2374-8141/1/00104
- Skorokhod, V. V. (2003). Layered composites: structural classification, thermos-physical and mechanical properties. *Powder Metallurgy and Metal Ceramics*, 42, 437–446. doi:10.1023/B:PMMC.0000013215.36378.50

- Souissi, S., Souissi, N., Barhoumi, H., et al. (2019). Characterization of the role of squeeze casting on the microstructure and mechanical properties of the t6 heat treated 2017A aluminum alloy, 1–9. <https://doi.org/10.1155/2019/4089537>
- Sunil, B. R. (2015). Developing surface metal matrix composites: a comparative survey. *International Journal of Advances in Materials Science and Engineering (IJAMSE)*, 4(3), 9–16.
- Surappa, M. K. (2003). Aluminum matrix composites: challenges and opportunities. *Sadhana*, 28, 319–334. doi:10.1007/BF02717141
- Tagore, G. R. N., Anjikar, S. D., and Gopal, A. V. (2007). Multi objective optimization of build orientation for rapid prototyping with fused deposition modeling (FDM). In: *Seventeenth Solid Freeform Fabrication (SFF) Symposium*, Austin, 246–255.
- Taya, M., and Arsenault, R. J. (1989). *Technology and engineering*. Pergamon Press: New York.
- Thandalam, S. K., Ramanathan, S., and Sundarraj, S. (2015). Synthesis, microstructural and mechanical properties of ex situ zircon particles ($ZrSiO_4$) reinforced metal matrix composites (MMCs): a review. *Journal of Material Research Technology*, 4(3), 333–347.
- Tither, D., Ahmed, W., Sarwar, M., and Ahmed, E. (1995). Application of diamond-like carbon coatings deposited by plasma-assisted chemical vapour deposition onto metal matrix composites for two-stroke engine components. *Journal of Materials Science Letters*, 14(15), 21–27.
- Waku, Y., and Nagasawa, T. (1994). Future trends and recent developments of fabrication technology for advanced metal matrix composites. *Material and Manufacturing Processes*, 9(5), 937–963.
- Wang, X., Jiang, M., Zhou, Z., Gou, J., and Hui, D. (2017). 3D printing of polymer matrix composites: a review and prospective, *Composites Part B: Engineering*, 110, 442–458, ISSN 1359-8368, doi:10.1016/j.compositesb.2016.11.034
- Wood, M., and Ward-Close, M. (1995). Fibre-reinforced intermetallic compounds by physical vapour deposition. *Materials Science and Engineering A*, 192/193, 590–596.
- Yap, C. Y., Chau, C. K., and Dong, Z. L. (2015). Review of selective laser melting: Materials and applications. *Applied Physics Reviews*, 2(4), doi:10.1063/1.493592
- York Duran, J. L., Kuhn, C., and Müller, R. (2017). Modeling of the effective properties of metal matrix composites using computational homogenization. *Applied Mechanics and Material*, 869, 94–111. doi:10.4028/www.scientific.net/AMM.869.94



Taylor & Francis

Taylor & Francis Group

<http://taylorandfrancis.com>

@seismicisolation
@seismicisolation

10 Advancement in Liquid Processing Techniques of Aerospace-Grade 7XXX Series Aluminium Alloy and Composites

Vasanthakumar Pandian and Sekar Kannan

Department of Mechanical Engineering, National Institute of Technology, Calicut, India

CONTENTS

10.1	Introduction.....	225
10.1.1	Research Objective and Published Research Related to the Theme of the Topic	227
10.1.2	Chemical Composition and Alloying Elements	227
10.2	Casting Techniques.....	229
10.2.1	Stir Casting Method	229
10.2.2	Squeeze Casting Method.....	233
10.2.3	Ultrasonic Assisted Casting Method	233
10.2.4	Other Casting Method.....	234
10.3	Microstructural Characterization.....	234
10.4	Mechanical Properties	237
10.5	Discussion.....	240
10.6	Conclusion	244
	References.....	245

10.1 INTRODUCTION

Aluminium metal has a less density of 2.7 g/cm^3 approximately one-third as much as steel 7.83 g/cm^3 (Davis, 1999; Davis, 2001). Aluminium metals are second to steels in use as structural members. Aluminium metal is lightweight, less costly, and more available and also physically, chemically, and mechanically comparable with other metals like steel, copper, brass, lead, zinc, nickel, and

titanium (Ahmad, 2012; Donatus et al., 2017). Aluminium metal can be casted, rolled, formed, and machined like other metals with less effort due to its soft and ductile nature. Alloying the pure aluminium with different elements like copper, manganese, silicon, magnesium, and zinc serves for various applications in all fields of Science and Engineering. More importantly, in recent research, aluminium and its alloying element are reinforced to form composites for the development of high-performance, environmentally friendly, and lightweight applications. Aluminium is alloyed with other elements to improve material properties. The principal divisions of alloys are: 1XXX series (Al alloy) in pure form; 2XXX series (Al-Cu alloy) used for structural and aircraft industry; 3XXX series (Al-Mn alloy) used mainly in canning industry; 4XXX series (Al-Si) used for welding rods and brazing; 5XXX series (Al-Mg alloy) used for architectural and automotive applications; 6XXX series (Al-Mg-Si alloy) used for universal building industry and automobile components; and (Al-Zn-Mg-Cu alloys) 7XXX series used as high strength alloys for aircraft, military and space vehicle applications (Ahmad, 2012). For several decades, aluminium 7XXX series alloy has been used as engineering components in various sectors like aerospace, marine, automotive, and space industries because of their lighter weight, high performance, and higher strength-to-weight ratio (Michael Rajan, Ramabalan, Dinaharan, & Vijay, 2013).

Aluminium metal matrix composites (AMMCs) have high strength, improved corrosive resistance, lightweight, and toughness. AMMCs are used globally due to their high material properties. AMMC, when reinforced with ceramic particles SiC, B₄C, Al₂O₃, TiC, has a better mechanical property than base alloys. The fabrication of AMMC can be done by various conventional liquid processing methods like stir, squeeze casting, compo-casting, ultrasonic-assisted casting, supersonic-assisted casting, and the powder metallurgy method (Biermann & Hartmann, 2006; Suresh, Mortensen, & Needleman, 2013; Delrue, Tabatabaeipour, Hettler, Van Abeele, & Den., 2016; Cuevas, Becerril, Martínez, & Ruiz, 2018; Vasanthakumar, Sekar, & Venkatesh, 2019). The liquid processing technique is one of the best common methods for fabricating metal matrix composite because of control over matrix structure, low cost, and near net shape forming, bulk production ability to form a uniform dispersion of the reinforcement particle in the matrix phase (Baradeswaran & Elaya Perumal, 2014, 2015; Baradeswaran, Elayaperumal, & Franklin Issac, 2013; Baradeswaran & Perumal, 2014a, 2014b; Basavarajappa, Chandramohan, Mukund, Ashwin, & Prabu, 2006; Fadavi Boostani et al., 2015; Gupta, Chaudhari, & Daniel, 2018; Imran & Khan, 2019; Jo et al., 2019; Kanth, Rao, & Krishna, 2019; A. Kumar, Pal, & Mula, 2017; Leng, Wu, Zhou, Dou, & Huang, 2008; Madhukar, Selvaraj, Rao, & Veeresh Kumar, 2019; Pandian & Kannan, 2021; Podymova & Karabutov, 2017; Priyadarshi & Sharma, 2016b; Priyadarshi & Sharma, 2016a; Ramanathan, Krishnan, & Muraliraja, 2019; Sekar, 2019; Singh, 2016; Sudhakar, Madhusudhan Reddy, & Srinivasa Rao, 2016; Suresha & Sridhara, 2010; Baradeswaran, & Perumal, 2014a; Vigneshwar, Divagar, & Selvamani, 2016).

10.1.1 RESEARCH OBJECTIVE AND PUBLISHED RESEARCH RELATED TO THE THEME OF THE TOPIC

This chapter studies the entire liquid processing methods, as shown in Figure 10.1(a) stir-squeeze casting, thixoforming, ultrasonic aid casting, compo-casting, high pressure die-casting of 7XXX series aluminium alloys and composites. In this chapter, improvements related to the liquid processing technique, material characterization, and mechanical properties were also studied. Figure 10.1(b) of the web of science metrics shows that 5% or less than 5% of the research article published related to the theme during the years 2000–2013. From 2014, there was a substantial increase up to 10% and further increased to 15% during 2016–2017, and 20% during 2018–2019. In Figure 10.1(c), the stir casting process covers 40%, followed by other casting methods like die casting and compo casting, occupying 34%. The squeeze and ultrasonic-assisted casting contribute 20% of the total research published. Figure 10.1 (d) shows research work distribution in material characterization techniques in optical microscopy at 33%, scanning electron microscopy 44%, X-ray diffraction 18%, and energy dispersive spectroscopy 5%. Figure 10.1 (e) shows the research works in mechanical testing and wear study. With more than 30% hardness and tensile test occupies whereas wear test –30%, fatigue –4%, and impact test-2% of entire research published associated to the theme of the topic. From preliminary data collection, current research focused on the processing of 7XXX series aluminium alloys and composites.

10.1.2 CHEMICAL COMPOSITION AND ALLOYING ELEMENTS

Aluminium (Al) with a weight percentage ranging from 87% to 91% is termed as a base element and other alloying elements like zinc (Zn), magnesium (Mg), and copper (Cu) are major alloys in the aerospace-grade aluminum 7XXX series. The effects of zinc (5.1% to 6.68%) when combined with magnesium (1.14% to 2.9%) and copper (0.08% to 2.5%) help in the improvement of natural aging conditions and the heat treatment process. Zinc also helps in weldability properties. The high content of magnesium will lead to oxidation losses in molten aluminium commonly. To avoid embrittlement in the casting process, low magnesium content is used, and this is also a significant factor for the acceleration of age hardening properties. Generally, copper improves hardness, strength, thermal conductivity, and machinability. The use of copper of more than 6% may decrease castability and hot tear resistance, and they are disposed to intergranular corrosion. Minor alloying elements like silicon (Si) improve feeding, fluidity, and hot tear resistance almost in all casting techniques. The addition of silicon elements in base compositions provides an increase in hardness to the alloy and decreases machinability and ductility, and it also lowers the melting point. The iron (Fe) element with less than 0.5% prevents the material from sticking over the die and maintains the castability, ductility, machinability, and shock resistance. The intermetallic formation in the alloy avoided by the addition of manganese

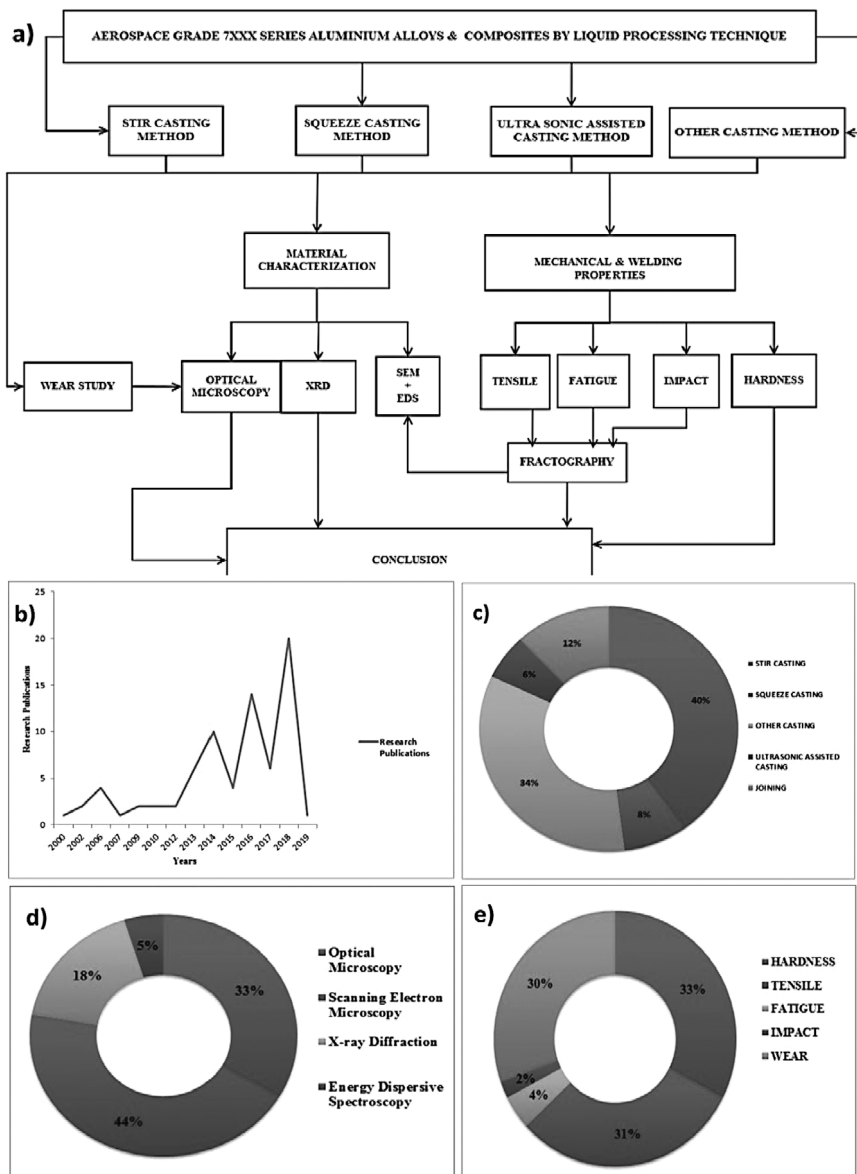


FIGURE 10.1 Published research related to the theme of the topic.

(Mn), further leads to improved ductility and shrinkage characteristics. The small percentage of chromium (Cr), titanium (Ti), and nickel (Ni) when combined with major alloying elements enhances strength and hardness (Davis, 1999; Davis, 2001; Divagar, Vigneshwar, & Selvamani, 2016; Mohanavel, Rajan, Suresh Kumar, Vijayan, & Vijayanand, 2018).

10.2 CASTING TECHNIQUES

Conventional casting methods are the oldest manufacturing process used, since the 4th century B.C. The evolution of casting methods is considered one of the significant impact factors on the World's economy. The evolution starts from the conventional method to fully automated methods like centrifugal casting, stir casting, squeeze casting, electro-magnetic stir casting, and ultrasonic-assisted casting. For the production of aluminium metal matrix composites, the liquid casting process is considered one of the most economical methods proven worldwide when compared with other methods.

10.2.1 STIR CASTING METHOD

Stir casting is the best inexpensive and simplest technique for the preparation of metal matrix composite (MMC), owing to its simplicity commonly used for the composite production of bulk quantity. In the liquid processing method, stir casting is used to produce the aluminium matrix composite materials in which the reinforcement act as a dispersed phase and AA7XXX as a matrix phase. Mixing the reinforcement particle in a molten matrix will lead to uniform distribution under controlled process parameters. Table 10.1 depicts various process parameters like matrix alloy, reinforcement details, stirring speed, stirring time, furnace temperature, post-process heat treatment, and other details.

Kannan and Ramanujam (2017) reported 1.2 kg of AA7075 with Al_2O_3 , SiC having three different reinforcement pre-heat temperatures of 400°C, 500°C, and 600°C cast in a stir casting machine. The stirring speed consists of 600 RPM with 4 minutes' stirring time and a furnace temperature of 850°C. The additional substance used consists of 10 g of Na_3AlF_6 with a reinforcement flow of 5 g/min. This work consists of three samples of the single reinforced composite and two-hybrid reinforced composite. Veeravalli et al. (2016) stated that 0.75 kg of AA7075 cast with TiC had a reinforcement pre-heat temperature of 300°C, and a stir speed of 300 RPM with 800°C furnace temperature. The additional substance consists of Mg ribbons to provide better wettability. Heat treatment post-process T6 is carried out in the sample size of $\varnothing 15 \times 150$ mm. Baradeswaran et al. (2013) provided information regarding 1 kg of AA7075 with Al_2O_3 reinforcement pre-heated at a temperature of 480°C with 10 minutes stir time and a furnace temperature of 800°C. The additional substance used consists of Nucleant,

TABLE 10.1
Stir Casting Method of 7XXX Series Aluminium Alloys and Composites

Reinforcement								
Matrix/ Weight of Ingots	Type	Preheat Temp. (°C)	Stir Speed (rpm)	Stirring Time (Min)	Furnace Temp. (°C)	Additional Substance Used	Specimen Details	Reference
AA7075/1.2 kg	Al ₂ O ₃ , SiC	400, 500, 600	600	4	850°C	Na ₃ AlF ₆ -10 g Reinforcement flow-5 g/min	3-single reinforced, 2-hybrid reinforced	(Kannan & Ramanujam, 2017)
AA7075 / 0.75 kg	TiC	300	300	—	800°C	Mg ribbons	Ø15 × 150 mm	(Veeravalli, Nallu, Mohiuddin, & S., 2016)*
AA7075 /1 kg	Al ₂ O ₃	480	—	10	800°C	Nucleant, Degasser-5 g	Preheat die Temp-350°C	(Baradeswaran et al., 2013)
AA7075	SiC	300	—	5-7	720°C -20 min	1.5 wt%- Mg, 2lpm – Argon gas	100 × 100 × 6 mm	(Deepandurai & Parameshwaran, 2016)
AA7075	WC	—	500	10-15	850°C	K ₂ TiF ₆ (Potassium fluotitanate) flux	150 × 100 × 10 mm	(Nallabelli & Ravi, 2018)
AA7075	SiC, Gr	—	600	—	700°C (under cover of nitrogen gas)	1 wt%- Mg	Preheat die Temp-300°C	(Kumar & Dhiman, 2013)*
AA7475	B4C, CeO ₂	400	—	3	800°C	—	100 × 100 × 10 mm	(Senthilnathan, Balachandar, & Author, 2018)
AA7075	Al ₂ O ₃ , Gr	480	450	10	850°C	—	—	(Baradeswaran & Elaya Perumal, 2014)

AA7075	Gr and bagasse-ash	—	200–300	15	750 °C	—	Circular metal mold- 250 mm length, Ø21 mm.	(Prabhu, 2017)
AA7075/500 g	Si ₃ N ₄ , Gr	—	250	10	950°C	—	—	(Mir Irfan Ul Haq, 2018)
AA7075-T651/ 2.6 kg	SiC, Al ₂ O ₃	600	—	—	810°C	—	12 mm Dia Ingots	(Selvamani, Vigneshwar, & Divagar, 2016)
AA7075	TiB ₂	—	500	—	700°C (under cover of nitrogen gas)	1 wt% Mg	—	(Chandana, Lawrence, & Jayabal, 2018)
AA7075	Graphite	—	500	—	850°C	—	—	(Baradeswaran & Perumal, 2014a, b)*
AA7075	Gr, TiB ₂	—	300	—	760°C	—	Circular die-250 mm length, Ø30 mm	(Ramkumar, Bekele, & Sivasankaran, 2015)
AA7075	SiC, Al ₂ O ₃	—	—	—	810°C	—	Preheated steel die-dia-20 mm and Height-140 mm	(Divagar et al., 2016)

Matrix	Reinforcement	Specimen Information	Reference
AA7075	B ₄ C	Two stirrers are used	(Dubey & Singh, 2018)
AA7075	SiC	Die –120 mm thickness –6 mm	(Bhushan, Kumar, & Das, 2013)
AA7009	SiC	Cylinder die –200 mm length, Ø16 mm	(Rao & Das, 2010)
AA7010	SiC	Cylinder die –200 mm length, Ø16 mm	(Rao, Das, Mondal, Dixit, & Tulasi Devi, 2013)
AA7075-T651	SiC, Al ₂ O ₃	No specimen information	(Vigneshwar et al., 2016)

* Post processed with T6-Heat Treatment.

Degasser 5 g with reinforcement pre-heat die temperature of 350°C. Deepandurai and Parameshwaran (2016) reported AA7075 cast with SiC reinforcement at a reinforcement pre-heat temperature of 300°C. The stirring time consists of 5–7 minutes and a furnace temperature of 720°C for 20 min. The additional substance used consists of 1.5 wt% Mg, 2 lpm argon gas to get a final cast size of 100 × 100 × 6 mm.

Nallabelli and Ravi (2018) provided information regarding AA7075-WC composite with a stir speed of 500 RPM and stir time of 10–15 minutes with a furnace temperature of 850°C. The additional substance used consists of K₂TiF₆ flux. Cast specimens with a size of 150 mm × 100 mm × 10 mm. Kumar and Dhiman (2013) stated AA7075 stir cast with SiC and Gr consists of 600 RPM stirring speed, a furnace temperature of 700°C (under cover of nitrogen gas), and 300°C reinforcement pre-heat die temperature. The additional substance used is 1 wt% Mg and a T6 post-process heat treatment is carried out. Senthilnathan et al. (2018) reported an AA7075 cast with B4C, CeO₂, with a reinforcement pre-heat temperature of 400°C. A stirring time of 3 minutes and furnace temperature of 800°C are needed to obtain final specimens sized 100 × 100 × 10 mm. Baradeswaran and Elaya Perumal (2014) provided information regarding AA7075 reinforced with Al₂O₃, Gr with the reinforcement pre-heat temperature of 480°C. The stirring speed is 450 RPM with 10 minutes stirring time and furnace temperature of 850°C. Imran, Khan, Megeri, and Sadik (2016) reported AA7075 with Gr and bagasse-ash with a stir speed of 200–300 RPM and 15 minutes stir time. The furnace temperature of 750°C and circular metal mold 250 mm length, Ø21 mm. Mir Irfan Ul Haq (2018) stated 500 g of AA7075 cast with Si₃N₄, Gr with stirring speed of 250 RPM, 10 minutes stirring time, with a furnace temperature of 950°C.

Selvamani et al. (2016) provided information regarding 2.6 kg of AA7075-T651 with reinforcement SiC, and Al₂O₃ with a pre-heat temperature of 600°C. The furnace temperature maintained at 810°C to obtain 12-mm diameter ingots. Chandana et al. (2018) stated that AA7075 cast with TiB₂ consists of a stir speed of 500 RPM. The furnace temperature of 700°C (under cover of nitrogen gas) with 1 wt% Mg as an additional substance. Ceschini, Boromei, Minak, Morri, & Tarterini (2007) reported AA7075 with graphite consists of a stir speed of 500 RPM with 850°C furnace temperature. The T6 post-process-heat treatment was used in fabricate cast samples. Ramkumar et al. (2015) stated AA7075 with Gr, TiB₂ consists of a stirring speed of 300 RPM. The furnace temperature is 760°C and circular die 250 mm length, and Ø30 mm used. Divagar et al. (2016) reported AA7075 with SiC, Al₂O₃, with a furnace temperature of 810°C. A pre-heated steel die diameter of 20 mm and height 140 mm are used for casting. Dubey and Singh (2018) provided information regarding two stirrer blades that were used to prepare AA7075-B4C composite. Bhushan et al. (2013) reported a die size of diameter 120 mm and 6 mm CeO₂ were used to obtain a AA7075-SiC composite. Rao and Das (2010) stated AA7010/AA7009-SiC composite was prepared in cylinder die of 200 mm length, Ø16 mm. Rao et al. (2013) reported a AA7010-SiC composite prepared in cylinder die of 200 mm length, Ø16 mm.

10.2.2 SQUEEZE CASTING METHOD

The squeeze casting generates high pressure to produce near net-shaped components to avoid porosity in the fabrication of MMC. Squeeze casting has its advantage when poured molten metal is forced with high pressure to decrease the adverse effects of porosity and reduces the gas entrapment and solidification shrinkage. Table 10.2 shows matrix alloy, reinforcement, and squeeze pressure of 7XXX series aluminium alloy and composites. Kannan and Ramanujam (2018) reported that AA7075 cast with Al_2O_3 , h-BN reinforcement with maximum squeeze pressure of 150 MPa. George and Knutsen (2012) used a 130-ton pressure for AA7075 without reinforcement. Blaz et al. (2010) suggested that the pressure of 100 Mpa can be used to cast AA7039-SiC composite. Kannan and Ramanujam (2017) used the same pressure as Blaz et al. (2010) suggested for AA7075- Al_2O_3 composite.

10.2.3 ULTRASONIC ASSISTED CASTING METHOD

The ultrasonic transducer produces high-intensity ultrasonic waves of frequency above 18 kHz in the liquid medium with alternate non-linear waves. Due to these non-linear waves, there is a small bubble growth formation, which leads to high energy absorption and massive collapse, with abrupt acoustic sound inside the molten metal causing cavitation. The ultrasonic waves further help in improving microstructure, reducing porosity, and homogenizing. Table 10.3 shows ultrasonic treated metal matrix composite with process parameters and reinforcement.

Haghayeghi et al. (2015) reported AA7075 without reinforcement and prepared with the help of ultrasonic transducer at 10, 14, 17.5, 20 KHz frequency with an input power of 4 kW for the 60 sec. Kannan and Ramanujam (2018) used the ultrasonic method for AA7075 + Al_2O_3 + h-BN hybrid composite. Gopalakannan and Senthilvelan (2015) reported on AA7075 + SiC + B_4C hybrid composite prepared through the ultrasonic technique with 18 KHz frequency and an input power of 4 kW.

TABLE 10.2

Squeeze Casting Method of 7XXX series Aluminium Alloys and Composites

Matrix	Reinforcement	Squeeze Pressure	Reference
AA7075	Al_2O_3 , h-BN	150 MPa	(Kannan & Ramanujam, 2018)
AA7075	—	130 ton	(George & Knutsen, 2012)
AA7075	Al_2O_3	101 MPa	(Kannan & Ramanujam, 2017)
AA7039	SiC	100 MPa	(Blaz et al., 2010)

TABLE 10.3**Ultrasonic Assisted Casting Method of 7XXX Series Aluminium Alloys and Composites**

Matrix/ Reinforcement	Frequency	Input Power	Time	Reference
AA7075	10,14,17.5,20 KHz	4 kW	60 s	(Haghayeghi, Heydari, & Kapranos, 2015)
AA7075 + Al ₂ O ₃ + h-BN	—	—	—	(Kannan & Ramanujam, 2018)
AA7075 + SiC + B4C	18 KHz	4 kW	—	(Gopalakannan & Senthilvelan, 2015)

10.2.4 OTHER CASTING METHOD

There is also a method called in-situ casting, which involves synthesizing reinforcement particles in the molten melt. The advantages of this fabrication are that they produce good bond strength between interfaces, uniform dispersion of reinforcement particles, stable-particle thermodynamics, and low-cost. There are various methods, like electromagnetic stir casting, compocasting, thixoforming, infiltration, which are used for the fabrication of composites. Apart from the above techniques, a combined casting technique with different (Kannan & Ramanujam, 2017; Sekar, Jayachandra, & Aravindan, 2018; Sekar & Ananda Rao, 2019; Sekar & Singh, 2019; Sekar & Vasanthakumar, 2019, 2020a, 2020b; Pandian & Kannan, 2021) reinforcement shows excellent mechanical properties and uniformed microstructure as compared to stir, squeeze, ultrasonic-assisted, and other casting techniques.

10.3 MICROSTRUCTURAL CHARACTERIZATION

Table 10.4 shows the detailed microstructural observations made in optical microscopy, scanning electron microscopy and elemental presence in energy dispersive spectroscopy of 7XXX series aluminium alloy and composites. Kannan and Ramanujam (2017) examined the processing methods on the hybrid nanocomposites (Al₂O₃ + hBN) produced through ultrasonic-assisted molten salt method, and T6 heat-treated with deep cryogenic treatment (DCT). They found that T6 enhances the properties of base alloys and nanocomposites more than the DCT method. The microstructure of base alloy and hybrid nanocomposite shows refined grains in hybrid nanocomposite than base alloy. Due to grain boundary pinning, the particle size, and their volume fraction change such that the grain size of matrix decreases and volume fraction increases, which restricts the grain growth. When compared to the DCT method, under T6-heat-treated conditions, the grains were found to be finer. When examined under T6 conditions, it forms

TABLE 10.4
Microstructural Characterization of 7XXX Series Aluminium Alloys and Composites

Composite	Findings	Reference
AA7075 + TiB ₂	No detrimental intermetallic compounds	(Pugazhenthi, Kanagaraj, Dinaharan, & David Raja Selvam, 2018)
AA7075 + TiB ₂	After FSP, voids became finer and there is intra-granular distribution of TiB ₂ particle for good interfacial bonding to the matrix alloy	(Rajan, Dinaharan, Ramabalan, & Akinlabi, 2016)
AA7075-T651 + SiC-10% + Al ₂ O ₃ -5%	Fatigue strength improved 12% in MMC compared base alloy and its composites	(Divagar et al., 2016)
AA7075	Homogenization by promoting porosity expansion at temperatures above 470°C	(George & Knutsen, 2012)
AA7075 + SiC + Al ₂ O ₃	The heat-affected zone: coarser grains, weld zone: much finer grains observed	(Vigneshwar et al., 2016)
AA7075 + TiC	With average grain size of be less than 2 µm, TiC particles are uniformly dispersed	(Baskaran, Anandakrishnan, & Duraiselvam, 2014)
AA7075 + TiB ₂	Absence of deleterious intermetallic compounds and homogeneous distribution of TiB ₂ particles in the aluminium matrix	(Michael Rajan, Ramabalan, Dinaharan, & Vijay, 2014)
AA7075	Presence of graphite increases the wear resistance and SiC significantly affect the wear	(Kumar & Dhiman, 2013)
AA7075 + Si ₃ N ₄ + Gr	Improved bond strength between matrix and reinforcement particles	(Mir Irfan Ul Haq, 2018)
AA7075	The microstructure of the base alloy contained secondary phases. Adding nickel into the base alloy formed new dispersion particles which restricted recrystallization and grain growth	(Naeem & Mohammed, 2013)
AA7075 + TiB ₂	Developed composite revealed a good bond strength and uniform dispersion of TiB ₂ particles	(Michael Rajan et al., 2013)
AA7075 + Al ₂ O ₃ + Graphite	Compared to base alloy and hybrid composites, monocomposite AA7075 + Al ₂ O ₃ exhibits superior properties	(Baradeswaran & Elaya Perumal, 2014)
AA7075 + SiC	Volume fraction of SiC increases, porosity also increases	(Prabhu, 2017)
AA7075 + TiB ₂	TiB ₂ particles are uniformly disturbed on the aluminium composites with better microstructures at 8 wt.%	(Chandana et al., 2018)
AA7075 + Al ₂ O ₃ + h-BN	Microstructure reveals that the grain refinement influences mechanical properties	(Kannan & Ramanujam, 2018)
AA7075 + TiC	TiC reinforcement particles are uniformly dispersed in AA7075-10 wt% composite	(Veeravalli et al., 2016)

(Continued)

TABLE 10.4 (Continued)**Microstructural Characterization of 7XXX Series Aluminium Alloys and Composites**

Composite	Findings	Reference
AA7075 + Gr	The graphite thickness layer act as the main role in wear behavior of AA7075	(Baradeswaran & Elaya Perumal, 2015)
AA7075 + SiC + Al ₂ O ₃	Observed that tear dimples like structure are elongated with ductile and cleavage fracture	(Selvamani et al., 2016)
AA7075 + SiC + Al ₂ O ₃	The reinforcement particle preheating temperatures produces uniform distribution and prevents agglomeration.	(Kannan & Ramanujam, 2017)
AA7075 + foamed SiC/ Al ₂ O ₃ /Fe ₂ O ₃	Observed pools of eutectic phase inside globules of primary phase.	(Ralph & Silberstein, 2015)
AA7075 Wrought + A359 Cast	AA7075 alloy with elongated grains along the extrusion direction. A359 cast alloy shows the microstructure of hypo-eutectic alloy	(Sabatini, Ceschini, Martini, Williams, & Hutchings, 2010)
AA7075 + SiC	Under optimum conditions distribution of reinforcement particles are homogeneous and absence of secondary phase particles	(Bhushan et al., 2013)
AA7075 + Gr + TiB ₂	No intermetallic phases. The uniform distribution of TiB ₂ and graphite reinforcement particles in the AA7075 matrix	(Ramkumar et al., 2015)
AA7010/ AA7009 + SiC	The microstructure reveals the presence of dendrites of aluminium and precipitates along the inter-dendritic regions	(Rao & Das, 2010)
AA7010 + SiC	The dendritic structure present in aluminium and precipitates along the inter-dendritic regions.	(Rao et al., 2013)
AA7039 + SiC _w	Very fine microstructure and uniform distribution of SiC _w particles	(Blaz et al., 2010)
AA7005 + Al ₂ O ₃ _p	Grain refinement due to plastic deformation of aluminium alloy matrix was observed	(Ceschini et al., 2007)
AA7075	A very fine equiaxed grains and partial precipitates was observed	(Zhang, Su, Chen, & Nie, 2015)
AA7475 + B4C + CeO ₂	Less cluster formation and B4C and CeO ₂ particles are uniformly distributed in matrix	(Senthilnathan et al., 2018)
AA7075 + WC	The reinforcement particle clustered and has been distributed in the matrix alloy	(Nallabelli & Ravi, 2018)
AA7075 + SiC + B4C	The nanoparticles uniformly distributed within the matrix alloy except some fine clusters	(Gopalakannan & Senthilvelan, 2015)

fine precipitates within the grains. These microstructural effects in the hybrid composites produce better mechanical properties than the monocomposite and base alloy.

10.4 MECHANICAL PROPERTIES

Hardness is well-defined as resistance to indentation and now and then resistance to deformation. Mostly for metals, hardness is the quantity of their resistance to plastic deformation. The various hardness measurement methods exist, but the indentation hardness test commonly chosen for all metal in engineering field. The test procedure and sample preparation were carried out as per ASTM E10 standard (Gajewska, Dutkiewicz, & Morgiel, 2014; Ramkumar et al., 2015; Sekar, Allesu, & Joseph, 2015; Imran et al., 2016; Kannan & Ramanujam, 2018; Karabulut, Gökmen, & Çinici, 2018; Mohanavel et al., 2018). A tensile test is executed to define properties such as strength and ductility of a material. The tensile test needs intended specimen as per the ASTM standard. Generally, ASTM E8M is used for testing metallic samples (Ceschini et al., 2007; Sabatini et al., 2010; Imran et al., 2016; Selvamani et al., 2016; Sekar et al., 2018). An impact test is executed under an impact load to estimate the energy absorbed during fracture and to measure the ability to absorb energy on shock loads. The test was performed on notched bar samples prepared by ASTM E23 standard, which specifies two methods; namely the Charpy method and the Izod method (Arjunan, 2019; Manikandan, Arjunan, & Akhil, 2020; Pandian & Kannan, 2021). Fatigue leads to disastrous failure under the action of a fluctuating load, the magnitude of which is much less as compared with the yield strength of the material. Failure under fatigue occurs in three stages: (i) initiation of crack, (ii) crack propagation, and (iii) unexpected sudden failure. The specimen preparation and test procedure under this type of load is prescribed in ASTM E466 standard (Ceschini et al., 2007; Effertz et al., 2016). Table 10.5 depicts the mechanical test value for Hardness, Tensile, Impact, and Fatigue test of 7XXX series aluminium alloys and composites performed as per ASTM standard.

Kannan and Ramanujam (2017) found that there was an increase of hardness values with an increase in wt.% of Al_2O_3 particles due to the uniform dispersion of nanoparticles in the matrix metal. When compared to the base cast alloy, there was an improvement of 63.7% and 90.5% in the hardness for a monocomposite prepared through stir-squeeze casting. Divagar et al. (2016) found that AA7075-T651 + SiC-10% + Al_2O_3 -5% exhibits 12.13% higher fatigue strength than the base metal and other composites due to uniform dispersion and dendritic cast structure and also due to early fracture of the particles during loading. Selvamani et al. (2016) found no defects in the friction welded zone and a higher tensile strength of around 370 MPa in the welded joints. Bhushan et al. (2013) found that composite with reinforcement 10 and 15 wt% of SiC in AA7075 matrix have the uniform distribution of reinforcement particles and products for secondary

TABLE 10.5
Mechanical Testing of 7XXX Series Aluminium Alloys and Composites

Composite	Hardness		Tensile		Reference
	Min	Max	Min (MPa)	Max (MPa)	
AA7075 + TiB ₂	63 VHN	128 VHN	130	280	(Michael Rajan et al., 2013)
AA7075 With & Without Ni	100 HV	225 HV	180	400	(Naeem & Mohammed, 2013)
AA7075 + Al ₂ O ₃ + hBN	—	—	180	450	(Kannan & Ramanujam, 2018)
AA7075 + TiB ₂	104.4 HV	132.82 HV	—	—	(Chandana et al., 2018)
AA7075 + Foamed SiO ₂ /Al ₂ O ₃ /Fe ₂ O ₃	128 HV	169 HV	—	—	(Ralph & Silberstein, 2015)
AA7075 + Al ₂ O ₃ + SiC	70 HB	142 HB	165	325	(Kannan & Ramanujam, 2017)
AA7075 + SiC + Al ₂ O ₃	—	—	370	584	(Selvamani et al., 2016)
AA7075 + TiC	95 VHN	190 VHN	300	600	(Veeravalli et al., 2016)
AA7075 + Gr	90 BHN	115 BHN	170	220	(Baradeswaran & Perumal, 2014a, b)
AA7075 + SiC	82.6 HV	127.5 HV	—	—	(Prabhu, 2017)
AA7075 + Al ₂ O ₃	—	—	—	—	(Divagar et al., 2016)
AA7075 + Gr + Bagasse-ash	87.3 BHN	99.6 BHN	259.3	299.4	(Imran et al., 2016)
AA7075 + Gr	205 RHN	275 RHN	—	—	(Ramkumar et al., 2015)
AA7075 + Al ₂ O ₃ /Gr	58 VHN	110 VHN	210	290	(Baradeswaran & Elaya Perumal, 2014)
AA7005 + Al ₂ O ₃ p	75 HV	110 HV	299	370	(Ceschini et al., 2007)
AA7075	100 HV	220 HV	373	484	(Zhang et al., 2015)
AA7475 + B4C + CeO ₂	—	—	49	210	(Senthilnathan et al., 2018)
AA7075 + WC	86 HV	—	101	197	(Nallabelli & Ravi, 2018)
AA7075 + SiC + B4C	96 HV	134 HV	85.37	138	(Gopalakannan & Senthilvelan, 2015)
AA7075 + SiC + Graphite	138BHN 146VHN	168BHN 168VHN	—	—	(Pandian & Kannan, 2021)

(Continued)

TABLE 10.5 (Continued)
Mechanical Testing of 7XXX Series Aluminium Alloys and Composites

Composite	Impact		Fatigue		Reference
	Min. (J)	Max. (J)	Min. (J)	Max. (J)	
AA7075 + Al ₂ O ₃ + SiC	3.5	8.5	—	—	(Kannan & Ramanujam, 2017)
AA7075 + SiC + Al ₂ O ₃	—	—	128	190	(Selvamani et al., 2016)
AA7075 + Al ₂ O ₃	—	—	173	194	(Divagar et al., 2016)
AA7075 + SiC + Graphite	4.5	5.1	—	—	(Pandian & Kannan, 2021)

chemical reactions on the SiCp/matrix interface. Baradeswaran and Elaya Perumal (2014) found that tensile strength increases with increasing wt.% of Al₂O₃ content. However, there was a decrease in the tensile strength of hybrid composite slightly due to the presence of graphite.

Veeravalli et al. (2016) found that there was an increase in strength of about 130 MPa after T6 heat treatment due to an increase in 8 wt% of reinforcement. The tensile tests also revealed that the decrease in % elongation from 8.34 to 7.14 was due to an increasing percentage of TiC reinforcement. Wear rate and coefficient of friction also decreased with an increase in weight percentage of the reinforcement. The reason behind this may be due to the increase in strain energy, the hardness of the composites increased at the peripheral of the particles in the matrix. Kumar and Dhiman (2013) examined wear test on reinforcement like SiC and graphite and used response surface methodology statistical techniques to validate it. The results revealed that the wear properties improved with the use of hybrid composite (SiC + Gr) than with the unreinforced aluminium alloy. Michael Rajan et al. (2014) examined the effect of wear and temperature content on AA7075 reinforced with TiB₂. They found that a constant amount of TiB₂ particle resistance to wear was lower at a higher temperature. Baradeswaran et al. (2013) found improvement in the wear properties due to the MML formation on the worn surface of the composite, and it acted as a controlling parameter for the wear properties. MML formed on the worn surface of the composite is the key role player in controlling the wear properties of the composites. Vigneshwar et al. (2016) found that rotational speed had more influence on the tensile strength of the joints, followed by forging pressure and friction pressure. So, there was an increase in the tensile strength. No defects were found in the friction welded

MMNC joints under optimized conditions. The optimized condition attains a tensile strength of 370 MPa under 21.67 MPa/s of friction pressure/time, 21.67 MPa/s of forging pressure/time, and 21.66 rps of rotational speed. A maximum tensile strength of 370 MPa could be attained in friction-welded MMNC joints under the welding conditions of 21.67 MPa/s of friction pressure/time, 21.67 MPa/s of forging pressure/time and 21.66 rps of rotational speed.

10.5 DISCUSSION

In this section, a brief discussion is presented to understand the preparation method, when aluminium 7XXX as a base matrix with reinforcement as mono composite or hybrid composite. After a detailed understanding of all research articles cited in reference, this chapter compares the more significant factors with or without the addition of reinforcement related to the casting method in Figures 10.2–10.5 and reinforcement related to mechanical properties in Figures 10.6–10.7. Figure 10.2 shows the weight percentage of different reinforcements in the stir casting technique. Here the reinforcements used were SiC (7–25 wt%), Al₂O₃ (2–8 wt%), TiB₂ (4–8 wt%), TiC (2–10 wt%), Gr (5–20 wt%), B₄C (5 wt%), Al₂O₃ + SiC (2,4 wt%), SiC + Gr (7,3 wt%), Al₂O₃ + Gr (10,5 wt%), Si₃N₄ + Gr (8,0–6 wt%), Nano SiC (10 wt%)+ Al₂O₃ (5 wt%). The reinforcements most commonly used are SiC and Al₂O₃, showing that they are having good wettability and easily mixed into one another. Figure 10.3 shows with weight percent of

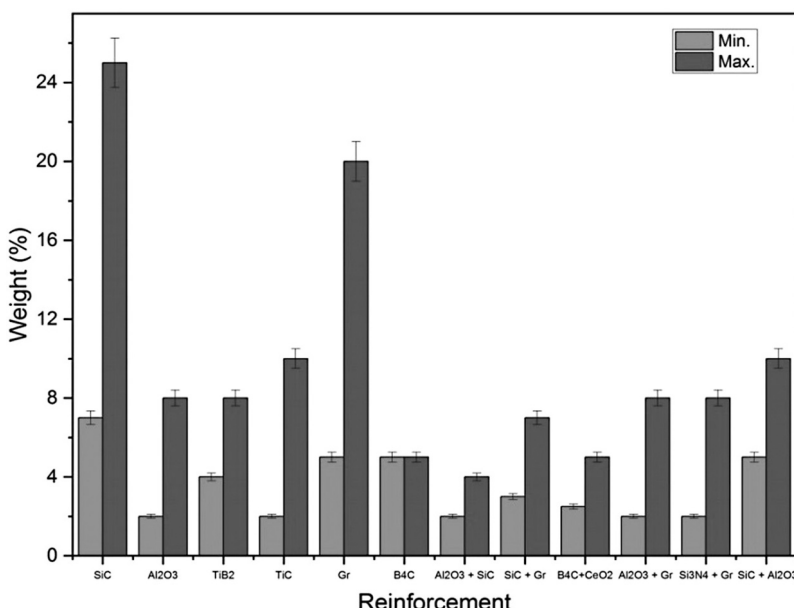


FIGURE 10.2 Reinforcement vs. weight percent for the stir casting technique.

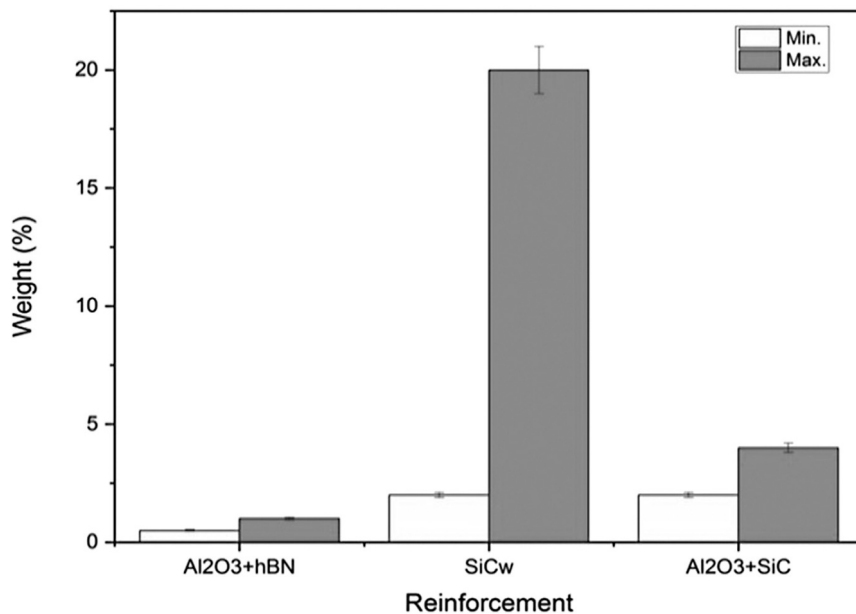


FIGURE 10.3 Reinforcement vs. weight percent for squeeze casting technique.

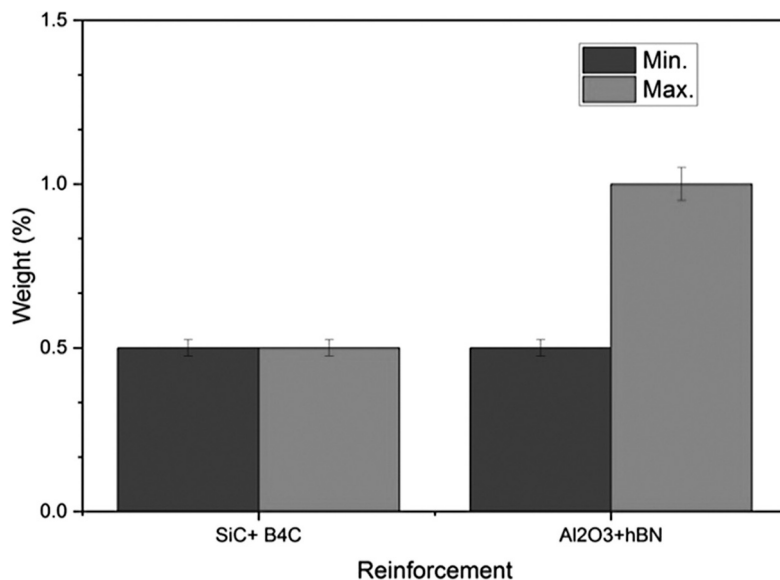


FIGURE 10.4 Reinforcement vs. weight percent for ultrasonic-assisted casting technique.

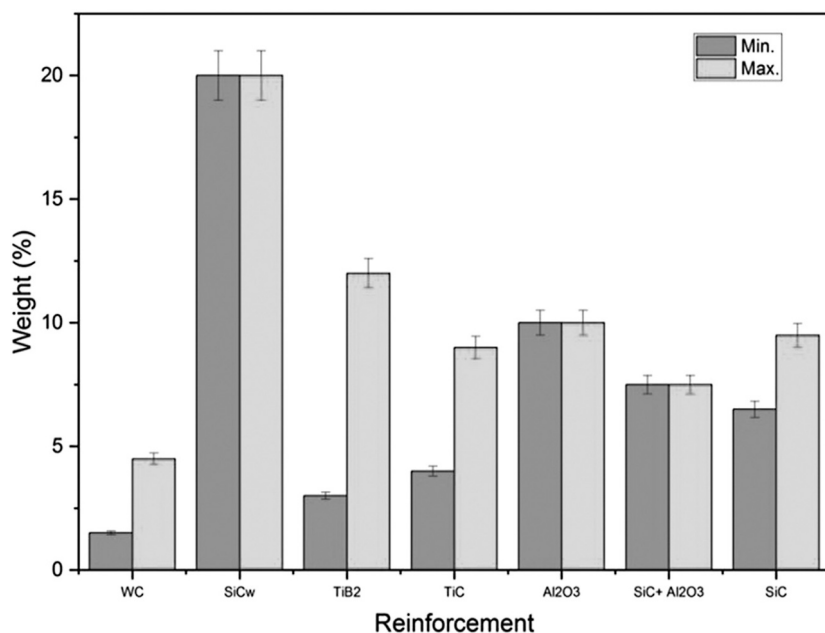


FIGURE 10.5 Reinforcement vs. weight percent for other casting techniques.

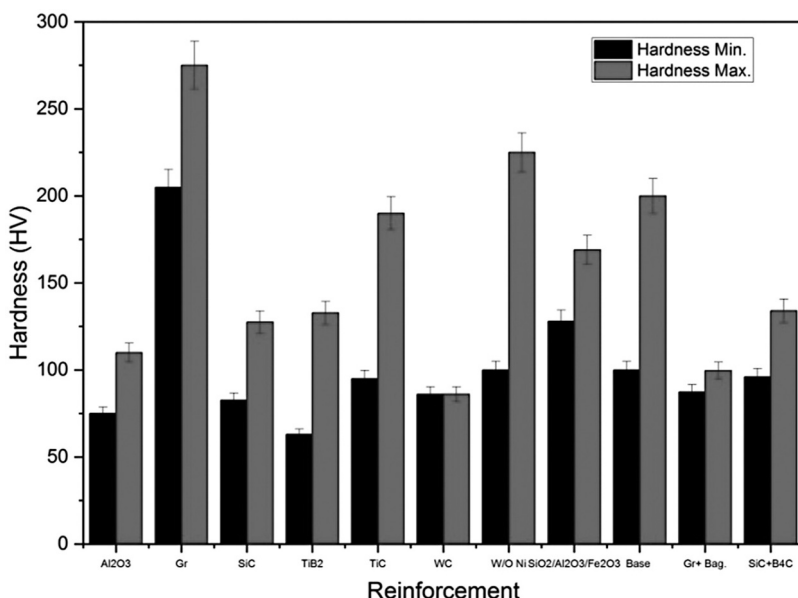


FIGURE 10.6 Reinforcement vs. hardness value of 7XXX series aluminium alloys and composites.

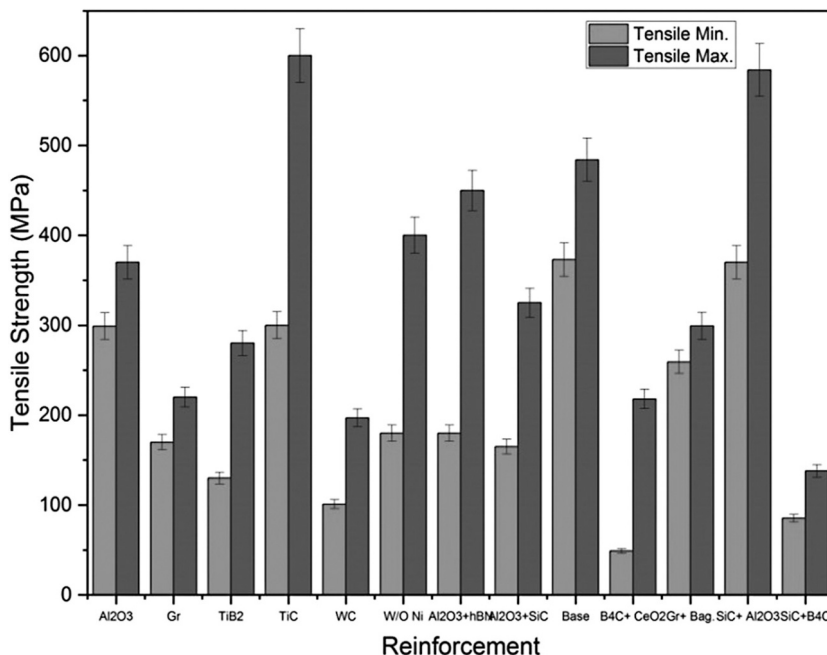


FIGURE 10.7 Reinforcement vs. tensile strength of 7XXX series aluminium alloys and composites.

different reinforcements in the squeeze casting technique with reinforcements like Al₂O₃ + hBN (0.5 wt%, 1 wt%), SiC_w (20 wt%), Al₂O₃ (2 wt%) (Blaz et al., 2010; Kannan & Ramanujam, 2017, 2018).

Figure 10.4 shows the weight percentages of different reinforcements of ultrasonic-assisted casting techniques, from minimum to maximum values. The reinforcements used were SiC + B₄C (0.5, 0.5 wt%), Al₂O₃ + hBN (0.5, 1 wt%) (Gopalakannan & Senthilvelan, 2015; Kannan & Ramanujam, 2018). The squeeze and ultrasonic method shows that they help in reducing porosity and giving fine grain structures and good mechanical properties.

Figure 10.5 shows with weight percent of different reinforcements of other casting techniques which comprises in-situ casting, centrifugal casting, electromagnetic stir casting, semi-direct chill casting, infiltrated casting, thixoforming from maximum to minimum values, and using reinforcements like WC (1.5–3.5 wt%), SiC_w (20w t%), TiB₂ (3–12 wt%), TiC (4 wt%), Al₂O₃ (10 wt%), SiC + Al₂O₃ (7.5 wt%, 15 wt%) (Blaz et al., 2010; Sabatini et al., 2010; George & Knutsen, 2012; Naeem & Mohammed, 2013; Baskaran et al., 2014; Lal, Kumar, Khan, & Siddiquee, 2014; Michael Rajan et al., 2014; Haghayeghi et al., 2015; Ralph & Silberstein, 2015; Prabhu, 2017).

The maximum and minimum ranges for composite making, up to different reinforcement weight percentages, were taken into consideration. Beyond the

limits of weight percent, there may be the presence of defects, which lead to the decreasing of microstructural and mechanical properties. Figures 10.2–10.5 show that the hybrid composite has better mechanical properties with fine-grained structure than monocomposite. Further, the combined casting technique for fabricating hybrid composite will be the better option to avoid defects as well to optimize grain size and mechanical properties.

Figure 10.6 shows that by varying the reinforcements, there is a variation in the hardness value from minimum to maximum. It signifies that the use of hybrid reinforcements leads to the increase of mechanical properties comparatively than the mono reinforcements. Figure 10.7 shows that varying the reinforcements, and there is a variation in the tensile strength value from minimum to maximum. TiC reinforcement is showing maximum values as compared to others may be due to strong bonding between the alloy and reinforcement when compared to others. For the case of hybrid reinforcements, the tensile values increased up to 584 MPa, which shows that there is a tremendous increase in the case of hybrid reinforcement as compared to mono reinforcements for the SiC and Al₂O₃ may be due to the excellent wettability with each other as compared to others.

10.6 CONCLUSION

The following are the conclusions drawn from the topical review on advancement in liquid processing techniques of aerospace-grade 7XXX series aluminium alloy and its composites.

- The stir casting method is used most commonly for the preparation of 7XXX series aluminium composites. Stir casting process parameters used by various researchers for mono composite with reinforcement pre-heat temperatures range from 300 to 400°C, stirring speeds range from 250 to 500 RPM with 4 to 15 minutes' stirring time, and a furnace temperature 750 to 850°C.
- Stir cast process parameters like reinforcement pre-heat temperatures range from 400 to 600°C, stirring speed range from 450 to 600 RPM with 10 to 15 minutes' stirring time and a furnace temperature of 800 to 950°C used for hybrid composite fabrication.
- In the squeeze casting method, 100 Mpa pressure is used for mono composite and 150 MPa pressure for hybrid composite preparation.
- Ultrasonic-assisted casting method is used only for the preparation of un reinforced base alloy and hybrid composite with 18 kHz frequency and 4 kW input power.
- In the 7XXX series, AMMC aluminium is used as the base metal matrix and SiC, Al₂O₃, graphite, TiB₂, B₄C (micro and nano size) in particulate or whiskers form are used as reinforcement.

- Al_2O_3 has been used as reinforcement mostly for aluminium composites as it helps increase the composite's tensile strength. The various other reinforcements like SiC, graphite, TiC, and TiB_2 were also studied. The reinforcements like SiC and Al_2O_3 support each other in the homogeneity aspect as they improve mechanical properties.
- SiC and graphite combined have the least value wear rate, and with the addition of graphite below 5 wt% show excellent mechanical and wear properties in the aerospace series. When SiC and graphite are combined in nanoparticle form, they exhibit high fatigue strength.
- Hybrid composite shows better mechanical properties and wear properties over mono composites and unreinforced aluminium alloys.
- The combined casting technique (stir, squeeze, and ultrasonic) for fabricating hybrid and mono composite will be the better option to avoid defects, as well to optimize grain size to obtain better microstructure and mechanical properties.
- In aerospace-grade aluminium alloys and composites, very few works have reported on impact testing, fatigue testing, wear and joining studies, which shows many possibilities for future research related to this area.

REFERENCES

- Ahmad, Z. (2012). *Recent Trends in Processing and Degradation of Aluminium Alloys. Recent Trends in Processing and Degradation of Aluminium Alloys*. <https://doi.org/10.5772/741>
- Arjunan, R. M. T. V. (2019). Microstructure and mechanical characteristics of CDA–B 4 C hybrid metal matrix composites. *Metals and Materials International*, (0123456789). <https://doi.org/10.1007/s12540-019-00518-6>
- Baradeswaran, A., & Elaya Perumal, A. (2014). Study on mechanical and wear properties of Al 7075/ Al_2O_3 /graphite hybrid composites. *Composites Part B: Engineering*, 56, 464–471. <https://doi.org/10.1016/j.compositesb.2013.08.013>
- Baradeswaran, A., & Elaya Perumal, A. (2015). Effect of graphite on tribological and mechanical properties of AA7075 composites. *Tribology Transactions*, 58(1), 1–6. <https://doi.org/10.1080/10402004.2014.947663>
- Baradeswaran, A., & Perumal, A. E. (2014a). Effect of graphite on tribological and mechanical properties of AA7075 composites, (December), 37–41. <https://doi.org/10.1080/10402004.2014.947663>
- Baradeswaran, A., & Perumal, A. E. (2014b). Wear and mechanical characteristics of Al 7075/graphite composites. *Composites Part B: Engineering*, 56, 472–476. <https://doi.org/10.1016/j.compositesb.2013.08.073>
- Baradeswaran, A., Elayaperumal, A., & Franklin Issac, R. (2013). A statistical analysis of optimization of wear behaviour of Al-Al 2O3 composites using taguchi technique. *Procedia Engineering*, 64, 973–982. <https://doi.org/10.1016/j.proeng.2013.09.174>
- Basavarajappa, S., Chandramohan, G., Mukund, K., Ashwin, M., & Prabu, M. (2006). Dry sliding wear behavior of Al 2219/SiCp-Gr hybrid metal matrix composites. *Journal of Materials Engineering and Performance*, 15(6), 668–674. <https://doi.org/10.1361/105994906X150803>

- Baskaran, S., Anandakrishnan, V., & Duraiselvam, M. (2014). Investigations on dry sliding wear behavior of in situ casted AA7075-TiC metal matrix composites by using Taguchi technique. *Materials and Design*, 60, 184–192. <https://doi.org/10.1016/j.matdes.2014.03.074>
- Bhushan, R. K., Kumar, S., & Das, S. (2013). Fabrication and characterization of 7075 Al alloy reinforced with SiC particulates. *International Journal of Advanced Manufacturing Technology*, 65(5–8), 611–624. <https://doi.org/10.1007/s00170-012-4200-6>
- Biermann, H., & Hartmann, O. (2006). Mechanical behavior and fatigue properties of metal-matrix composites. *Metal Matrix Composites: Custom-made Materials for Automotive and Aerospace Engineering*. <https://doi.org/10.1002/3527608117.ch7>
- Blaz, L., Kula, A., Kaneko, J., Sugamata, M., Wloch, G., & Sobota, K. (2010). Microstructure and mechanical properties of AA7039+20%SiCw composite. *Journal of Microscopy*, 237(3), 416–420. <https://doi.org/10.1111/j.1365-2818.2009.03276.x>
- Ceschini, L., Boromei, I., Minak, G., Morri, A., & Tarterini, F. (2007). Effect of friction stir welding on microstructure, tensile and fatigue properties of the AA7005/10 vol.%Al₂O₃p composite. *Composites Science and Technology*, 67(3–4), 605–615. <https://doi.org/10.1016/j.compscitech.2006.07.029>
- Chandana, A., Lawrence, I. D., & Jayabal, S. (2018). Characterization of particulate-reinforced aluminium 7075/TiB₂ composites. *Materials Today: Proceedings*, 5(6), 14317–14326. <https://doi.org/10.1016/j.matpr.2018.03.014>
- Cuevas, A. C., Becerril, E. B., Martínez, M. S., & Ruiz, J. L. (2018). *Metal matrix composites: Wetting and infiltration. Metal Matrix Composites: Wetting and Infiltration*. <https://doi.org/10.1007/978-3-319-91854-9>
- Davis JR. (1999). *Corrosion of aluminum and aluminum alloys*. ASM International. <https://doi.org/10.5860/choice.37-2798>
- Davis, J. R. (2001). *Aluminum and Aluminum Alloys*. ASM International. <https://doi.org/10.1361/autb2001p351>
- Deepandurai, K., & Parameshwaran, R. (2016). Multiresponse optimization of FSW parameters for cast AA7075/SiCp composite. *Materials and Manufacturing Processes*, 31(10), 1333–1341. <https://doi.org/10.1080/10426914.2015.1117628>
- Delrue, S., Tabatabaeipour, M., Hettler, J., & Abeele, K. Van Den. (2016). Applying a non-linear, pitch-catch, ultrasonic technique for the detection of kissing bonds in friction stir welds. *Ultrasonics*, 68, 71–79. <https://doi.org/10.1016/j.ultras.2016.02.012>
- Divagar, S., Vigneshwar, M., & Selvamani, S. T. (2016). Impacts of nano particles on fatigue strength of aluminum based metal matrix composites for aerospace. *Materials Today: Proceedings*, 3(10), 3734–3739. <https://doi.org/10.1016/j.matpr.2016.11.021>
- Donatus, U., Thompson, G. E., Omotoyinbo, J. A., Alaneme, K. K., Aribi, S., & Agbabiaka, O. G. (2017). Corrosion pathways in aluminium alloys. *Transactions of Nonferrous Metals Society of China (English Edition)*, 27(1), 55–62. [https://doi.org/10.1016/S1003-6326\(17\)60006-2](https://doi.org/10.1016/S1003-6326(17)60006-2)
- Dubey, V., & Singh, B. (2018). Study of material removal rate in powder mixed EDM of AA7075/B4C composite. *Materials Today: Proceedings*, 5(2), 7466–7475. <https://doi.org/10.1016/j.matpr.2017.11.418>
- Effertz, P. S., Infante, V., Quintino, L., Suhuddin, U., Hanke, S., & Dos Santos, J. F. (2016). Fatigue life assessment of friction spot welded 7050-T76 aluminium alloy using Weibull distribution. *International Journal of Fatigue*, 87, 381–390. <https://doi.org/10.1016/j.ijfatigue.2016.02.030>

- Fadavi Boostani, A., Tahamtan, S., Jiang, Z. Y., Wei, D., Yazdani, S., Azari Khosroshahi, R., ... Gong, D. (2015). Enhanced tensile properties of aluminium matrix composites reinforced with graphene encapsulated SiC nanoparticles. *Composites Part A: Applied Science and Manufacturing*, 68, 155–163. <https://doi.org/10.1016/j.compositesa.2014.10.010>
- Gajewska, M., Dutkiewicz, J., & Morgiel, J. (2014). Effect of reinforcement particle size on microstructure and mechanical properties of AlZnMgCu/AlN nano-composites produced using mechanical alloying. *Journal of Alloys and Compounds*, 586(SUPPL. 1), S423–S427. <https://doi.org/10.1016/j.jallcom.2012.10.055>
- George, S. L., & Knutson, R. D. (2012). Composition segregation in semi-solid metal cast AA7075 aluminium alloy. *Journal of Materials Science*, 47(11), 4716–4725. <https://doi.org/10.1007/s10853-012-6340-3>
- Gopalakannan, S., & Senthilvelan, T. (2015). Synthesis and characterisation of Al 7075 reinforced with SiC and B4C nano particles fabricated by ultrasonic cavitation method. *Journal of Scientific and Industrial Research*, 74(5), 281–285.
- Gupta, R., Chaudhari, G. P., & Daniel, B. S. S. (2018). Strengthening mechanisms in ultrasonically processed aluminium matrix composite with in-situ Al3Ti by salt addition. *Composites Part B: Engineering*, 140, 27–34. <https://doi.org/10.1016/j.compositesb.2017.12.005>
- Haghayeghi, R., Heydari, A., & Kapranos, P. (2015). The effect of ultrasonic vibrations prior to high pressure die-casting of AA7075. *Materials Letters*, 153, 175–178. <https://doi.org/10.1016/j.matlet.2015.04.034>
- Imran, M., & Khan, A. R. A. (2019). Characterization of Al-7075 metal matrix composites: a review. *Journal of Materials Research and Technology*, 8(3), 3347–3356. <https://doi.org/10.1016/j.jmrt.2017.10.012>
- Imran, M., Khan, A. R. A., Megeri, S., & Sadik, S. (2016). Study of hardness and tensile strength of Aluminium-7075 percentage varying reinforced with graphite and bagasse-ash composites. *Resource-Efficient Technologies*, 2(2), 81–88. <https://doi.org/10.1016/j.refft.2016.06.007>
- Jo, M. C., Choi, J. H., Yoo, J., Lee, D., Shin, S., Jo, I., ... Lee, S. (2019). Novel dynamic compressive and ballistic properties in 7075-T6 Al-matrix hybrid composite reinforced with SiC and B4C particulates. *Composites Part B: Engineering*, 174(March), 107041. <https://doi.org/10.1016/j.compositesb.2019.107041>
- Kannan, C., & Ramanujam, R. (2017). Comparative study on the mechanical and microstructural characterisation of AA 7075 nano and hybrid nanocomposites produced by stir and squeeze casting. *Journal of Advanced Research*, 8(4), 309–319. <https://doi.org/10.1016/j.jare.2017.02.005>
- Kannan, C., & Ramanujam, R. (2018). Effectiveness evaluation of molten salt processing and ultrasonic cavitation techniques during the production of aluminium based hybrid nanocomposites - an experimental investigation. *Journal of Alloys and Compounds*, 751, 183–193. <https://doi.org/10.1016/j.jallcom.2018.04.112>
- Kanth, U. R., Rao, P. S., & Krishna, M. G. (2019). Mechanical behaviour of fly ash/SiC particles reinforced Al-Zn alloy-based metal matrix composites fabricated by stir casting method. *Journal of Materials Research and Technology*, 8(1), 737–744. <https://doi.org/10.1016/j.jmrt.2018.06.003>
- Karabulut, Ş., Gökmən, U., & Çinici, H. (2018). Optimization of machining conditions for surface quality in milling AA7039-based metal matrix composites. *Arabian Journal for Science and Engineering*, 43(3), 1071–1082. <https://doi.org/10.1007/s13369-017-2691-z>

- Kumar, R., & Dhiman, S. (2013). A study of sliding wear behaviors of Al-7075 alloy and Al-7075 hybrid composite by response surface methodology analysis. *Materials and Design*, 50, 351–359. <https://doi.org/10.1016/j.matdes.2013.02.038>
- Kumar, A., Pal, K., & Mula, S. (2017). Simultaneous improvement of mechanical strength, ductility and corrosion resistance of stir cast Al7075-2% SiC micro- and nanocomposites by friction stir processing. *Journal of Manufacturing Processes*, 30, 1–13. <https://doi.org/10.1016/j.jmapro.2017.09.005>
- Lal, S., Kumar, S., Khan, Z. A., & Siddiquee, A. N. (2014). Wire electrical discharge machining of AA7075/SiC/Al₂O₃ hybrid composite fabricated by inert gas-assisted electromagnetic stir-casting process. *Journal of the Brazilian Society of Mechanical Sciences and Engineering*, 36(2), 335–346. <https://doi.org/10.1007/s40430-013-0087-x>
- Leng, J., Wu, G., Zhou, Q., Dou, Z., & Huang, X. L. (2008). Mechanical properties of SiC/Gr/Al composites fabricated by squeeze casting technology. *Scripta Materialia*, 59(6), 619–622. <https://doi.org/10.1016/j.scriptamat.2008.05.018>
- Madhukar, P., Selvaraj, N., Rao, C. S. P., & Veeresh Kumar, G. B. (2019). Tribological behavior of ultrasonic assisted double stir casted novel nano-composite material (AA7150-hBN) using Taguchi technique. *Composites Part B: Engineering*, 175(June), 107136. <https://doi.org/10.1016/j.compositesb.2019.107136>
- Manikandan, R., Arjunan, T. V., & Akhil, A. R. (2020). Studies on micro structural characteristics, mechanical and tribological behaviours of boron carbide and cow dung ash reinforced aluminium (Al 7075) hybrid metal matrix composite. *Composites Part B: Engineering*, 183(AI 7075), 107668. <https://doi.org/10.1016/j.compositesb.2019.107668>
- Michael Rajan, H. B., Ramabalan, S., Dinaharan, I., & Vijay, S. J. (2013). Synthesis and characterization of in situ formed titanium diboride particulate reinforced AA7075 aluminum alloy cast composites. *Materials and Design*, 44, 438–445. <https://doi.org/10.1016/j.matdes.2012.08.008>
- Michael Rajan, H. B., Ramabalan, S., Dinaharan, I., & Vijay, S. J. (2014). Effect of TiB₂ content and temperature on sliding wear behavior of AA7075/TiB₂ in situ aluminum cast composites. *Archives of Civil and Mechanical Engineering*, 14(1), 72–79. <https://doi.org/10.1016/j.acme.2013.05.005>
- Mir Irfan Ul Haq, A. A. (2018). Dry sliding friction and wear behaviour of Hybrid AA7075/Si₃N₄/Gr self lubricating composites. *Nanotechnology*, 29(27).
- Mohanavel, V., Rajan, K., Suresh Kumar, S., Vijayan, G., & Vijayanand, M. S. (2018). Study on mechanical properties of graphite particulates reinforced aluminium matrix composite fabricated by stir casting technique. *Materials Today: Proceedings*, 5(1), 2945–2950. <https://doi.org/10.1016/j.matpr.2018.01.090>
- Naeem, H. T., & Mohammed, K. S. (2013). Retrogression and re-aging of aluminum alloys (AA 7075) containing nickel. *Digest Journal of Nanomaterials and Biostructures*, 8(4), 1621–1632.
- Nallabelli, A. B., & Ravi, B. (2018). Effect of tool rotational speed on microstructure and mechanical behavior of friction stir welded AA7075/WC metal matrix composites, 9(6), 746–754.
- Pandian, V., & Kannan, S. (2021). Processing and preparation of aerospace-grade aluminium hybrid metal matrix composite in a modified stir casting furnace integrated with mechanical supersonic vibration squeeze infiltration method. *Materials Today Communications*, 26(May 2020), 101732. <https://doi.org/10.1016/j.mtcomm.2020.101732>

- Podyanova, N. B., & Karabutov, A. A. (2017). Combined effects of reinforcement fraction and porosity on ultrasonic velocity in SiC particulate aluminum alloy matrix composites. *Composites Part B: Engineering*, 113, 138–143. <https://doi.org/10.1016/j.compositesb.2017.01.017>
- Prabhu, T. R. (2017). Processing and properties evaluation of functionally continuous graded 7075 Al alloy/SiC composites. *Archives of Civil and Mechanical Engineering*, 17(1), 20–31. <https://doi.org/10.1016/j.acme.2016.08.004>
- Priyadarshi, D., & Sharma, R. K. (2016a). Effect of type and percentage of reinforcement for optimization of the cutting force in turning of Aluminium matrix nanocomposites using response surface methodologies. *Journal of Mechanical Science and Technology*, 30(3), 1095–1101. <https://doi.org/10.1007/s12206-016-0255-x>
- Priyadarshi, D., & Sharma, R. K. (2016b). Optimization for turning of Al-6061-SiC-Gr hybrid nanocomposites using response surface methodologies. *Materials and Manufacturing Processes*, 31(10), 1342–1350. <https://doi.org/10.1080/10426914.2015.1070427>
- Pugazhenthi, A., Kanagaraj, G., Dinaharan, I., & David Raja Selvam, J. (2018). Turning characteristics of in situ formed TiB₂ ceramic particulate reinforced AA7075 aluminium matrix composites using polycrystalline diamond cutting tool. *Measurement: Journal of the International Measurement Confederation*, 121, 39–46. <https://doi.org/10.1016/j.measurement.2018.02.039>
- Rajan, H. B. M., Dinaharan, I., Ramabalan, S., & Akinlabi, E. T. (2016). Influence of friction stir processing on microstructure and properties of AA7075/TiB₂ in situ composite. *Journal of Alloys and Compounds*, 657, 250–260. <https://doi.org/10.1016/j.jallcom.2015.10.108>
- Ralph, C., & Silberstein, M. (2015). *Mechanics of Composite and Multi-functional Materials, Volume 7* (Vol. 7).
- Ramanathan, A., Krishnan, P. K., & Muraliraja, R. (2019). A review on the production of metal matrix composites through stir casting – Furnace design, properties, challenges, and research opportunities. *Journal of Manufacturing Processes*, 42, 213–245. <https://doi.org/10.1016/j.jmapro.2019.04.017>
- Ramkumar, K. R., Bekele, H., & Sivasankaran, S. (2015). Experimental investigation on mechanical and turning behavior of al 7075/x % wt. TiB₂-1% Gr in situ hybrid composite. *Advances in Materials Science and Engineering*, 2015. <https://doi.org/10.1155/2015/727141>
- Rao, R. N., & Das, S. (2010). Effect of matrix alloy and influence of SiC particle on the sliding wear characteristics of aluminium alloy composites. *Materials and Design*, 31(3), 1200–1207. <https://doi.org/10.1016/j.matdes.2009.09.032>
- Rao, R. N., Das, S., Mondal, D. P., Dixit, G., & Tulasi Devi, S. L. (2013). Dry sliding wear maps for AA7010 (Al-Zn-Mg-Cu) aluminium matrix composite. *Tribology International*, 60, 77–82. <https://doi.org/10.1016/j.triboint.2012.10.007>
- Sabatini, G., Ceschini, L., Martini, C., Williams, J. A., & Hutchings, I. M. (2010). Improving sliding and abrasive wear behaviour of cast A356 and wrought AA7075 aluminium alloys by plasma electrolytic oxidation. *Materials and Design*, 31(2), 816–828. <https://doi.org/10.1016/j.matdes.2009.07.053>
- Sekar, K. (2019). Mechanical and tribological properties of Al7475-SiCp composites by stir casting method and wear rate modeling using RSM. *Sadhana-Academy Proceedings in Engineering Sciences*, 44(5), 1–8. <https://doi.org/10.1007/s12046-019-1105-1>

- Sekar, K., & Ananda Rao, D. V. (2019). Investigation of hybrid composite A7075/SiC/B4C by stir and squeeze casting method. *Materials Today: Proceedings*, 22, 1398–1408. <https://doi.org/10.1016/j.matpr.2020.01.483>
- Sekar, K., & Singh, R. (2019). Mechanical and tribological properties of a7050 hybrid composite reinforced with nano Al₂O₃/micro ZrO₂ particles by stir casting method. *Materials Science Forum*, 969, 576–581. <https://doi.org/10.4028/www.scientific.net/MSF.969.576>
- Sekar, K., & Vasanthakumar, P. (2019). Mechanical properties of Al-Cu alloy metal matrix composite reinforced with B4C, graphite and wear rate modeling by Taguchi Method. *Materials Today: Proceedings*, 18, 3150–3159. <https://doi.org/10.1016/j.matpr.2019.07.190>
- Sekar, K., & Vasanthakumar, P. (2020a). Mechanical and tribological properties of Al6063 hybrid composites reinforced with SiC/ZrO₂ by stir casting and thixoforming process. *Materials Science Forum*, 979, 47–51. <https://doi.org/10.4028/www.scientific.net/MSF.979.47>
- Sekar, K., & Vasanthakumar, P. (2020b). Microstructural evaluation of similar and dissimilar welding of aluminum metal matrix hybrid composite by friction stir welding. *Materials Science Forum*, 979, 124–128. <https://doi.org/10.4028/www.scientific.net/MSF.979.124>
- Sekar, K., Allesu, K., & Joseph, M. A. (2015). Mechanical and wear properties of Al-Al₂O₃ metal matrix composites fabricated by the combined effect of stir and squeeze casting method. *Transactions of the Indian Institute of Metals*, 68(2), 115–121. <https://doi.org/10.1007/s12666-015-0520-1>
- Sekar, K., Jayachandra, G., & Aravindan, S. (2018). Mechanical and welding properties of A6082-SiC-ZrO₂ hybrid composite fabricated by stir and squeeze casting. *Materials Today: Proceedings*, 5(9), 20268–20277. <https://doi.org/10.1016/j.matpr.2018.06.398>
- Selvamani, S. T., Vigneshwar, M., & Divagar, S. (2016). Establishing the relationship between fatigue and tensile strength of frictionally joined metal matrix nanocomposite autogeneous joints for aerospace. *Transactions of the Indian Institute of Metals*, 69(2), 431–437. <https://doi.org/10.1007/s12666-015-0791-6>
- Senthilnathan, T., Balachandar, K., & Author, C. (2018). Friction stir welding of AA7475 hybrid composites, 9(8), 582–588.
- Singh, J. (2016). Fabrication characteristics and tribological behavior of Al/SiC/Gr hybrid aluminum matrix composites: a review. *Friction*, 4(3), 191–207. <https://doi.org/10.1007/s40544-016-0116-8>
- Sudhakar, I., Madhusudhan Reddy, G., & Srinivasa Rao, K. (2016). Ballistic behavior of boron carbide reinforced AA7075 aluminium alloy using friction stir processing – An experimental study and analytical approach. *Defence Technology*, 12(1), 25–31. <https://doi.org/10.1016/j.dt.2015.04.005>
- Suresh, S., Mortensen, A., & Needleman, A. (2013). Fundamentals of Metal-Matrix Composites. *Fundamentals of Metal-Matrix Composites*. <https://doi.org/10.1016/b978-0-12-819724-0-00001-x>
- Suresha, S., & Sridhara, B. K. (2010). Effect of silicon carbide particulates on wear resistance of graphitic aluminium matrix composites. *Materials and Design*, 31(9), 4470–4477. <https://doi.org/10.1016/j.matdes.2010.04.053>
- Vasanthakumar, P., Sekar, K., & Venkatesh, K. (2019). Recent developments in powder metallurgy based aluminium alloy composite for aerospace applications. *Materials Today: Proceedings*, 18, 5400–5409. <https://doi.org/10.1016/j.matpr.2019.07.568>

- Veeravalli, R. R., Nallu, R., & Mohammed Moulana Mohiuddin, S. (2016). Mechanical and tribological properties of AA7075-TiC metal matrix composites under heat treated (T6) and cast conditions. *Journal of Materials Research and Technology*, 5(4), 377–383. <https://doi.org/10.1016/j.jmrt.2016.03.011>
- Vigneshwar, M., Divagar, S., & Selvamani, S. T. (2016). Mechanical and metallurgical behavior of friction welded dual nano particles reinforced armour grade Al based nanocomposite joints in optimized condition. *Materials Today: Proceedings*, 3(10), 3740–3745. <https://doi.org/10.1016/j.matpr.2016.11.022>
- Zhang, F., Su, X., Chen, Z., & Nie, Z. (2015). Effect of welding parameters on microstructure and mechanical properties of friction stir welded joints of a super high strength Al-Zn-Mg-Cu aluminum alloy. *Materials and Design*, 67, 483–491. <https://doi.org/10.1016/j.matdes.2014.10.055>



Taylor & Francis

Taylor & Francis Group

<http://taylorandfrancis.com>

@seismicisolation
@seismicisolation

Index

3D laser cladding, 177

A

Additive Manufacturing, 118, 128, 149, 158, 168, 211, 228
Aerospace industry, 169, 188, 200
Aspect ratio, 21, 62, 109
Atoms, 19, 20, 48
Automotive industry, 16, 168, 188

B

Binder jetting (BJG), 184, 188
Biomedical industry, 197, 200

C

Carbon nanotubes, 95, 109, 110
Casting process, 30, 31, 36
Cause and Effect Analysis, 79, 80
Centrifugal infiltration route, 22
Ceramic matrix composites, 215
Chemical Vapor Deposition, 123, 126
Coating Technique, 120, 124
Coefficient of thermal expansion, 29, 60, 71, 109
Cold Spray, 120, 126, 128
Composite Material, 131, 168, 188, 192
Consolidation Techniques, 42
Construction industry, 197, 201
Conventional sintering, 30, 31, 56
Copper Matrix Composites, 47, 50

D

Decision Matrix, 71–73
Defects, 129, 137, 145
Design flexibility, 171, 190
Detonation Gun, 126, 128, 129
Different casting routes, 1
Diffusion bonding route, 17
Direct metal laser sintering (DMLS), 169, 172
Directed energy deposition (DED), 169, 172, 177

E

Elastoplastic, 84, 104, 105
Electrical, 128, 182, 184
Electron Beam Melting, 215, 216
Electron Beam Welding, 136, 137, 149

F

Fiber, 26, 182, 199
Fiber Reinforced Composites, 49, 199, 201
Finite element method, 91, 93, 94
Forced infiltration route, 17
Freeform design, 189
Friction Stir Welding, 136, 137, 140, 144
Fusion Deposition Modeling, 211, 216
Fusion Filament Fabrication, 212

G

Geometrical shape, 171, 185, 191

H

High energy ball milling, 28, 29
Homogenization, 86, 91, 93
Hot pressing sintering, 30, 31, 41

I

Imperfect bonding, 109
Infiltration route, 21, 22, 24
Ink Jet Printing, 225
Interphase, 97, 98, 101
Iron Matrix Composites, 167

J

Just in time (JIT), 190

L

Laminated Object Manufacturing, 172, 179
Laser engineered net shaping (LENS), 169, 177
Laser metal deposition (LMD), 169, 177
Laser Welding, 136, 137, 148
Liquid binder, 176
Liquid infiltration process, 51, 52
Liquid state processing techniques, 18, 19, 28
Lubrication, 118, 129, 182

M

Material characterization, 227
Mechanical properties, 130, 138, 139, 155
Micro and Nanocomposites, 1, 66
Micro-mechanics, 86, 91
Microstructure, 92, 98, 130

Mori-Tanaka, 91, 93, 95
 Multi-axis metal deposition, 178
 Multi-scale, 81, 83, 84

N

Nanocomposites, 98, 99, 101, 103
 Nickel Matrix Composites, 167

O

Orientation, 183, 187, 223

P

Particle Reinforced Composites, 201
 Pattern tracing, 173
 Perfect bonding, 109
 Phase deposition processing techniques, 18, 34
 Physical Vapor Deposition, 34, 57
 Poly Lactic Acid, 211
 Polymer Matrix Composites, 200, 203
 Powder metallurgy (PM), 203, 204, 210
 Powder-bed fusion (PBF), 169, 174

R

Rapid tooling, 172, 185
 Reinforcement, 173, 175, 180
 Representative volume element, 91, 103
 Reuss, 81, 87, 88

S

Scanning Electron Microscopy, 150, 227, 234
 Selective Laser Melting, 169, 172
 Selective Laser Sintering, 214, 216
 Self-consistent model, 203
 Solid state processing techniques, 18, 27, 47
 Spark Plasma Sintering, 30, 56, 57
 Spontaneous infiltration route, 17, 21

Spray deposition route, 17, 37
 Sputtering deposition process, 17, 36, 37
 Squeeze infiltration route, 22, 24
 Stereo lithography, 211, 212, 216
 Stir casting route, 19
 Super-alloy, 83, 178, 182
 Sustainable manufacturing, 168
 SWOT, 63, 73, 75

T

T6 Heat treatment, 7–9, 231, 239
 Thermal conductivity, 17, 40, 59
 Thermal Spray Process, 124–126
 Thermo-mechanical, 98, 105, 107, 109
 Titanium Matrix Composites, 167

U

Ultrasonic additive manufacturing (UAM), 137, 179
 Ultrasonic infiltration route, 17, 22, 26
 Ultrasonic Welding, 146

V

Voigt, 81, 87, 88
 Volume fraction, 88, 92, 97, 98

W

Welding Speed, 138, 139, 141, 142
 Wire+Arc AM (WAAM), 177

X

XRD, 69, 123, 129, 131

Z

Zinc Matrix Composites, 167, 185